eman ta zabal zazu

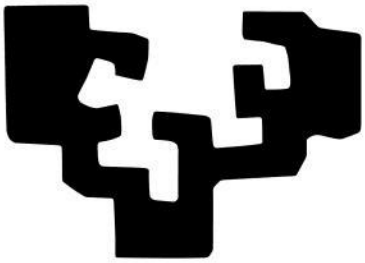

Universidad del País Vasco

Euskal Herriko Unibertsitatea

Post-processing Routes for Design of Giant Magnetoimpedance Response and Domain Wall Dynamics Control in Glass-coated Magnetic Microwires

by
Paula Corte-León

Supervisors
Prof. Dr. Arkady Zhukov Egorova
Prof. Dr. Julián María González Estévez

Departamento de Polímeros y Materiales Avanzados: Física, Química y Tecnología
Facultad de Ciencias Químicas
San Sebastián, 2022

Abstract

The principal objective of this thesis is to investigate the post-processing routes for the optimization of the magnetic properties of cobalt and iron based glass-coated microwires according to their applications. For this purpose several series of microwires were prepared and characterized paying attention on the effect of post-processing conditions allowing maximizing magnetic softness, Giant Magnetoimpedance (GMI) effect and/or fast domain wall (DW) dynamics control.

The work attempts to give an overview of the tuning possibilities of glass-coated microwires, which is one of the characteristics, in addition to their simple fabrication method and inexpensiveness that make them quite attractive and suitable for an enormous range of applications.

We have worked with nearly-zero magnetostriction amorphous Co-rich glass-coated microwires, of CoFeBSiC composition with small additions of Ni, Mo and C or Cr and different diameters, which present magnetic softness in as-prepared state. The results show that appropriate post-processing allows further improvement of magnetic softness and GMI effect. It is noteworthy the remarkable GMI ratio enhancement (up to 650%) achieved by Joule heating at optimal conditions of CoFeNiBSiMoC amorphous glass-coated microwires.

For Fe and Fe-Ni based glass-coated microwires, with rectangular hysteresis loops and hence, single DW propagation in as-prepared state, DW dynamics is further improved by furnace annealing owing to the internal stresses relaxation. On the other hand, low GMI ratio is enhanced more than an order of magnitude after stress-annealing, Joule heating or combined stress-annealed followed by conventional furnace annealing. Induced anisotropy depends on the post-processing conditions.

Annealing was demonstrated as an effective tool for optimizing magnetic softness and GMI effect of FeSiBNbCu devitrified microwires, but deterioration and poor mechanical properties lead to focus on post-processing that allows maintaining the amorphous structure.

Unique combination of GMI effect and fast single DW propagation is obtained for FeBSiC amorphous glass-coated microwires with moderate stress-annealing induced anisotropy. Such stress-annealing induced anisotropy is found to possess a partially reversible character. Subsequent annealing of stress-annealed samples allowed reversing part of the anisotropy induced by the stress-annealing.

As a rule, Co- & Fe-based microwires present amorphous structure if their diameters are below 30 μm. Furthermore, Fe-rich glass coated microwires of FeBSiNbNi composition of about 100 μm of metallic nucleus, considered as "thick" microwires, are successfully obtained by modified Taylor Ulitovsky technique. "Thick" microwires are highly demanded for certain applications and few documented. After proper annealing desirable combination of high GMI effect and single DW propagation is exhibited.

Likewise, for samples of both groups of microwires a simple route to achieve graded magnetic anisotropy along the sample length is proposed. Graded magnetic anisotropy is satisfactorily achieved after stress-annealing under temperature gradient.

Finally, among the many possibilities, a novel sensing technology is proposed and explored in order to illustrate the possibility of implementing the use of glass-coating microwires in sensing technologies. With this aim, as-prepared Co-based microwires and stress-annealed Fe-based microwires were used for non-destructive and non-contact monitoring of a composite material with microwire inclusions. Sensitivity of such microwires to tensile stress and temperature allows monitoring matrix polymerization process of the composite through the changes in the hysteresis loops of the microwires. The sensitivity of Fe-rich microwires to tensile stress can be improved by the stress-annealing induced anisotropy. Composite polymerization effect is observed to be opposite to the effect of applied tensile stress on the hysteresis loops of the microwire inclusions. Therefore, allows assuming compressive character of stresses acting upon the microwires during the polymerization process. Additionally, upon polymerization considerable variation of the transmission and reflection parameters (in the range of 4-7 GHz) of the composite with microwire inclusions is also observed by means of free space technique.

Resumen (Spanish)

El principal objetivo de esta tesis es investigar las rutas de posprocesamiento para la optimización de las propiedades magnéticas de microhilos recubiertos de vidrio basados en cobalto y hierro de acuerdo con sus aplicaciones. Para ello, se prepararon y caracterizaron varias series de microhilos prestando atención al efecto de las condiciones de posprocesado que permitieran maximizar el comportamiento magnético blando, el efecto de magnetoimpedancia gigante (GMI) y/o el control de la dinámica de paredes de dominio.

El trabajo intenta dar una visión general de las posibilidades de ajuste de las propiedades de los microhilos recubiertos de vidrio, que es una de las características, además de su sencillo método de fabricación y bajo costo, que los hacen bastante atractivos y aptos para una enorme gama de aplicaciones.

Se ha trabajado con microhilos amorfos recubiertos de vidrio ricos en Co de magnetostricción casi nula, de composición CoFeBSiC con pequeñas adiciones de Ni, Mo y C ó Cr y de diferentes diámetros, que presentan comportamiento magnético blando sin necesidad de posprocesado. Los resultados muestran que el procesamiento posterior adecuado permite una mejora de la suavidad magnética y el efecto GMI. Cabe destacar la notable mejora del efecto GMI (hasta un 650 %) lograda optimizando las condiciones de calentamiento por efecto Joule en microhilos amorfos recubiertos de vidrio de composición CoFeNiBSiMoC.

Para los microhilos recubiertos de vidrio basados en Fe y Fe-Ni, con ciclos de histéresis rectangulares y, que por lo tanto, presentan propagación de una única pared de dominio sin necesidad de tratamiento de posprocesado, la dinámica de paredes de dominio se mejora aún más mediante el recocido en horno debido a la relajación de las tensiones internas. Por otro lado, el bajo ratio GMI mejora más de un orden de magnitud después del recocido bajo tensión, el calentamiento Joule o el recocido bajo tensión combinado seguidamente de recocido en horno convencional. La anisotropía inducida depende de las condiciones de posprocesamiento.

Se demostró que el recocido es una herramienta eficaz para optimizar la suavidad magnética y el efecto GMI en microhilos desvitrificados de FeSiBNbCu, pero el deterioro de las propiedades mecánicas llevan a centrarse en posprocesado que permita mantener la estructura amorfa.

Se obtiene una combinación única de efecto GMI y propagación rápida de una única pared de dominio para microhilos amorfos recubiertos de vidrio FeBSiC con anisotropía inducida por recocido bajo tensión moderada aplicada. Se encuentra que tal anisotropía inducida por recocido bajo tensión posee un carácter parcialmente reversible. El recocido posterior de muestras recocidas bajo tensión permitió revertir parte de la anisotropía inducida por el recocido bajo tensión.

Generalmente, los microhilos basados en Fe y Co presentan estructura amorfa cuando sus diámetros están por debajo de 30 μm. Se han obtenido con éxito mediante la técnica modificada de Taylor Ulitovsky microhilos recubiertos de vidrio ricos en Fe de composición FeBSiNbNi de aproximadamente 100 μm de núcleo metálico, considerados como microhilos "gruesos". Los microhilos “gruesos” son muy demandados para ciertas aplicaciones y están poco documentados. Después de un recocido adecuado, exhiben una combinación deseable de alto efecto GMI y propagación de una única pared de dominio.

Asimismo, para muestras de ambos grupos de microhilos se propone una ruta sencilla para lograr una anisotropía magnética graduada a lo largo de la longitud de la muestra. La anisotropía magnética graduada se logra satisfactoriamente después del recocido bajo tensión bajo un gradiente de temperatura.

Finalmente, entre las muchas posibilidades, se propone y explora una nueva tecnología de detección para ilustrar la posibilidad de implementar el uso de microhilos recubiertos de vidrio en tecnologías de detección. Con este objetivo, se utilizaron microhilos a base de Co sin posprocesar y microhilos a base de Fe recocidos bajo tensión para el control no destructivo y sin contacto de un material compuesto con inclusiones de microhilos. La sensibilidad de tales microhilos a la tensión de tracción y la temperatura permite monitorear el proceso de polimerización de la matriz del material compuesto a través de los cambios en los ciclos de histéresis de los

microhilos. La sensibilidad de los microhilos ricos en Fe a la tensión de tracción puede mejorarse mediante la anisotropía inducida por recocido de tensión. A través de los ciclos de histéresis, se observa que la polimerización de la matriz del material compuesto tiene un efecto sobre las inclusiones de microhilo de carácter opuesto a la aplicación de tensión de tracción sobre los microhilos. Por lo tanto, permite asumir el carácter compresivo de las tensiones que actúan sobre los microhilos durante el proceso de polimerización. Además, tras la polimerización también se observa una variación considerable de los parámetros de transmisión y reflexión (en el rango de 4-7 GHz) del compuesto con inclusiones de microhilos.

Acknowledgments

First of all, I want to mention Prof. Ignacio Guerra, for being so much more than a friend over the years and our first guide in the research world.

I would be grateful for life to Prof. Blanca Hernando for giving me the opportunity and the encouragement to take this path, how not to do it keeping in mind her enthusiasm. Also Prof. Víctor de la Prida and all the Magnetic Materials and Nanomaterials research group at the University of Oviedo.

All my gratitude to my Supervisors Prof. Julián González Estévez and Prof. Arkady Zhukov for the support, guidance and continuous help received from them and especially from Prof. Valentina Zhukova, I admire her in many aspects, the most important her human quality, and I will be always grateful for their tireless help, also she introduce me to the use of the equipments needed and made me familiar in working on microwires. I deeply appreciate the time and efforts they made for me. This work has been accomplished thanks to them.

Many sincere thanks to our entire group, Juan María Blanco, Alexander Chizhik and especially Mihail Ipatov for helping me in uncountable occasions, I honestly appreciate them, their friendship and the things they made for me. Working with them was gratifying and a great pleasure. I am very glad for the place they gave me in their group making me feel part of it since the first day, and making easy my day to day, I am very thankful to them for their help in all aspects that could continue saying so much more. I want to give a huge thank you to all of them.

I want to give special thanks to Prof. Carlos García, for the acceptance of my stay at his laboratory in the Department of Physics of the Universidad Técnica Federico Santa María in Valparaíso, Chile, for his kind welcome, his help, friendship and support and the rest of the group, especially Dra. Marián Abellán, for making the time spent there a valuable and unforgettable experience.

I greatly thank Prof. Ivan Škorvánek, Head of Department of Applied Magnetism and Nanomaterials at the Institute of Experimental Physics of the Slovak Academy of Sciences in Košice, Slovakia for the acceptance of my virtual stay, the fruitful collaboration carried out, his invaluable discussions and his kindness and efficiency and Dr. František Andrejka for his crucial and extremely useful assistance and help.

Special thanks to Alexander Torcunov and Victor Muhortov for letting me introduce in the microwires fabrication procedure, sharing their priceless experience and also unforgettable anecdotes.

I would also like to give special thanks to Dra. Lorena González-Legarreta and Dra. Andrea Džubinská, co-workers for short time, but their great help and friendship has been essential, and Ahmed Talaat, doing the same path before me, for his kindness and support.

Many thanks to PhD colleagues Alfonso García and Álvaro González who came to bring freshness to the group and also Dr. Mohamed Salaheldeen for his significant help and support in the final strech.

I would like to thank Dr. Koldo Gondra and Dra. Sandra Allue, our collaboration established in the framework of ELKARTEK project, allowed me introduce myself in the field of smart composite materials with the help of their expertise.

I am truly grateful to my friends, especially Coral, Alba, Cristina and Bea, for always being there for me.

I must express my gratitude to Touseef, my husband, for been by my side, I want to promise him that all our efforts will be worth it. My children, Hakim and Ayra, born at the same time that this thesis bringing the biggest joy to my life, for them everything makes sense.

For my parents I will never have enough words of gratitude for their efforts in helping me, to them belongs the greatest merit of this work. To my brother for been always the best companion and counselor.

I would like to acknowledge for the technical and human support provided by SGiker of UPV/EHU (Medidas Magnéticas Gipúzcoa) and the Government of the Basque Country in the framework of HAZITEK and ELKARTEK projects and under the scheme of “Ayuda a Grupos Consolidados” and Spanish MINECO for the financial support of the group.

Finally, I thank the following grant for financial support: NEOHIRE-NEOdymium-Iron-Boron base materials, fabrication techniques and recycling solutions to HIghly REduce the consumption of Rare Earths in Permanent Magnets for Wind Energy Application, H2020-NMBP-720838, European Comission (Horizon 2020).

This thesis is also devoted to those who are no longer but made us being here.

Thanks to everyone who has contributed to this work.

Contents

Part I: Fundamentals 1-52

1. Introduction **1**

1.1. Metallic glasses 2
1.2. Soft magnetic materials 3
1.3. Amorphous glass coated microwires 4
1.3.1. Fabrication method 4
1.3.2. Effect of composition on magnetic properties 6
1.3.3. Hysteresis loops and domain structure 7
1.3.4. Induced anisotropies 9
1.3.5. Nanocrystalline glass-coated microwires 11
1.4. Giant magnetoimpedance (GMI) effect 11
1.5. Magnetic bistability and Fast domain wall (DW) propagation 13
1.6. Technological applications of magnetic glass-coated microwires 15
1.7. Research structure 18
1.8. References 19

2. Experimental techniques **25**

2.1. Glass-coated microwires fabrication: Taylor Ulitovsky method 25
2.2. Post-processing techniques: Annealing procedures 27
2.2.1. Conventional furnace annealing 27
2.2.2. Stress annealing 27
2.2.3. Current annealing 28
2.3. Magnetic characterization techniques 29
2.3.1. Hysteresis in ferromagnetic materials 29
2.3.2. Flux-metric method for hysteresis loops measurements 30
2.3.3. PPMS Magnetometer 33
2.3.4. Giant Magneto-Impedance (GMI) effect measurements 34
2.3.5. Free space electromagnetic parameters measurement system 37
2.3.6. Domain wall (DW) propagation measurements 39
2.3.7. Small angle magnetization rotation (SAMR) technique for magnetostriction measurements 40
2.4. Microstructural characterization techniques 43
2.4.1. Powder X-ray diffraction (XRD) 43
2.4.2. Optical microscopy (OM) 45
2.4.3. Scanning Electron Microscopy (SEM) 46
2.4.4. Differential Scanning Calorimetry (DSC) 47
2.5. References 51

Part II: Results and discussion **54-187**

3. Engineering of magnetic properties of Co-rich microwires **54**

3.1. As-prepared Co-rich microwires 55

3.2. Post-processing effect on magnetic properties, GMI effect and DW dynamics for Co-rich microwires 58
3.2.1. Conventional furnace annealing in Co-rich microwires 58
3.2.2. Stress-annealing in Co-rich microwires 61
3.2.3. Controlling the domain wall dynamics in Co-based magnetic microwires 68
3.2.4. Joule heating in Co-rich microwires 71
3.2.5. Effect of tensile stress in Co-rich microwires 79
3.2.5.1. Tuning of DW dynamics in Co-rich microwires by applied tensile stress 81
3.2.6. Graded magnetic anisotropy in Co-rich microwires 82
3.3. Concluding remarks 89
3.4. References 90

4. Engineering of magnetic properties of Fe-rich microwires with positive magnetostriction coefficient (Fe-, Fe-Ni- and Fe-Co-rich) 93

4.1. As-prepared Fe-rich microwires 94
4.1.1. FeBSiC microwires 94
4.1.2. Magnetoelastic anisotropy effect on as-prepared Fe-rich amorphous microwires 95
4.1.3. Fe-Ni microwires 97
4.1.4. "Thick" glass-coated Fe-rich microwires 99
4.2. Post-processing effect on magnetic properties, GMI effect and DW dynamics for Fe-rich microwires 102
4.2.1. Effect of annealing on magnetic properties and GMI effect in nanocrystalline and devitrified microwires 102
4.2.2. Tuning of magnetic properties of amorphous microwires by furnace annealing 108
4.2.2.1. Effect of furnace annealing on magnetic properties of FeBSiC microwires 109
4.2.2.2. Effect of furnace annealing on magnetic properties of Fe-Ni based microwires 112
4.2.3. Stress annealing in FeBSiC microwires 117
4.2.3.1. Tuning of domain wall dynamics by stress-annealing 117
4.2.3.2. Effect of stress-annealing on GMI effect of Fe-rich microwires 124
4.2.3.3. Effect of stress-annealing on applied stress dependence of hysteresis loops of Fe-rich microwires 128
4.2.4. Reversibility of the stress-annealing anisotropy 133
4.2.5. GMI effect and DW propagation in "thick" glass-coated Fe-rich microwires 141
4.2.6. Graded magnetic anisotropy in Fe-rich microwires and its effect on DW dynamics 146
4.3. Concluding remarks 162
4.4. References 164

5. Application: Magnetic microwire inclusions in smart composites allowing non-contact stress and temperature monitoring 168

5.1. Effect of the matrix polymerization in the hysteresis loops of the microwire inclusions of the composite material 170
5.2. Effect of the matrix polymerization in the electromagnetic parameters of the FRC with embedded microwires 173
5.3. Effect of the composite matrix polymerization process in the internal stresses of the microwires 177
5.4. Concluding remarks 184

5.5. References 186

6. Conclusions and future outlook **188**

7. Conclusiones (Spanish) **193**

List of Publications **198**

Part I: Fundamentals

1. Introduction

Magnetic materials are highly demanded for a wide range of technological applications including: magnetic sensors, microelectronics, security electronic surveillance, automobile, aerospace and aircraft industries, energy harvesting and conversion, magnetic refrigeration, home entertainment, electrical engineering, magnetic recording, magnetic memories, wireless communications, non-destructive testing in civil construction, medicine and biomedical engineering, among others [1-5]. This fuels the development of new materials, and at the same time, trying to balance cost and performance, forces to optimise existing ones towards specific applications. The latter route, also splits onto two main lines of research, again balancing cost and performance, optimization based on combining different materials (usually involving a rare earth which increases the cost), and optimization based on post-processing treatments that can be applied to the existing material (e.g., annealing). The latter are usually referred to as functional materials [5].

One particular area of research involving functional materials is that of microwires. Magnetically soft microwires hold great promise for many of the above mentioned technological applications due to their exceptional, and tunable, magnetic and magneto-transport properties, the possibility of remote sensing through giant magnetoimpedance (GMI) effect, the fact that magnetization can be linked to the applied mechanical stress, and primarily, that due to their extremely cheap and rather simple production, they can be easily adopted by industry.

In this context, further tuning and optimization of the mentioned properties of magnetic microwires is essentially necessary for the actual and

emerging applications and it is therefore the essential purpose of the present work.

The next few paragraphs attempt to set the background knowledge needed to understand the experimental results presented in this thesis.

1.1. Metallic glasses

The main term to describe amorphous magnetically soft microwires is metallic glasses. Metallic glasses, also called amorphous metals, are a family of metallic materials obtained by the rapid cooling of liquid alloys and characterized by their metastable glassy states. A great amount of alloy compositions have been quenched into this particular state by different processes since extensive research led to its discovery in the late '50s. [6]. Their main distinctive characteristic is their similarity with liquids, with atomic short-range ordering and a non-totally random like distribution of the atoms, reflected in the smooth peaks present in their X-ray diffraction patterns [7].

The particular amorphous structure of metallic glasses, with absence of long-range atomic order, gives to them an exceptional combination of mechanical, physical and chemical properties [8]. Hence, compared to conventional metals and alloys, metallic glasses are preferable for specific scientific and technological applications and consequently they attract great and continuous interest [9].

In the early years of metallic glasses, the main interest was concentrated on Fe-based systems characterized by soft magnetic properties [7]. However, nowadays this area of research involves many other materials and alloys, and distinguishes between completely random assemblies, those with nano-sized order, i.e., nanocrystalline, and those with large range order (a perfect crystal can be considered a metallic glass where the minimum domain size is infinite).

In magnetic metallic glasses, the rapid solidification preparation method involves the induction of large internal stresses that are the origin of the magnetoleastic anisotropy responsible of the magnetic behaviour of these materials. The main interest in amorphous soft magnetic materials lies in the low coercivities, and high permeabilities due to the absence of magnetocrystalline anisotropy [10].

In the case of magnetic microwires made with metallic glasses, magnetoelastic interactions link magnetic properties, the stress, and the increased tensile strength, this fact allows tailoring the magnetic properties through mechanical and/or thermal treatments (reversible or irreversible) such as stress annealing at temperatures lower than the crystallization temperature. [11].

In addition to the aforementioned properties, in general, metallic glasses have low conductivity, originated from the absence of long-range atomic order, they posses great flexibility and some of them corrosion resistance [12,13].

1.2. Soft magnetic materials

As above described, soft ferromagnetic materials are those magnetic materials with high permeability, low coercivity and low hysteresis loss [14].

Relative permeability, μ_r, which measures the response of a material to an applied magnetic field, ranges from $\mu \approx 10^6$ in soft magnetic materials to $\mu_r \approx 1$ in some permanent magnets [15]. It is known that in broad terms, initial permeability and coercivity have a reciprocal relationship, therefore the low coercivity values (lower than 1000 A/m) of soft magnetic materials that can be of about 0.4 A/m in nickel alloys such as permalloy [14].

On the other hand, the highest magnetization saturation, M_s, values ($\mu M_s \approx 2.45$ T) are obtained in Fe-Co alloy containing 35% cobalt, and then range continuously to effectively zero.

Historically, research into the magnetism field has been dominated by hard magnetic materials, being the main applications magnetic recording media, however, in recent years the trend has changed. This is mainly due to two factors: soft magnetic materials are usually made out of cheaper abundant materials (e.g., Fe); and the appearance of phenomena producing large signals when magnetization changes (e.g., the giant magneto impedance (GMI) effect, that can produce changes up to 600%) [14,16]. These two reasons, i.e., cheap abundant materials, and large signals, are why the microwires studied in the present thesis are composed of soft magnetic materials.

Note that for the fabrication of magnetic microwires with soft magnetic characteristics Fe, Ni and Co are the alloy main elements, additions of elements such as Si, B, C and Al allow to ensure the amorphicity of the produced microwires [17].

1.3. Amorphous glass coated microwires

1.3.1. Fabrication method

Magnetically soft, amorphous and nanocrystalline microwires, as previously mentioned, have great potential in terms of applications and industry adoption due to their low cost and relatively simple manufacturing method (as shown in *Figure 1a*). However, the materials they are typically made of (e.g., Fe), tend to oxidize in air rapidly, and thus, to make these systems viable for practical applications, the microwires need to be encapsulated. To do so, the addition of a vitreous layer attract great scientific-technological interest (*Figure 1b-c*), because, to the excellent magnetic and

mechanical properties aforementioned wire properties, the glass coating adds anticorrosive properties and biocompatibility [18].

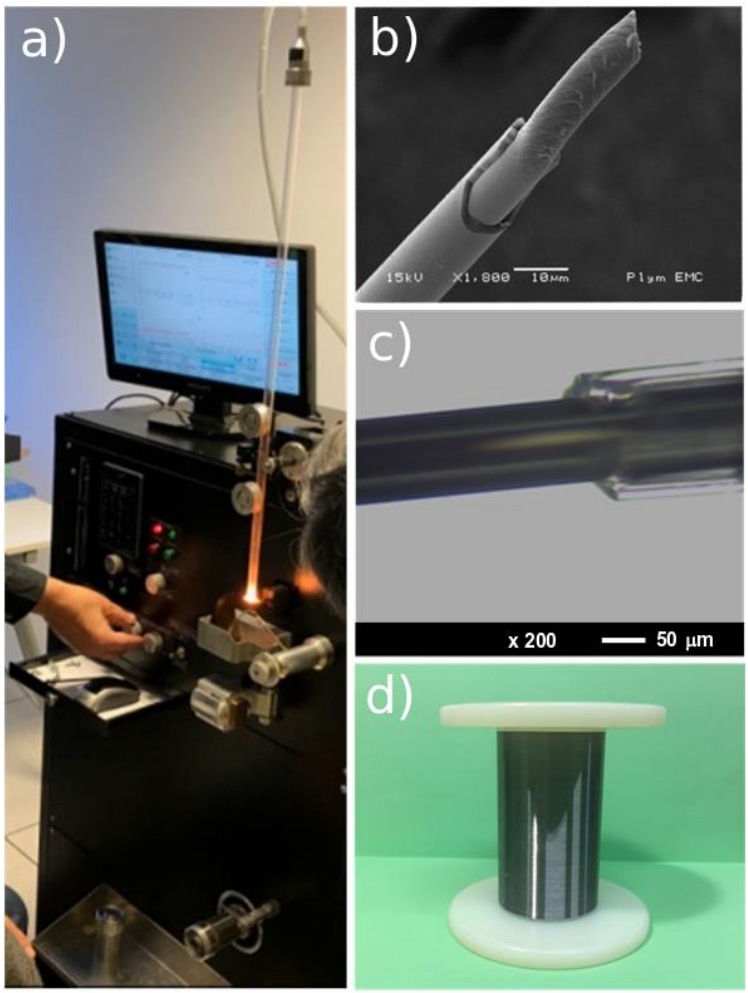

Figure 1.1. *Glass-coated microwires casting at TAMAG Iberica, S.L., Spain (a). SEM (b) and optical (c) images of glass-coated microwire samples (the glass coating has been cut and the metallic core is exposed) and sample of a microwire bobbin produced (d).*

Among the rapid melt quenching methods to produce glass-coated microwires, the process used in this thesis consists on the modified Taylor-Ulitovsky technique, based on rapid cooling of the molten alloy. The main reasons are: because of the dimensionality reduction that it allows, with the production of the thinnest amorphous glass-coated metal microwires (typically with 1 - 30 μm in diameter) [19,20]; It is well known, being known since the '60s [18], and including magnetic materials since the '70s [21]; because it allows a controlled manufacture of continuous and homogeneous metallic microwires

(*Figure 1d*) (up to a few kilometres) [22]; and it is suitable for fabrication of magnetic microwires with either amorphous or nanocrystalline structure [22-23].

As compared with crystalline microwires, amorphous microwires present high tensile strength values that are observed to decrease with the increase in the metallic core diameters. This tendency is explained by higher cooling rates with decreasing metallic core diameters [24,25]. Now, while the tensile strength in amorphous state seems to be due to the metallic core of the microwire, the addition of the glass coating does not seem to contribute significantly in the fracture toughness. The glass around the fracture point breaks, not because of the stress, but because of the sound wave produced by the rupture or the metallic core [26].

1.3.2. Effect of composition on magnetic properties

The energy balance between long and short-range interactions determines the magnetic properties of a material. In the case of amorphous materials, the absence of magnetocrystalline anisotropy, gives a main role to the magnetoelastic anisotropy, K_{me}, given as [27,28]:

$$K_{me} = 3/2\lambda_S\sigma \tag{1.1}$$

where λ_s is the magnetostriction coefficient, $\sigma = \sigma_i + \sigma_{app}$ the total stresses and σ_i and σ_{app} the internal and applied stresses, respectively. Therefore, in amorphous microwires, stress and magnetization are linked and stress can either be sensed, or used as a mean to tune the magnetic properties.

The λ_s sign and value of amorphous materials primary depends on the chemical composition. Accordingly, the easiest way to tune the λ_s sign and value in amorphous alloys is to modify their chemical composition [27,28]. Thus, Fe-rich compositions possess high and positive λ_s -values (up to $\lambda_s \approx 40 \times 10^{-6}$), while for the Co-rich alloys the magnetostriction is low (up to $\lambda_s \approx -5 \times 10^{-}$

^{6}) [28]. Even lower λ_s values can be obtained by doping of Co-rich alloy with Fe or Mn: λ_s can take vanishing values in $Co_{1-x}Fe_x$ or $Co_{1-x}Mn_x$ amorphous alloys at $0.05 \leq x \leq 0.1$ [27,28]. Alternatively, low λ_s -values can be achieved in $Ni_{1-x}Fe_x$ alloys, while such alloys present a low saturation magnetization, M_s, and hence are less interesting for applications [28].

Internal stresses in glass-coated microwires (of the order of 100-1000 MPa) arise from the difference in the thermal expansion coefficients of metallic nucleus and glass coating [29]. They strongly depend on the ratio between the glass coating thickness and metallic core diameter, increasing with the glass coating thickness. Such large internal stresses give rise to a drastic change of the magnetoelastic energy, K_{me}, even for small changes of the glass-coating thickness at fixed metallic core diameter [11].

Magnetic behaviour of each group of microwires depends on the internal stresses value and distribution. Therefore, magnetic properties of the glass–coated microwires can be tailored through the change of magnetic anisotropy by tailoring the internal stresses with adequate post-processing (furnace annealing, chemical etching, etc.) or changing the compositions of the metallic nucleus.

1.3.3. Hysteresis loops and domain structure

Depending on the magnetostriction sign and value amorphous glass-coated microwries can be divided in three groups. *Figure 1.2* reflects the hysteresis behaviour and domain structure of the amorphous-glass coated microwires related to each group.

Co-based microwires with negative magnetostriction coefficient usually possess circular magnetic easy axis [30] and therefore are characterized by a domain structure consisting of circular domains [31]. Magnetization process in axial direction runs through reversible rotation of magnetic moments inside

domains. Almost linear loop with quite low hysteresis is observed for these microwires when an axial magnetic field is applied (*Figure 1.2a*).

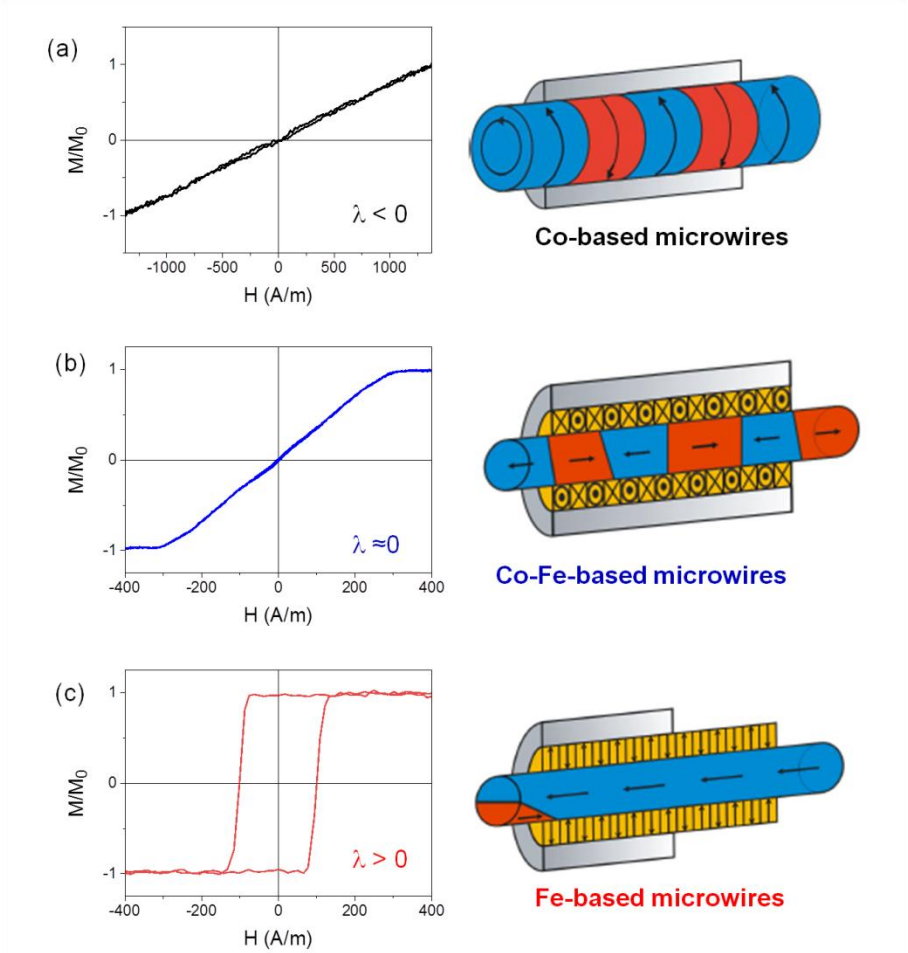

Figure 1.2. *Typical hysteresis loops and domain structures of glass-coated microwires with negative (a), nearly zero (b) and positive (c) magnetostriction coefficient. Adapted from [32].*

Nearly zero or low magnetostriction coefficients are found for Co-Fe-based glass-coated microwires. The domain structure of such microwires consists of axial domain structure surrounded by circular domains [26]. Hysteresis loops of such microwires present very low coercivity and high permeability (*Figure 1.2b*).

Finally, Fe-based based glass-coated microwires with positive magnetostriction usually present rectangular hysteresis loop related to their domain structure consisting of a large axially magnetized single domain

surrounded by outer domains with radial magnetization orientation. In addition to small closure domains at the microwire ends in order to decrease the stray fields [32] (*Figure 1.2c*). Magnetic bistability presented for such microwires will be further discussed later.

1.3.4. Induced anisotropies

The metastable amorphous structure of glass-coated microwires makes them quite sensitive to their environment and past history. One of the important sources of anisotropies is the stress induced during their fabrication. Anisotropy control is extremely important for specific technological applications.

Annealing, at temperatures below crystallization, allows to relax the induced anisotropies as well as to create new ones. However, the rate of change of structural relaxation is a complex function depending on the annealing temperature and time. Thus in order to understand how anisotropies are affected by annealing processes, the relaxation phenomena itself has to be understood [33].

The relaxation mechanism that comprises changes in volume, diffusivity or viscosity of the metallic glass is of irreversible and monotonic character (except very close to and above glass transition temperature, T_g) [34]. On the other hand, a reversible relaxation phenomena occurs when achieving a saturated pseudo-equilibrium state after prolonged annealing. Usually, the system can move from one equilibrium state to another changing the annealing temperature [35].

Several mechanisms are proposed for induced anisotropies including: ordering of atomic pairs that results in directional ordering; easy-axis alignment; structural relaxation; shape anisotropy influence due to mechanical

grain alignment or structural anisotropy associated to small anisotropic structural rearrangements in short atomic range [36,37].

Annealing at modest temperatures and annealing times causes a decrease in the magnetoelastic anisotropy. Accordingly, elevated annealing temperature induces macroscopic magnetic anisotropy with the preferential axis determined by the direction of magnetization during the annealing [37].

Here, as an example the complex mechanism of induced anisotropies is described for the case of Fe-rich microwires subjected to stress-annealing (see *Figure 1.3*) [38-40]. In this case, stress-annealing induced anisotropy is associated to so called "back-stresses". Annealing induces transversal anisotropy and the stress applied during the annealing induces longitudinal anisotropy, resulting in drastic decrease in the longitudinal stress component and appearance of compressive longitudinal stress. Magnetoelastic energy is minimized, with the redistribution of the internal stresses and/or local microstructure.

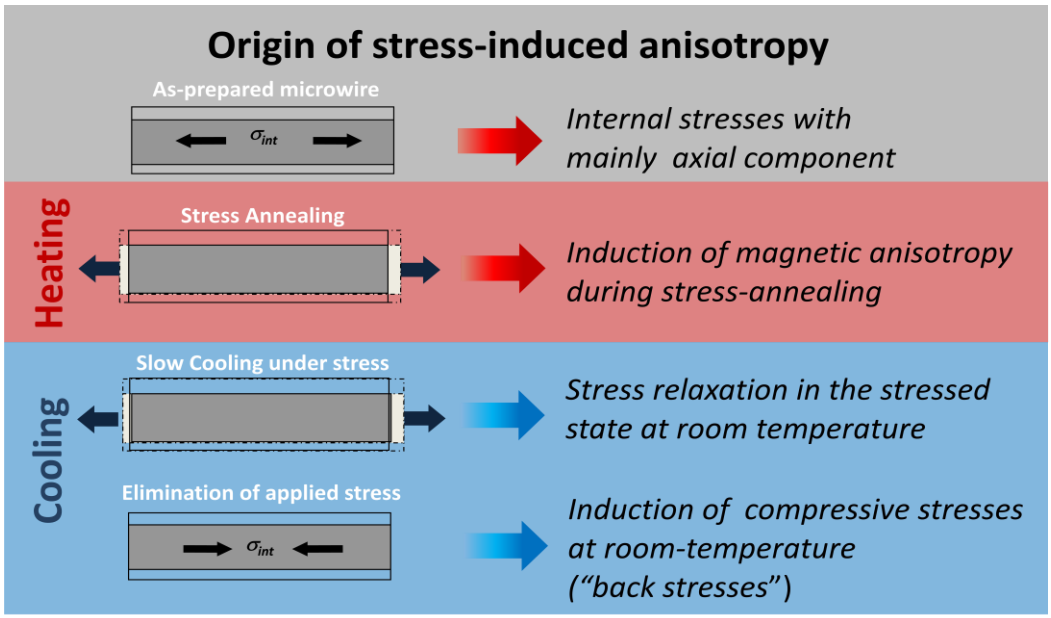

Figure 1.3. *Schematic illustration of effect of stress annealing in Fe-based glass-coated microwires (Adapted from [39]).*

1.3.5. Nanocrystalline glass-coated microwires

Nanocrystalline soft magnetic materials are two-phase materials consisting of nanocrystallites randomly distributed in a soft magnetic amorphous phase. This group of magnetic materials is considered of great interest due to their exceptional soft magnetic properties [10].

The nanocrystalline state is achieved by crystallization of conventional Fe-Si-B amorphous alloys, produced since the '70s [41] with small addition of Cu and Nb [42]. Fe-Si-B-Cu-Nb alloys obtained are usually known by trademark name *Finemet*. Ultrafine grain structure with small crystallites (around 10 nm grain size) embedded in a residual amorphous matrix is obtained after carefully annealing the amorphous precursor, at temperatures between partial and full crystallization processes in order to avoid the deterioration of soft magnetic properties.

The adjustment of the chemical compositions and the annealing parameters for the devitrification process allow obtaining materials with rather different microstructures. Although, most results have been reported on ribbons and wires, recently great attention has been paid also on nanocrystalline microwires [43,44].

The origin of excellent soft magnetic properties in nanocrystalline microwires as well as the routes for their optimization will be further address in the section particularly devoted to them.

1.4. Giant magnetoimpedance (GMI) effect

First discovered in the '30s [45], it was not until the late '90s [46-48], when high frequency equipment was available, that GMI research took off. The GMI effect is a skin effect where the electrical impedance of a material is linked to its magnetization, thus becoming an ideal way of probing magnetization

remotely [49]. Initially studied in wires, GMI has been also reported in glass-coated microwires [50], ribbons [51], micro-patterned ribbons [52] and multilayers [53].

The key advantage of magnetic sensors based on GMI is their ultra-high sensitivity (up to 10% / A/m) [5,54]. When combining the large effect of GMI, with the capability to perform remote measurements, and the relatively inexpensiveness of soft magnetic materials, with their low coercivities, the mixture produces an ideal combination to produce sensors at a low-cost and with high signal-to-noise ratio.

Consequently, for the magnetic microwires studied here, the research pays attention on this effect to track magnetization, and through magnetization changes sense other magnitudes (e.g., stress).

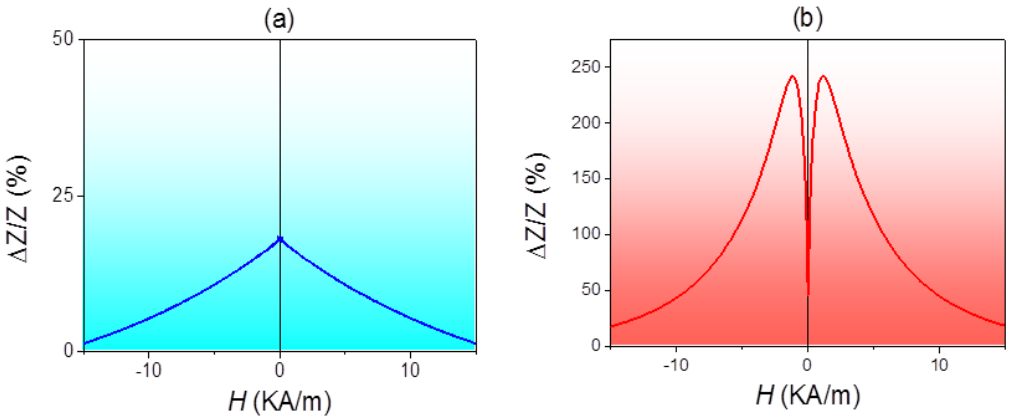

Figure 1.4. *Typical GMI behaviour of Fe-rich microwires (a) and nearly zero magnetostriction Co-rich microwires (b).*

Figure 1.4 schematically shows the GMI behaviour exhibited by Fe-rich microwires with axial magnetic anisotropy and nearly zero magnetostriction Co-rich glass-coated microwires. GMI response of Fe-rich glass-coated microwires presents a single maximum for $H = 0$ (*Figure 1.4a*). On the other hand, double-peak behaviour is observed for nearly zero magnetostriction samples (*Figure 1.4b*). The later samples are the most interesting due to the larger GMI effect

and better softness. However, Co belongs to critical raw materials; therefore, great efforts are paid to optimize the GMI response in less–expensive Fe-rich glass-coated microwires as promising solution [55].

1.5. Magnetic bistability and Fast domain wall (DW) propagation

A magnetic material is considered bi-stable when its magnetization has two preferred orientations, and the transition between these two states occurs through a single domain wall (DW) that travels the material without suffering any pinning. This is a desired behavior in certain situations, because it simplifies analyzing the behavior of the material.

Such DW propagation can be driven either by a magnetic field [56] or by an electric current [50]. Roughly linear dependencies of DW velocity, *v*, on magnetic field, *H*, reported for a magnetic field driven DW dynamics are well understood in terms of the viscous DW motion [56].

DW propagation in a viscous regime with a velocity, *v*, can be given as [56]:

$$v = S(H - H_0) \tag{1.2}$$

where *S* is the DW mobility, *H* is the axial magnetic field and H_0 is the critical propagation field.

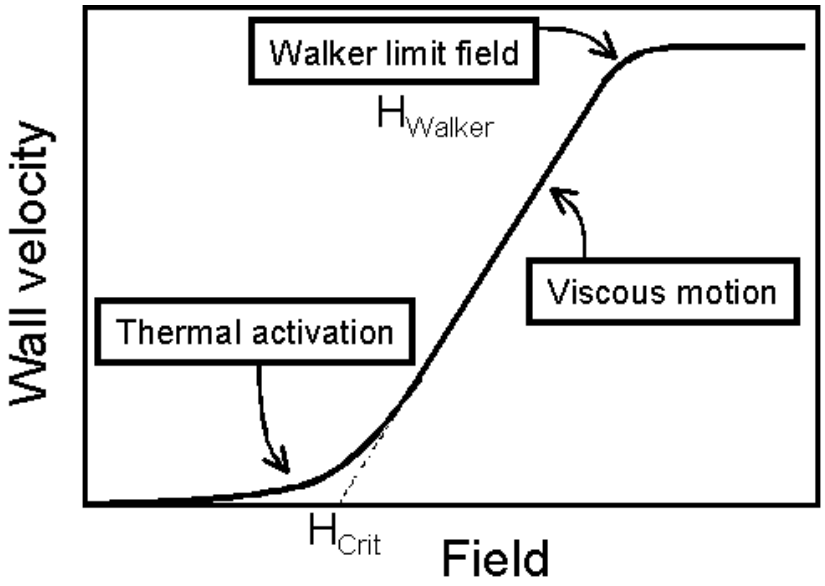

Figure 1.5. *Typical v(H) dependence for magnetic field driven DW dynamics [57].*

Non-linear *v(H)* dependencies can be observed either in low field or at high field regions (see *Figure 1.5*).

After S. Parkin racetrack memory proposal in 2008 [58], using the concept of DWs to store information, DW motion control has attracted increasing attention for a vast number of promising applications (racetrack memories, magnetic sensors, magnetic tags, etc.). Such applications require fast magnetization switching and controllable DW propagation. Despite their great stability, thermal activation and pinning lead to stochastic behavior of the DW motion that needs to be addressed [59].

Amorphous glass coated microwires with positive magnetostriction constant generally exhibit spontaneous magnetic bistability originated by a single and large Barkhausen jump between two remanent states with opposite magnetization. As above described, perfectly rectangular hysteresis loops observed for these microwires are related to axial magnetization orientation within the most part of the metallic core of the microwire [60,61]. The magnetization switching (between the two remanent states) runs by fast DW propagation, starting from the closure domains at the microwire ends [62]. Thus, magnetically bistable microwires are a unique material for DW

propagation studies providing the possibility to study the influence of various factors such as applied or internal stresses, magnetoelastic and induced magnetic anisotropies, transverse or local magnetic field.

1.6. Technological applications of magnetic glass-coated microwires

The main interest in magnetic microwires lies in the outstanding magnetic softness exhibited by the amorphous microwires that possess nearly zero magnetostriction coefficient, λ_s [63]. For this reason, as a rule, the highest GMI response, linked with magnetic softness, is reported for as-prepared cobalt rich microwires that present circumferential magnetic permeability [64]. This fact, promoted since the end of the '90s the development of several magnetic sensors and devices for applications determined by the combination of their characteristics and cost [65-67]. In this sense, were developed electronic compasses for mobile phones, mass-produced by the Japanese company Aichi Steel Co. since 2005, Smart phones since 2011, and the use of amorphous wires for 3-axis MI sensor chips of wristwatches [65].

The use of magnetic microwires for GMI technology is presented as quite competitive and promising among the other actual various sensor technologies (e.g., Hall effect, magnetoresistance and fluxgates) due to its characteristics such as low noise and high magnetic field resolution [5,66]. Now, while size used to be a deficit for microwire technology, recent works, have reported the reduction of the volume needed to achieve a significant GMI by using glass-coated microwires excited by a pulsed GHz current [68,69], thus putting microwires at the vanguard in terms of sensing technologies.

Additionally, the fact that GMI technology operates at GHz frequencies and allows a fast response, greatly satisfies the needs of fields as different as automotive and transport industries, informatics, automation or biomedicine [70-74].

However, microwires not only offer advantages compared to other sensing technologies, they also add new functionalities. For instance, it has been reported that in thin ferromagnetic wires embedded onto a dielectric matrix (and whose properties have been tuned through stress and/or temperature treatments) the effective microwave permittivity depends on an external dc magnetic field, applied stress or temperature [70,71], thus opening the possibility of sensing inside of larger structures (e.g., concrete) [70,72]. The short wire inclusions inside of the dielectric matrix play a role of "the elementary scatterers", when the electromagnetic wave irradiates the composite and induces a longitudinal current distribution and electrical dipole moment in each inclusion. The important advantage of sensing inside of large structures is that the soldering problems are avoided because of the wireless detection of the signals.

On the other hand, magnetically bistable microwires are adequate for applications such as magnetic memory, magnetic logic, magnetoelastic sensors and electronic article surveillance, in which is crucial fast magnetization switching, controllable DW propagation and a harmonic response [4,60,75-78]. The extremely fast DW dynamics reported for these microwires (DW velocities up to 3-4 km/s and mobility up to almost 50 $m^2/A{\cdot}s$) is essential for mentioned applications and it can be tuned by magnetoelastic anisotropy, induced magnetic anisotropy or application of transverse magnetic field [75].

Manipulation and control of the DW propagation is satisfactorily achieved in bistable magnetic microwires through various techniques, including DW injection by local magnetic field or creation of artificial defects allowing either DW pinning or nucleation [4,60,75-80].

It is worth mentioning, that despite having excellent properties, and being quite competitive in the sensing market, magnetic microwires still need a significant effort in terms of development. For instance, despite the great efforts to find post-processing routes for the magnetic properties optimization that allowed a significant improvement of the magnetic softness and therefore

the GMI effect improvement, GMI ratios achieved are still below those predicted by the theory. But there are promising reports indicating that further enhancement is possible (e.g, better magnetic softness and wider switching field range) [81]. Recently, has been obtained, either by Joule heating or stress annealing of magnetic microwires with moderate transverse anisotropy, a singular combination of magentic properties in the same microwire: high GMI effect and fast magnetization switching related to a single and large Barhausen jump [82]. This unique excellent magnetic properties combination is added to the outstanding mechanical properties, high corrosion resistance, biocompatibility, reduced dimensionality and the fact that amorphous microwires allow to achieve 1-2 higher orders of magnitude of magnetic field sensitivity, as compared with thin films, up to 10% / A/m [83].

In addition, the thin flexible glass coating, apart from biocompatibility, provide the microwires with enhanced corrosion resistance and adhesion to polymer matrices and makes them appropiate candidates not only for biomedical applications [84,85] but also for smart composites with embedded microwire inclusions and non-destructive stress and temperature monitoring. [86,87].

Consequently, due to the mentioned high performance, durability, robust and cost-effective of magnetic microwires, the continuos development of emerging appplications for them is expected. Thus, it can be concluded that research in the field of magnetic microwires is challenging, competitive, and has a great potential for impact. However, there are challenges that need addressed, e.g., optimization by post-processing to achieve the predicted theoretical GMI, and also new applications that need to be further characterizeD to pave their adoption by the industry. Through this thesis several optimization routes will be explored for potential applications.

1.7. Research structure

The main objective of this thesis is to obtain amorphous and nanocrystalline magnetic microwires with optimal properties for their application in advanced magnetic sensors based on the effect of giant magnetoimpedance (GMI) and bistable magnetic behavior. In order to achieve this goal the work has been divided as follows:

Chapter 1 pretends to serve as a brief overview of the state of the art of amorphous glass coated microwires and their main magnetic and structural properties.

Chapter 2 describes the experimental techniques employed in the production and characterization of the samples studied.

The second part of the work is devoted to the results and discussion. **Chapter 3** and **Chapter 4** are related to the engineering of the magnetic properties of Cobalt and Iron rich microwires, respectively, with a convenient selection of microwires with different chemical compositions and diameters to cover the entire spectrum and that allow setting the route for the parameters optimization procedure. The effect of the post-processing method selected on the magnetic properties, GMI effect and domain wall dynamics of each of the microwires selected is analyzed.

Chapter 5 is focused on the technical applications, with the detailed description of one of the possible uses of the produced amorphous glass coated microwires that was carried out in the field of smart composites using magnetic microwire inclusions for non-contact stress and temperature monitoring.

Finally, the most important results are summarized in the conclusions presented in **Chapter 6**.

1.8. References

[1] J. Lenz, S. Edelstein, Magnetic sensors and their applications, IEEE Sens. J. 6 (2006) 631–649, doi:10.1109/JSEN.2006.874493.

[2] M. Vazquez, H. Chiriac, A. Zhukov, L. Panina, T. Uchiyama, On the state-of-the-art in magnetic microwires and expected trends for scientific and technological studies, Phys. Status Solidi A 208(3) (2011) 493–501

[3] F. Fiorillo, G. Bertotti, C. Appino, M. Pasquale, Soft Magnetic Materials. In Wiley Encyclopedia of Electrical and Electronics Engineering, J. Webster Ed., p. 42, John Wiley & Sons, Inc., Torino, Italy (1999).

[4] G. Herzer, Magnetic materials for electronic article surveillance, J. Magn. Magn. Mater. 254–255 (2003) 598–602.

[5] A. Zhukov, M. Ipatov, P. Corte-Leon, J.M. Blanco, V. Zhukova, Advanced functional magnetic microwires for magnetic sensors suitable for biomedical applications. In Magnetic Materials and Technologies for Medical Applications, Tishin, A.M., Ed., Ch. 18, Elsevier: Amsterdam, The Netherlands (2022).

[6] W. Klement, R.H. Willens, P. Duwez, Non-crystalline Structure in Solidified Gold-Silicon Alloys, Nature 187 (1960) 869–870.

[7] R. Hasegawa, Properties and Applications of Nanocrystalline Alloys from Amorphous Precursors, NATO Science Series (Series II: Mathematics, Physics and Chemistry), B. Idzikowski, P. Švec, M. Miglierini, Eds., vol. 184, pp. 189–198, Springer, Dordrecht, The Netherlands (2005).

[8] J. Durand, Magnetic Properties of Metallic Glasses. In: H. Beck, H.-J. Giintherodt, Eds., Topics in Applied Physics. Glassy Metals II, vol. 53, Springer, New York (1983).

[9] A.L. Greer, Metallic glasses…on the threshold, Mater. Today. 12 (2009) 14–22, doi:10.1016/S1369-7021(09)70037-9.

[10] G. Herzer, Grain size dependence of coercivity and permeability in nanocrystalline ferromagnets, IEEE Trans. Magn. 26 (1990) 1397–1402.

[11] A. Inoue, Bulk amorphous and nanocrystalline alloys with high functional properties, Mater. Sci. Eng. A, 304–306 (2001) pp. 1-10, ISSN: 0921-5093, doi:10.1016/S0921-5093(00)01551-3.

[12] R. Zallen, The Physics of Amorphous Solids, pp. 274–289, Wiley, New York (1983).

[13] D. Jiles, Introduction to magnetism and magnetic materials, Taylor & Francis Group CRC, USA (1998).

[14] D.C. Jiles, Recent advances and future directions in magnetic materials, Acta Mater. 51 (2003) 5907-5939.

[15] Soft magnetic materials - technologies, materials, devices, new developments, industry structure and global markets. Report summary, LONDON (Aug. 26th. 2015).

[16] M. Vázquez, Giant magneto-impedance in soft magnetic “Wires”, J. Magn. Magn. Mat. 226–230, Part 1 (2001) pp. 693-699, ISSN: 0304-8853, doi:10.1016/S0304-8853(01)00013-0.

[17] V.S. Larin, A.V. Torcunov, A. Zhukov, J. González, M. Vazquez, L. Panina, Preparation and properties of glass-coated microwires, J. Magn. Magn. Mater. 249 (1–2) (2002) 39-45, ISSN: 0304-8853. doi:10.1016/S0304-8853(02)00501-2.

[18] V. Zhukova, Soft magnetic Wires for Sensor Applications in Novel Functional Magnetic Materials, Fundamentals and Applications, A. Zhukov Ed., Springer Series in Materials Science, vol. 231, ch. 6, Springer International Publishing, (2016), ISSN: 0933-033X, doi:10.1007/978-3-319-26106-5.

[19] A.V. Ulitovsky, I.M. Maianski, A.I. Avramenco, Method of continuous casting of glass coated microwire, USSR Patent, No. 128427, 15.05.60. Bulletin No. 10, p. 14.

[20] S.A. Baranov, V.S. Larin, A.V. Torcunov, Technology, Preparation and Properties of the Cast Glass-Coated Magnetic Microwires, Crystals 7 (2017) 136, doi:10.3390/cryst7060136.

[21] L. Kraus, J. Schneider, H. Wiesner, Ferromagnetic resonance in amorphous alloys prepared by rapid quenching from the melt, Czech. J. Phys. B 26 (1976) 601-602.

[22] A. Zhukov, M. Ipatov, A. Talaat, J.M. Blanco, B. Hernando, L. Gonzalez-Legarreta, J.J. Suñol, V. Zhukova, Correlation of Crystalline Structure with Magnetic and Transport Properties of Glass-Coated Microwires, Crystals 7 (2017) 41, doi: 10.3390/cryst7020041.

[23] A. Zhukov, V. Zhukova, J.M. Blanco, J. Gonzalez, Recent research on magnetic properties of glass-coated microwires, J. Magn. Magn. Mater. 294 (2005) 182–192, doi:10.1016/j.jmmm.2005.03.033.

[24] T. Goto, M. Nagano, N. Wehara, Mechanical Properties of Amorphous $Fe_{80}P_{16}C_3B_1$ Filament Produced by Glass-Coated Melt Spinning, Trans JIM 18 (1977) 759-764.

[25] T. Goto, Fe-B and Fe-Si-B System Alloy Filaments Produced by Glass-Coated Melt Spinning, Trans JIM 21 (1980) 219-225.

[26] A.F. Cobeño, A. Zhukov, A.R. de Arellano-López, F. Elías, J.M. Blanco, V. Larin, J. González, Physical properties of nearly zero magnetostriction Co-rich glass-coated amorphous microwires, J. Mat. Res. 14(9) (1999) 3775-3783.

[27] A. Zhukov, M. Ipatov, M. Churyukanova, A. Talaat, J.M. Blanco, V. Zhukova, Trends in optimization of giant magnetoimpedance effect in amorphous and nanocrystalline materials, J. Alloys Compd. 727 (2017) 887–901.

[28] G. Herzer, Amorphous and Nanocrystalline Soft Magnets, in Proc. NATO Adv. Study Inst. Magn. G.C. Hadjipanayis (Ed.), Hysteresis Nov. Mater., pp. 711–730, Springer Netherlands, Dordrecht (1997), doi:10.1007/978-94-011-5478-9_77.

[29] A.S. Antonov, V.T. Borisov, O.V. Borisov, A.F. Prokoshin, N.A. Usov, Residual quenching stresses in glass-coated amorphous ferromagnetic microwires, J. Phys. D: Appl. Phys. 33 (2000) 1161-1168.

[30] A.V. Torcunov, S.A. Baranov, V.S. Larin, The magnetic properties of glass-covered microwire with negative magnetostriction constant, J. Magn. Magn. Mater. 215–216 (2000) 303-306, ISSN: 0304-8853, doi:10.1016/S0304-8853(00)00140-2.

[31] Yu. Kabanov, A. Zhukov, V. Zhukova, J. Gonzalez, Magnetic domain structure of microwires studied by using the magneto-optical indicator film method, Appl. Phys. Lett. 87(14) (2005) 142507.

[32] R. Varga, Magnetization processes in glass-coated microwires with positive magnetostriction, Acta Phys. Slovaca 62(5) (2012) 411-518.

[33] A.L. Greer, J.A. Leake, Structural relaxation and cross-over effect in a metallic glass, J. Non-Cryst. Solids 33 (1979) 291-297.

[34] T. Egami, Magnetic amorphous alloys: physics and technological applications, Rep. Prog. Phys. 47 (1984) 1601-1725.

[35] A. Zhukov, J. Gonzalez, J.M. Blanco, M.J. Prieto, E. Pina, M. Vazquez, Induced magnetic anisotropy in Co-Mn-Si-B amorphous microwires, J. Appl. Phys. 87 (2000) 1402-1408.

[36] H. Fujimori, Magnetic anisotropy, Chapter 16 in Amorphous Metallic Alloys, F. Luborsky Ed., Butterworths Monographs in Materials (1983) 300-316.

[37] F.E. Luborsky, J.L. Walker, Magnetic anneal anisotropy in amorphous alloys, IEEE Trans. Magn. Mag-13, 2 (1977) 953-956.

[38] A. Zhukov, Design of the magnetic properties of Fe-rich, glass-coated microwires for technical applications, Adv. Funct. Mater. 16(5) (2006) 675-680.

[39] A. Zhukov, V. Zhukova, V. Larin, J.M. Blanco, J. Gonzalez, Tailoring of magnetic anisotropy of Fe-rich microwires by stress induced anisotropy, Physica B 384 (2006) 1-4.

[40] D.X. Chen, Induced anisotropy and magnetostriction in metallic glasses, J. Appl. Phys. 61 (1987) 3781-3783.

[41] M.G. Poletti, L. Battezzati, Assessment of the ternary Fe-Si-B phase diagram, Calphad Comput. Coupling Ph. Diagr. Thermochem. 43 (2013) 40–47.

[42] Y. Yoshizawa, S. Oguma, K. Yamauchi, New Fe-based soft magnetic alloys composed of ultrafine grain structure, J. Appl. Phys. 64 (1988) 6044.

[43] V. Zhukova, A.F. Cobeño, A. Zhukov, J.M. Blanco, V. Larin, J. Gonzalez, Coercivity of glass-coated $Fe_{73.4-x}Cu_1Nb_{3.1}Si_{13.4+x}B_{9.1}$ ($0 \le x \le 1.6$) microwires, Nanostructured Materials 11(8) (1999) 1319-1327, ISSN: 0965-9773, doi:10.1016/S0965-9773(99)00424-9.

[44] C. Garcia, A. Zhukov, M. Ipatov, V. Zhukova, J.J. del Val, L. Domínguez, J.M. Blanco, V. Larin, J. González, Soft magnetic behaviour of nanocrystalline Fe-based glass-coated microwires, J. Optoelectron. Adv. Mater. 8(5) (2006) 1667-1671.

[45] E.P. Harrison, G.L. Turney, H. Rowe, Electrical properties of wires of high permeability, Nature 135 (1935) 961.

[46] K. Mohri, T. Kohsawa, K. Kawashima, H. Yoshida, L.V. Panina, Magneto-inductive effect (MI effect) in amorphous wires, IEEE Trans. Magn. 28(5) (1992) 3150-3152. doi:10.1109/20.179741.

[47] L.V. Panina, K. Mohri , Magneto-impedance effect in amorphous wires, Appl. Phys. Lett. 65 (1994) 1189-1191, doi:10.1063/1.112104.

[48] R.S. Beach, A.E. Berkowitz, Giant magnetic field dependent impedance of amorphous FeCoSiB wire, Appl. Phys. Lett. 64 (1994) 3652.

[49] L. Kraus, GMI modeling and material optimization, Sens. Actuator A Phys. 106, 1–3 (2003) pp. 187-194, ISSN 0924-4247, doi:10.1016/S0924-4247(03)00164-X.

[50] A. Zhukov, J. González, J.M. Blanco, M. Vázquez, V. Larin, Microwires coated by glass: A new family of soft and hard magnetic materials, J. Mater. Res. 15 (2000) 2107.

[51] B. Hernando, M.L. Sánchez, V.M. Prida, M. Tejedor, M. Vázquez, Magnetoimpedance effect in amorphous and nanocrystalline ribbons, J. Appl. Phys. 90 (2001) 4783.

[52] L. Chen, Y. Zhou, C. Lei, Z.-M. Zhou, W. Ding, Effect of meander structure and line width on GMI effect in micro-patterned Co-based ribbon, J. Phys. D: Appl. Phys. 42 (2009) 145005.

[53] C. García, J.M. Florez, P. Vargas, C.A. Ross, Asymmetrical giant magnetoimpedance in exchange-biased NiFe, Appl. Phys. Lett. 96 (2010) 232501.

[54] P. Ripka, Magnetic sensors and magnetometers. Artech House Publishers, 2001.

[55] A. Zhukov, M. Ipatov, V. Zhukova, Advances in giant magnetoimpedance of materials, chapter 2 in Handbook of Magnetic Materials, K.H.J. Buschow Ed., vol. 24 , pp. 139-236, (2015).

[56] A. Zhukov, J. M. Blanco, M. Ipatov, V. Zhukova, Fast magnetization switching in thin wires: Magnetoelastic and defects contributions, Sensor Letters 11(1) (2013) 170-176, doi:10.1166/sl.2013.2771.

[57] K. Fukumoto, Magnetization Reversal Dynamics in Magnetically Coupled Trilayer Systems, Ph.D. Thesis, Freien Universität Berlin, Berlin, Germany, May 2005.

[58] S.S.P. Parkin, M. Hayashi, L. Thomas, Magnetic domain-wall racetrack memory, Science 320(5873) (2008) pp. 190–194.

[59] M. Muñoz, J.L. Prieto, Suppression of the intrinsic stochastic pinning of domain walls in magnetic nanostripes, Nat. Commun. 2 (2011) p. 562.

[60] A. Zhukov, J. González, M. Vázquez, V. Larin, A. Torcunov, Nanocrystalline and Amorphous Magnetic Microwires, chapter 6, pp. 365-387 in Encyclopedia of Nanoscience and Nanotechnology, American Scientific Publishers: Valencia, USA (2004).

[61] H. Chiriac, T.A. Ovari, Amorphous glass-covered magnetic wires: Preparation, properties, applications, Prog. Mater. Sci. 40 (1996) 333-407.

[62] V. Zhukova, A. Zhukov, J.M. Blanco, J. Gonzalez, B.K. Ponomarev, Switching field fluctuations in a glass coated Fe-rich amorphous microwire, J. Magn. Magn. Mater. 249 (2002) 131–135.

[63] A. Zhukov, V. Zhukova, Magnetic sensors based on thin magnetically soft wires with tuneable magnetic properties and its applications (International Frequency Sensor Association (IFSA) Publishing, Ronda de Ramon Otero Pedrayo, 42C, 1-5, 08860, Castelldefels - Barcelona, Spain), 2014, 154 p, ISBN-10: 84-617-1866-6.

[64] K.R. Pirota, L. Kraus, H. Chiriac, M. Knobel, Magnetic properties and giant magnetoimpedance in a CoFeSiB glass-covered microwire, J. Magn. Magn. Mater. 221 (2000) L243–L247, doi:10.1016/S0304-8853(00)00554-0.

[65] K. Mohri, T. Uchiyama, L.V. Panina, M. Yamamoto, K. Bushida, Recent Advances of Amorphous Wire CMOS IC Magneto-Impedance Sensors: Innovative High-Performance Micromagnetic Sensor Chip, J. Sens. (2015) 718069, doi: 10.1155/2015/718069.

[66] K. Mohri, T. Uchiyama, L.P. Shen, C.M. Cai, L.V. Panina, Amorphous wire and CMOS IC-based sensitive micro-magnetic sensors (MI sensor and SI sensor) for intelligent measurements and controls, J. Magn. Magn. Mater. 249 (2002) 351-356.

[67] T. Kanno, K. Mohri, T. Yagi, T. Uchiyama, L.P. Shen, IEEE Trans. Magn. 22 (5) (1997) 3358.

[68] Y. Honkura, S. Honkura, The Development of ASIC Type GSR Sensor Driven by GHz Pulse Current Sensors 20 (2020) 1023, doi:10.3390/s20041023.

[69] Y. Honkura, S. Honkura, The Development of ASIC Type GSR Sensor Driven by GHz Pulse Current, Proceedings of The Ninth International Conference on Sensor Device Technologies and Applications, SENSORDEVICES 2018, IARIA, 2018, pp. 15-22, ISBN: 978-1-61208-660-6.

[70] A. Uddin, D. Estevez, F.X. Qin, From functional units to material design: A review on recent advancement of programmable microwire metacomposites, Compos. Part A Appl. Sci. 153 (2022) 106734, ISSN: 1359-835X, doi:10.1016/j.compositesa.2021.106734.

[71] D.P. Makhnovskiy, L.V. Panina, S.I. Sandacci, Tuneable microwave composites based on ferromagnetic microwires, Book chapter in Progress in Ferromagnetism Research, V.N. Murray Ed., ISBN: 1-59454-335-6, Nova Science Publishers Inc., USA (2005).

[72] Y. Honkura, Development of amorphous wire type MI sensors for automobile use J. Magn. Magn. Mater. 249 (2002) 375-381.

[73] T. Uchiyama, J. Ma, Development of pico tesla resolution amorphous wire magneto-impedance sensor for bio-magnetic field measurements, J. Magn. Magn. Mater. 514 (2020) 167148.

[74] V. Zhukova, P. Corte-Leon, J.M. Blanco, M. Ipatov, J. Gonzalez, A. Zhukov, Electronic Surveillance and Security Applications of Magnetic Microwires Chemosensors 9 (2021) 100, doi:10.3390/chemosensors9050100.

[75] V. Zhukova, P. Corte-Leon, L. González-Legarreta, A. Talaat, J.M. Blanco, M. Ipatov, J. Olivera, A. Zhukov, Review of Domain Wall Dynamics Engineering in Magnetic Microwires, Nanomaterials 10(12) (2020) 2407, doi:10.3390/nano10122407.

[76] R. Sabol, P. Klein, T. Ryba, L. Hvizdos, R. Varga, M. Rovnak, I. Sulla, D. Mudronova, J. Galik, I. Polacek, J. Zivcak, R. Hudak, Novel Applications of Bistable Magnetic Microwires, Acta Phys. Pol. A 131(4) (2017) 1150-1152.

[77] D.A. Allwood, G. Xiong, C.C. Faulkner, D. Atkinson, D. Petit, R.P. Cowburn, Magnetic domain-wall logic, Science 309 (2005) 1688-1692.

[78] A. Jiménez, R.P. del Real, M. Vázquez, Controlling depinning and propagation of single domain-walls in magnetic microwires, Eur. Phys. J. B 86 (2013) 113, doi:10.1140/epjb/e2013-30922-9.

[79] A. Zhukov, J.M. Blanco, A. Chizhik, M. Ipatov, V. Rodionova, V. Zhukova, Manipulation of domain wall dynamics in amorphous microwires through domain wall collision, J. Appl. Phys. 114 (2013) 043910, doi:10.1063/1.4816560.

[80] P. Corte-León, V. Zhukova, J.M. Blanco, A. Chizhik, M. Ipatov, J. Gonzalez, A. Fert, A. Zhukov, Engineering of domain wall propagation in magnetic microwires with graded magnetic anisotropy, Appl. Mater. Today 26 (2021) 101263, ISSN 2352-9407, doi: 10.1016/j.apmt.2021.101263.

[81] M.H. Phan, H.X. Peng, Giant magnetoimpedance materials: Fundamentals and applications, Prog. Mater. Sci. 53(2) (2008) 323-420.

[82] P. Corte-Leon, V. Zhukova, A. Chizhik, J.M. Blanco, M. Ipatov, L. Gonzalez-Legarreta, A. Zhukov, Magnetic Microwires with Unique Combination of Magnetic Properties Suitable for Various Magnetic Sensor Applications, Sensors 20(24) (2020) 7203, doi:10.3390/s20247203. PMID: 33339238; PMCID: PMC7767316.

[83] A. Zhukov, V. Zhukova, J.M. Blanco, J. Gonzalez, Recent research on magnetic properties of glass-coated microwires J. Magn. Magn. Mater. 294 (2005) 182–192, doi:10.1016/j.jmmm.2005.03.033.

[84] D. Kozejova, L. Fecova, P. Klein, R. Sabol, R. Hudak, I. Sulla, D. Mudronova, J. Galik, R. Varga, Biomedical applications of glass-coated microwires, J. Magn. Magn. Mater. 470 (2019) 2-5, doi:10.1016/J.JMMM.2017.11.004.

[85] O. Mitxelena-Iribarren, J. Campisi, I. Martínez de Apellániz, S. Lizarbe-Sancha, S. Arana, V. Zhukova, M. Mujika, A. Zhukov, Glass-coated ferromagnetic microwire-induced magnetic hyperthermia for in vitro cancer cell treatment, Mater. Sci. Eng. C 106 (2020) 110261, doi:10.1016/j.msec.2019.110261.

[86] M. Churyukanova, S. Kaloshkin, E. Shuvaeva, A. Stepashkin, M. Zhdanova, A. Aronin, O. Aksenov, P. Arakelov, V. Zhukova, A. Zhukov, Non-contact method for stress monitoring based on stress dependence of magnetic properties of Fe-based microwires, J. Alloys Compd. 748(5) (2018) 199-205.

[87] D.P. Makhnovskiy, L.V. Panina, Field dependent permittivity of composite materials containing ferromagnetic wires, J. Appl. Phys. 93 (2003) 4120–4129.

2. Experimental techniques

This chapter is dedicated to the description of the different experimental techniques employed in this research work. A brief description of the fundamental background of each technique and the particular experimental set-up conditions used is given, from sample preparation to magnetic, microstructural and compositional characterization of the glass coated microwires produced.

2.1. Glass-coated microwires fabrication: Taylor Ulitovsky method

Figure 2.1. *Glass coated microwires casting machine.*

Taylor Ulitovsky rapid solidification technique for glass-coated microwires manufacturing allows the preparation of thinnest amorphous microwires (with

metallic nucleus diameters ranging from 0.5-40 μm). This fabrication method consists of melting a pre-prepared ingot of metallic alloy inside a glass (typically Pyrex or Duran) tube using a high frequency inductor [1,2].

Figure 2.1. shows the casting machine for the glass-coated microwires production. Few grams of the metal alloy with the suitable chemical composition are placed inside a glass tube. A high frequency inductor melts the metal forming a droplet which softens the glass tube adjacent allowing a capillary to form. Then, the capillary filled with the molten alloy is drawn and wound on a rotating bobbin. As a result, a microwire with metallic core and flexible and insulating glass coating is obtained.

Table 2.1. *Compositions and geometry of studied glass-coated microwires.*

Composition	**Metallic Nucleus Diameter *d* (μm)**	**Total Diameter *D* (μm)**	**Ratio *ρ=d/D***	**Magnetostriction Coefficient $\lambda_s \times 10^{-6}$**
$Fe_{77.5}B_{15}Si_{7.5}$	15.1	35.8	0.42	38
$Fe_{75}B_9Si_{12}C_4$	15.2	17.2	0.88	38
$Fe_{70}B_{15}Si_{10}C_5$	3	18,75	0.16	35
$Fe_{70}B_{15}Si_{10}C_5$	6	23,08	0.26	35
$Fe_{70}B_{15}Si_{10}C_5$	10.8	22.5	0.48	35
$Fe_{70}B_{15}Si_{10}C_5$	15	23,8	0.63	35
$Fe_{71.7}B_{13.4}Si_{11}Nb_3Ni_{0.9}$	103	158	0.65	35
$Fe_{71,8}Cu_1Nb_{3,1}Si_{15}B_{9.1}$	7.0	24.8	0.282	30
$Fe_{71,8}Cu_1Nb_{3,1}Si_{15}B_{9.1}$	18.2	39	0.467	30
$Fe_{70.8}Cu_1Nb_{3.1}Si_{14.5}B_{10.6}$	11.8	14.4	0.8	30
$Fe_{70.8}Cu_1Nb_{3.1}Si_{14.5}B_{10.6}$	15.6	21.8	0.7	30
$Fe_{70.8}Cu_1Nb_{3.1}Si_{14.5}B_{10.6}$	10.7	16.4	0.6	30
$Fe_{62}Ni_{15.5}Si_{7.5}B_{15}$	14.35	33.25	0.43	27
$Fe_{47.4}Ni_{26.6}Si_{11}B_{13}C_2$	29	32.2	0.9	25
$Fe_{49.6}Ni_{27.9}Si_{7.5}B_{15}$	14.2	33.85	0.42	20
$(Fe_{0.7}Co_{0.3})_{83.7}Si_4B_8P_{3.6}Cu_{0.7}$	26.5	22.3	0.84	
$Fe_{83.7}Si_4B_8P_{3.6}Cu_{0.7}$	15.5	17.5	0.89	
$Co_{65.4}Fe_{3.8}Ni_1B_{13.8}Si_{13}C_{1.65}Mo_{1.35}$	18.8	22.2	0.85	−1
$Co_{69.2}Fe_{3.6}Ni_1B_{12.5}Si_{11}C_{1.2}Mo_{1.5}$	22.8	23.2	0.98	−1
$Co_{69.2}Fe_{4.1}B_{11.8}Si_{13.8}C_{1.1}$	25.6	30.2	0.85	−0.3
$Co_{67}Fe_{3.9}Ni_{1.5}B_{11.5}Si_{14.5}Mo_{1.6}$	25.6	26.6	0.96	−0.29
$Co_{64.04}Fe_{5.71}B_{15.88}Si_{10.94}Cr_{3.4}Ni_{0.03}$	95	130	0.73	
$Co_{66}Cr_{3.5}Fe_{3.5}B_{16}Si_{11}$	20.1	24.8	0.81	

Fe-, Ni-, Fe-Co- and Co- based microwires with minor metalloid additions (Si, B, P, C) or non-magnetic metals have been prepared and studied. The compositions, geometry and magnetostriction coefficient, λ_s, of studied microwires are shown in *Table 2.1*.

2.2. Post-processing techniques: Annealing procedures

2.2.1. Conventional furnace annealing

The most extended annealing technique is the heating of the sample at a given temperature, T_{ann}, in air or vacuum for a given time, t_{ann}, in a conventional furnace. A single piece or a bunch of microwires can be treated at the same time.

The samples were heat treated at a temperature, T_{ann}, typically ranging from 200 °C to 500 °C in a conventional furnace, Thermolyne 62700. Typically, the crystallization of amorphous microwires was reported for $T_{ann} \geq 490$ °C. The advantage of amorphous microwires is their superior mechanical properties typically reported for amorphous materials [3]. In most cases, we fixed the annealing time, t_{ann}, of 60 min which is usually used for heat treatment of amorphous and nanocrystalline materials [4]. The samples were slow cooled to room temperature within the furnace.

2.2.2. Stress annealing

In several cases, tensile stress was applied with a mechanical load attached to one microwire end during the annealing, as well as during the sample cooling in the furnace.

The stress value in the metallic nucleus, σ_m, was evaluated considering different Young's modulus of metal, E_2, and glass, E_1, as follows [5]:

$$\sigma_m = \frac{K \cdot P}{K \cdot S_m + S_{gl}} \quad ; \quad \sigma_{gl} = \frac{K}{K S_m + S_{gl}} \tag{2.1}$$

where $K = E_2 / E_1$, P is the applied mechanical load and S_m, and S_{gl} are the cross sections of the metallic nucleus and the glass coating, respectively.

2.2.3. Current annealing

Also know as Joule heating, in this technique a sample is annealed by the current that passes through it causing its heating by Joule effect. It is widely used due to its simplicity and low cost, the equipment needed is similar as the one used for resistivity measurements [6].

Current annealing allows a better control of the annealing time without compromising the mechanical and chemical properties of the microwires as compared with conventional furnace annealing [7].

The current density is directly related to the sample heating [8]. The dc current value, I, needs to be set clearly below the value that can produce magnetic hardening and/or crystallization of the samples in order to avoid the deterioration of magnetic properties [9]. Structural relaxation and crystallization also depend on a great extend on the annealing time [10].

For our studies, electrical contacts were prepared by mechanically removing the insulating glass coating on the very end of microwires. Current annealing, with different durations and applying different currents was performed in air on 8 cm long samples. The insulating glass-coating of the microwires allows performing the thermal treatments in air.

In order to avoid the inhomogeneities of the microwire diameter (and corresponding current density variation) and stresses related to the sample cutting, we used the same microwire for studies of the influence of annealing time, for a fixed DC current value, on magnetic properties and GMI effect.

2.3. Magnetic characterization techniques

2.3.1. Hysteresis in ferromagnetic materials

The graphical representation of the magnetization versus the applied field for a ferromagnet in the processes of magnetization and demagnetization gives as a result a closed curve, called the hysteresis loop.

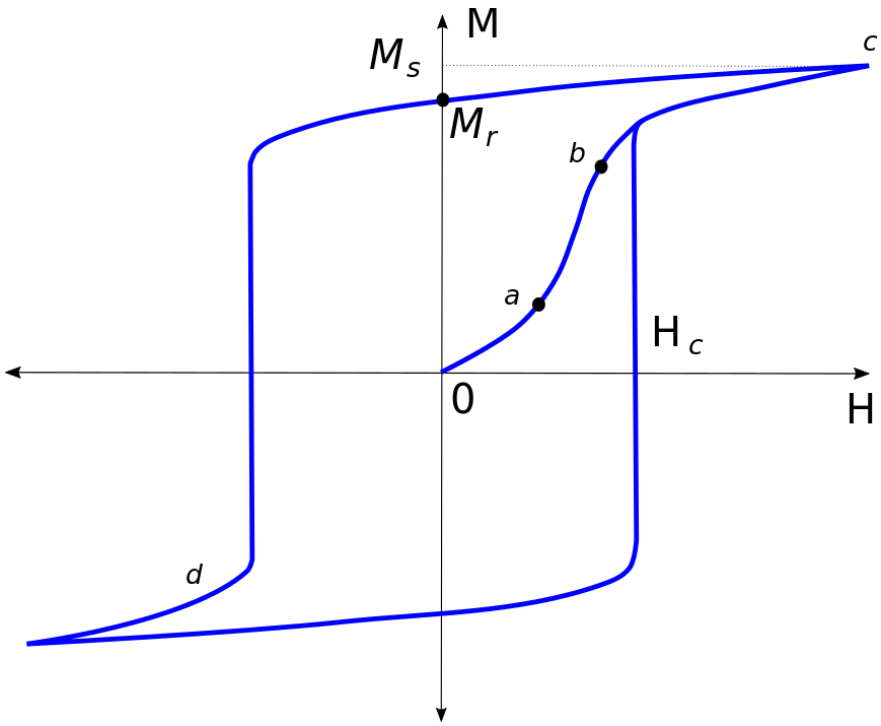

Figure 2.2. *Typical hysteresis loop of a ferromagnetic material.*

Hysteresis loops characterize the state of the sample studied. *Figure 2.2* shows a typical hysteresis loop of a bulk ferromagnetic sample [11]. Initially, the material is demagnetized and the applied field is zero ($M = H = 0$), increasing the value of the field H the first magnetization curve O_{abc} is obtained. From zero to the point *a* the sample is magnetized by the reversible process of the domain frontiers movement. Between *a* and *b* the magnetization increases by an irreversible process of the domains frontiers movement and between *b* and *c* increases mainly by the domains magnetization rotation, being *c* the point of magnetization saturation, M_s. Decreasing from *c* the value of the field H up to zero we reach the point of remanent magnetization or

remanence, M_r, since the magnetization of the sample is not cancelled due to the non reversibility of the domains frontiers movement, the sample magnetization does not return to the initial demagnetized state, each magnetization domain rotates back to the nearest easy direction. To cancel this magnetization it is needed to apply a field with the appropriate value and in the opposite direction, called coercive field or coercivity, H_c. Increasing the field in this direction the saturation is also reached.

The saturation magnetization, M_s, is determined by the composition, internal structure and temperature of the material and the coercive field, H_c, and remanence M_r, are determined by the anisotropy of the sample. The coercivity also depends on the imperfections (internal stresses distribution or defects).

The ratio between the magnetization and the applied field, given by the slope of the hysteresis curve, is called the susceptibility, χ, of the material [12]:

$$\chi = \frac{M}{H} \tag{2.2}$$

The area enclosed by the hysteresis loop is equal to the energy dissipated by the sample in a magnetization cycle. Hard magnetic materials typically have a square shape hysteresis loop, with high coercive field, H_c, (a requirement for many applications, such as memory devices), as the material is softer the hysteresis loop tends to be more linear, the area inside the cycle is smaller and hence, the hysteresis loss is lower, a desirable characteristic of soft magnetic materials (for applications like magnetic sensors).

2.3.2. Flux-metric method for hysteresis loops measurements

One of the main and first steps of the characterization of magnetic microwires is its hysteresis loop analysis, that will allow us to obtain magnetic parameters such us coercive field, H_c, anisotropy field, H_k, remanent magnetization, M_r and magnetic saturation, M_s. Hysteresis loops can be obtained by the induction fluxmetric method based on the Faraday-Lenz law, that establishes that with the magnetic flux, ϕ,

temporal variation in a circuit an electromotive force ε proportional to this variation is induced [11]:

$$\varepsilon = -N\frac{d\phi}{dt} \tag{2.3}$$

where *N* is the number of turns in a coil.

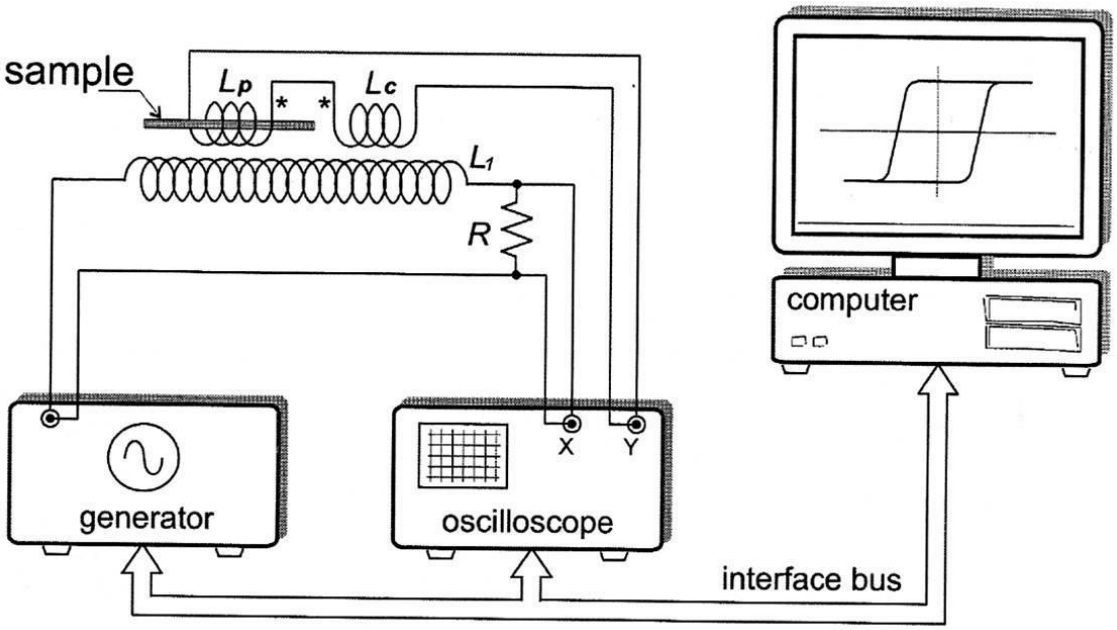

Figure 2.3. *Scheme of the hysteresis loops measurement set-up [13].*

The measurement set-up (shown in *Figure 2.3*) consists of the primary exciting system (in our case a solenoid) to generate the magnetic field and the secondary pick-up system, composed of two coils, the pick-up coil and the compensation coil. Once an alternating magnetic field is applied at a fixed frequency (in our case 50 Hz) provided by the power supply, the change in the magnetization of the sample is detected by the pick-up coil. The induced pick-up coil signal, proportional to the magnetization of the sample, is integrated by the fluxmeter and generally has two components, the first due to the change in the magnetic field *H* and the second due to the change in the magnetization of the sample, *M* [11]:

$$\varepsilon = -N\mu_0\frac{d(A_cH + A_sM)}{dt} = -N\mu_0\left[A_c\frac{dH}{dt} + A_s\frac{dM}{dt}\right] \tag{2.4}$$

where A_c and A_s are the coil and the sample cross section areas.

The magnetic field *H*, has two components, the first related to the field produced by the primary exciting system and the second related to the demagnetizing factor that can be neglected when the section of the sample adjusts well with the secondary's section. This demagnetizing factor produces a field inside the sample opposite to the magnetization that tends to zero in the case that ratio between the length and the diameter also tends to zero, as in the case of the microwires.

The compensation coil, connected in series-opposition with the pick-up coil and identical to it, is used to eliminate the component due to the external magnetic field in order to get an induced electromotive force only dependent of the change in the magnetization of the sample

$$\varepsilon = N\mu_0 A_s \frac{dM}{dt} \tag{2.5}$$

Integrating this signal, by means of the fluxmeter, the magnetization of the sample is obtained:

$$M = \frac{1}{N\mu_0 A_s} \int \epsilon dt \tag{2.6}$$

This integrated signal is taken by the *Y* channel of the oscilloscope (Tektronix TDS3012B). The solenoid is in series with a pattern resistance (1 Ω) whose voltage drop, proportional to the magnetic field produced by the solenoid, is taken by the *X* channel of the oscilloscope. The *XY* mode of the oscilloscope gives the hysteresis loop. The whole system is oriented to minimize the interference with the terrestrial magnetic field.

The magnetization *M* is normalized, M/M_s, in our hysteresis loops representation, being M_s the magnetic moment of the sample at the maximum magnetic field amplitude, H_o.

Among other advantages, this method allows the measurement of sufficiently long samples (of about 10 cm and longer), an important factor for the case of microwires whose bistability vanishes at a critical length. The system can also be adjusted to apply tensile and/or torsion stress during the measurements and evaluate

the evolution of the characteristic magnetic parameters under the influence of the torsion and/or tensile stress applied.

2.3.3. PPMS magnetometer

The Physical Property Measurement System, PPMS, is a versatile measurement platform, capable to measure a wide range of materials and properties as a function of temperature and magnetic field. Provides information of the magnetic, thermal and electric properties of a sample, such as magnetoresistivity and magnetization in direct current (DC) and alternating current (AC) and resistivity (using a typical 4-point configuration) or heat capacity (with a micro-calorimeter platform), among others. The advantages of this technique are speed and high sensitivity. The addition of different functional options allows enlarging the measurement range and customize the capabilities of the system.

Figure 2.4. *Figure 2.3. PPMS QD 6000 at the SGIker of the University of the Basque Country (UPV/EHU).*

The PPMS Quantum Design Model 6000 employed in our studies (*Figure 2.4*) works in a wide range of temperatures that spans from 1.9 K up to 1000 K (in the *DC* mode) and external magnetic fields, generated by a superconducting coil, from -9 to +9 T. For frequencies ranging from 10 Hz to 10 kHz fields of 0.002 to 15 Oe are available in the *AC* excitation mode. The main part of the device is the probe placed inside a dewar containing liquid helium, the refrigeration system is controlled by a temperature hardware. Parallel and perpendicular orientations with respect of the applied magnetic field are allowed. A detailed description of the capabilities is given in the device manual [13].

The AC measurement system uses an alternating field, generated by a drive coil, in the measurement region with the sample located in the center of a detection coil that measures the change in the applied field due to the presence of the sample. Sensitivity of the order of 2×10^{-8} emu can be achieved in these measurements.

In the DC mode, a constant field is applied and the system fasten scrolls (with a maximum speed of 100 cm/s) the position of the sample with respect to the two detection coils while synchronously records the induced voltage on the detection coils. The sensitivity in this mode is of the order of 2×10^{-5} emu.

2.3.4. Giant Magnetoimpedance (GMI) effect measurements

The giant magnetoimpedance (GMI) effect usually observed in soft magnetic materials phenomenologically consists of a change of the AC impedance, $Z = R + iX$ (where R is the real part, or resistance, and X is the imaginary part, or reactance), when submitted to an external magnetic field, H_0.

The electrical impedance, Z, of a magnetic conductor is given by [14]:

$$Z = R_{dc} kr J_0(kr)/2J_1(kr) \qquad (2.7)$$

where R_{dc} is the electrical resistance for a DC current, $k = (1 + j) / \delta$, J_0 and J_1 are the Bessel functions, r is the radius of the wire and δ the penetration depth given by [15]:

$$\delta = \left(\pi\sigma\mu_\phi f\right)^{-1/2} \tag{2.8}$$

being σ the electrical conductivity, f the frequency of the current along the sample and μ_ϕ the circular magnetic permeability assumed to be scalar. The DC applied magnetic field induces significant changes in the circular permeability, μ_ϕ. Thus, the penetration depth also changes and as a result there is a change of Z [15,16].

The GMI ratio, $\Delta Z/Z$, used for the GMI effect characterization, has been defined as [17]:

$$\Delta Z/Z = [Z(H) - Z(H_{max})]/Z(H_{max}) \cdot 100 \tag{2.9}$$

where H is the applied axial *DC*-field with a maximum value, H_{max}, up to a few kA/m.

The magnetic permeability in ferromagnetic materials with high circumferential anisotropy (as in the case of magnetic wires) possesses tensor character and therefore the classic form of impedance definition is not valid. The relation between the electric field, $\vec{e}$, (which determines the voltage) and the magnetic field, h, (which determines the current) is defined by means of the surface impedance tensor, $\hat{\varsigma}$, [18]:

$$\vec{e} = \hat{\varsigma}\vec{h} \quad \text{or} \quad \left\{\begin{array}{l} e_z = \varsigma_{zz} h_\varphi - \varsigma_{z\varphi} h_z \\ e_\varphi = \varsigma_{\varphi z} h_\varphi - \varsigma_{\varphi\varphi} h_z \end{array}\right\} \tag{2.10}$$

The circular magnetic field h_φ is produced by the currents i_w running through the wire. At the wire surface $h_\varphi = i/2\pi r$, where r is the wire radius. The longitudinal magnetic field h_z is produced by the currents i_c running through the exciting coil, $h_z = N_1 i_c$, with N_1 the number of turns in the exciting coil.

The longitudinal electrical field on the wire surface can be measured as the voltage drop along the wire, v_w, and the circumferential electrical field as the voltage induced in the pickup coil, v_c, wounded on it [16]:

$$v_w \equiv e_z l_w = (\varsigma_{zz} h_\varphi - \varsigma_{z\varphi} h_z) l_w \tag{2.11}$$

$$v_c \equiv e_\varphi l_t = (\varsigma_{\varphi z} h_\varphi - \varsigma_{\varphi\varphi} h_z) l_t \qquad (2.12)$$

being l_w the length of the wire and $l_t = 2\pi r N_2$ the total length of the pickup coil turns N_2 wounded directly on the wire.

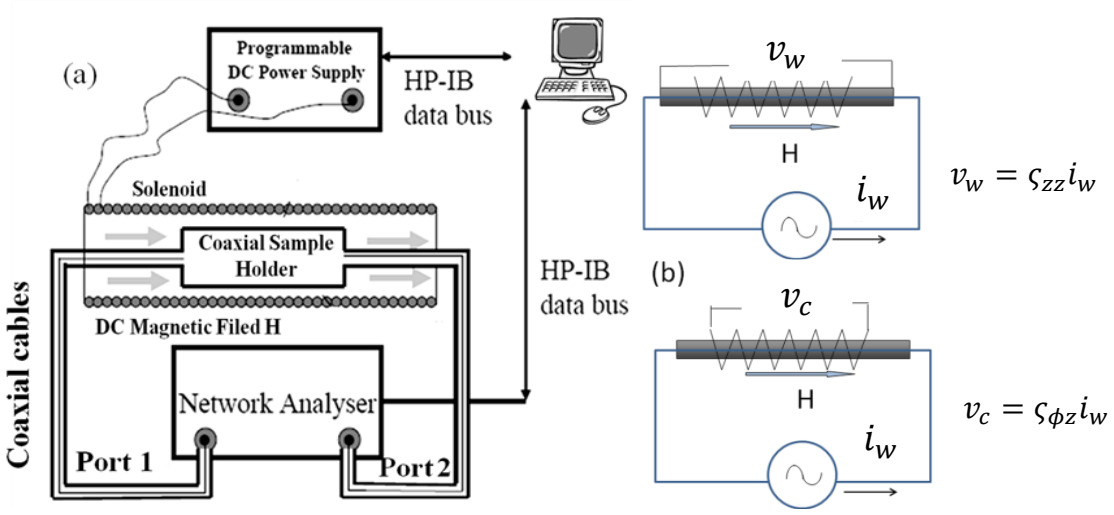

Figure 2.5. *Schematic picture of the experimental set-up for measurements of the GMI effect (a), methods for revealing the diagonal, ς_{zz}, and off-diagonal, $\varsigma_{z\varphi}$, impedance matrix elements (b) [19].*

Figure 2.5a shows a schematic picture of the experimental set-up employed for the GMI effect characterization. The methods for revealing the components of the impedance tensor are shown in *Figure 2.5b*. The longitudinal diagonal component ς_{zz} is defined as the voltage drop along the wire and corresponds to the impedance definition in the classical model (*Figure 2.5b*):

$$\varsigma_{zz} \equiv \frac{v_w}{h_\varphi l_w} = \left(\frac{2\pi r}{l_w}\right)\left(\frac{v_w}{i_w}\right) \qquad (2.13)$$

The off-diagonal components, $\varsigma_{z\varphi}$ and $\varsigma_{\varphi z}$, and the circumferential diagonal component $\varsigma_{\varphi\varphi}$ arise from cross sectional magnetization process ($h_\varphi \rightarrow m_z$ and $h_z \rightarrow m_\varphi$) [20].

A specially designed microstrip sample holder (shown in *Figure 2.6*) placed inside a solenoid sufficiently long to provide a homogeneous field allows measuring of the magnetic field dependence of sample impedance, *Z(H)*, using vector network analyzer (Agilent N5230A VNA) from the reflection coefficient, S_{11}, taking into account the following expression [21]:

$$Z = Z_0 \frac{(1 + S_{11})}{(1 - S_{11})} \tag{2.14}$$

being Z_0 = 50 Ω the characteristic impedance of the coaxial line and S_{11} is the reflection coefficient. Described technique allows measuring the GMI effect in an extended frequency, *f*, range, up to GHz frequencies.

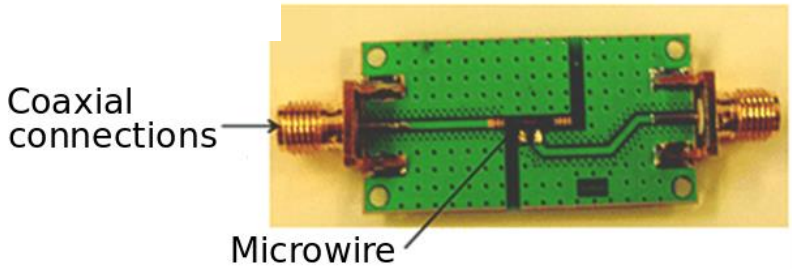

***Figure 2.6**. Microstrip line for GMI measurements of the microwires.*

2.3.5. Free-space electromagnetic parameters measurement system

Free-space technique offers several advantages for measurement of electromagnetic parameters of composite materials. This non-contact method allows non-destructive measurements under different temperature or environmental conditions [22,23].

The experimental set-up used in this work for reflection (*R*) and transmission (*T*) coefficients measurement consists of a pair of broadband horn antennas (1-17 GHz), a

vector network analyzer (Agilent N5230A VNA) and an anechoic chamber (see *Figure 2.7*).

The composite is placed in the middle of the anechoic chamber with the microwires orientation along the electric-field of the incident electromagnetic wave. The desired frequency range for measurement of the scattering parameters, determines the requirements to the operating frequency of the VNA, antennas and to the chamber size (distance between antennas and sample) [23].

The size of the sample needs to be larger than the wavelength of the incident electromagnetic wave in order to achieve convincing results. In fact, to further minimize the effects of the scatterings from the sample boundary, the sample size should be at least twice larger than the wavelength [24]. According to this, in our experiments, the composite was placed in 20 x 20 cm^2 window to avoid the edge effects. This window limits the applicable frequency range in 4-17 GHz.

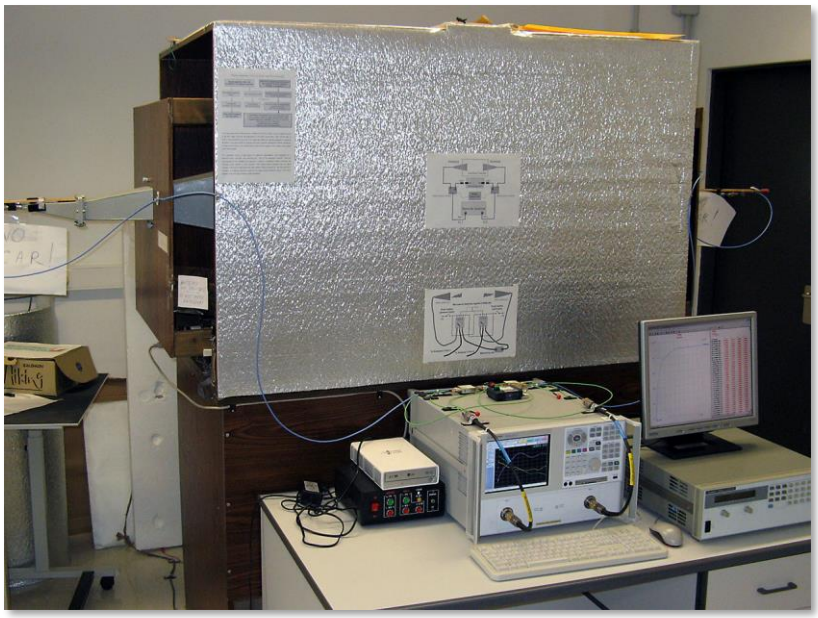

Figure 2.7. *Free space microwave measurement set-up for measurement of the electromagnetic parameters in composite material at the Applied Physics Dept. of UPV/EHU.*

2.3.6. Domain Wall (DW) propagation measurements

The magnetic field driven domain wall (DW) propagation has been studied using modified Sixtus-Tonks method c The main differences of used method from the classical Sixtus-Tonks [25] set-up are the following: a system of three pick-up coils is employed (see *Figure 2.8*) [26], instead of a nucleation coil, since small closure domains spontaneously appear at the end of the wire in order to decrease the stray field. In addition, one sample end is placed outside the magnetization coil to ensure a single DW propagation avoiding multiple DW propagation and hence overestimating the magnitude of DW velocity.

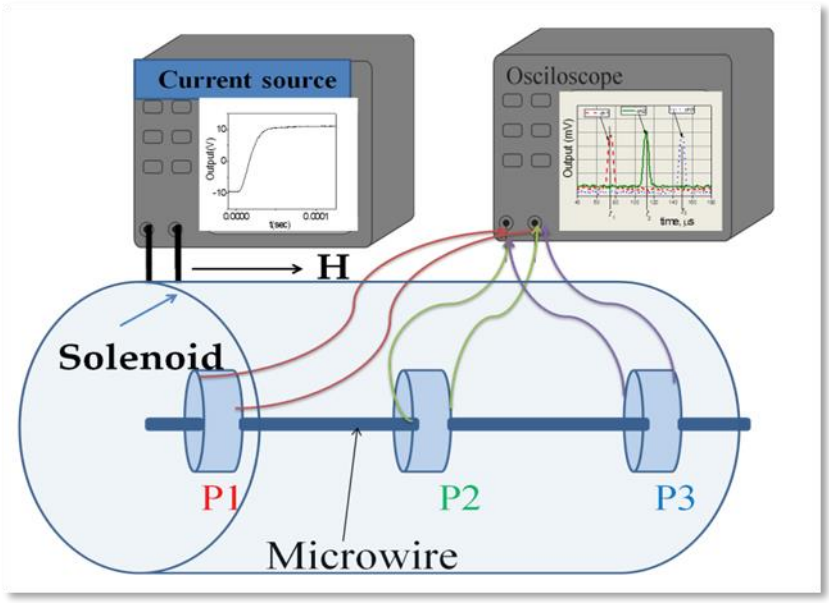

Figure 2.8. *Schematic picture of the experimental set-up for DW dynamics measurements in microwires [27].*

Studied microwire samples (usually of about 10 cm long) were placed inside the three coaxially pick-up coils. Rather homogeneous axial magnetic field was generated by a 140 mm long solenoid (10 mm in diameter). The DW travelling along the sample induces an electromotive force (*EMF*) in the pick-up coils that is recorded by an oscilloscope. Then, velocity, *v,* of a DW travelling along the sample can be estimated as [27]:

$$v = \frac{l}{\Delta t} \tag{2.15}$$

with l the distance between pick-up coils and Δt the time interval between the *EMF* peaks generated when moving DW crosses the pick-up coils [26].

For evaluation of the DW injection inside the sample and nucleation field profile, we used a short magnetizing coil to apply local magnetic field [28,29]. Located next to the short pick-up coil, the short magnetizing coil allows detecting local magnetization reversal at sufficiently large distance from the ends of the wire. Then, by slowly moving the wire through the short magnetizing coil is possible to measure the length distribution of the local magnetization reversal (DW injection) fields of each sample.

2.3.7. Small angle magnetization rotation (SAMR) technique for magnetostriction measurements

Magnetic properties of amorphous alloys strongly depend on the magnitude of the magnetostriction, which causes the change in the dimensions of a magnetic material during the magnetization. Direct magnetoelastic effect has small influence (of the order of $\approx 10^{-5}$-10^{-7}) but the inverse effect, i.e., the change in the magnetization of a ferromagnetic material due to the applied mechanical stress is significant. Therefore, for the optimization of the magnetic properties of magnetic microwires it is relevant to quantify the value of the magnetostriction. There are several indirect methods for the determination of the saturation magnetostriction constant, λ_S. In the present work, Small Angle Magnetization Rotation (SAMR) technique, introduced in 1980s [26,28], is employed.

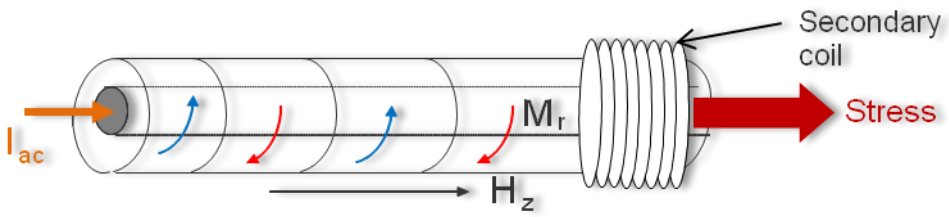

Figure 2.9. *Schematic picture of the set-up for magnetostriction measurements in microwires.*

As can be seen from *Figure 2.9*, during the measurements the initial tensile stress, σ_0, is created by a weight, *P,* attached to the microwire end. In this method the sample (of about 10 cm long) is saturated by an axial DC magnetic field, H_z, created along the microwire *z* -axis using a solenoid, while applying simultaneously a small *ac* transverse field, H_y, created by an AC electric current flowing along the sample. The combination of these fields leads to a reversible rotation of the magnetization within a small angle, θ, out of the axial direction. The induction voltage, $V(2\omega)$, due to the magnetization rotation, is detected by a pick-up coil wounded around the microwire. This signal is amplified for its detection in the measuring block. The AC current value, flowing through the wire is selected to avoid possible Joule heating of the sample: the current amplitude does not exceed 10-30 mA.

The magnetostriction coefficient, λ_s, is determined from the measurement of the dependence on axial magnetic field, H_z, versus applied stress σ, for different mechanical loads, at fixed value of induction voltage $V(2\omega)$, according to the expression [30,31]:

$$\lambda_S = -\frac{\mu_0 M_S}{3}\left(\frac{dH}{d\sigma}\right) \tag{2.16}$$

where $\mu_0 M_s$ is the saturation magnetization of the sample obtained from magnetization curves measured at high applied field and room temperature.

Additional details on SAMR method and set-up features designed for evaluation of magnetostriction coefficient, λ_s, can be found in refs. [30,31].

The SAMR method is successfully employed for the evaluation of Co-rich glass-

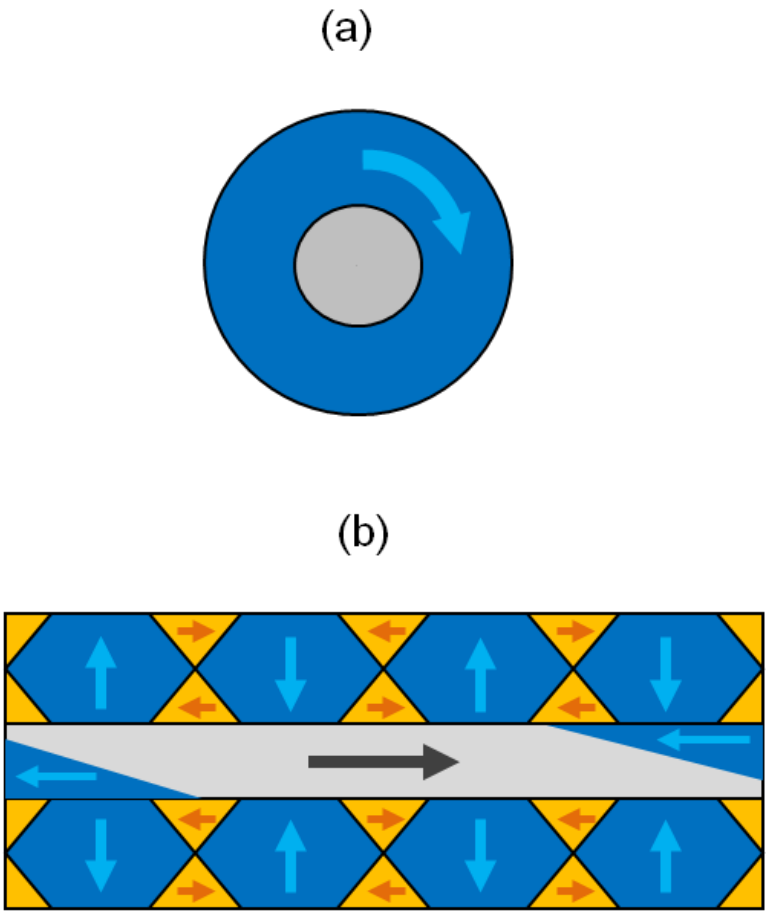

Figure 2.10. *Schematic picture illustrating domain structure of Co-rich (a) and Fe-rich (b) microwires.*

coated microwires with negative magnetostriction coefficient as it was originally developed for magnetic materials in which magnetization rotation governs the magnetization process. Recently, it has also been extended for evaluation of microwires with positive magnetostriction coefficient [32,33]. Indeed, in Co-rich microwires circular magnetization orientation was experimentally observed by various experimental techniques (*Figure 2.10a*), while Fe-rich microwires present radial magnetization orientation (*Figure 2.10b*) [34]. Accordingly, magnetization rotation in the outer domain shell can be observed in both kinds of microwires [32,33].

2.4. Microstructural characterization techniques

2.4.1. Powder X-ray diffraction (XRD)

X-ray diffraction allows the structural characterization of amorphous and crystalline materials. Electromagnetic waves, in this case X-rays, are diffracted when they encounter an obstacle, and this effect is increased when the size of the obstacle is comparable to the wavelength incident on the material. Then, it is possible to explore the structure of solids by studying the diffraction patterns of an incident wave with wavelength comparable to the distance between atoms.

When an X-ray beam strikes a solid material, part of this beam is scattered in all directions by the electrons associated with the atoms of the material or ions that encounters along the way, but the rest of the beam can give rise to the X-ray diffraction phenomenon, which takes place if there is an ordered arrangement of atoms (long range) and are fulfilled the conditions given by Bragg's Law [35] (*Figure 2.11*) that relate the wavelength, λ, of the X-rays and the interatomic distance, d_{hkl}, between the family of planes (*hkl*), with the angle of incidence of the diffracted beam, θ (Bragg angle). This law is described by the following equation [35]:

$$n\lambda = 2d_{hkl}sin\theta \qquad (2.17)$$

where *n* is an integer that represents the order of reflection. This equation allows us to obtain the angular position of the diffraction peaks of the crystalline solid that is analyzed.

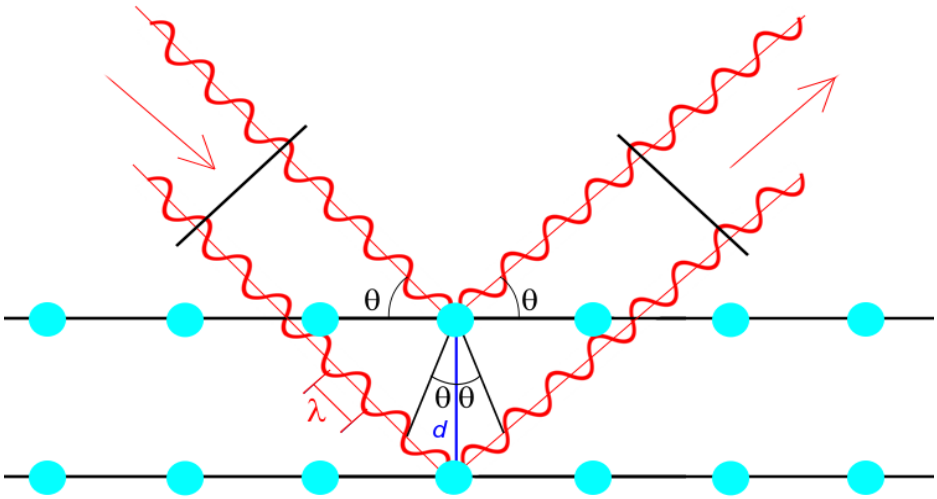

Figure 2.11. *Schematic picture illustrating Bragg's Law of diffraction.*

The structure of the samples in the present work has been analyzed using Bruker (D8 Advance) X-ray diffractometer (*Figure 2.12*) with CuK_α (λ = 1.54 Å) radiation, operated at applied voltage of 40 KV and filament current of 30 mA. The sample is attached to the diffractometer sample holder and each scan is made over the two theta angular range of 30 to 90 degrees, step size of 0.05°and a step time of 30 second for each step. The diffraction peaks are indexed using JCPDS (Joint Committee on Powder Diffraction Standards) database.

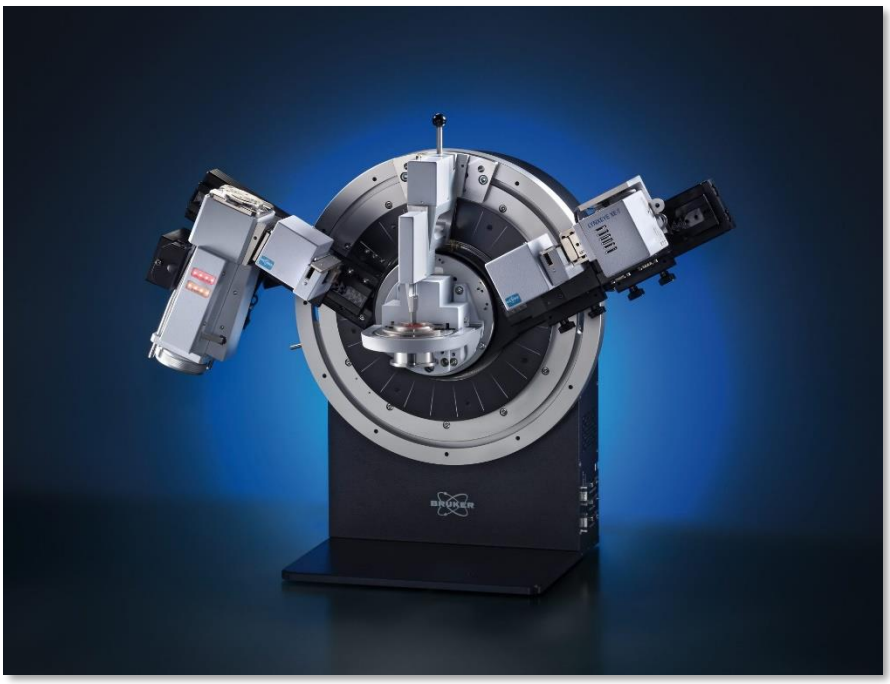

Figure 2.12. *Bruker (D8 Advance) X-ray diffractometer picture [36].*

A wide halo characteristic of completely amorphous materials was observed in the case of amorphous (as-prepared or annealed) glass-coated microwires.

2.4.2. Optical Microscopy (OM)

The diameters of the metallic nucleus and glass coating of the different microwires employed in this work and the homogeneity along their length was checked by means of an optical microscopy, in our case Microscope Axio Scope A1 (as shown in *Figure 2.13*), that uses visible light and a system of lenses to magnify images. This microscopy allows to obtain a two-dimensional image of the microwires. The microwire is placed in the microscope stage on a slide (a thin flat piece of glass) to check its geometry.

Figure 2.13. *Microscope Axio Scope A1. Source Carl Zeiss Microscopy GmbH and own elaboration (Adapted from Microscope Axio Scope A1 user manual).*

The system contents various lenses, which are placed in the microscope column below the emission chamber and situated one above the other. The condenser lens allows to obtain a parallel and thin beam of light form the illuminator to proper illuminate and focus the light on the sample. The objective lens collects the light diffracted from the sample and forms the first image of the object and the intermediate lens or group of lenses (called the eyepiece) amplify this image that finally is projected by the projection lens. The quality of the image depends on the contrast, resolution and the focal depth of the microscope. Illumination sources and objectives can be manipulated to adjust the image.

2.4.3. Scanning Electron Microscopy (SEM)

Chemical composition, microstructure and external morphology of the microwires once they are obtained and after the thermal treatments, were characterized by Scanning Electron Microscopy, (SEM). The equipment employed at the UPV/EHU was a MEB JEOL JSM-7000F (*Figure 2.14*) with energy-dispersive X-ray spectroscopy (EDX) option with an Inca Energy 350 spectrometer. The microscope has a field emission source (Schottky type).

In this technique, a thin beam of high-energy accelerated electrons is concentrated by electromagnetic lenses and focuses on the surface of a thick an opaque sample. The beam scans the surface of the sample in a raster scan pattern, with a velocity synchronized with the position in a computer screen to create the image. As a result of the interaction, different types of radiation are produced. The emitted electrons and those that bounce off the surface (Auger electrons, secondary and backscattered electrons) are collected by a sensor. Secondary electrons emitted by the nearest to the surface atoms of the sample allow to obtain the images of the surface. Their intensity depends on the incident angle and thus, on the topography of the surface, and it is proportional to the correspondent spot on the image of the sample at the screen. To facilitate the emission of the electrons the sample is coated with a conductive metal, usually Au.

Backscattered electrons are those reflected after the interaction with the sample. Their intensity depends on the mean atomic number of the atoms of the sample. The image generated by backscattered electrons reveals differences in the chemical composition by differences in the contrast.

Most electronic microscopes have a microprobe coupled to perform a elemental analysis, at selected points of the sample, by X-ray emission. The X-ray spectra allows to obtain a semi-quantitative chemical composition analysis.

With this technique, by the examination of selected areas of the surface of the sample, can be estimated the grain size of the nanostructures and the homogeneity in the composition along the microwire length and at different points of the diameter

Figure 2.14. *Scanning Electron Microscope* MEB JEOL JSM-7000F *at the SGIker of the University of the Basque Country (UPV/EHU).*

2.4.4. Differential Scanning Calorimetry (DSC)

Differential Scanning Calorimetry, DSC, is a thermal analysis technique in which the heat flow of the sample is measured as a function of time or temperature when the temperature of the sample is scanned, in a controlled atmosphere. DSC calorimetry is one of the most useful tools for the characterization of the structural and magnetic transitions of the samples

The system maintains the sample and the reference at the same temperature, while continuously records, in the whole temperature interval, the supply of heat needed to maintain both at identical temperature. The measurement of the difference in the heat flow between a crucible containing the sample and a reference crucible (contains a thermally inert material at the temperature range studied, with a specific heat capacity, or may be empty) gives a direct calorimetric measure of the absorbed or released energy. When the sample undergoes a physical transformation, like a phase transition, it will be needed to supply more (or less) heat to maintain it at the same temperature than the reference.

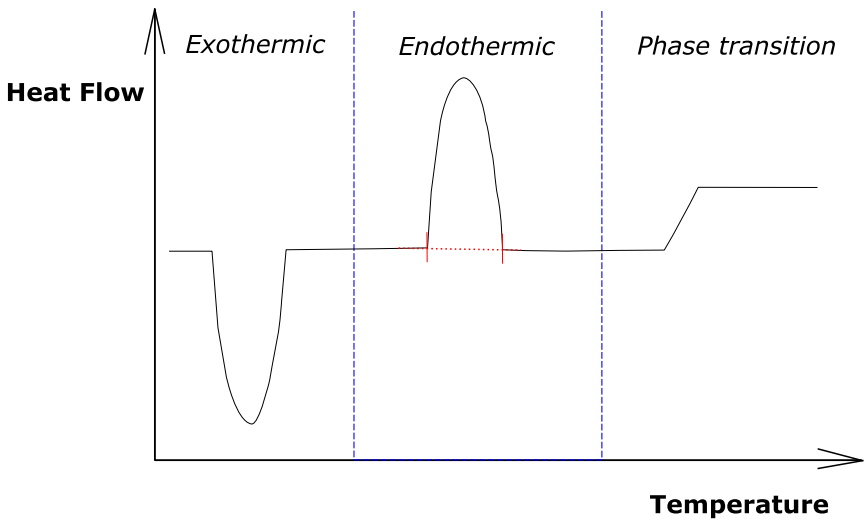

Figure 2.15. *Schematic example of a DSC curve showing the common features.*

In *Figure 2.15* it is shown a thermogram, in which the heat flow, *DH/dt*, is represented *versus* the temperature, with the three main processes that can take place, the heat difference is obtained subtracting the heat flow from the sample to the heat flow of the reference. When there is no thermodynamic process the heat flow difference between sample and reference is not significant and a base plane line is reflected on the DSC curve. *i*) When the sample undergoes an exothermic process (e.g. crystallization) *($\Delta H < 0$)* the sample yields heat, being necessary to supply power to the reference in order to maintain sample and reference both at the same temperature,

the extra power supplied is shown in the diagram as a negative peak, following the convention mentioned above. In contrast, *ii*) an endothermic process *($\Delta H > 0$)* implies absorption of heat by the sample from the surroundings so, in this case, it is needed to supply power to the sample in order to maintain it at the same temperature than the reference and it will be reflected on the diagram as a positive peak. *iii*) A change in the slope of the *DSC* curve will indicate a phase transition, involving a change in the heat capacity, $C_p = \Delta H/\Delta T$. The area of the peaks is proportional to the thermal effects.

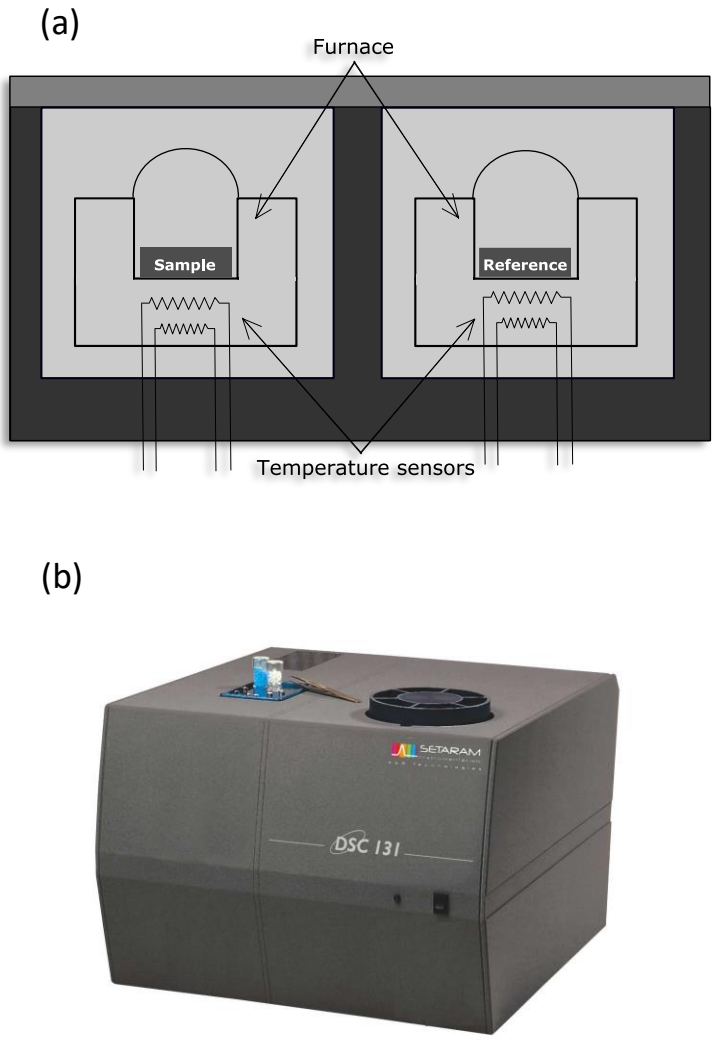

Figure 2.16. *Power-compensation differential scanning calorimeter diagram (a) and Differential scanning calorimeter DSC 131 Setaram (image taken from DSC 131 Setaram user manual) (b).*

This technique allows a direct determination of the enthalpy of the transitions, from the area of the peak, the mass of the sample and a calorimetric constant dependent on the instrument.

The experimental set up as shown in *Figure 2.16a* consists of two sample holders (the crucibles are generally made of Al), one for the sample, *S*, and the other for the reference, *R*, that are heated with independent heating systems while monitorizing the difference in the heat flow between both. The measurement can be carried out at constant temperature or changing the temperature at a constant rate. The differences in the temperatures between *S* and *R* are detected by temperature sensors and sent to an output device, normally a computer, that allows to obtain the calorimetric curves. In the present work, to determine the transitions and critical temperatures (crystallization temperature, T_{cr}, and Curie temperature, T_C) of the samples and also in some cases to anneal them following a controlled temperature program, it was employed a DSC-131 Setaram Calorimeter (*Figure 2.16b*) in Ar atmosphere, employing different heating rates.

2.5. References

[1] G.F. Taylor, A Method of Drawing Metallic Filaments and a Discussion of their Properties and Uses, Phys. Rev. 23 (1924) 655–660, doi:10.1103/PhysRev.23.655.

[2] G.F. Taylor, Process and apparatus for making filaments, Patent N.1 793 529 US, 1931.

[3] T. Goto, M. Nagano, N. Wehara, Mechanical Properties of Amorphous $Fe_{80}P_{16}C_3B_1$ Filament Produced by Glass-Coated Melt Spinning, Trans. Japan Inst. Met. 18 (1977) 759–764, doi:10.2320/matertrans1960.18.759.

[4] A. Zhukov, M. Ipatov, P. Corte-León, L. Gonzalez-Legarreta, J.M. Blanco, V. Zhukova, Soft magnetic microwires for sensor applications, J. Magn. Magn. Mater. 498 (2020) 166180, doi:10.1016/j.jmmm.2019.166180.

[5] E. Ia. Badinter, E.M. Lysko, Microwire and resistivity devices, Shtinitsa, Kishinev, 1962, pp. 52–62.

[6] V. Zhukova, A.F. Cobeño, A. Zhukov, J.M. Blanco, S. Puerta, J. Gonzalez, M. Vázquez, Tailoring of magnetic properties of glass-coated microwires by current annealing, J. Non. Cryst. Solids. 287 (2001) 31–36, doi:10.1016/S0022-3093(01)00536-1.

[7] M.G. Nematov, I. Baraban, N.A. Yudanov, V. Rodionova, F.X. Qin, H.-X. Peng, L.V. Panina, Evolution of the magnetic anisotropy and magnetostriction in Co-based amorphous alloys microwires due to current annealing and stress-sensory applications, J. Alloys Compd. 837 (2020) 155584, ISSN 0925-8388, doi:10.1016/j.jallcom.2020.155584.

[8] H. Chiriac, M. Knobel, T. Ovari, Temperature Distribution in a Joule effect Annealed Amorphous Glass-Covered Wire, Mater. Sci. Forum 302-3 (1999) 239.

[9] A.V. Popova, V.I. Odintsov, S.A. Menshov, E.V. Kostitsyna, V.P. Tarasov, V. Zhukova, A. Zhukov, S.A. Gudoshnikov, Continuous control of a resistance in Co-rich amorphous ferromagnetic microwires during DC Joule heating, Intermetallics 99 (2018) 39–43, doi:10.1016/j.intermet.2018.05.012.

[10] I. Astefanoaei, D. Radu, H. Chiriac, Internal stress distribution in DC joule-heated amorphous glass-covered microwires, J. Phys. Condens. Matter. 18 (2006) 2689–2716, doi:10.1088/0953-8984/18/9/008.

[11] R.C. O'Handley, Modern Magnetic Materials Principles and Applications, ISBN-13: 978-0471155669 (1999).

[12] B.D. Cullity, Introduction to magnetic materials, Addison-Wesley (1972).

[13] L. Gonzalez-Legarreta, P. Corte-Leon, V. Zhukova, M. Ipatov, J.M. Blanco, J. Gonzalez, A. Zhukov, Optimization of magnetic properties and GMI effect of Thin Co-rich Microwires for GMI Microsensors, Sensors (2020) 20(6) 1558, doi:10.3390/s20061558.

[14] Quantum Desing, Inc., (n.d.). http://qdusa.com/products/ppms.html.

[15] E.C. Jordan, Electromagnetic Waves and Radiating Systems, Prentice Hall (1968), ISBN 978-0-13-249995-8.

[16] L.V. Panina, K. Mohri, Magneto-impedance effect in amorphous wires, Appl. Phys. Lett. 65 (1994) 1189–1191.

[17] R.S. Beach, A.E. Berkowitz, Giant magnetic field dependent impedance of amorphous FeCoSiB wire, Appl. Phys. Lett. 64 (1994) 3652–3654.

[18] M. Knobel, Giant Magnetoimpedance in Handbook of Magnetic Materials, K.H.J. Buschow (ed.), Elsevier (2003).

[19] A. Zhukov, A. Talaat, M. Ipatov, V. Zhukova, High frequency giant magnetoimpedance effect of amorphous microwires for magnetic sensors applications, Proc. Int. Conf. Sens. Technol. ICST. (2014) 624–629.

[20] S. Sandacci, D. Makhnovskiy, L. Panina, K. Mohri, Y. Honkura, Off-diagonal impedance in amorphous wires and its application to linear magnetic sensors, IEEE Trans. Magn. 40 (2004) 3505–3511. doi:10.1109/TMAG.2004.835676.

[21] D. González-Alonso, L. González-Legarreta, P. Corte-León, V. Zhukova, M. Ipatov, J.M. Blanco, A. Zhukov, Magnetoimpedance Response and Field Sensitivity in Stress-Annealed Co-Based Microwires for Sensor Applications, Sensors 20(11) (2020) 3227, doi:10.3390/s20113227.

[22] D. Makhnovskiy, A. Zhukov, V. Zhukova, J. Gonzalez, Tunable and Self-Sensing Microwave Composite Materials Incorporating Ferromagnetic Microwires, Adv. Sci. Technol. 54 (2009) 201–210, doi:10.4028/www.scientific.net/AST.54.201.

[23] L. Panina, M. Ipatov, V. Zhukova, J. Gonzalez, A. Zhukov, Tuneable composites containing magnetic microwires, in: J. Cuppoletti (Ed.), Met. Ceram. Polym. Compos. Var. Uses, InTech - Open Access Publisher, Janeza Trdine, 9, 51000 Rijeka, Croatia, 2011, pp. 431–460, doi:10.5772/21423.

[24] L.F. Chen, C.K. Ong, C.P. Neo, V.V. Varadan, V.K. Varadan, Microwave Electronics Measurement and Materials Characterization, John Wiley & Sons, 0-47084-492-2, England 2004.

[25] K.J. Sixtus, L. Tonks, Propagation of Large Barkhausen Discontinuities. II, Phys. Rev. 42 (1932) 419–435, doi:10.1103/PhysRev.42.419.

[26] V. Zhukova, J.M. Blanco, A. Chizhik, M. Ipatov, A. Zhukov, AC-current-induced magnetization switching in amorphous microwires, Front. Phys. 13 (2017) 137501, doi:10.1007/s11467-017-0722-6.

[27] V. Zhukova, P. Corte-Leon, L. González-Legarreta, A. Talaat, J.M. Blanco, M. Ipatov, J. Olivera, A. Zhukov.. Review of Domain Wall Dynamics Engineering in Magnetic Microwires, Nanomaterials 10(12) (2020) 2407, doi:10.3390/nano10122407.

[28] M. Ipatov, N.A. Usov, A. Zhukov, J. Gonzalez, Local nucleation fields of Fe-rich microwires and their dependence on applied stresses, Phys. B Condens. Matter. 403 (2008) 379–381, doi:10.1016/j.physb.2007.08.054.

[29] V. Zhukova, J.M. Blanco, V. Rodionova, M. Ipatov, A. Zhukov, Domain wall propagation in micrometric wires: Limits of single domain wall regime, J. Appl. Phys. 111 (2012) 07E311.

[30] A. Siemko, H. Lachowicz, On indirect measurements of saturation magnetostriction in low-magnetostrictive metallic glasses, IEEE Trans. Magn. (1987) 2563–2565.

[31] K. Narita, J. Yamasaki, H. Fukunaga, Measurement of Saturation Magnetostriction of a Thin Amorphous Ribbon by Means of Small-Angle Magnetization Rotation, IEEE Trans. Magn. 16 (1980) 435–439.

[32] A. Zhukov, M. Churyukanova, S. Kaloshkin, V. Sudarchikova, S. Gudoshnikov, M. Ipatov, A. Talaat, J.M. Blanco, V. Zhukova, Magnetostriction of Co–Fe-Based Amorphous Soft Magnetic Microwires, J. Electron. Mater. 45 (2016) 226–234, doi:10.1007/s11664-015-4011-2.

[33] M. Churyukanova, V. Semenkova, S. Kaloshkin, E. Shuvaeva, S. Gudoshnikov, V. Zhukova, I. Shchetinin, A. Zhukov, Magnetostriction investigation of soft magnetic microwires, Phys. Status Solidi A 213 (2016) 363–367, doi:10.1002/pssa.201532552.

[34] Y. Kabanov, A. Zhukov, V. Zhukova, J. Gonzalez, Magnetic domain structure of wires studied by using the magneto-optical indicator film method, Appl. Phys. Lett. 87 (2005) 142507, doi:10.1063/1.2077854.

[35] D.B. Cullity, Elements of x-ray diffraction, 2-Edition: Addison-Wiley Publishing Company Reading (1978).

[36] Bruker Corporation, https://www.bruker.com/en/products-and-solutions/diffractometers and-scattering-systems/x-ray-diffractometers/d8-advance-family/d8-advance.html.

Part II: Results and discussion

3. Engineering of magnetic properties of Co-rich microwires

As mentioned before, non-existence of magnetocrystalline anisotropy in amorphous materials makes the magnetoelastic anisotropy the main source of magnetic anisotropy [1]. Magnetoelastic anisotropy depends on the magnetostriction coefficient, λ_s, and the applied and internal stresses (*eq. (1.1)*).

The λ_s sign and value of amorphous materials is mainly given by the chemical composition. Therefore, chemical composition modification allows to adjust λ_s sign and value [1,2]. Co-based alloys posses low magnetostriction values (up to $\lambda_s \approx -5 \times 10^{-6}$) and early zero magnetostriction values can be obtained doping Co-based alloys with Fe or Mn [1,2].

The other important parameter is the internal stresses, σ_i, value. Once the composition is chosen, the magnetic properties can be optimized by modifying the internal stresses with the selection of the sample geometry, described by the ρ-ratio between the metallic nucleus diameter, *d*, and the total microwire diameter, *D*, and the appropriate post-processing. In this chapter, Co-based microwires of different characteristics, i.e., compositions and diameters, and hence different magnetostriction coefficients, λ_s, will be presented with the description and discussion of the post-processing selected for them with the aim to optimize its magnetic softness and improve the Giant Magnetoimpedance (GMI) effect and domain wall dynamics.

The magnetic softness is intrinsically related to the GMI effect originated by the dependence of the skin depth, δ, of a magnetic conductor on applied magnetic field, *H*, as previously defined by *eq. (2.8)* [1]. For characterization of the GMI effect it will be used the GMI ratio, $\Delta Z/Z$, as defined in *eq. (2.9)* [1]. The GMI ratio optimization is linked to improvement of magnetic softness.

The influence of each controllable parameter in all the post-processing types selected has been studied, in order to get a complete overview of the adjusting parameters for the optimization of the magnetic properties.

Table 3.1 summarizes the main characteristics of the Co-rich microwires studied.

Table 3.1. *Compositions, geometry and magnetostriction coefficients of studied Co-rich glass-coated microwires.*

Sample Nº	***Composition***	***d* (μm)**	***D* (μm)**	**$\rho = d/D$**	**λ_s x 10^{-6}**
1	$Co_{69.2}Fe_{3.6}Ni_1B_{12.5}Si_{11}Mo_{1.5}C_{1.2}$	22.8	23.2	0.98	-1
2	$Co_{69.2}Fe_{4.1}B_{11.8}Si_{13.8}C_{1.1}$	25.6	30.2	0.85	-0,3
3	$Co_{65.4}Fe_{3.8}Ni_1B_{13.8}Si_{13}Mo_{1.35}C_{1.65}$	18.8	22.2	0.85	-1
4	$Co_{67}Fe_{3.9}Ni_{1.5}B_{11.5}Si_{14.5}Mo_{1.6}$	25.6	26.6	0.96	-0.29
5	$Co_{64.04}Fe_{5.71}B_{15.88}Si_{10.94}Cr_{3.4}Ni_{0.03}$	95	130	0.73	
6	$Co_{66}Cr_{3.5}Fe_{3.5}B_{16}Si_{11}$	20.1	24.8	0.81	

3.1. As-prepared Co-rich microwires

Figure 3.1a-d shows the hysteresis loops of 4 of the Co-rich microwires selected. The microwire samples have negative magnetrostriction coefficient and in as-prepared state exhibit quite soft magnetic properties, reflected in a typical linear and inclined hysteresis loop with low coercivity [1], below $H_c \approx 10$ A/m.

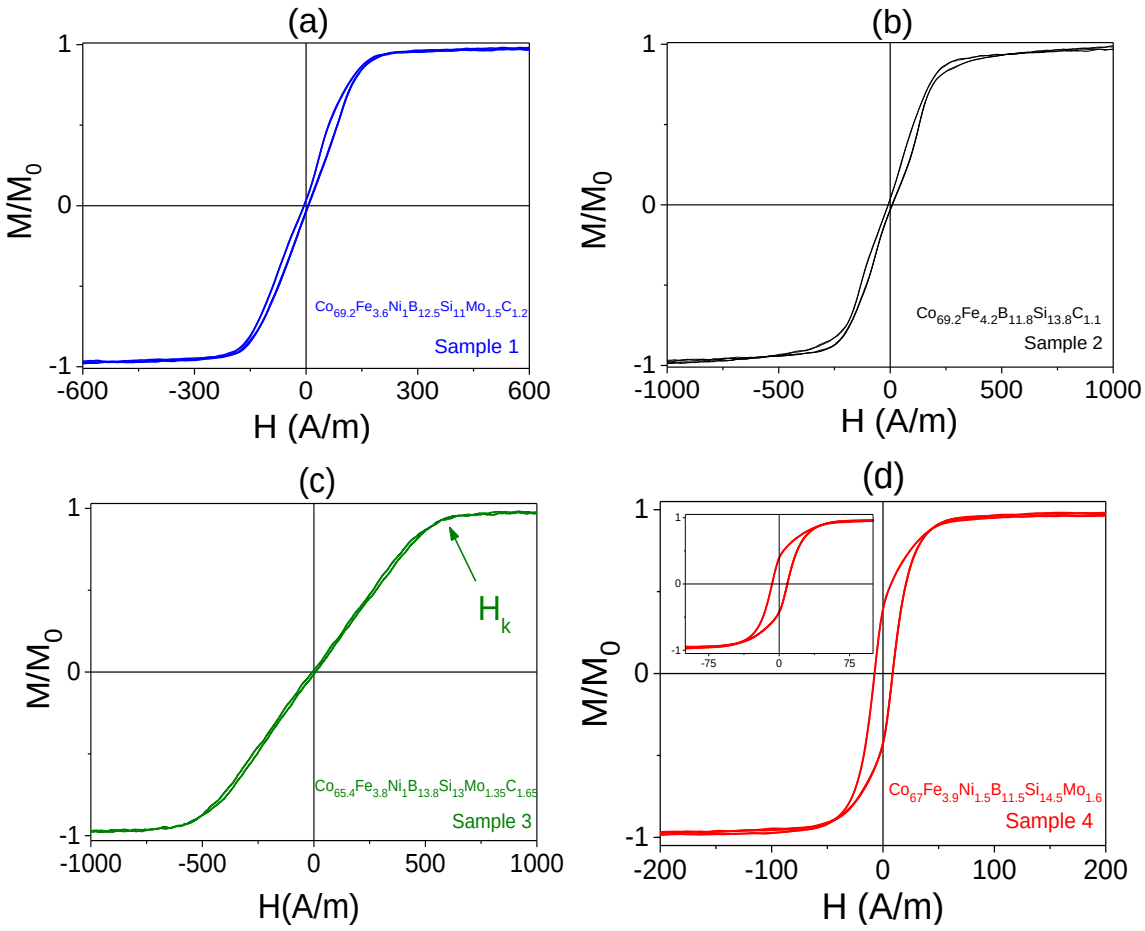

Figure 3.1. *Hysteresis loops of as-prepared $Co_{69.2}Fe_{3.6}Ni_1B_{12.5}Si_{11}Mo_{1.5}C_{1.2}$ (a), $Co_{69.2}Fe_{4.1}B_{11.8}Si_{13.8}C_{1.1}$ (b), $Co_{65.4}Fe_{3.8}Ni_1B_{13.8}Si_{13}Mo_{1.35}C_{1.65}$ (c) and $Co_{67}Fe_{3.9}Ni_{1.5}B_{11.5}Si_{14.5}Mo_{1.6}$ (d) microwires.*

X-ray diffraction (XRD) patterns of studied microwires present a wide halo, in as-prepared and annealed state, characteristic of completely amorphous materials [3], as can be seen in *Figure 3.2* for sample 3.

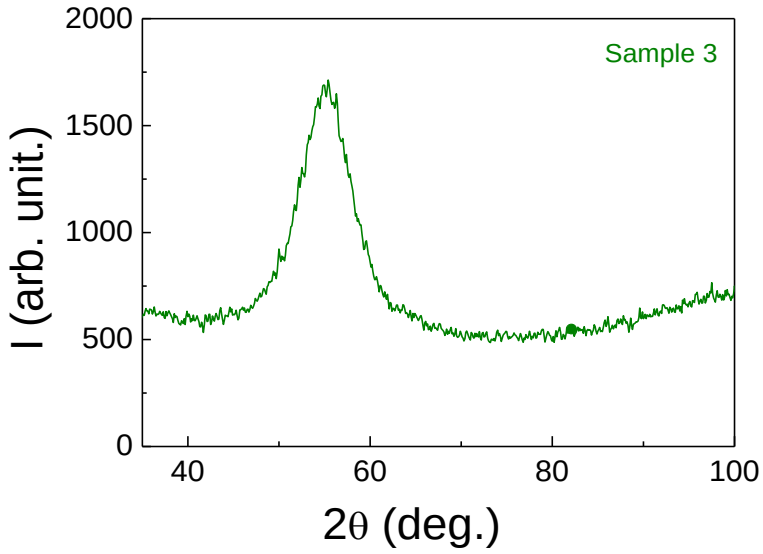

Figure 3.2. *XRD diffraction pattern of as-prepared* $Co_{65.4}Fe_{3.8}Ni_1B_{13.8}Si_{13}Mo_{1.35}C_{1.65}$ *microwire.*

From the studied microwires, in *Figure 3.3a* are presented the samples with similar composition for comparison of the evolution of the hysteresis loop with the ρ –ratio increase. In *Figure 3.3b* can be seen the decrease of the anisotropy field, H_k, as the ρ –ratio increases.

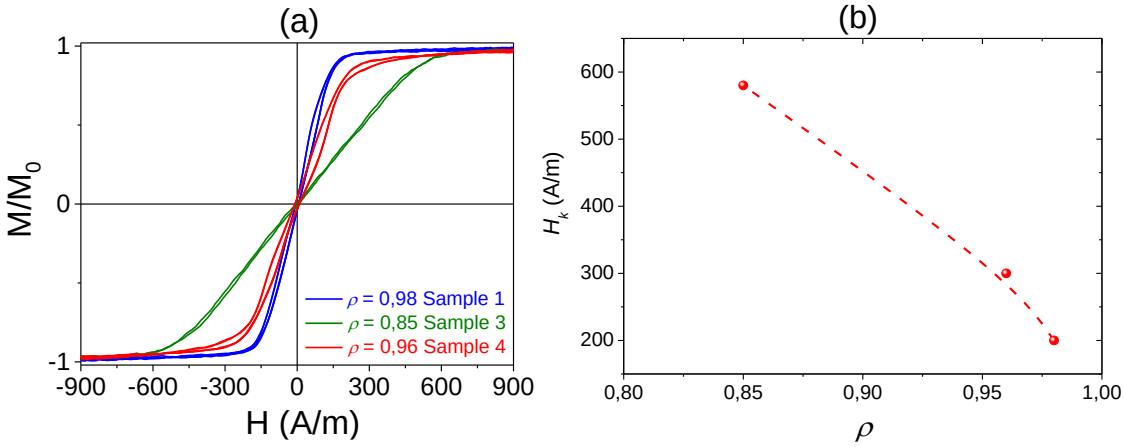

Figure 3.3. *Hysteresis loops of as-prepared Co-rich microwires of similar composition studied (a) and* $H_k(\rho)$ *dependence of microwires samples 1, 3 and 4 (b).*

3.2. Post-processing effect on magnetic properties, GMI effect and DW dynamics for Co-rich microwires

3.2.1. Conventional furnace annealing in Co-rich microwires

After annealing at sufficiently high temperature, similarly to reported results for Co-rich microwires with vanishing λ_s [4], the hysteresis loop shape turns into rectangular. $Co_{69.2}Fe_{3.6}Ni_1B_{12.5}Si_{11}Mo_{1.5}C_{1.2}$ microwires (sample 1) annealed at 250 °C and 350 °C during 60 min present considerable magnetic hardening, perfectly rectangular hysteresis loops with almost the same coercivity, $H_c \approx 90$ A/m, can be seen in

Figure **3.4**, for the different annealing temperatures, and an increase in the remanent magnetization, M_r, is observed.

The influence of the annealing temperature on GMI ratio presented in

Figure **3.4** was studied at a frequency of 200 MHz, given that Co-rich microwires present maximum GMI ratio values at a frequency, f, ranging from 100 to 200 MHz [5].

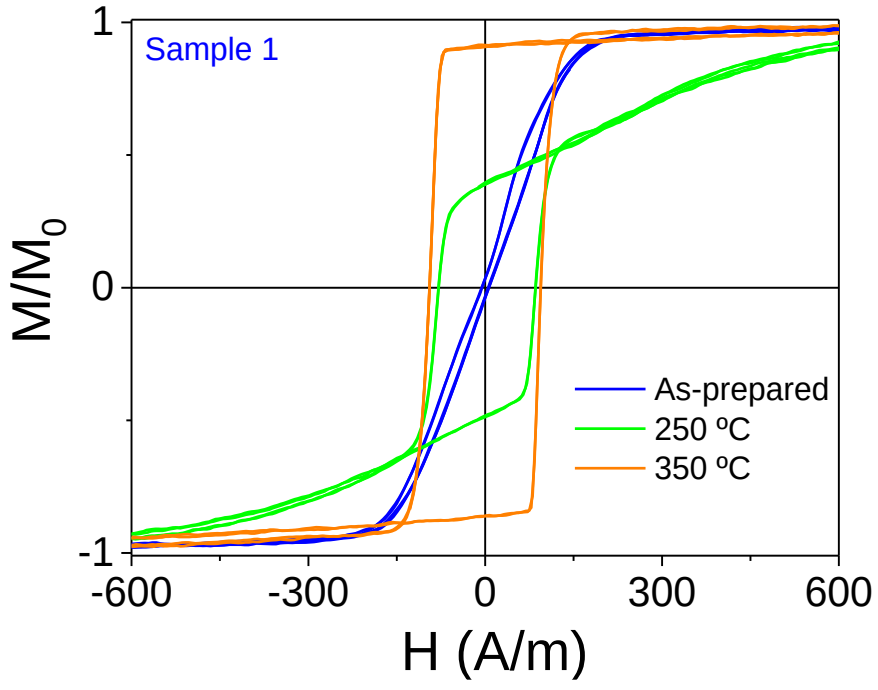

Figure 3.4. *Hysteresis loop of $Co_{69.2}Fe_{3.6}Ni_1B_{12.5}Si_{11}Mo_{1.5}C_{1.2}$ microwire as-prepared and annealed at different temperatures during 60 min.*

Similar tendency was observed in several Co-rich microwires with vanishing magnetostriction coefficient [1,4]. Consequently, observed tendency in hardening of Co-rich microwires and transformation of inclined hysteresis loops into rectangular is of general character.

ΔZ/Z(H) dependences observed in *Figure 3.5* show a decrease after annealing at 200 °C, however, annealing at higher temperatures, T_{ann} of 250 °C and 300 °C, give as a result an increase in the maximum GMI ratio, $\Delta Z/Z_{max}$. H_{max}, the field of maximum *ΔZ/Z(H)*, becomes lower with increasing the annealing time, changing *ΔZ/Z(H)* dependence shape, from the double-peak dependence shown in as-prepared and annealed at 200 °C samples to a shape of decay with the magnetic field increase presented for the samples annealed at higher annealing temperature, T_{ann}.

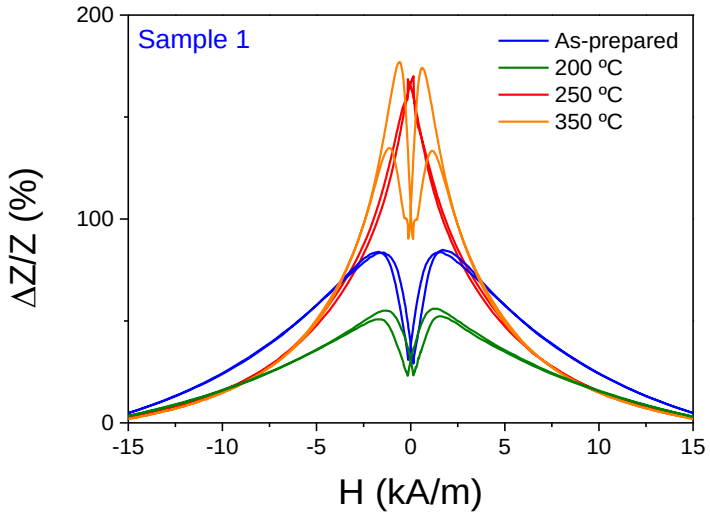

Figure 3.5. *ΔZ/Z(H) dependences measured at 200 MHz for $Co_{69.2}Fe_{3.6}Ni_1B_{12.5}Si_{11}Mo_{1.5}C_{1.2}$ microwire as-prepared and annealed at different temperatures during 60 min.*

ΔZ/Z(H) dependence shape, can be explained in terms of the magnetic anisotropy distribution of the microwire metallic nucleus and the skin penetration depth, δ, and its dependence on the frequency given by *eq. (2.8)* [1,6].

According to *eq. (2.8)*, δ as a function of the ratio between R_{DC}, the DC-resistance of the wire, and R_{AC}, the real component of the impedance, R_{DC}/R_{AC}, can be expressed as [7]:

$$\delta = r\left[1 - (1 - R_{DC}/R_{AC})^{1/2}\right] \quad (3.1)$$

where *r* is the wire radius.

The inner axially microwire radius, R_c, is related to the remanent magnetization and therefore, can be estimated from the reduced remanence, M_r/M_s, using the relation [1,3]:

$$R_C = r(M_r/M_S)^{1/2} \quad (3.2)$$

One of the important parameters for GMI effect characterization is the maximum GMI ratio, $\Delta Z/Z_{max}$, determined from the *ΔZ/Z(H)* dependencies [1,3].

$\Delta Z/Z_{max}$ evolution upon annealing, as it is reflected in *Figure 3.6*, for annealing temperatures of 250 °C and 300 °C gives higher $\Delta Z/Z_{max}$ values for the whole frequency range studied.

It is important to note, that for Co-rich microwires with magnetic bistability induced by annealing it was previously reported a decrease in the GMI ratio [4].

The magnetic hardening observed in

Figure **3.4** can be explained by the change of the magnetostriction coefficient from negative to positive associated to the internal stresses relaxation or to the domain structure modification consisting of the onset and growth of the inner axially magnetized single domain at the expense of the outer domain shell with transverse magnetic anisotropy [1,4,5]. Obviously, conventional furnace annealing cannot be considered as appropriate processing for magnetic softness improvement of Co-rich microwires.

Accordingly, additional efforts have been paid to improve magnetic softness of Co-rich microwires.

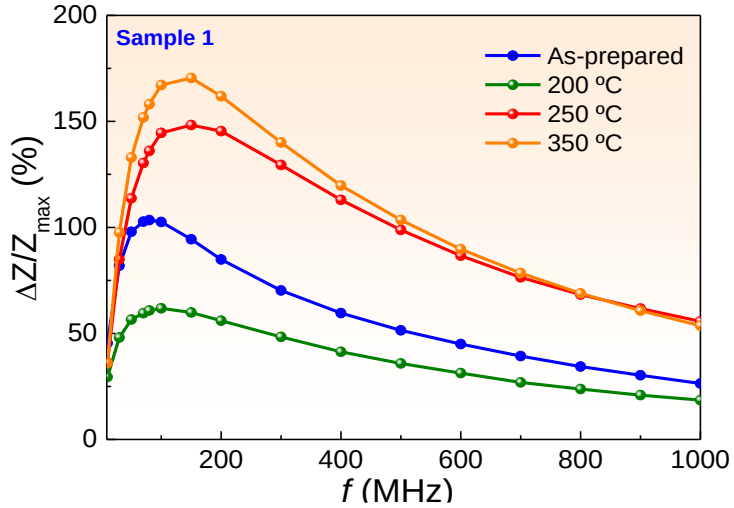

***Figure 3.6.** Maximum GMI ratio dependences on frequency for $Co_{69.2}Fe_{3.6}Ni_1B_{12.5}Si_{11}Mo_{1.5}C_{1.2}$ microwire as-prepared and annealed at different temperatures for T_{ann} = 60 min.*

3.2.2. Stress-annealing in Co-rich microwires

A systematic study of the influence of applied tensile stress during the annealing for different applied stresses, temperatures and annealing times was carried out for $Co_{69.2}Fe_{3.6}Ni_1B_{12.5}Si_{11}Mo_{1.5}C_{1.2}$ microwire, corresponding to labeled sample 1 and $Co_{69.2}Fe_{4.1}B_{11.8}Si_{13.8}C_{1.1}$, sample 2.

The tensile stress within the metallic nucleus, applied to the sample hanging a mechanical load to one end of the microwire during the sample heating and slow cooling within the furnace, has been evaluated following the equation previously described (*eq.(2.1)*):

$$\sigma_m = \frac{K \cdot P}{K \cdot S_m + S_{gl}} \tag{3.3}$$

being $K = E_2/E_1$, the ratio of the Young's moduli at room temperature of the metallic alloy, E_1, and the glass, E_2. P is the mechanical load applied and S_m and S_{gl} are the cross

sections of the metallic nucleus and glass coating, respectively. The applied stress within the metallic nucleus ranges from 0 to 472 MPa.

Similarly to the case shown in

Figure **3.4**, magnetic hardening is achieved upon conventional annealing [8]. The linear hysteresis loop of as prepared sample turns into rectangular (*Figure 3.7a*) for the sample annealed without applied stress, with an increase in the coercivity,

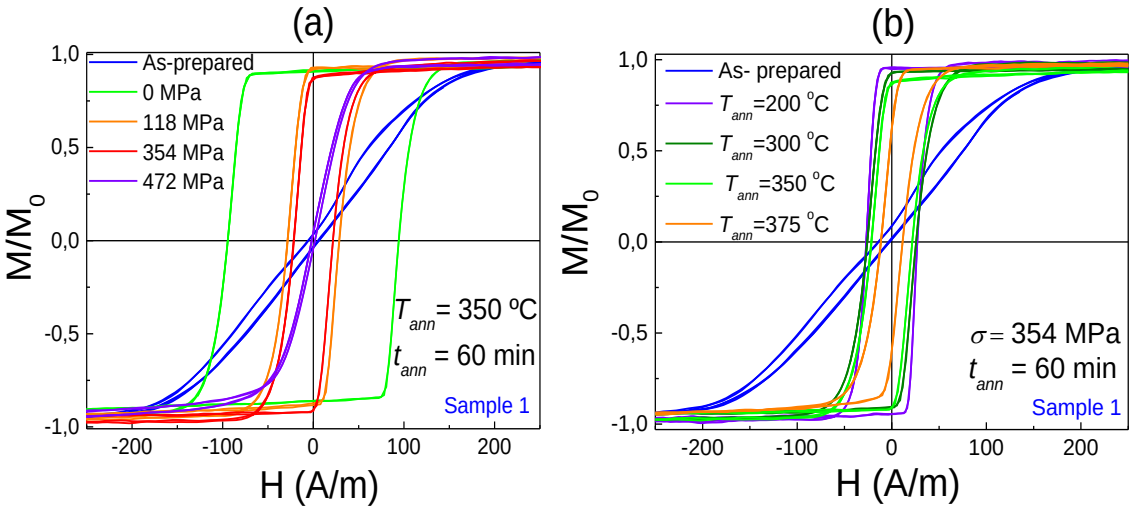

Figure 3.7. *Hysteresis loop of as-prepared and stress annealed with different applied stresses at 350 °C (a), as-prepared and stress annealed with 354 MPa at different temperatures (b)* $Co_{69.2}Fe_{3.6}Ni_1B_{12.5}Si_{11}Mo_{1.5}C_{1.2}$ *microwires.*

from $H \approx 5$ A/m up to $H_c \approx 93$ A/m.

Stress-annealing allows to manipulate the hysteresis loop character and the magnetic softness: at intermediate T_{ann} and σ_m with the application of stress during the annealing, the coercivity experiments a noticeable decrease and the remanent magnetization increases. *Figure 3.7b* shows the influence of the temperature in the stress-annealing treatment, coercivity decreases with the temperature increase.

This tendency changes with the increase of T_{ann} and σ_m, at T_{ann} = 300 ºC, H_c continues to decrease, while M_r/M_0 begins to decrease with increasing σ (see *Figure 3.8a*). Stress-annealed at T_{ann} = 300 ºC samples present rectangular hysteresis loops shape with rather low H_c (*Figure 3.8a*).

The comparison of the hysteresis loops of the sample conventionally annealed at 300 °C and stress-annealed (T_{ann} = 300 °C, σ = 472 MPa) presented in *Figure 3.8b* reflects better magnetic softness of the stress-annealed sample, with H_k ≈ 50 A/m, lower than the value observed for as-prepared sample, H_k ≈ 200 A/m.

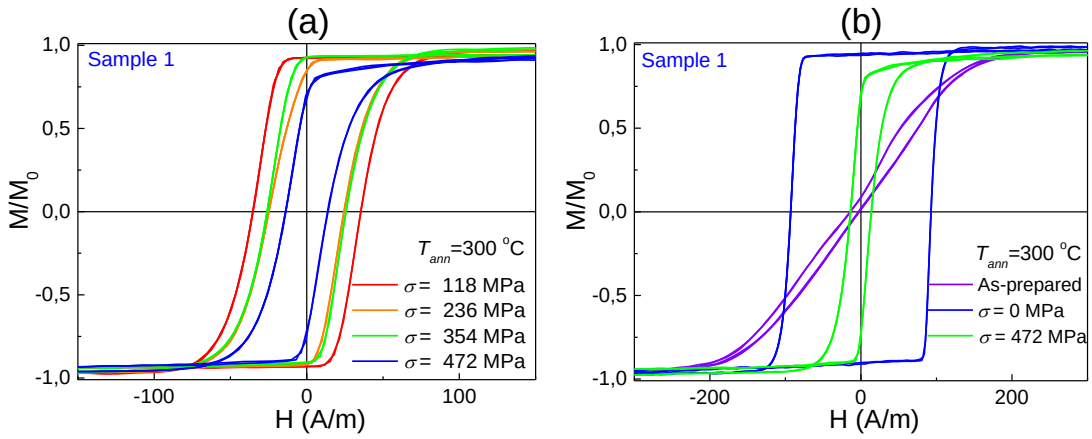

Figure 3.8. *Hysteresis loops of $Co_{69.2}Fe_{3.6}Ni_1B_{12.5}Si_{11}Mo_{1.5}C_{1.2}$ microwires stress-annealed at T_{ann} = 300 °C, 1 h (a) and hysteresis loops of as-prepared, annealed (T_{ann} = 300 °C, 1 h) and stress-annealed (T_{ann} = 300 °C, σ = 472 MPa) microwires (b).*

The increase in the annealing temperature, follows the same tendency of better magnetic softness for the stress-annealed sample as compared with annealed sample, as presented in *Figure 3.9*, where the temperature is set to T_{ann} = 325 °C. The influence of the variation of the stress applied during the annealing, evidences a remarkable decrease in H_c and M_r/M_0 (*Figure 3.9a*) with the increase in σ. The hysteresis loop of the stress-annealed microwire at higher applied stress is no more rectangular, with H_c ≈ 3 A/m and H_k ≈ 35 A/m (*Figure 3.9*).

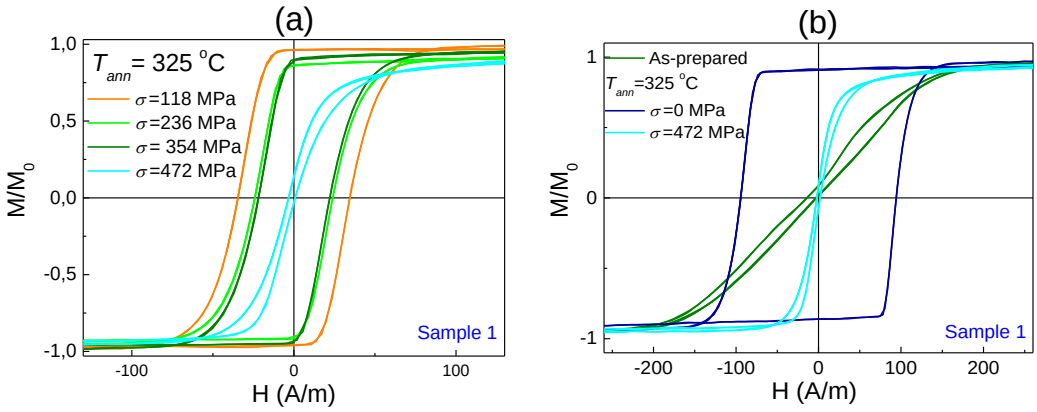

Figure 3.9. *Hysteresis loops of $Co_{69.2}Fe_{3.6}Ni_1B_{12.5}Si_{11}Mo_{1.5}C_{1.2}$ microwires stress-annealed at T_{ann} = 325 °C, 1 h (a) and hysteresis loops of as-prepared, annealed (T_{ann} = 325 °C, 1 h) and stress-annealed (T_{ann} = 325 °C, σ = 472 MPa, 1 h) microwires (b).*

Stress-annealed $Co_{69.2}Fe_{3.6}Ni_1B_{12.5}Si_{11}Mo_{1.5}C_{1.2}$ microwire at higher temperatures, T_{ann} = 350 ºC (*Figure 3.10*), exhibits a more remarkable coercivity decrease, with $H_c \approx 2$ A/m, for the sample stress annealed with σ = 472 MPa, however, in this case, $H_k \approx 50$ A/m [9].

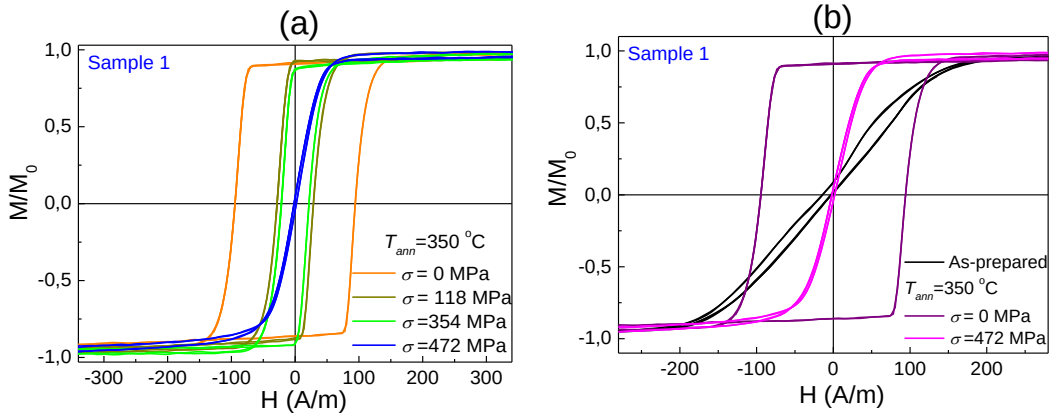

Figure 3.10. *Hysteresis loops of $Co_{69.2}Fe_{3.6}Ni_1B_{12.5}Si_{11}Mo_{1.5}C_{1.2}$ microwires annealed and stress-annealed at T_{ann} = 350 °C (a) and hysteresis loops of as-prepared, annealed (T_{ann} = 350 °C) and stress-annealed (T_{ann} = 350 °C, σ = 472 MPa) microwires (b).*

Correspondingly, above mentioned modification of the hysteresis loops induced by the stress annealing is affected by both T_{ann} and σ. As for the case of Fe-rich microwires [10], although at higher temperatures and stresses values than for Fe-rich microwires, the stress-annealing induces transverse magnetic anisotropy.

It can be expected that the stress-induced anisotropy, depending on the annealing temperature and the stress applied during the annealing, affects the GMI ratio dependences, which are discussed below.

A comparison of $\Delta Z/Z_{max}$ *(f)* dependencies for as-prepared and stress-annealed at 472 MPa $Co_{69.2}Fe_{3.6}Ni_1B_{12.5}Si_{11}Mo_{1.5}C_{1.2}$ samples is shown in *Figure 3.11a*. In spite of better magnetic softness of the stress-annealed at 472 MPa $Co_{69.2}Fe_{3.6}Ni_1B_{12.5}Si_{11}Mo_{1.5}C_{1.2}$ samples, they present similar $\Delta Z/Z_{max}$ -values.

Figure 3.11b shows the influence, at a fixed annealing temperature, of the stress applied during the annealing on the maximum GMI ratio, $\Delta Z/Z_{max}$ –values.

It is interesting that the optimum frequency for as-prepared sample is about 100 MHz, however, for stress-annealed samples the optimal frequency shifts to about 150 MHz. We can conclude that the stress-induced anisotropy allows tuning of both the GMI ratio value and the $\Delta Z/Z_{max}$ *(f)* dependencies.

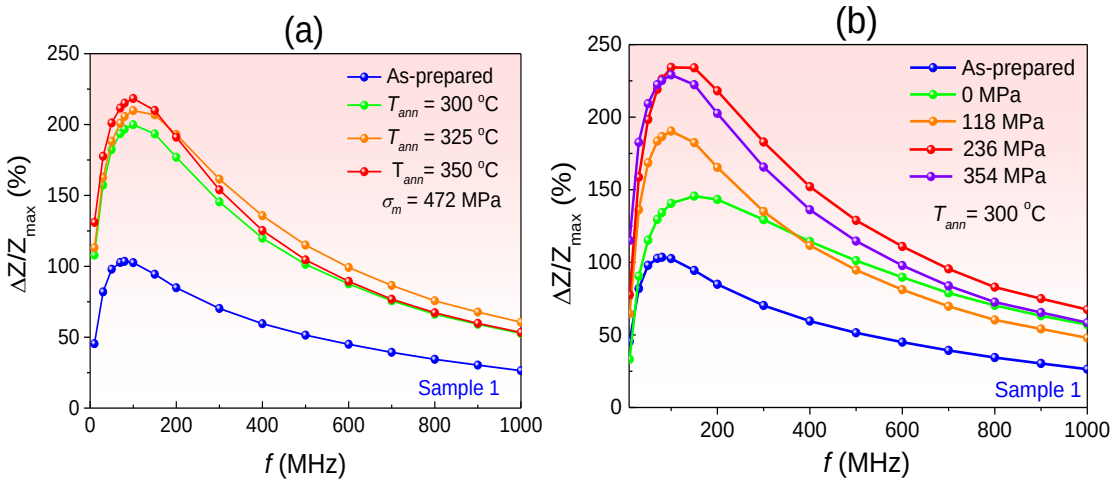

Figure 3.11. *$\Delta Z/Z_{max}$ (f) dependencies for as-prepared and stress-annealed $Co_{69.2}Fe_{3.6}Ni_1B_{12.5}Si_{11}Mo_{1.5}C_{1.2}$ samples at different annealing temperatures (a) and at 300 °C during 60 min for different applied stresses (b).*

For the study of the influence of the annealing time in the $\Delta Z/Z(H)$ and $\Delta Z/Z_{max}$ dependences $Co_{69.2}Fe_{4.1}B_{11.8}Si_{13.8}C_{1.1}$ microwire was employed.

After even short annealing of $Co_{69.2}Fe_{4.1}B_{11.8}Si_{13.8}C_{1.1}$ microwires, considerable magnetic hardening is achieved (see *Figure 3.12b*), coercivity rises by more than an order of magnitude and the hystereis loops transforms into rectangular, as compared with the behaviour displayed for as-prepared microwire, with almost anhysteretic hysteresis loop (see *Figure 3.12a*), typical for microwires with low negative magnetostriction values [11]. Stress-annealed $Co_{69.2}Fe_{4.1}B_{11.8}Si_{13.8}C_{1.1}$ microwires showed lower coercivity, H_c, as observed from *Figure 3.12c.*

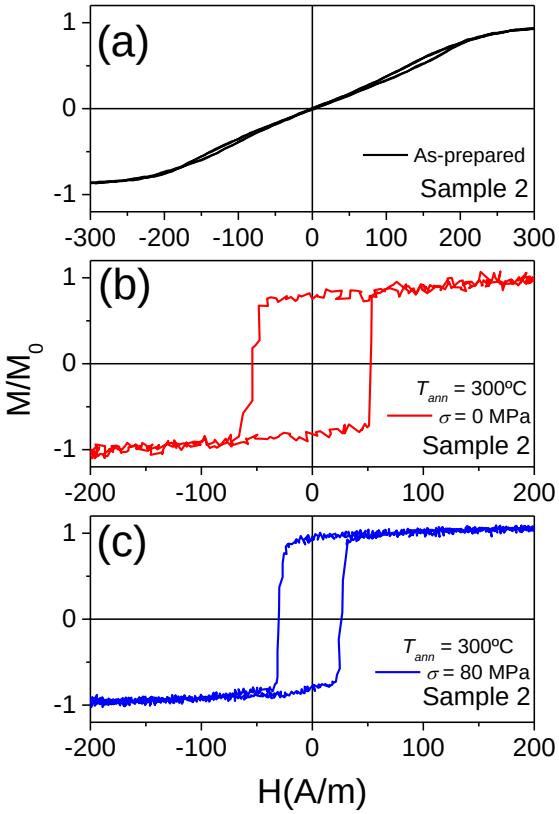

Figure 3.12. *Hysteresis loops of as-prepared (a), annealed at T_{ann} = 300 °C for σ = 0 MPa (b), and for σ = 80 MPa (c) $Co_{69.2}Fe_{4.1}B_{11.8}Si_{13.8}C_{1.1}$ microwires.*

The rectangular character observed for the hysteresis loop of stress-annealed $Co_{69.2}Fe_{4.1}B_{11.8}Si_{13.8}C_{1.1}$ microwire can be related to low enough σ_m-value (80 MPa).

$Co_{69.2}Fe_{4.1}B_{11.8}Si_{13.8}C_{1.1}$ microwire presents enhanced GMI effect as shown in *Figure 3.13* (GMI ratio up to 285%) with double peak behavior. This peak behavior is ascribed to circular magnetic anisotropy with high initial permeability and low coercivity.

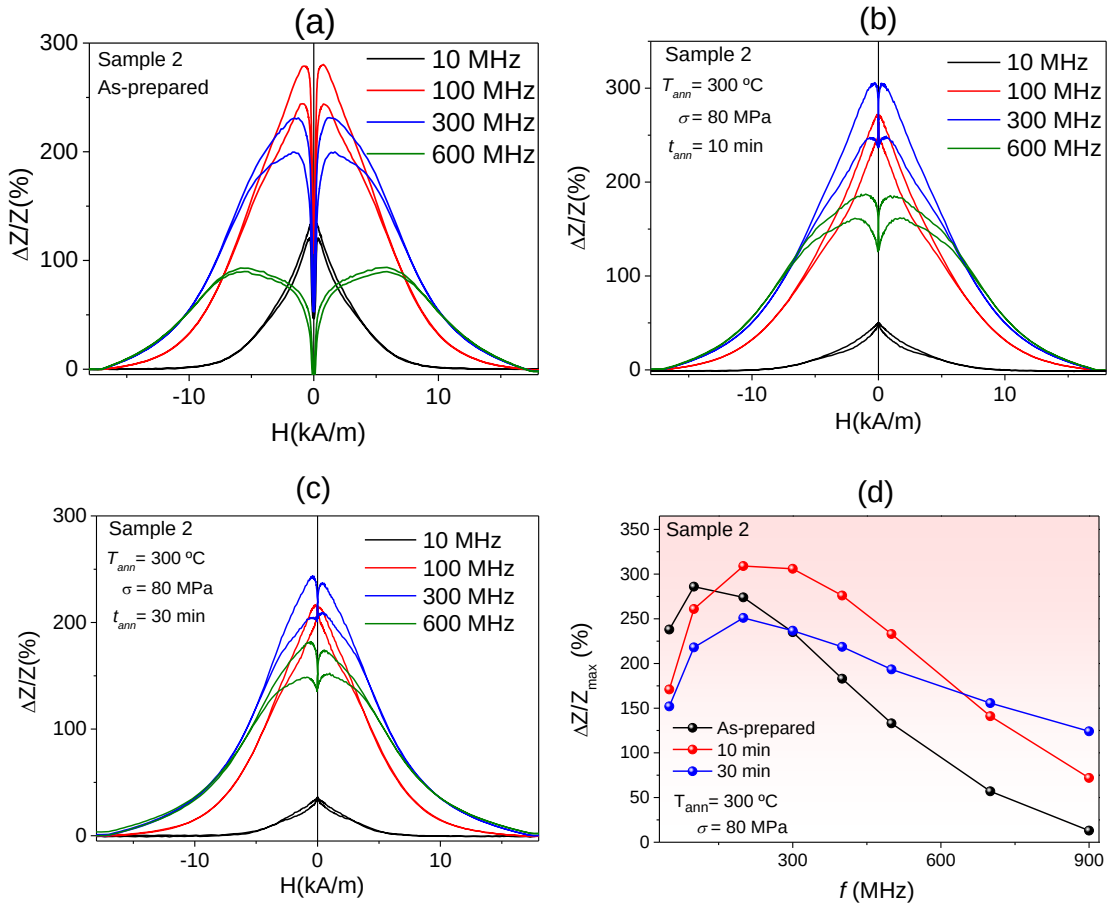

Figure 3.13. *ΔZ/Z(H) dependences of as-prepared (a), stress-annealed (T_{ann} = 300 ˚C, σ = 80 MPa) t_{ann} = 10 min (b), t_{ann} = 30 min (c), and $\Delta Z/Z_{max}$ (f) dependencies of as-prepared and stress annealed (d) $Co_{69.2}Fe_{4.1}B_{11.8}Si_{13.8}C_{1.1}$ microwires.*

Upon stress annealing at a fixed temperature (T_{ann} = 300 ˚C) and applied stress (σ_a = 80 MPa) for different annealing time, a noticeable modification of the *ΔZ/Z(H)* dependences has been observed (*Figure 3.13b-c*). $\Delta Z/Z_{max}$ at f = 100 MHz decreases from 280% to 265% and 250% for samples stress annealed at 10 min and 30 min, respectively. However, the samples stress-annealed present higher $\Delta Z/Z_{max}$ –values at higher frequencies (*Figure 3.13b-d*). *Figure 3.13d* shows maximum on $\Delta Z/Z_{max}$ *(f)* dependence at about 200 MHz for both stress-annealed samples. $\Delta Z/Z_{max}$ ≈ 310% is achieved for the stress-annealed sample for t_{ann} = 10 min (*Figure 3.13b-d*).

Moreover, *ΔZ/Z(H)* dependence exhibits single peak character at lower frequencies (10 MHz) associated with axial anisotropy induced upon stress annealing.

Observed frequency dependence on *ΔZ/Z(H)* can be related to the radial distribution of magnetic anisotropies in the core-shell domain structure [11]. In consequence, as can be seen in *Figure 3.13d,* GMI ratio optimization after stress-annealing of Co-rich microwires is achieved at frequencies above 400 MHz

Based on these observed dependencies, it can be concluded that stress annealing is an efficient method for improving the GMI effect for Co-rich microwires with low negative magnetostriction values.

3.2.3. Controlling the domain wall dynamics in Co-based magnetic microwires

The evolution of the hysteresis loops, presented in *Figure 3.8*, shows the annealing induced magnetic bistabilty, similar to other Co-rich microwires [4,12].

As seen in *Figure 3.8b*, as prepared sample presents a linear hysteresis loop with very low remanent magnetization, M_r, and in consequence, it does not exhibit single DW propagation. In contrast, annealed samples, present perfectly rectangular hysteresis loop, and hence, single DW propagation can be observed in the inner axially magnetized domain.

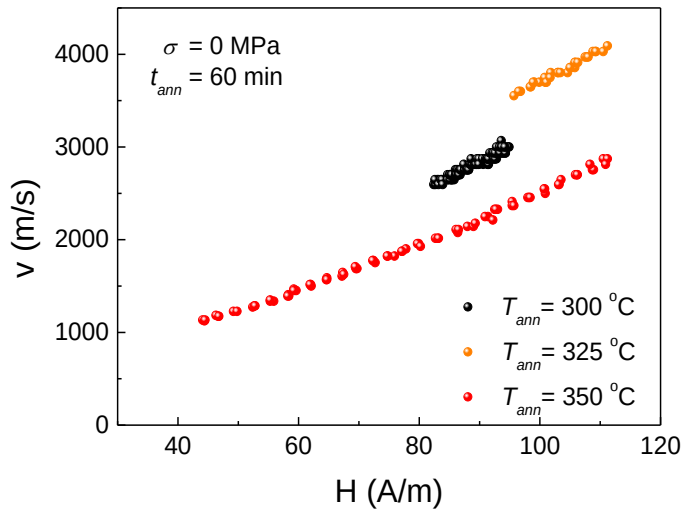

Figure. 3.14. *v(H) dependences measured for $Co_{69.2}Fe_{4.1}B_{11.8}Si_{13.8}C_{1.1}$ microwires annealed during t_{ann} = 60 min at different temperatures.*

Therefore, the DW propagation was measured for the samples presenting induced magnetic bistability. Obtained *v(H)* dependencies are presented in *Figure 3.14*, where it can be appreciated the influence of annealing temperature.

High DW velocity is observed for the microwires annealed at 325 ºC (see *Figure 3.14*) with a non-monotonic dependence of the DW velocity on the annealing temperature. The latter can be associated to the annealing influence on the sign and value of the magnetostriction coefficient, λ_s, [12]. As a rule, an increase of λ_s upon annealing is found for Co-based microwires [13].

Consequently, the annealing influence on the magnetoleastic anisotropy, i.e, stresses relaxation and magnetostriction coefficient modification, is reflected on the evolution of the DW dynamics and as well as in the GMI effect previously analyzed.

Stress annealing was presented as a useful tool for the improvement of the GMI effect. The stress-induced anisotropy is expected to affect both GMI ratio and DW dynamics.

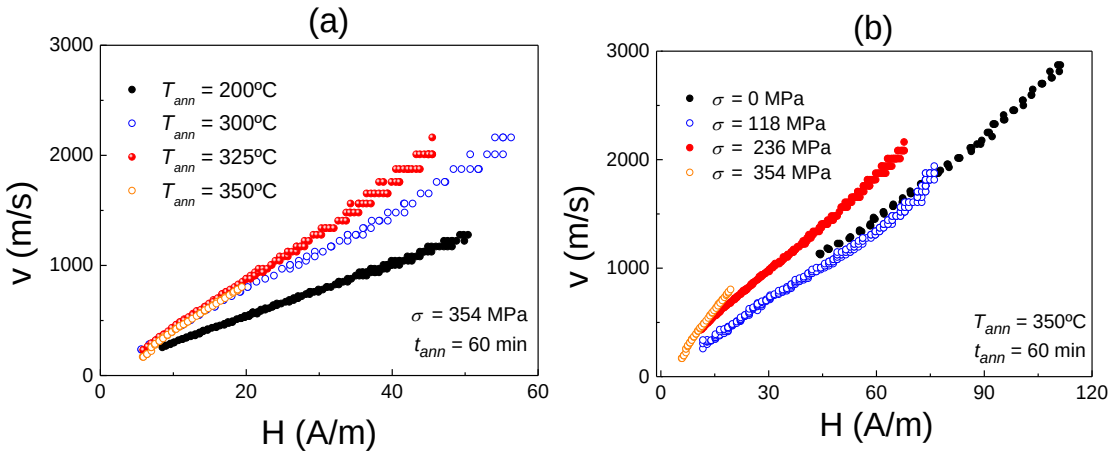

Figure 3.15. *v(H) dependences measured for $Co_{69.2}Fe_{4.1}B_{11.8}Si_{13.8}C_{1.1}$ microwires stress-annealed with 354 MPa at different T_{ann} (a) and for the sample annealed at T_{ann} = 350 ºC with different applied stresses during the annealing.*

At selected stress-annealing conditions, where the hysteresis loops shape remains rectangular, it can be assumed that the samples can present single domain wall propagation related to a single Barkhausen jump.

*Figure 3.15*a presents the influence of the annealing temperature for a fixed value of the applied stress during the annealing. It can be observed upon increase of the annealing temperature a gradual increase of the mobility, *S*, (slope of the curve) and the DW velocity. In the same way, in *Figure 3.15b* there is reflected an increase of *S* -values upon σ rising for a fixed T_{ann}.

Figure 3.16 shows the influence of the tensile stress applied during the annealing at T_{ann} = 300 ºC for t_{ann} = 60 min. All the samples present single DW propagation with almost perfectly linear *v(H)* dependencies (described by *eq. (1.2)*) and quite high DW velocities.

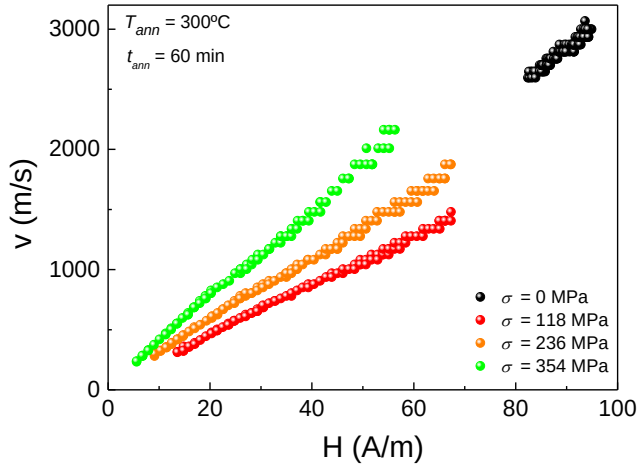

Figure 3.16. *v(H) dependencies for $Fe_{3.6}Co_{69.2}Ni_1B_{12.5}Si_{11}Mo_{1.5}C_{1.2}$ microwires annealed at T_{ann} = 300 ºC for t_{ann} =60 min without stress (σ_m = 0 MPa) and under different stresses.*

$Fe_{3.6}Co_{69.2}Ni_1B_{12.5}Si_{11}Mo_{1.5}C_{1.2}$ microwires annealed without stress present the highest DW velocity of about 3 km/s (*Figure 3.16*). However, the field range of single DW propagation is rather short (between 83 and 93 A/m). Extended field range is observed for stress-annealed $Fe_{3.6}Co_{69.2}Ni_1B_{12.5}Si_{11}Mo_{1.5}C_{1.2}$ microwires. DW velocity and *S* -values are affected by σ values, similarly to the case of T_{ann} = 350 ºC (*Figure 3.15b*). There is a gradual increase of the mobility upon increase of the stress applied during the annealing. The observed shift of the linear *v(H)* dependences of stress-annealed microwires with induced magnetic bistability to low field region (*Figure 3.15b* and *Figure 3.16*) is explained by the lower coercivity values of stress-annealed samples (see *Figure 3.8*).

3.2.4. Joule heating in Co-rich microwires

Throughout this section the influence of Joule heating on the magnetic properties of Co-based microwires and its comparison with conventional furnace annealing is systematically investigated. Accordingly, the experimental results of $Co_{69.2}Fe_{4.1}B_{11.8}Si_{13.8}C_{1.1}$ and $Co_{67}Fe_{3.9}Ni_{1.5}B_{11.5}Si1_{4.5}Mo_{1.6}$ microwires, samples 2 and 4, respectively, are presented.

The microwires were subjected to a series of current annealing treatments in which different currents were applied during different time. Direct current (DC) values for the heat treatments were selected clearly below the values that could produce hardening and/or crystallization of the samples, as described in annealing procedures section [14]. Current densities of 58.3 and 77.7 A/mm^2 were selected for time ranging from 3 to 20 minutes for both samples.

Accordingly, $Co_{69.2}Fe_{4.1}B_{11.8}Si_{13.8}C_{1.1}$ microwire (sample 1), with d = 22.8 µm, was subjected to currents of 24 and 32 mA. Hysteresis loops of current annealed samples are presented in *Figure 3.17*. Joule heated at I = 24 mA samples, *Figure 3.17a*, present similar character as hysteresis loops of as-prepared microwire, with low coercivity values. A slight decrease in the magnetic anisotropy field can be observed (*Figure 3.17c*).

Current annealed samples at I= 32 mA (*Figure 3.17b*), show similar behaviour, linear hysteresis loop with a decrease in H_k, that becomes more remarkable for t_{ann} = 10 min (*Figure 3.17c*).

Although Joule heating at $j \approx 80$ A/mm^2 causes a sample heating up to approximately 200 °C [12], as compared with conventional furnace annealing of studied microwire at 200 °C presented in *Figure 3.17b*, Joule heated samples present lower H_c.

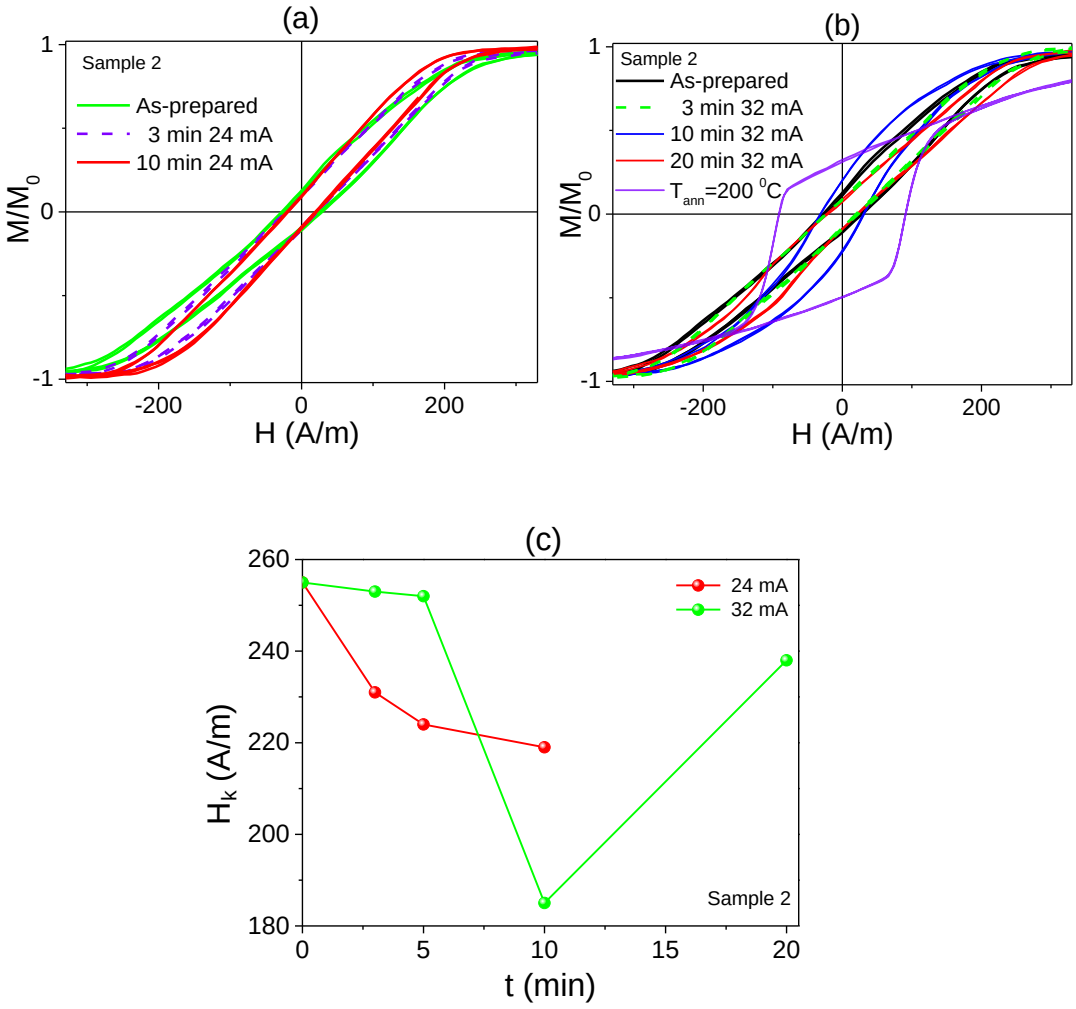

Figure 3.17. *Hysteresis loops of sample 1 as-prepared and Joule heated at 24 mA (a), Joule heated at 32 mA and annealed at 200 °C for 60 min (b) and H_k (t_{ann}) dependence evaluated from hysteresis loops of current annealed samples (c).*

Magnetic hardening observed for Co-rich microwires after conventional furnace annealing is avoided with current annealing, as is also observed in amorphous ribbons [14].

ΔZ/Z(H) dependence of Joule heated sample with *j* = 24 mA during 3 min, presented in *Figure 3.18a for f = 150 MHz*, shows a remarkable improvement of $\Delta Z/Z_{max}$ from $\Delta Z/Z_{max} \approx 100\%$ to $\Delta Z/Z_{max} \approx 300\ \%$, as compared to as-prepared sample.

Double-peak shape of *ΔZ/Z(H)* dependencies, similar to as-prepared sample, is observed for all Joule heated samples at all frequencies measured (see *Figure 3.18b* and *Figure 3.18c*, where results for Joule heating for t_{ann} = 3 min are shown).

The double-peak *ΔZ/Z(H)* dependence observed is associated to circumferential magnetic anisotropy and the maximum field, H_m, to magnetic anisotropy field [15]. Joule heated samples present lower H_m values than those of as-prepared sample (*Figure 3.18a*), that correlate with lower H_k values for Joule heated sample than for as-prepared, obtained from bulk hysteresis loops measured of both samples (see *Figure 3.17a,b*).

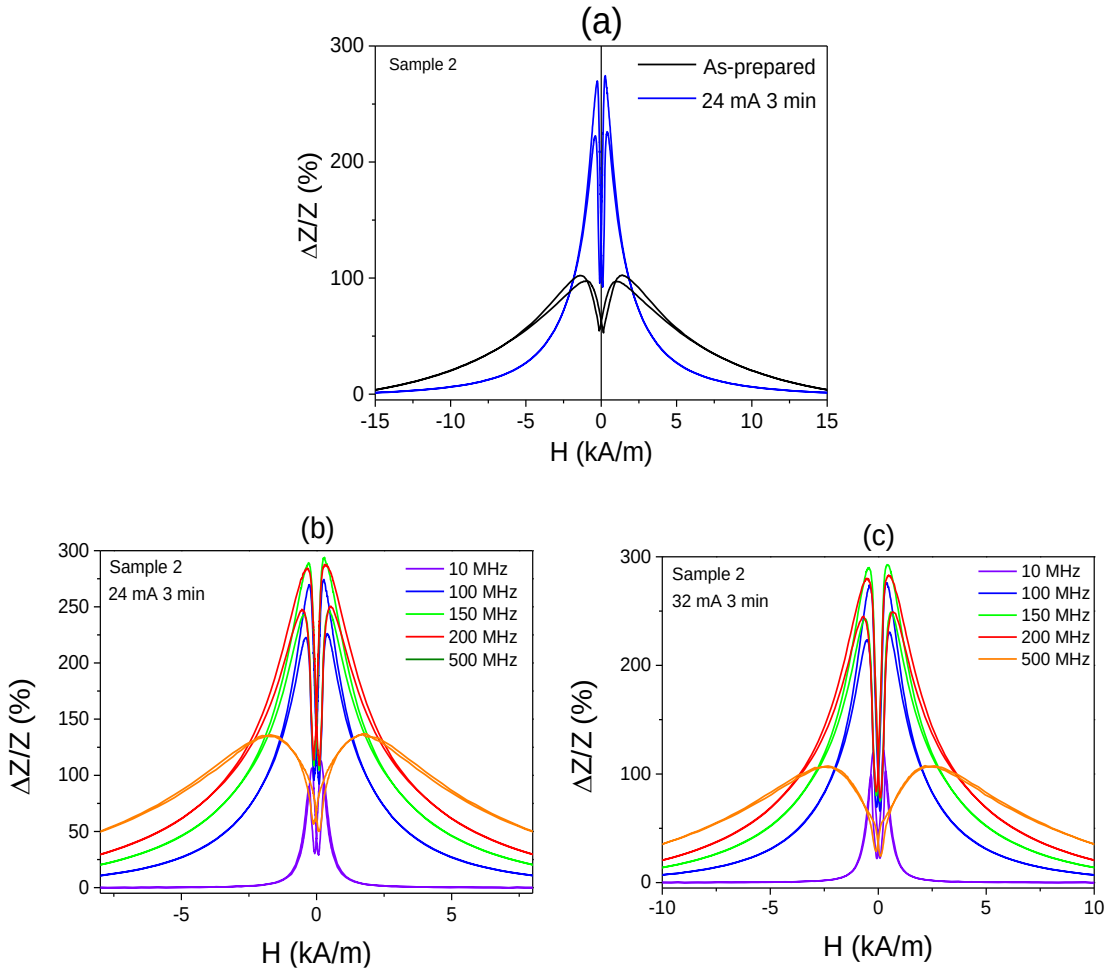

Figure 3.18. *$Co_{69.2}Fe_{4.1}B_{11.8}Si_{13.8}C_{1.1}$ microwire ΔZ/Z(H) dependencies measured in as-prepared and Joule heated (24 mA, 3 min) samples measured at 150MHz (a), ΔZ/Z(H) dependencies measured at different frequencies for Joule heated 3 min at 24 mA (b) and at 32 mA (c), respectively.*

Maximum GMI ratio, $\Delta Z/Z_{max}$, dependence on frequency presented in *Figure 3.19a* shows a GMI ratio improvement, with $\Delta Z/Z_{max}$ close to 300% for all current annealed samples in an extended frequency range. It is important to note, that the optimum frequency, at which maximum on $\Delta Z/Z_{max}(f)$ dependence is observed is

shifted to higher frequencies of about 150-200 MHz as compared to as prepared sample, in which such maximum takes place at a frequency of about 100 MHz (*Figure 3.19a*).

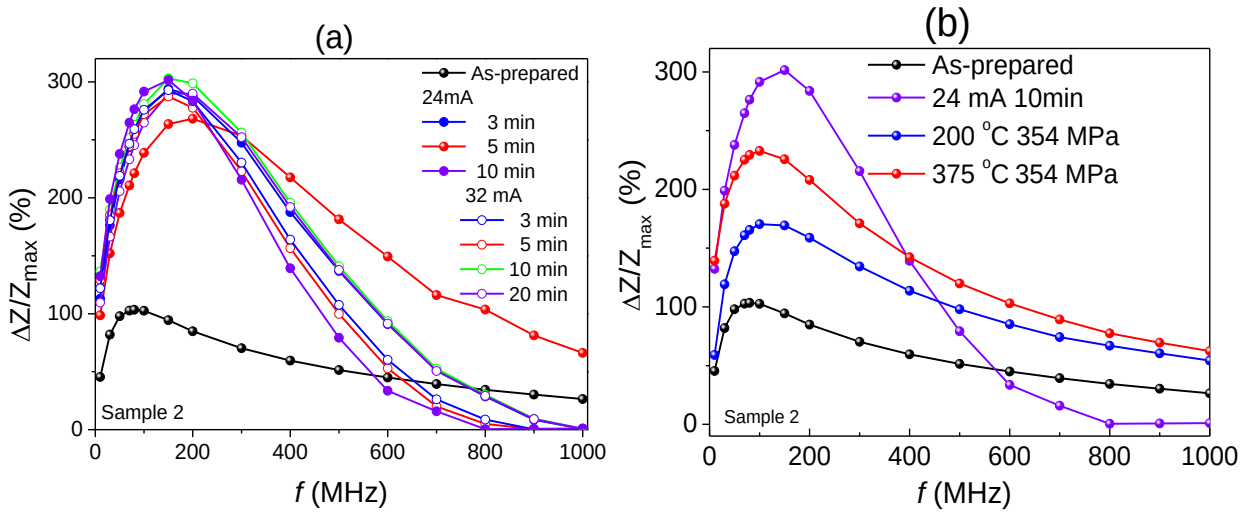

Figure 3.19. *$Co_{69.2}Fe_{4.1}B_{11.8}Si_{13.8}C_{1.1}$ microwire $\Delta Z/Z_{max}$ (f) dependences observed in as-prepared and Joule heated at different annealing conditions samples (a) and $\Delta Z/Z_{max}$ (f) dependencies of as-prepared, stress-annealed (T_{ann} = 200 and 375 °C, with 354 MPa, for 60 min) and Joule annealed (24 mA, 10 min) samples (b).*

Comparison of $\Delta Z/Z_{max}$ *(f)* dependencies of as-prepared, stress-annealed and Joule heated samples presented in *Figure 3.19b* reflects the beneficial influence of Joule heating, Joule heated sample presents the highest $\Delta Z/Z_{max}$ -value up to f = 400 MHz.

Influence of Joule heating on the hysteresis loops and GMi effect for $Co_{67}Fe_{3.9}Ni_{1.5}B_{11.5}Si_{14.5}Mo_{1.6}$ microwire, sample 4, is studied below. The hysteresis loops of the samples current annealed are presented in *Figure 3.20*, coercive field, H_c, and effective anisotropy field, H_k, evaluated from the knee area just before the approach of magnetization saturation, M_s, were obtained from the hysteresis loops and compiled in *Table 3.2*.

Current annealed $Co_{67}Fe_{3.9}Ni_{1.5}B_{11.5}Si_{14.5}Mo_{1.6}$ glass coated microwires present extremely soft magnetic properties. The samples current annealed at 30 mA for 3 min and 5 min present the lowest coercivities of about 2 A/m and $H_k \approx 32$ A/m, as can be seen from H_k evolution with Joule heating time, in *Figure 3.18d*. Increasing the annealing time a slight increase in the coercivity and the anisotropy field is observed. The character of the hysteresis loop remains the same for longer current annealed time [16]. Similar behaviour is observed for the sample current annealed at 40 mA.

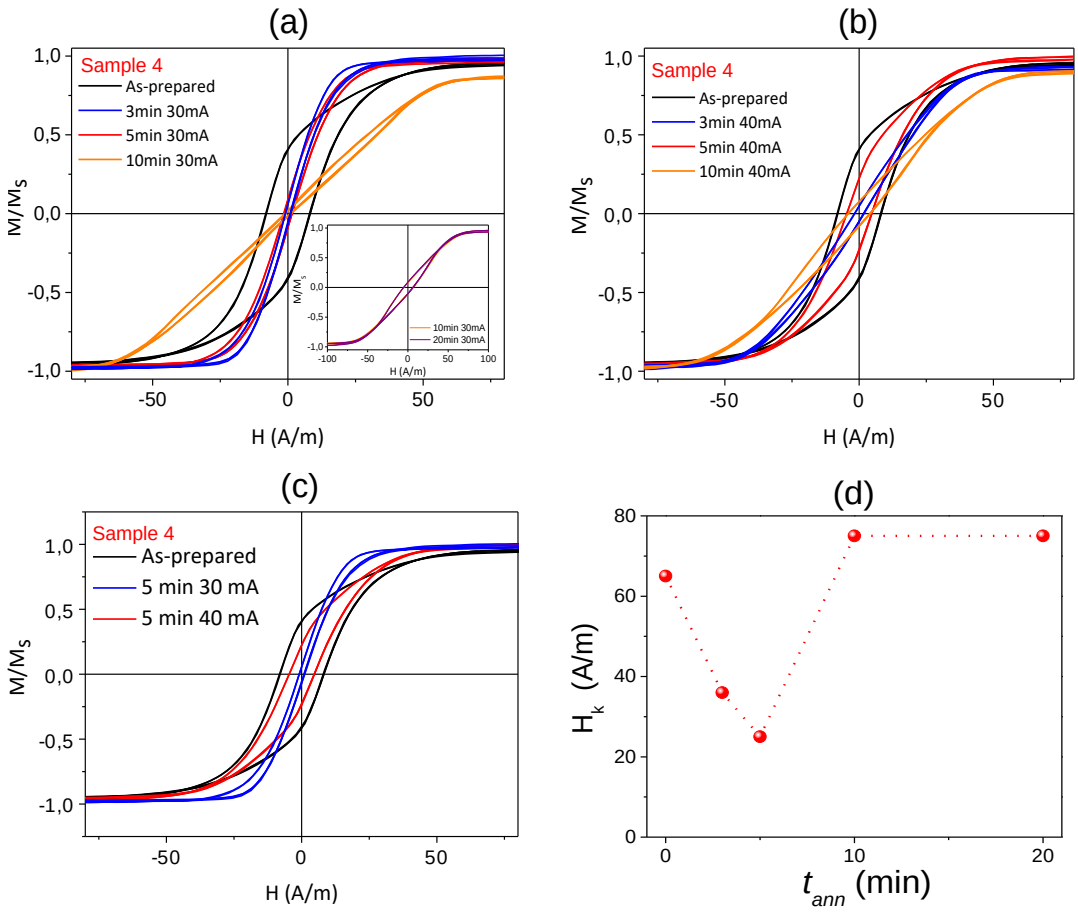

Figure 3.20. *Hysteresis loops of $Co_{67}Fe_{3.9}Ni_{1.5}B_{11.5}Si_{14.5}Mo_{1.6}$ microwires Joule heated at 30 mA for 3, 5, 10 and 20 min (inset) (a), Joule heated at 40 mA for 3, 5 and 10 min (b) and comparison between the hysteresis loops of the sample Joule heated at 30 mA and 40 mA for 5 min (c) and H_k dependence on Joule annealing time for I = 30 mA (d).*

Table 3.2. *Magnetic properties of studied $Co_{67}Fe_{3.9}Ni_{1.5}B_{11.5}Si_{14.5}Mo_{1.6}$ microwires subjected to different post-processing.*

Post-processing type	***I applied (mA)***	***Duration (min)***	***H_c (A/m)***	***H_k (A/m)***
As-prepared			7	65
Joule heated	30	3	2	32
		5	2	32
		10	6	75
		20	6	75
	40	3	5	50
		5	5	55
		10	4	63
Annealed (T_{ann} = 300 °C)		60	6	21

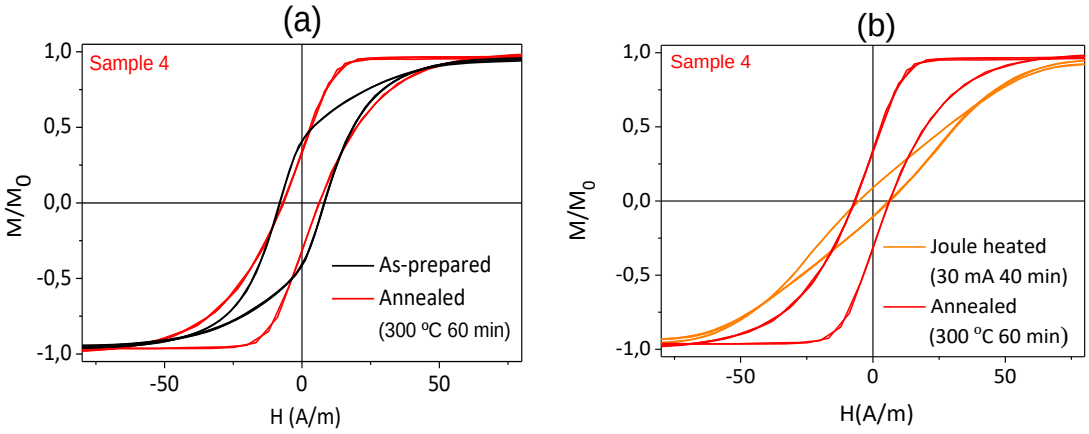

Figure 3.21. *Hysteresis loops of $Co_{67}Fe_{3.9}Ni_{1.5}B_{11.5}Si1_{4.5}Mo_{1.6}$ microwire as-prepared and annealed at 300°C 60 min (a) and annealed at the same conditions and current annealed with 30 mA for 40 min (b).*

The results obtained for $Co_{67}Fe_{3.9}Ni_{1.5}B_{11.5}Si_{14.5}Mo_{1.6}$ microwire annealed in conventional furnace, at 300 °C during 60 min (*Figure 3.21a*) and its comparison with Joule heated sample with 30 mA during 40 min (*Figure 3.21b*) show that in contrast to Joule heated sample, conventional annealing leads to a drastic magnetic hardening of the sample [17].

ΔZ/Z(H) representation of as-prepared and current-annealed $Co_{67}Fe_{3.9}Ni_{1.5}B_{11.5}Si_{14.5}Mo_{1.6}$ microwires gives as a result a double-peak dependence (*Figure 3.22*) typically reported for Co-rich microwires with low negative magnetostriction coefficient and weak circumferential magnetic anisotropy [15,18]. Even in as-prepared state, $Co_{67}Fe_{3.9}Ni_{1.5}B_{11.5}Si_{14.5}Mo_{1.6}$ microwire presents high *ΔZ/Z(H)* values with a maximum GMI ratio, $\Delta Z/Z_{max}$, of about 550% at a frequency of 300 MHz (*Figure 3.22* and *Figure 3.23*).

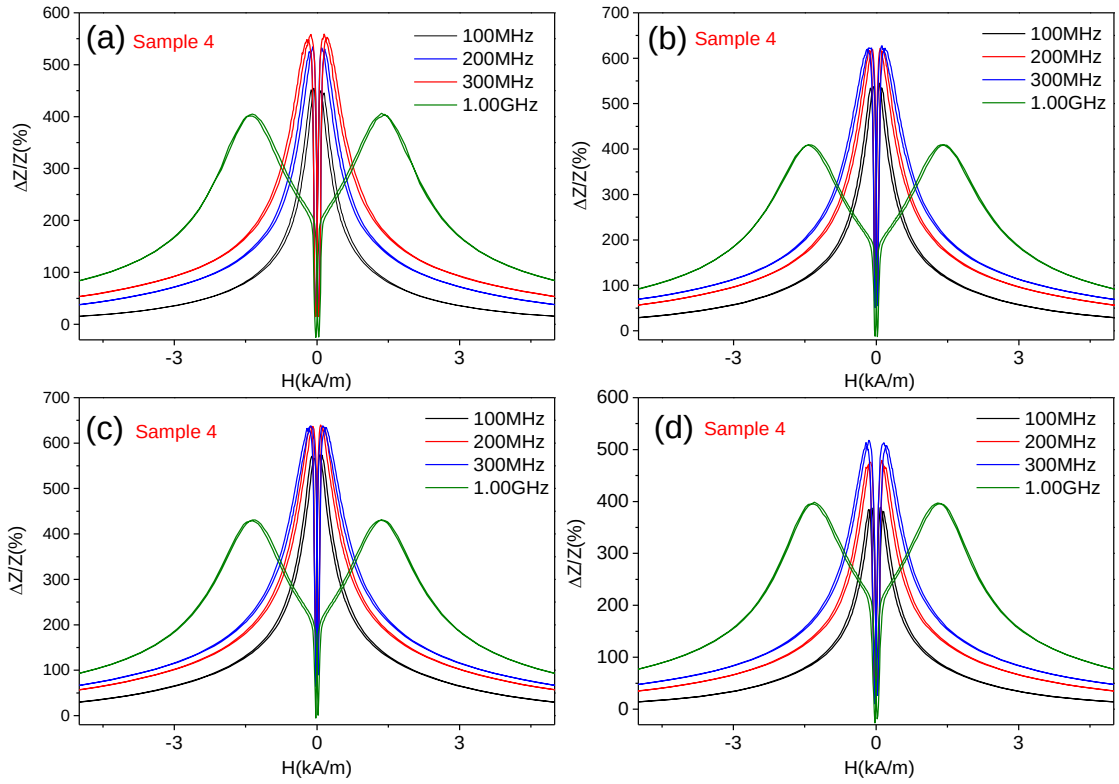

Figure 3.22. *ΔZ/Z(H) dependences for $Co_{67}Fe_{3.9}Ni_{1.5}B_{11.5}Si_{14.5}Mo_{1.6}$ microwire as-prepared (a) current annealed at 40 mA for 3 min (b), 5 min (c) and 10 min (d) measured at different frequencies.*

An increase in the GMI ratio is observed after Joule-heating at the selected conditions. Highest GMI ratio enhancement is attained for short current-heating times as can be appreciated in *Figure 3.22*, for samples annealed at 30 and 40 mA during 3 min and 5 min, related to the magnetic softening observed in the hysteresis loops of current annealed microwires at these conditions. The highest $\Delta Z/Z_{max}$ value of about

650% is obtained for sample current-annealed at 40mA during 5 minutes. An increase in the annealing time correlates with a decrease in $\Delta Z/Z_{max}$ (*Figure 3.22d*).

A noticeable improvement of the GMI ratio is obtained for the whole MHz frequency range. The optimum frequency moves from 300 MHz for as-prepared sample to 200 MHz for current-annealed ones.

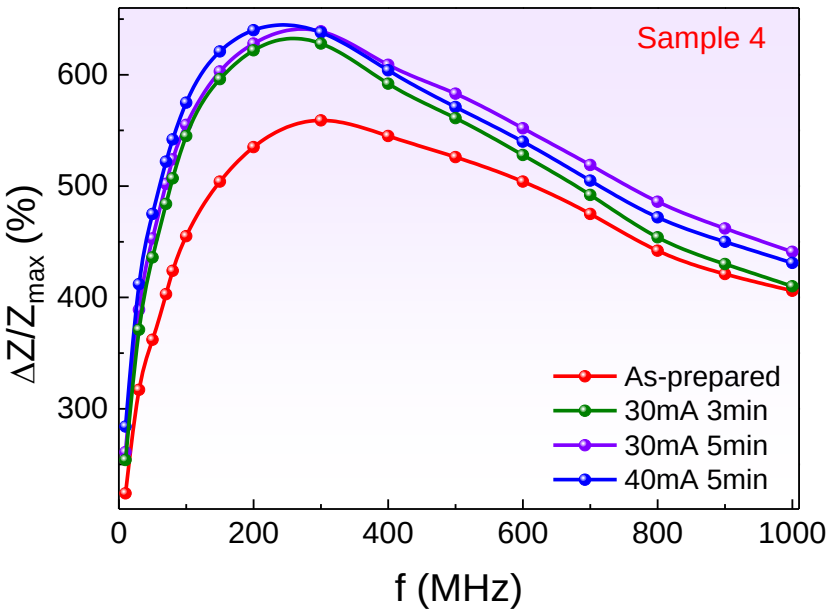

Figure 3.23. *Maximum GMI ratio dependences on frequency for $Co_{67}Fe_{3.9}Ni_{1.5}B_{11.5}Si1_{4.5}Mo_{1.6}$ microwire as-prepared and current annealed at different conditions.*

In the current annealing process, the sample, besides the heating, is affected by the circumferential magnetic field associated to the current flowing through it. The circumferential magnetic field, H_{circ}, produced from the current passing through the microwire (Oersted's law) can be estimated in the metallic nucleus as following [3]:

$$H_{circ} = I/2\pi r \tag{3.4}$$

with I the current value and r the radial distance.

H_{circ} values change to zero to its maximum value at the surface of the microwire, which is the one involved in the GMI effect. Obtained values for the studied microwire for the applied currents are $H_{circ} \approx 0.375$ kA/m and 0.5 kA/m for I = 30 mA

and 40 mA respectively, these values are well above H_k values extracted from the hysteresis loops (see *Figure 3.20* and *Table 3.*). Therefore, the magnetization near the surface can be affected by the circumferential magnetic field during the current annealing process that prevents the magnetic hardening of conventional annealing leading to the magnetic softening observed.

Magnetic anisotropy induced by the circumferential magnetic field and stresses relaxation explain the evolution of magnetic properties and GMI ratio dependences.

3.2.5. Effect of tensile stress in Co-rich microwires

We have evaluated the influence of applied stress for $Co_{65.4}Fe_{3.8}Ni_1B_{13.8}Si_{13}Mo_{1.35}C_{1.65}$ (d = 18.8 μm, D = 22.2 μm) glass coated microwires (sample 3). This sample was subjected to a series of applied stresses in as-prepared state, by means of a mechanical load attached to one end of the microwire (sample length of 10 cm). The applied stresses value, σ, ranges from 0 to 472 MPa.

Crystallization temperature of the sample, T_{cr} ≈ 554 °C, was determined by DSC measurements [19].

From *Figure 3.24* it can be seen that the hysteresis loop character does not change under applied stresses, nevertheless the anisotropy field, H_k, increases with the increase in the applied stress.

The representation of H_k versus σ (*Figure 3.25a*) gives as a result a linear dependence, in accordance with the magnetoelastic anisotropy, K_{me}, expression for low magnetostrictive amorphous materials [20], given by *eq. (1.1)*, and its relation with the anisotropy field [21]:

$$\lambda_S = \mu_0 M_S (H_k / 3\sigma) \tag{3.5}$$

being $\mu_o M_s$, the saturation magnetization.

In order to analyze the linear dependence of the magnetostriction coefficient on the applied stresses we have to take into account the expression [22]:

$$\lambda_{S,\sigma} = \lambda_{S,0} - B\sigma \tag{3.6}$$

where $\lambda_{s,\sigma}$ is the magnetostriction coefficient under applied stress, $\lambda_{s,0}$ is the magnetostriction coefficient value when there is no applied stress and *B* is a positive constant of the order of 10^{-10} MPa.

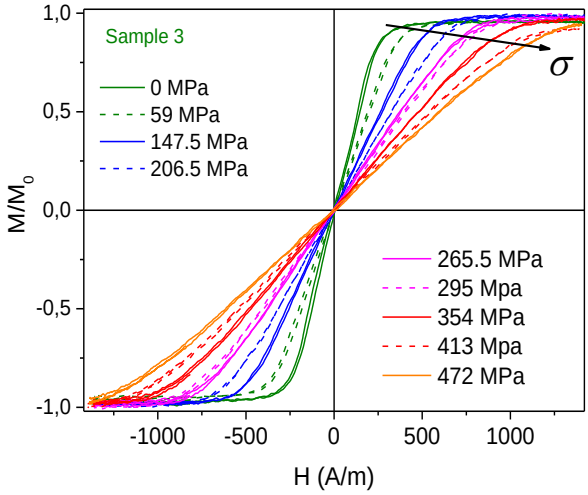

Figure 3.24. *Hysteresis loops of as-prepared and subjected to different applied stresses $Co_{65.4}Fe_{3.8}Ni_1B_{13.8}Si_{13}Mo_{1.35}C_{1.65}$ microwire.*

From *eq.* (*3.5*), it can be explained that for Co-rich microwires with negative magnetostriction coefficient the stress application produces a further decrease in λ_s, with the subsequent linear increase of the anisotropy field observed.

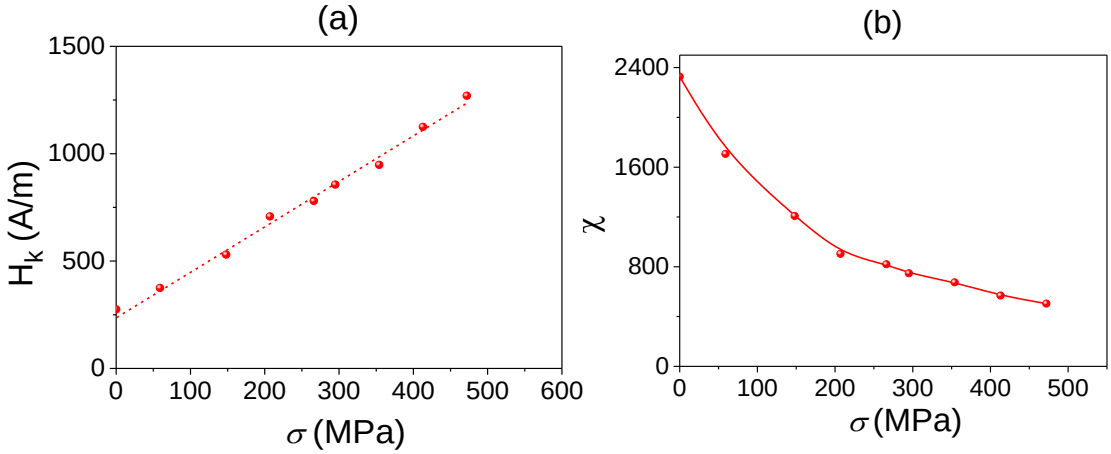

Figure 3.25. *Anisotropy field H_k dependence on applied stresses (a), and magnetic susceptibility, χ, dependence on applied stresses (b) of as-prepared $Co_{65.4}Fe_{3.8}Ni_1B_{13.8}Si_{13}Mo_{1.35}C_{1.65}$ microwire.*

Since the saturation magnetization, $\mu_o M_s$, of studied $Co_{65.4}Fe_{3.8}Ni_1B_{13.8}Si_{13}Mo_{1.35}C_{1.65}$ microwire is about 0.8 T [23], we calculate the magnetic susceptibility, χ, as a function of the applied stress in *Figure 3.25b*, where a monotonous decrease with the increase in the value of the applied stress can be observed.

3.2.5.1. Tuning of DW dynamics in Co-rich microwires by applied tensile stress

Stress dependence of the DW dynamics for $Co_{69.2}Fe_{4.1}B_{11.8}Si_{13.8}C_{1.1}$ microwires with annealing induced magnetic anisotropy is studied in *Figure 3.26*.

A considerable increase in the DW velocity upon applied tensile stress can be observed. Such stress dependence of DW dynamics, reported for various Co-rich microwires with annealing-induced magnetic bistability [24], is opposite to that reported for magnetic microwires with positive λ_s [25]. Additionally, high *v*-values (up to 3.5 km/s) can be observed in such Co-rich microwires.

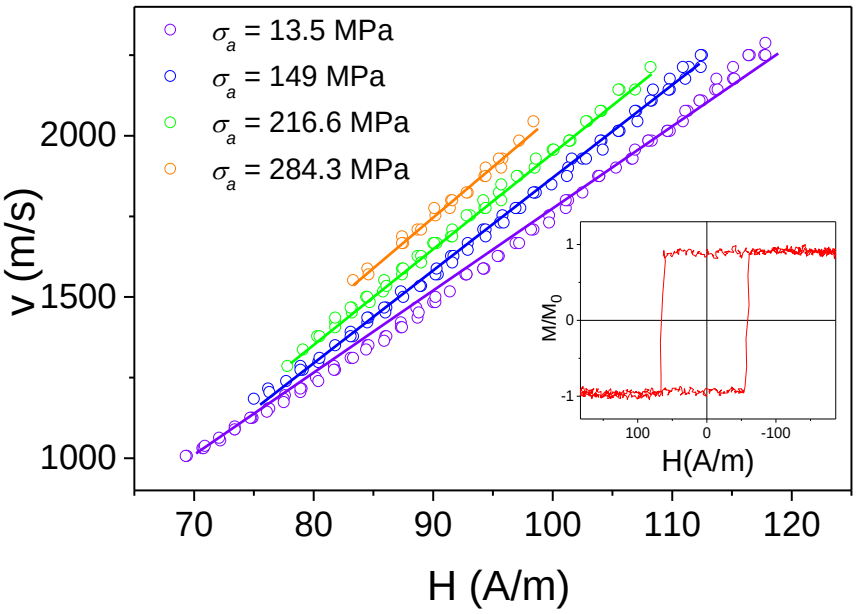

Figure. 3.26. *v(H) dependencies of $Co_{69.2}Fe_{4.1}B_{11.8}Si_{13.8}C_{1.1}$ microwires annealed at T_{ann} = 300 °C for 45 min measured under different applied tensile stresses. Hysteresis loop of the microwire annealed (T_{ann} = 300 °C for 45 min) (inset).*

3.2.6. Graded magnetic anisotropy in Co-rich microwires

The main interest in magnetic materials with graded magnetic anisotropy is the possibility to control the spatial distribution of the magnetic anisotropy. Such graded anisotropy has been proposed for the DW propagation engineering either by controllable DW injection or trapping [10,26].

Usually, graded magnetic anisotropy is obtained by chemical composition modification during the sample fabrication [27,28]. The magnetic properties tunability by stress-annealing at variable temperature was recently proposed for the development of Fe-rich microwires with graded magnetic anisotropy [10].

As we have seen above, and similarly to Fe-rich microwires, stress-annealing can considerably modify the magnetic properties of Co-rich microwires [8,9]. For this reason, it is expected that stress-annealing of Co-rich microwires at variable temperature will allow obtaining graded magnetic anisotropy in Co-rich microwires.

For the studies of graded magnetic anisotropy $Co_{64.04}Fe_{5.71}B_{15.88}Si_{10.94}Cr_{3.4}Ni_{0.03}$ (sample 5: d = 95 μm, D = 130 μm) and $Co_{66}Cr_{3.5}Fe_{3.5}B_{16}Si_{11}$ (sample 6: d = 20.1 μm, D = 24.8 μm) glass-coated microwires, prepared using Taylor-Ulitovsky method were selected.

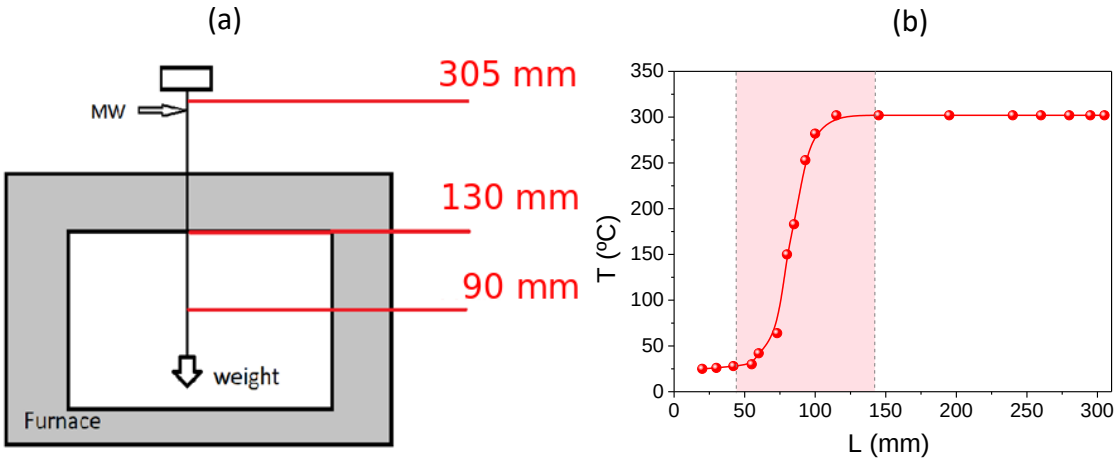

Figure 3.27. Diagram of the assembly for the microwire stress-annealing treatment at variable T (a) and temperature distribution inside the furnace (b).

The annealing at variable temperature was performed as follows: 30 cm long microwire was furnace annealed under tensile stress, $\sigma \approx 500$ MPa (sample 5) and 400 MPa (sample 6), created by a mechanical load attached to one of the microwire ends (*Figure 3.27a*). The magnitude of the applied stress σ, was selected considering the different Young moduli of the metallic nucleus and glass coating of the microwire as before described [8,9].

For the annealing treatment one end of the microwire sample was inserted into the furnace through the orifice to the central zone of the furnace where temperature, *T*, is constant, while the opposite sample end was kept outside the furnace.

By means of a commercial (NiCr-Ni) thermocouple it was measured the temperature distribution (with *T* set at 300 °C) inside the furnace and in the orifice, through which the sample is introduced (*Figure 3.27b*). Therefore, the part of the microwire placed outside the furnace was subjected to tensile stress, while the microwire portion placed inside the furnace was stress-annealed (part with constant *T* and the part of the sample placed in the temperature gradient zone was stress-annealed under variable *T)*.

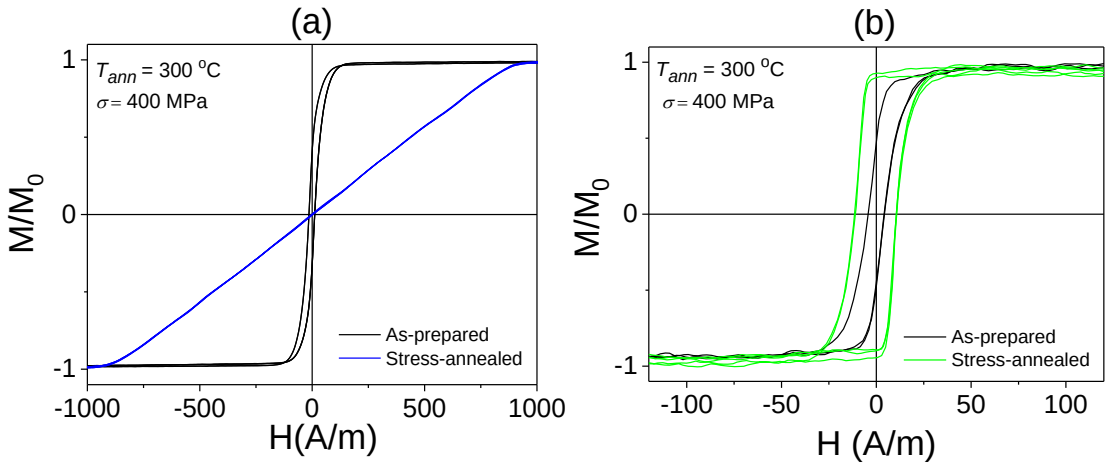

Figure 3.28. *Effect of stress-annealing at T_{ann} = 300 °C on hysteresis loops of sample 5 (σ = 500 MPa) (a) and for sample 6 (σ = 400 MPa) (b).*

Both as-prepared microwire samples present excellent magnetic softness with low coercivity, H_c, 14 A/m and 3 A/m and magnetic anisotropy field, H_k, 100 A/m and 40 A/m, for sample 5 and sample 6, respectively, typical of amorphous materials (see

Figure 3.28a and *Figure 3.28b*). Like for previously studied Co-rich microwires, a modification of the hysteresis loops of studied microwires is observed upon stress-annealing as can be seen in *Figure 3.28*.

Figure 3.28a shows the effect of stress-annealing at T_{ann} = 300 ºC in sample 5, there is a decrease in the coercivity, to almost unhysteretic loop, and the anisotropy field increases up to $H_k \approx$ 900 A/m. The observed modification of the hysteresis loop upon stress-annealing must be related to the transverse character of the induced magnetic anisotropy by stress-annealing and magnetization process by magnetization rotation.

On the other hand, the opposite tendency is observed for the sample 6, the hysteresis loop turns into almost perfectly rectangular with $H_c \approx$ 11 A/m (see *Figure 3.28b*).

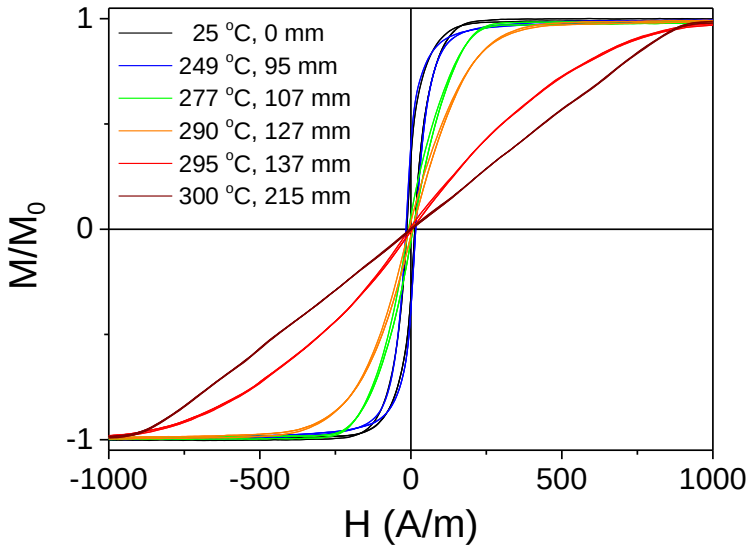

Figure 3.29. *Hysteresis loops of sample 5 stress-annealed (σ = 500 MPa) at variable T_{ann}. T_{ann} are evaluated from Figure 3.23b.*

The difference observed in the effect of stress-annealing on the hysteresis loops of both samples (see *Figure 3.28a* and *Figure 3.28b*) can be associated to the different value of the applied stresses. It has been recently reported [8,9], that even for the same Co-based microwire, the anisotropy induced by stress-annealing is considerably affected by the σ–values (the character of the induced anisotropy of

$Fe_{3.6}Co_{69.2}Ni_1B_{12.5}Si_{11}Mo_{1.5}C_{1.2}$ microwire stress-annealed for $\sigma \geq 470$ MPa changes form axial to transverse) [8,9]. Furthermore, the difference in the hysteresis loops of both stress-annealed samples can be also related to the difference in chemical compositions and thus different λ_s –values.

As previously shown, the stress-annealing induced magnetic anisotropy of microwires depends on the annealing conditions, T_{ann}, t_{ann} and σ [10]. Consequently, stress-annealing of Fe- rich microwires under temperature gradient was satisfactorily employed for obtaining controllable spatial distribution of the magnetic anisotropy [10].

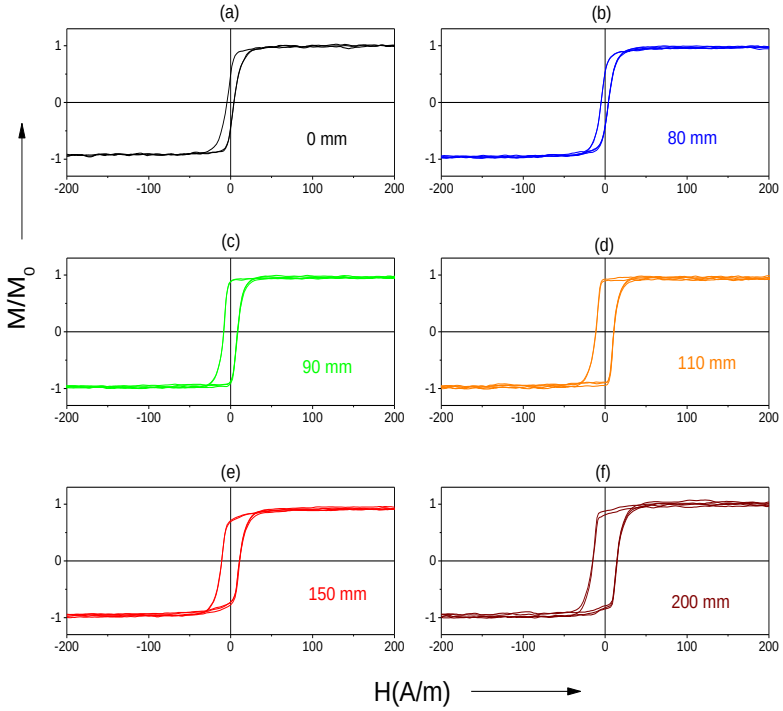

Figure 3.30. *Hysteresis loops of sample 6 stress-annealed (σ = 400 MPa) at variable T_{ann}. T_{ann} evaluated from Figure 3.23b are: 25 °C (a); 160 °C (b); 251 °C (c); 290 °C (d); 295 °C (e) and 300 °C (f), respectively.*

The same concept is used for studied Co-rich microwires. In fact, as can be seen in *Figure 3.29* and *Figure 3.30*, there is a gradual modification of the hysteresis loop (measured by the short pick-up coil along the samples length) of both samples stress-annealed at variable T_{ann}.

As has been evaluated from the hysteresis loops (shown in *Figure 3.29* and *Figure 3.30*), both samples present variation of the magnetic properties along the wires length that correlate with T_{ann} gradient during the stress-annealing. Accordingly,

Figure 3.31a and *Figure 3.31b* show the evolution of the hysteresis loops in terms of remanent magnetization, M_r/M_0, and magnetic anisotropy field, H_k, variation along the microwire length, *L,* for sample 5.

Likewise, *Figure 3.32* shows the evolution of the hystereis loops of sample 6 subjected to stress-annealing in T_{ann} gradient, reflected in M_r/M_0, and coercivity, H_c, variation along the microwire length.

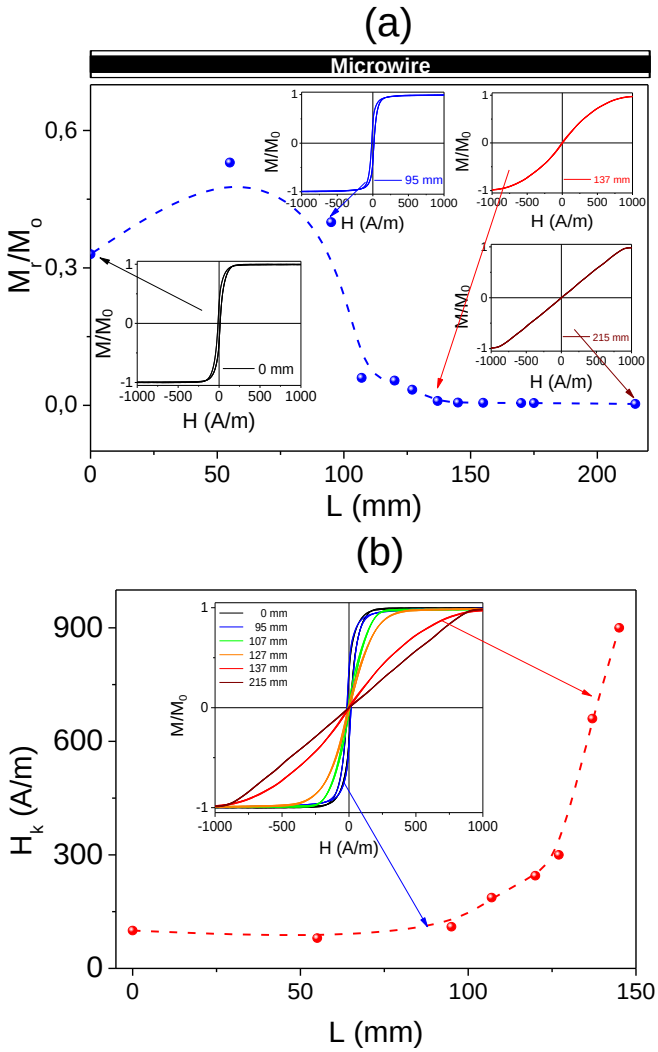

Figure 3.31.*Variation of M_r/M_0 (a) and H_k (b) along the sample length in the sample 5 annealed at variable T_{ann}. The lines are just guides for the eyes.*

The evolution upon stress-annealing under T_{ann} gradient presents features similar to those reported for stress-annealing induced anisotropy in Co-based microwires [29]. Both samples present an increase in M_r/M_0 followed by a decrease with T_{ann} increasing.

The hysteresis loops modification is explained by the microwires domain structure, which is affected by the λ_s value and sign, the internal stresses distribution and the shape magnetic anisotropy. As a consequence, axial magnetization alignment is promoted by the exchange energy contribution, especially relevant for thin and long enough magnetic microwires, with high shape anisotropy [30,31].

The internal stresses origin in glass-coated microwires is explained taking into account that in addition to quenching internal stresses, σ_{iq}, arising from the rapid melt quenching itself, there are two more internal stresses contributions: the difference in thermal expansion coefficients of the metallic alloy and the glass coating, σ_{it}, and the drawing stresses, σ_{id}, [32,33]. Different theoretical approaches and indirect experimental results (e.g., effect of glass-coating etching, influence of applied stresses) manifest that the σ_{it} contribution arising from the difference in thermal expansion coefficients of metal and glass is the most relevant [15,31]. Correspondingly, $\sigma_{it} \gg \sigma_{iq}$ and $\sigma_{it} \gg \sigma_{id}$.

The value of internal stresses is affected by the microwire geometry: glass-coating thickness, metallic nucleus diameter, *d*, and total microwire diameter, *D*. In the most simplified approximation σ_{it} has been expressed as [34]:

$$\sigma_\phi = \sigma_r = P = \frac{\varepsilon E k \Delta}{\left(\frac{k}{3}+1\right)\Delta} + \frac{4}{3}; \quad \sigma_z = P(k+1)\Delta + \frac{2}{(k\Delta+1)} \qquad (3.7)$$

where σ_ϕ, σ_r and σ_z are circular, radial and axial stresses, $\Delta = (1-\rho^2)/\rho^2$, $k = E_g/E_m$, E_m, E_g- Young modulus of metallic nucleus and glass, respectively, $\varepsilon = (\alpha_m - \alpha_g)(T_m - T_{room})$, α_m, α_g are thermal expansion coefficients of metallic nucleus and glass, respectively, and T_m, T_{room} are melting and room temperatures.

Therefore, the hysteresis loops variation, seen in *Figure 3.31* and *Figure 3.32*, is the result of the balance between the shape magnetic anisotropy, the magnetoelastic anisotropy and the stress-annealing induced anisotropy.

According to the core-shell domain structure model the modification in M_r/M_o along the microwire can be associated with the change in the inner axially magnetized core radius, R_c, related with M_r/M_o, by *eq. (3.2)*.

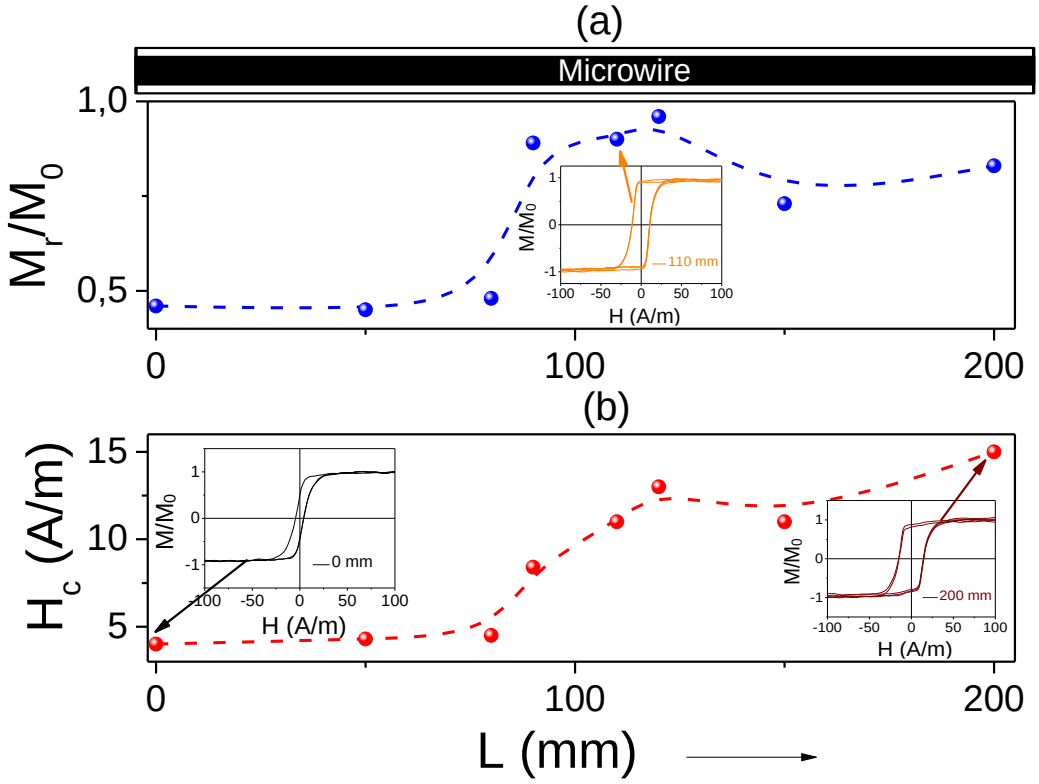

Figure 3.32. *Variation of M_r/M_0 (a) and H_c (b) along the sample length for the sample 6 annealed at variable T_{ann}. The lines are just guides for the eyes.*

Consequently, the spatial distribution of the hysteresis loops, must be consequence of the gradual modification of the domain structure along the microwires stress-annealed under a temperature gradient.

3.3. Concluding remarks

Amorphous Co-rich microwires can present excellent magnetic softness and giant magnetoimpedance (GMI) effect. High GMI effect, obtained even in as-prepared Co-rich microwires, can be further improved by appropriate heat treatment (including conventional annealing, stress-annealing and Joule heating).

It is worth mentioning the considerable improvement of $\Delta Z/Z_{max}$ values up to 650%, obtained for $Co_{67}Fe_{3.9}Ni_{1.5}B_{11.5}Si_{14.5}Mo_{1.6}$ microwire after appropriate current annealing conditions. Such microwires current annealed at optimal conditions, additionally present enhanced magnetic softness.

Conventionally furnace annealed and stress-annealed, under appropriately selected conditions, Co-based microwires can present rectangular hysteresis loops and therefore single and fast domain wall propagation. However, generally Co-based stress-annealed microwires present high magnetoimpedance ratio. Therefore, combination of both high GMI effect and fast single DW propagation can be obtained in the same Co-based microwire. The appropriate regimes allowing observation of fast and single DW propagation and high GMI effect in the same microwire were found.

DW velocity is observed in annealed Co-based microwires under application of tensile stresses due to the induced magnetic bistability.

We propose a rather simple method for preparation of Co rich microwires with graded magnetic anisotropy consisting of stress- annealing under temperature gradient. A gradual change in the hysteresis loop of Co-rich glass-coated microwire stress-annealed at variable temperature is observed.

3.4. References

[1] A. Zhukov, M. Ipatov, M. Churyukanova, A. Talaat, J.M. Blanco, V. Zhukova, Trends in optimization of giant magnetoimpedance effect in amorphous and nanocrystalline materials, J. Alloys Compd., 727 (2017) 887–901.

[2] G. Herzer, Amorphous and Nanocrystalline Soft Magnets, G.C. Hadjipanayis Ed., pp. 711–730, in Proc. NATO Adv. Study Inst. Magn. Hysteresis Nov. Mater., Springer Netherlands, Dordrecht (1997), doi:10.1007/978-94-011-5478-9_77.

[3] P. Corte-León, V. Zhukova, M. Ipatov, J.M. Blanco, J. Gonzalez, A. Zhukov, Engineering of magnetic properties of Co-rich microwires by joule heating, Intermetallics 105 (2019) 92–98, doi:10.1016/j.intermet.2018.11.013.

[4] A. Zhukov, A. Talaat, M. Ipatov, J.M. Blanco, V. Zhukova, Tailoring of magnetic properties and GMI effect of Co-rich amorphous microwires by heat treatment, J. Alloys Compd. 615 (2014) 610–615, doi: 10.1016/j.jallcom.2014.07.079.

[5] V. Zhukova, P. Corte-Leon, M. Ipatov, J.M. Blanco, L. Gonzalez-Legarreta, A. Zhukov, Development of Magnetic Microwires for Magnetic Sensor Applications, Sensors 19 (2019) 4767, doi:10.3390/s19214767.

[6] M. Knobel, M.L. Sanchez, C. Gómez-Polo, P. Marin, M. Vazquez, A. Hernando, Giant magneto-impedance effect in nanostructured magnetic wires, J. Appl. Phys. 79 (1996) 1646–1654.

[7] H.K. Lachowicz, K.L. Garcia, M. Kuźmiński, A. Zhukov, M. Vázquez, Skin-effect and circumferential permeability in micro-wires utilized in GMI-sensors, Sens. Actuators A Phys. 119 (2005) 384–389, doi: 10.1016/j.sna.2004.10.017.

[8] V. Zhukova, M. Ipatov, A. Talaat, J.M. Blanco, M. Churyukanova, A. Zhukov, Effect of stress annealing on magnetic properties and GMI effect of Co- and Fe-rich microwires, J. Alloys Compd. 707 (2017) 189–194. doi:10.1016/j.jallcom.2016.10.178.

[9] A. Zhukov, L. Gonzalez-Legarreta, P. Corte-Leon, M. Ipatov, J.M. Blanco, J. Gonzalez, V. Zhukova, Tailoring of Magnetic Softness and Magnetoimpedance of Co-Rich Microwires by Stress Annealing, Phys. Status Solidi. 218 (2021) 2100130, doi:10.1002/pssa.202100130.

[10] V. Zhukova, J.M. Blanco, P. Corte-Leon, M. Ipatov, M. Churyukanova, S. Taskaev, A. Zhukov, Grading the magnetic anisotropy and engineering the domain wall dynamics in Fe-rich microwires by stress-annealing, Acta Mater. 155 (2018) 279–285, doi:10.1016/j.actamat.2018.05.068.

[11] P. Corte-León, A. Talaat, V. Zhukova, M. Ipatov, J.M. Blanco, J. Gonzalez, A. Zhukov, Stress-Induced Magnetic Anisotropy Enabling Engineering of Magnetic Softness and GMI Effect of Amorphous Microwires, Appl. Sci. 10 (2020), doi:10.3390/app10030981.

[12] A. Zhukov, A. Talaat, M. Churyukanova, S. Kaloshkin, V. Semenkova, M. Ipatov, J.M. Blanco, V. Zhukova, Engineering of magnetic properties and GMI effect in Co-rich amorphous microwires, J. Alloys Compd. 664 (2016) 235–241. doi: 10.1016/j.jallcom.2015.12.224.

[13] V. Zhukova, J. M. Blanco, V. Rodionova, M. Ipatov, A. Zhukov, Domain wall propagation in micrometric wires: Limits of single domain wall regime, J. Appl. Phys. 111 (2012) 07E311.

[14] V. Zhukova, A.F. Cobeño, A. Zhukov, J.M. Blanco, S. Puerta, J. Gonzalez, M. Vázquez, Tailoring of magnetic properties of glass-coated microwires by current annealing, J. Non. Cryst. Solids. 287 (2001) 31–36, doi:10.1016/S0022-3093(01)00536-1.

[15] N.A. Usov, A.S. Antonov, A.N. Lagar'kov, Theory of giant magneto-impedance effect in amorphous wires with different types of magnetic anisotropy, J. Magn. Magn. Mater. 185 (1998) 159–173, doi:10.1016/S0304-8853(97)01148-7.

[16] P. Corte-León, V. Zhukova, M. Ipatov, J.M. Blanco, J. González, A. Zhukov, Optimization of GMI Effect and Magnetic Properties of Co-Rich Microwires by Joule Heating, IEEE Trans. Magn. 55 (2019) 2018–2021.

[17] V. Zhukova, P. Corte-Leon, L. Gonzalez-Legarreta, A. Talaat, J.M. Blanco, M. Ipatov, J. Olivera, A. Zhukov, Optimization of Magnetic Properties of Magnetic Microwires by Post-Processing, Processes 8 (2020) 1006, doi:10.3390/pr8081006.

[18] M.-H. Phan, H.-X. Peng, Giant magnetoimpedance materials: Fundamentals and applications, Prog. Mater. Sci. 53 (2008) 323–420, doi:10.1016/j.pmatsci.2007.05.003.

[19] L. Gonzalez-Legarreta, P. Corte-León, V. Zhukova, M. Ipatov, J.M. Blanco, M. Churyukanova, S. Taskaev, A. Zhukov, Route of magnetoimpedance and domain walls dynamics optimization in Co-based microwires, J. Alloys Compd. 830 (2020) 154576, doi:10.1016/j.jallcom.2020.154576.

[20] A. Siemko, H. Lachowicz, On indirect measurements of saturation magnetostriction in low-magnetostrictive metallic glasses, IEEE Trans. Magn. 23 (1987) 2563–2565, doi:10.1109/TMAG.1987.1065684.

[21] J.M. Barandiarán, A. Hernando, V. Madurga, O. V Nielsen, M. Vázquez, M. Vázquez-López, Temperature, stress, and structural-relaxation dependence of the magnetostriction in $(Co_{0.94}/BFe_{0.06})_{75}/BSi_{15}B_{10}$ glasses, Phys. Rev. B. 35 (1987) 5066–5071, doi:10.1103/PhysRevB.35.5066.

[22] K. Chichay, V. Rodionova, V. Zhukova, S. Kaloshkin, M. Churyuknova, A. Zhukov, Investigation of the magnetostriction coefficient of amorphous ferromagnetic glass coated microwires, J. Appl. Phys. 116 (2014) 173904, doi:10.1063/1.4900481.

[23] K. Mohri, F.B. Humphrey, K. Kawashima, K. Kimura, M. Mizutani, Large Barkhausen and Matteucci effects in FeCoSiB, FeCrSiB, and FeNiSiB amorphous wires, IEEE Trans. Magn. 26 (1990) 1789–1791.

[24] P. Corte-León, L. Gonzalez-Legarreta, V. Zhukova, M. Ipatov, J.M. Blanco, M. Churyukanova, S. Taskaev, A. Zhukov, Controlling the domain wall dynamics in Fe-, Ni- and Co-based magnetic microwires. J. Alloys Compd. 2020, 834, 155170.

[25] V. Zhukova, P. Corte-Leon, L. González-Legarreta, A. Talaat, J.M. Blanco, M. Ipatov, J. Olivera, A. Zhukov. Review of domain wall dynamics engineering in magnetic microwires, Nanomaterials 10(12) (2020) 2407.

[26] R. Skomski, T.A. George, D.J. Sellmyer, Nucleation and wall motion in graded media, J. Appl. Phys. 103 (2008) 07F531.

[27] Jai-Lin Tsai, Hsin-Te Tzeng, Bing-Fong Liu, Magnetic properties and microstructure of graded Fe/FePt films, J. Appl. Phys. 107 (2010) 113923.

[28] C.L. Zha, R.K. Dumas, Y.Y. Fang, V. Bonanni, J. Nogués, J. Åkerman, Continuously graded anisotropy in single $(Fe_{53}Pt_{47})_{100-x}Cu_x$ films, Appl. Phys. Lett. 97 (2010) 182504.

[29] L. Gonzalez-Legarreta, P. Corte-Leon, V. Zhukova, M. Ipatov, J.M. Blanco, J. Gonzalez, A. Zhukov, Optimization of magnetic properties and GMI effect of Thin Co-rich Microwires for GMI Microsensors, Sensors 20 (2020) 1558, doi:10.3390/s20061558.

[30] J.N. Nderu, J. Yamasaki, F. Humphrey, Switching mechanism in Co based amorphous wire, J. Appl. Phys. 81 (8) (1997) 4036-4038.

[31] V. Zhukova, J.M. Blanco, A. Chizhik, M. Ipatov, A. Zhukov, AC-current-induced magnetization switching in amorphous microwires, Front. Phys. 13 (2018) 137501.

[32] H. Chiriac, T.A. Ovari, Gh. Pop, Internal stress distribution in glass-covered amorphous magnetic wires, Phys. Rev. B 42 (1995) 10105.

[33] S.A. Baranov, V.S. Larin, A.V. Torcunov, Technology, Preparation and Properties of the Cast Glass-Coated Magnetic Microwires, Crystals 7 (2017) 136, doi:10.3390/cryst7060136.

[34] V. Zhukova, P. Corte-Leon, J.M. Blanco, M. Ipatov, L Gonzalez-Legarreta, A.Gonzalez, A. Zhukov, Development of Magnetically Soft Amorphous Microwires for Technological Applications (Review), Chemosensors, 10 (2022) 26, doi:10.3390/chemosensors10010026.

[35] J. Velázquez, M. Vázquez, A. Hernando, H.T. Savage, M. Wun-Fogle, Magnetoelastic anisotropy in amorphous wires due to quenching, J. Appl. Phys. 70 (1991) 6525–6527.

[36] A.S. Antonov, V.T. Borisov, O.V. Borisov, A.F. Prokoshin, N.A. Usov, Residual quenching stresses in glass-coated amorphous ferromagnetic microwires, J. Phys. D Appl. Phys. 33 (2000) 1161–1168.

4. Engineering of magnetic properties of microwires with positive magnetostriction coefficient (Fe-, Fe-Ni- and Fe-Co-rich)

This chapter summarizes the results obtained by selecting different chemical compositions and post-processing steps with the aim to optimize the magnetic properties for different Fe-rich compositions and geometric characteristics of amorphous glass coated microwires as presented in the table below (*Table 4.1*).

The microwires selected pretend to give a complete overview of the behaviour of Fe-rich microwires from the metallic alloy groups Co_xFe_{1-x} and Ni_xFe_{1-x}, for $0 \leq x \leq 1$, and *Finemet-type* FeCuNbSiB microwires.

Table 4.1. *Compositions, geometry and magnetostriction coefficients of studied Fe-rich glass-coated microwires.*

Composition	***d* (μm)**	***D* (μm)**	**$\rho = d/D$**	**λ_s x 10^{-6}**
$Fe_{77.5}B_{15}Si_{7.5}$	15.1	35.8	0.42	38
$Fe_{70}B_{15}Si_{10}C_5$	3	18,75	0.16	35
$Fe_{70}B_{15}Si_{10}C_5$	6	23,08	0.26	35
$Fe_{70}B_{15}Si_{10}C_5$	10.8	22.5	0.48	35
$Fe_{70}B_{15}Si_{10}C_5$	15	23,8	0.63	35
$Fe_{75}B_9Si_{12}C_4$	15.2	17.2	0.88	38
$Fe_{71.7}B_{13.4}Si_{11}Nb_3Ni_{0.9}$	103	158	0.65	35
$Fe_{47.4}Ni_{26.6}Si_{11}B_{13}C_2$	29	32.2	0.9	25
$Fe_{49.6}Ni_{27.9}Si_{7.5}B_{15}$	14.2	33.85	0.42	20
$Fe_{62}Ni_{15.5}Si_{7.5}B_{15}$	14.35	33.25	0.43	27
$Fe_{70.8}Cu_1Nb_{3.1}Si_{14.5}B_{10.6}$	11.8	14.4	0.8	30
$Fe_{70.8}Cu_1Nb_{3.1}Si_{14.5}B_{10.6}$	15.6	21.8	0.7	30
$Fe_{70.8}Cu_1Nb_{3.1}Si_{14.5}B_{10.6}$	10.7	16.4	0.6	30
$Fe_{71.8}Cu_1Nb_{3.1}Si_{15}B_{9.1}$	7.0	24.8	0.282	30
$Fe_{71.8}Cu_1Nb_{3.1}Si_{15}B_{9.1}$	18.2	39	0.467	30
$(Fe_{0.7}Co_{0.3})_{83.7}Si_4B_8P_{3.6}Cu_{0.7}$	26.5	22.3	0.84	
$Fe_{83.7}Si_4B_8P_{3.6}Cu_{0.7}$	15.5	17.5	0.89	
$Fe_{38.5}Co_{38.5}B_{18}Mo_4Cu_1$	10	16.6	0,6	

4.1. As-prepared Fe-rich microwires

4.1.1. FeBSiC microwires

As-prepared $Fe_{75}B_9Si_{12}C_4$ amorphous glass coated microwire with metallic nucleus diameter d = 15.2 μm and total diameter D = 17.2 μm, and with magnetostriction coefficient, λ_s, positive value of about 35 x 10^{-6}, presents a rectangular hysteresis loop (*Figure 4.1*) with $H_c \approx 48$ A/m.

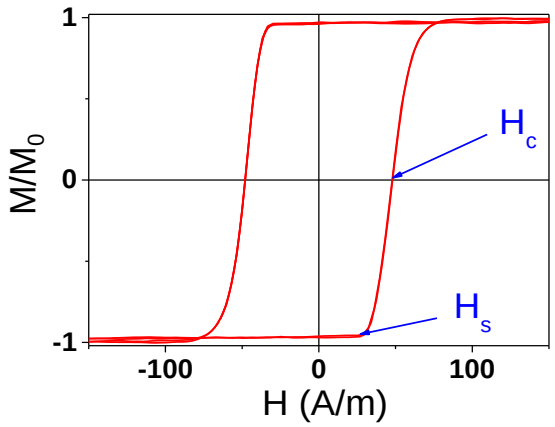

Figure 4.1. *Hysteresis loop of as-prepared $Fe_{75}B_9Si_{12}C_4$ amorphous glass-coated microwire.*

Amorphous state of the as-prepared microwire was confirmed by XRD pattern (*Figure 4.2a)* and DSC curve of as-prepared $Fe_{75}B_9Si_{12}C_4$ microwire (*Figure 4.2b*) shows a crystallization temperature, T_{cr1}, of about 522 °C, and the estimation of the Curie temperature is about T_c = 413 °C. Therefore, the annealing temperatures, T_{ann}, for this sample, in order to prevent crystallization, should be maintained below these temperatures.

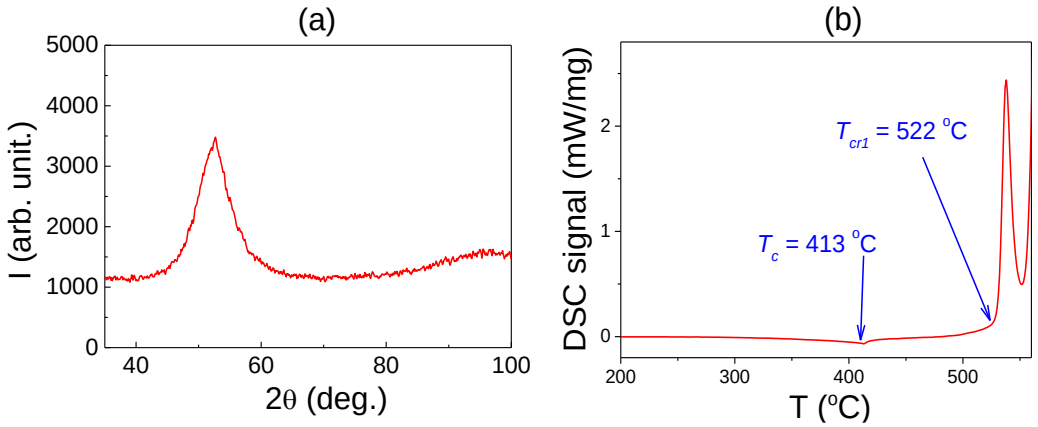

Figure 4.2. *XRD diffraction pattern (a) and DSC curve (b) of as-prepared $Fe_{75}B_9Si_{12}C_4$ microwire.*

4.1.2. Magnetoelastic anisotropy effect on as-prepared Fe-rich amorphous microwires

As mentioned in the previous chapter, the magnetoelastic anisotropy, K_{me}, together with the shape anisotropy, are the key factors that determine the character of the hysteresis loops of amorphous microwires [1]:

The magnetic softness of the microwires, reflected on the hysteresis loops is quite sensitive to their composition and geometry, as reported also for cobalt rich compositions [1]. By changing the composition of the microwires, we can study the effects of the changes in the magnetoelastic anisotropy on hysteresis loops.

On the other hand, the internal stresses arising during the glass-coated microwires preparation have three sources: *i*) quenching stresses originated by the rapid melt quenching; *ii*) complex tensor stresses associated with the different thermal expansion coefficients of metallic nucleus and glass-coating, and *iii*) axial stresses associated with wire drawing [1-3].

However, it is recognized that the internal stresses, σ_i, arising from different thermal expansion coefficients of the glass coating and the metallic alloy are the largest [4]. The internal stresses depend mainly on the difference of thermal expansion coefficients and on ρ-ratio ($\rho = d/D$) (*eq. 3.9*). The more detailed theoretical estimations give σ_i up to 4 GPa [3,5]. Although internal stresses are distributed in a complex way, the important point is that the axial internal stresses are the largest ones.

The quenching stresses and stresses originated by the microwire drawing are roughly an order of magnitude lower [3].

Accordingly, the σ_i value can be controlled by modifying the ρ-ratio [3-5].

Fe-rich microwires have positive magnetostriction coefficient with λ_s values ranging from $\lambda_s \sim$ (20-40) x 10^{-6}. The rectangular character of the hysteresis loops of amorphous microwires with positive λ_s values is rather

different of that of the microwires with negative λ_s values that present low coercivity and almost non-hysteretic behaviour [6].

The axial magnetic anisotropy of microwires with positive λ_s values, due to its particular domain structure consisting of an inner axially magnetized single domain and an outer domain shell with radial magnetization orientation, explains the rectangular character of the hysteresis loops, related to an extremely fast magnetization switching by single domain wall propagation.

On the other hand, microwires with the same composition and consequently same λ_s values, can present different magnetic properties depending on the diameters of their nucleus and glass coating, as we will see with the following example in *Figure 4.3*.

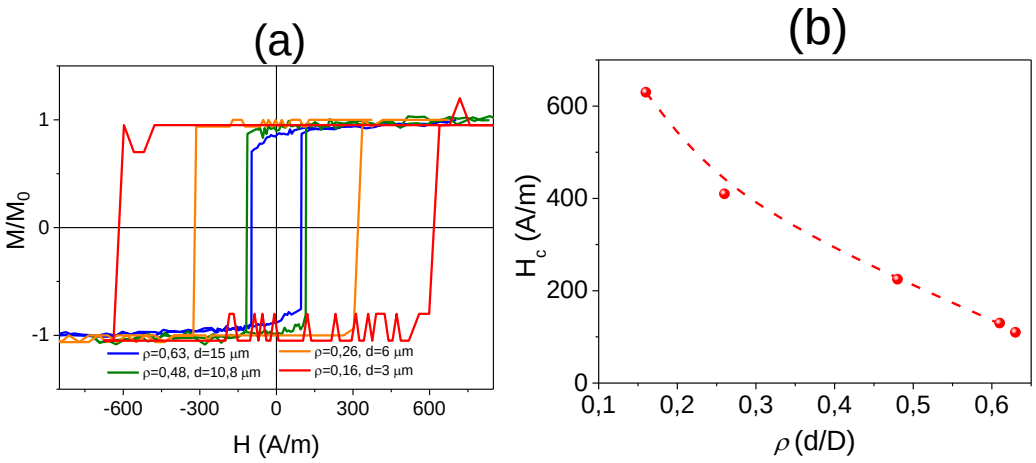

Figure 4.3. *Hysteresis loops of as-prepared $Fe_{70}B_{15}Si_{10}C_5$ amorphous microwires with different ρ ratios (a) and $H_c(\rho)$ dependence (b) of the same microwires.*

In *Figure 4.3a*, hysteresis loops of microwires with a given composition, in this case $Fe_{70}B_{15}Si_{10}C_5$ amorphous glass-coated microwires, and different internal stresses, obtained by means of ρ ratio variation, are presented, H_c variation by almost an order of magnitude can be observed from the H_c (ρ) dependence (*Figure 4.3b*), similarly as observed for the case of Co-rich microwires [8]. From the hysteresis loops representation it can also be

appreciated the influence of the internal stresses in the switching field, H_s, exhibiting, coupled *with* H_c (ρ), a decrease as ρ ratio increases.

On the other hand, λ_s sign and value of amorphous materials is primary influenced by the chemical composition. Therefore, the hystereris loops are also considerably affected by the chemical composition of the metallic nucleus [1].

Thus, Fe-rich amorphous alloys possess high and positive λ_s -values (up to $\lambda_s \approx 40 \times 10^{-6}$) [9,10], while in amorphous Co-rich alloys λ_s is low and negative (up to $\lambda_s \approx -5 \times 10^{-6}$) [9,10]. Vanishing λ_s values can be obtained by doping of Co-rich alloy with Fe or Mn: λ_s can take nearly-zero values in $Co_{1-x}Fe_x$ or $Co_{1-x}Mn_x$ amorphous alloys at $0.05 \leq x \leq 0.1$ [9,10]. Alternatively, low λ_s -values can be achieved in $Ni_{1-x}Fe_x$ alloys, while such alloys present a low saturation magnetization, M_s, and hence, are less interesting for applications [10].

The observed correlation of magnetic properties and magnetoelastic anisotropy lead us to expect a significant change in the magnetic properties of the microwires by change of chemical composition or by heat treatment and the consequent stress relaxation.

4.1.3. Fe-Ni microwires

The effect of the change in the magnetic anisotropy due to the change in the composition is evidenced by *Figure 4.4* and *Figure 4.5*, where rectangular hysteresis loops shown, for microwires with positive λ_s values, reflect the axial magnetic anisotropy of the samples, and it can be observed that the increase in the magnetostriction coefficient correlates with an increase in the coercivity [11].

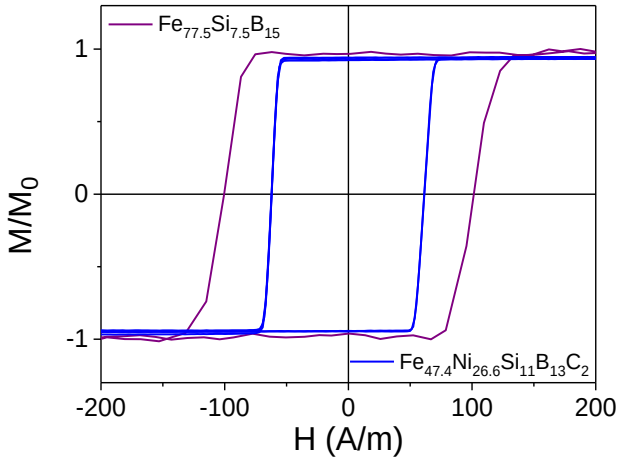

Figure 4.4. *Hysteresis loops of as-prepared $Fe_{77.5}Si_{7.5}B_1$ and $Fe_{47.4}Ni_{26.6}Si_{11}B_{13}C_2$ microwires.*

Properly post-processed crystalline Fe-Ni alloys (such as Invar and Permalloy alloys) can present excellent magnetic properties. Fast DW dynamics is reported for Fe-Ni rich materials, mainly planar nanowires and ribbons, although it has also already been reported for Fe-Ni based microwires [11,12]. To observe soft magnetic properties it is essential to identify the correct post-processing route in Fe-Ni rich crystalline materials. Therefore, it is relevant to study the influence on annealing on the magnetic properties and DW dynamics of Fe-Ni glass-coated microwires.

Spontaneous magnetic bistability, related to positive λ_s, is not only reduced to Fe-B-Si-C microwires, it is also observed for as-prepared Fe-Ni-based microwires (*Figure 4.4* and *Figure 4.5)*. Substitution of Fe by Ni and Co in Fe-B-Si-C microwires allows to modify considerably the magnetostriction coefficient [6,9,10], and hence, to tune the coercivity and further improve the DW dynamics.

Modification of λ_s by doping of Fe-rich alloy with Ni gives as a result a decrease in λ_s with increasing the Ni content in Ni_xFe_{1-x} ($0 \leq x \leq 1$) system that correlates with the decrease in the saturation magnetization, as can be appreciated from *Figure 4.4* and *Figure 4.5*, where lower H_c values correlate with lower λ_s and increase of the Ni content. High Ni contents give rise to zero

λ_s values corresponding to paramagnetic ordering of Ni_xFe_{1-x} alloys at room temperature [10].

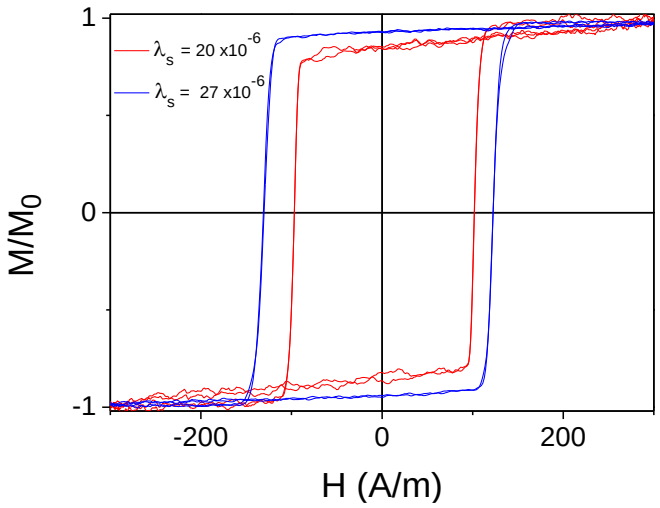

Figure 4.5. *Hysteresis loops of as-prepared $Fe_{49.6}Ni_{27.9}Si_{7.5}B_{15}$ (represented in red) and $Fe_{62}Ni_{15.5}Si_{7.5}B_{15}$ (represented in blue) microwires.*

4.1.4. "Thick" glass-coated Fe-rich microwires

Taylor Ulitovsky technique is usually considered to be restricted to the preparation of magnetic wires with thin diameters [1], but thicker microwires, of diameters above 50 μm, can be also produced by this technique [13,14]. This type of microwires are suitable for some industrial applications, like non-contact stress monitoring in composite materials [15], or magnetic tags for medical devices, which require microwires of higher diameters [16].

We summarized, later on this chapter, the experimental results carried out on post-processing of "thick" Fe-based, $Fe_{71.7}B_{13.4}Si_{11}Nb_3Ni_{0.9}$ glass coated microwires, of metallic nucleus diameter d = 103 μm and total diameter D = 158 μm. The purpose of this study is to obtain "thick" microwires maintaining the excellent magnetic properties and advanced functionalities achieved for thinner microwires.

The chemical composition, Fe-based amorphous material with small additions of Ni and Nb and its similarity with *Finemet-type* (Fe-Si-B-Cu-Nb) alloys, which present magnetic softening due to internal stresses relaxation at temperatures about 300 ℃ and first crystallization process at temperatures about 550 ℃ [17,18], lead us to select these annealing temperatures to study the evolution of the magnetic properties of the microwire. Then, the microwires were annealed in a conventional furnace at T_{ann} = 300 ℃ and 550 ℃ during different t_{ann}, up to 6 h.

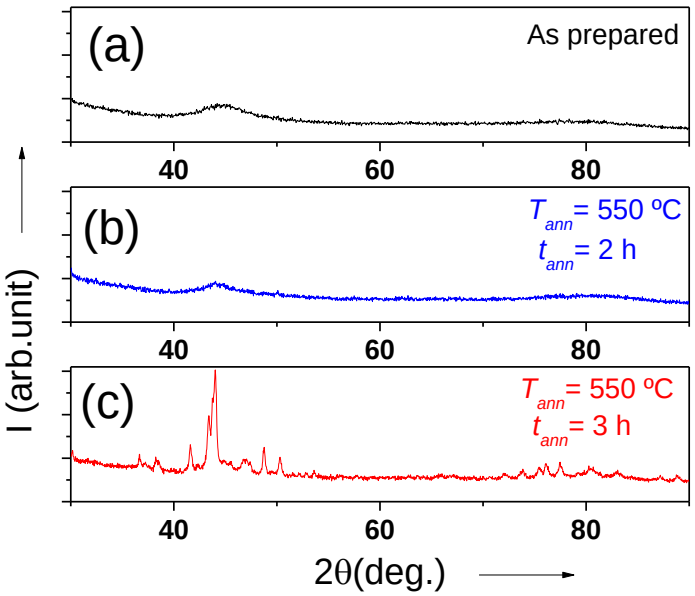

Figure 4.6. *XRD diffraction pattern of as-prepared $Fe_{71.7}B_{13.4}Si_{11}Nb_3Ni_{0.9}$ microwire (a) and annealed at 550 ℃ for t_{ann} = 2 h (b) and t_{ann} = 3 h (c).*

The microwires structure in as-prepared and annealed state was checked (*Figure 4.6*) by XRD diffraction. The measurement conditions were 0.3 degrees and 90 s of measurement step and time in each point, respectively. As-prepared sample presents a XRD diffraction pattern (*Figure 4.6a*) with a wide halo (at $2\Theta \approx 45^{o}$) reflecting the amorphous character of the material [18]. After annealing at 550 °C during 2 h, the same XRD pattern is observed (see *Figure 4.6b*). XRD patterns shown in *Figure 4.6a* and *Figure 4.6b*, for as-prepared and annealed sample, respectively, exhibit the same features as those observed for *Finemet-type* microwires before crystallization [18,19]. And finally, in *Figure*

4.6c, in sample annealed at 550 °C during 3 h, it can be seen that first crystallization peaks, related to the precipitation of fine Fe_3B crystals, begin to appear in the XRD pattern. The overlap between the broad halo and the sharp peaks can be understood as the coexistence of both phases, amorphous and crystalline (consisting of α-Fe, Fe_3B).

By means of a Scanning Electron Microscope (MEB JEOL JSM-7000F), the chemical composition and microstructure of the microwire in as-prepared and annealed state was characterized (*Figure 4.7*). The images were obtained working at 5 kV and $I \approx 0.1$ nA. For the compositional analysis, we employed the energy-dispersive X-ray spectroscopy (EDX) mode, with an Inca Energy 350 spectrometer, adjusting the measurement conditions at 20 kV and $I \approx 1$ nA. SEM analysis of as-prepared and annealed samples, presented in *Figure 4.7*, correlates with the XRD patterns. SEM image of the metallic nucleus of as-prepared sample (*Figure 4.7a*) is typical for amorphous samples. In *Figure 4.7b*, of SEM picture of annealed microwire at 550 °C during 3 h, crystallites of about 25 nm size can be appreciated. Nanocrystalline structure can be explained due to the particular composition of the microwires under study, given that the Nb impedes hinders the crystallites upon annealing [9].

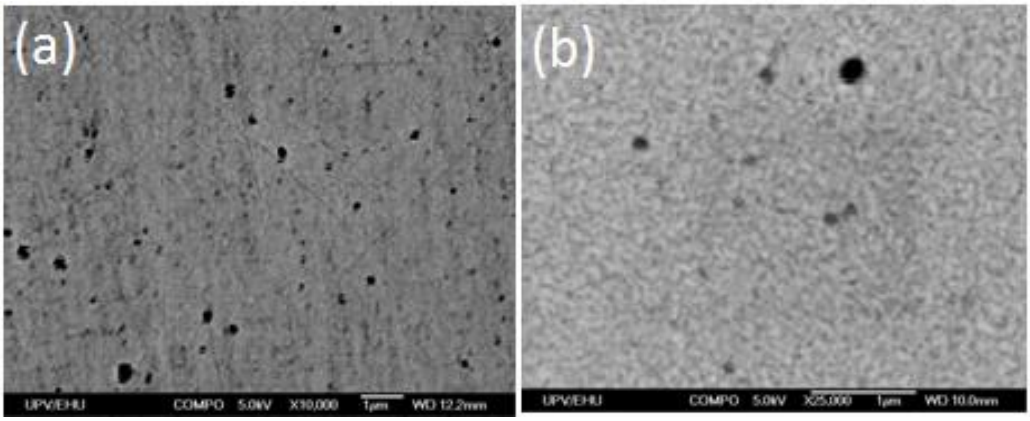

Figure 4.7. *SEM images of the metallic nucleus of $Fe_{71.7}B_{13.4}Si_{11}Nb_3Ni_{0.9}$ microwires as-prepared (a) and annealed at 550 °C for t_{ann} = 3 h (b).*

As prepared hysteresis loop of $Fe_{71.7}B_{13.4}Si_{11}Nb_3Ni_{0.9}$ microwire (*Figure 4.8*) is characterized by its rectangular shape with low coercivity, $H_c \approx 25$ A/m, correspondingly with the amorphous structure.

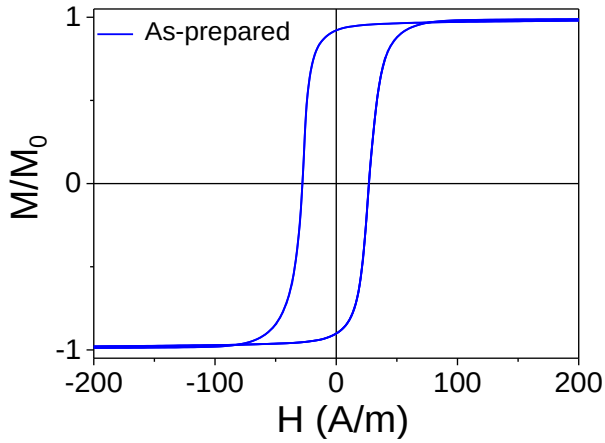

Figure 4.8. *Hysteresis loop of as-prepared $Fe_{71.7}B_{13.4}Si_{11}Nb_3Ni_{0.9}$ microwire.*

4.2. Post-processing effect on magnetic properties and GMI effect for Fe-rich microwires

4.2.1. Effect of annealing on magnetic properties and GMI effect in nanocrystalline and devitrified microwires

The devitrification of amorphous nucleus reached by post annealing process is a useful tool allowing considerable modification of the magnetic properties and even magnetic softening in some Fe-rich microwires [9,18,19].

In the case of FeSiBNbCu (so-called *Finemet*) alloys low magnetostriction values and better magnetic softness can be achieved by the devitrification of amorphous precursor [9,18-20]. The magnetic softening of the devitrified *Finemet* alloys is commonly explained considering the vanishing magnetocrystalline anisotropy, as well as the vanishing λ_s –value of the material, consisting of nano-sized grains with an average size on the order of 10

nm, embedded in an amorphous matrix obtained by nanocrystallization of the amorphous precursors [9,17,18].

The average magnetostriction coefficient takes nearly zero values [9,17,18], due to the control of the crystalline volume fraction: the existence of two phases (amorphous and crystalline) provides a good balance of a negative magnetostriction of α-Fe-Si nanocrystallites of about ($\lambda_s^{FeSi} \approx$ -6 x 10^{-6}) and a positive one for the amorphous matrix of about ($\lambda_s^{am} \approx$ 20 x 10^{-6}) resulting finally in vanishing net magnetostriction values [9]:

$$\lambda_s^{eff} \approx V_{cr}\,\lambda_s^{FeSi} + (1 - V_{cr})\,\lambda_s^{am} \tag{4.1}$$

where λ_s^{eff} is the saturation magnetostriction coefficient, and V_{cr} is the crystalline volume fraction.

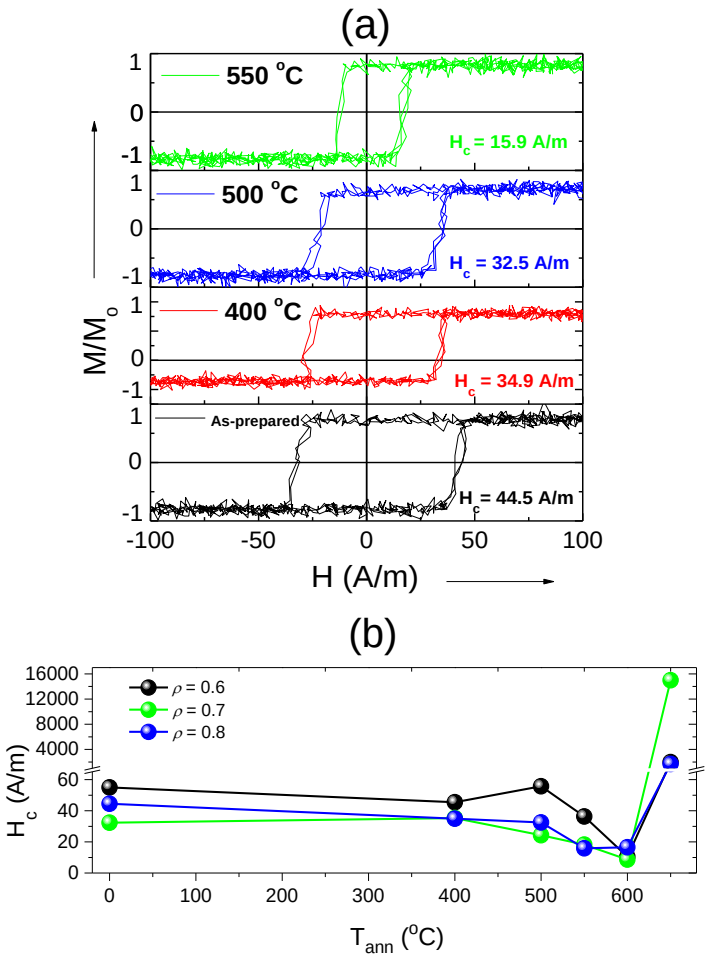

Figure 4.9. *Hysteresis loops of as-prepared and annealed $Fe_{70.8}Cu_1Nb_{3.1}Si_{14.5}B_{10.6}$ microwire samples at T_{ann} between 400-600 °C (a) and H_c (T_{ann}) dependence of $Fe_{70.8}Cu_1Nb_{3.1}Si_{14.5}B_{10.6}$ microwires for different ρ-ratios (b).*

This nanocrystallization of FeSiBNbCu alloys is usually observed after annealing in the range of 500-600 ºC for 1 h (i.e., at temperatures between the first and second crystallization stages). One of the examples of the evolution of the hysteresis loops of *Finemet-type* microwires upon nanocrystallization is shown in *Figure 4.9*. As can be observed from *Figure 4.9*, in the case of the $Fe_{70.8}Cu_1Nb_{3.1}Si_{14.5}B_{10.6}$ microwire, annealing at T_{ann} up to 550 ºC allows considerable decrease of coercivity. For these annealing conditions the character of hysteresis loops does not change: all the hysteresis loops present rectangular shape.

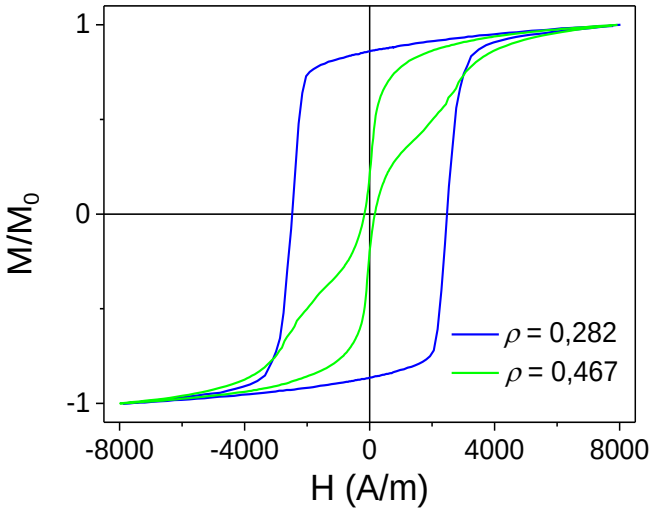

Figure 4.10. *Hysteresis loops of $Fe_{71,8}Cu_1Nb_{3,1}Si_{15}B_{9,1}$ microwires with different ρ-ratios annealed at 700 ºC.*

In some cases rectangular hysteresis loops are reported not only upon devitrification of *Finemet-type*, but even after second crystallization process when values up to 2400 A/m are observed [17-19]. One of the examples is shown in *Figure 4.10*, where hysteresis loop of $Fe_{71.8}Cu_1Nb_{3.1}Si_{15}B_{9.1}$ microwire (ρ = 0.282) annealed at T_{ann} = 700 ºC is shown. However, $Fe_{71.8}Cu_1Nb_{3.1}Si_{15}B_{9.1}$ microwire (ρ = 0.467) present rather different step-wise hysteresis loops (see *Figure 4.10*) that can be attributed to partially crystalline (bi-phase) structure. Such partially crystalline magnetic microwires, with step-wise hysteresis loops related to magnetic interaction between crystals or mixed amorphous-

crystalline structure, can be interesting for applications in electronic surveillance systems [17-20].

The microwires obtained by devitrification exhibit higher saturation magnetization and at certain annealing conditions can present better magnetic softness and GMI response than as-prepared Fe-rich microwires and therefore they are useful for GMI sensors and metacomposites applications [9,20,21].

In fact, microwires with nanocrystalline structure can be obtained even directly in as-prepared state without annealing [9,20,21]. The advantage of such microwires is that they can present better mechanical properties [9,20,21].

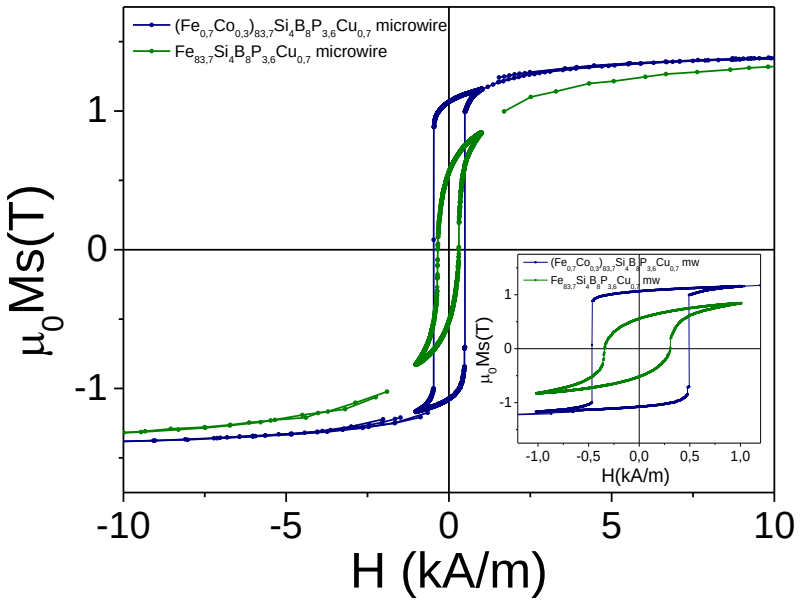

Figure 4.11. *Hysteresis loops of $(Fe_{0.7}Co_{0.3})_{83.7}Si_4B_8P_{3.6}Cu_{0.7}$ $Fe_{83.7}Si_4B_8P_{3.6}Cu_{0.7}$ microwires as-prepared.*

It is worth mentioning, that the use of specially designed compositions allows further increase of saturation magnetization, $\mu_o M_s$, and also obtain extremely magnetically soft nanocrystalline materials [21]. In the case of microwires, the use of a similar chemical composition allows preparation of nanocrystalline microwires with improved DW mobility without any post

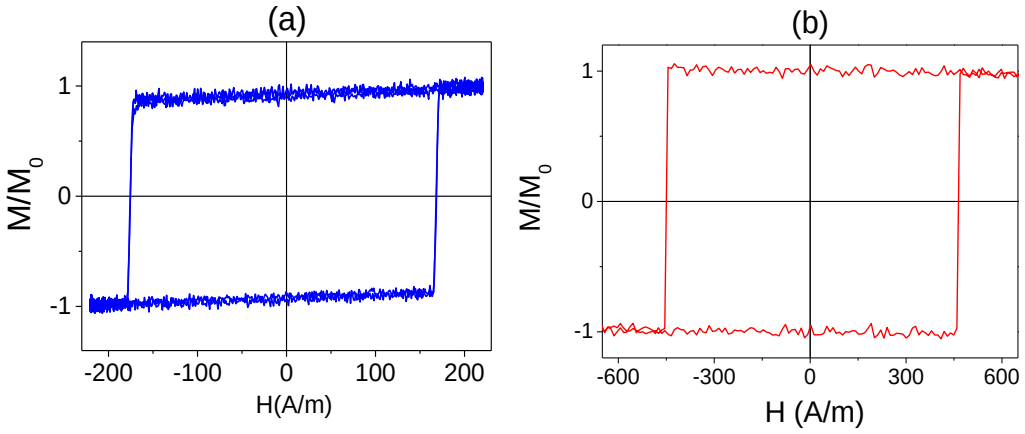

Figure 4.12. *Hysteresis loops of $Fe_{70.8}Cu_1Nb_{3.1}Si_{14.5}B_{10.6}$ (ρ = 0.38) (a) and $Fe_{38.5}Co_{38.5}B_{18}Mo_4Cu_1$ (ρ = 0.6) (b) as-prepared microwires.*

processing [21]. The partially crystalline $(Fe_{0.7}Co_{0.3})_{83.7}Si_4B_8P_{3.6}Cu_{0.7}$ microwire presents elevated values of H_c (about 480 A/m) and rather high saturation magnetization of about 1.6 T (see *Figure 4.11*).

Such elevated H_c -values are quite similar to that exhibited by other partially nanocrystalline microwires, i.e., Hitperm-like $Fe_{38.5}Co_{38.5}B_{18}Mo_4Cu_1$ microwires with similar average grain size (about 38 nm and 23-33 nm for $(Fe_{0.7}Co_{0.3})_{83.7}Si_4B_8P_{3.6}Cu_{0.7}$ and Hitperm-like microwires, respectively) [21]. Accordingly, even partially crystalline or nanocrystalline microwires can present perfectly rectangular hysteresis loops. For $(Fe_{0.7}Co_{0.3})_{83.7}Si_4B_8P_{3.6}Cu_{0.7}$ microwire elevated $\mu_o M_s$ -values allowed to obtain extremely fast domain wall velocity even in as-prepared state [21].

As-prepared *Finemet-like* and Hitperm-like glass-coated microwires also present perfectly rectangular hysteresis loops, as presented in *Figure 4.12*. $Fe_{38.5}Co_{38.5}B_{18}Mo_4Cu_1$ microwire present nanocrystalline structure in as-prepared state [22]. Higher H_c -values of $Fe_{38.5}Co_{38.5}B_{18}Mo_4Cu_1$ and $(Fe_{0.7}Co_{0.3})_{83.7}Si_4B_8P_{3.6}Cu_{0.7}$ microwires have been attributed to elevated magnetostriction coefficient of these microwires as-compared to *Finemet-type* microwires.

For nanocrystalline materials, consisting of nano-sized grains distributed randomly in an amorphous matrix, magnetic softening and considerable GMI enhancement correlates with the devitrification process [9,17-22].

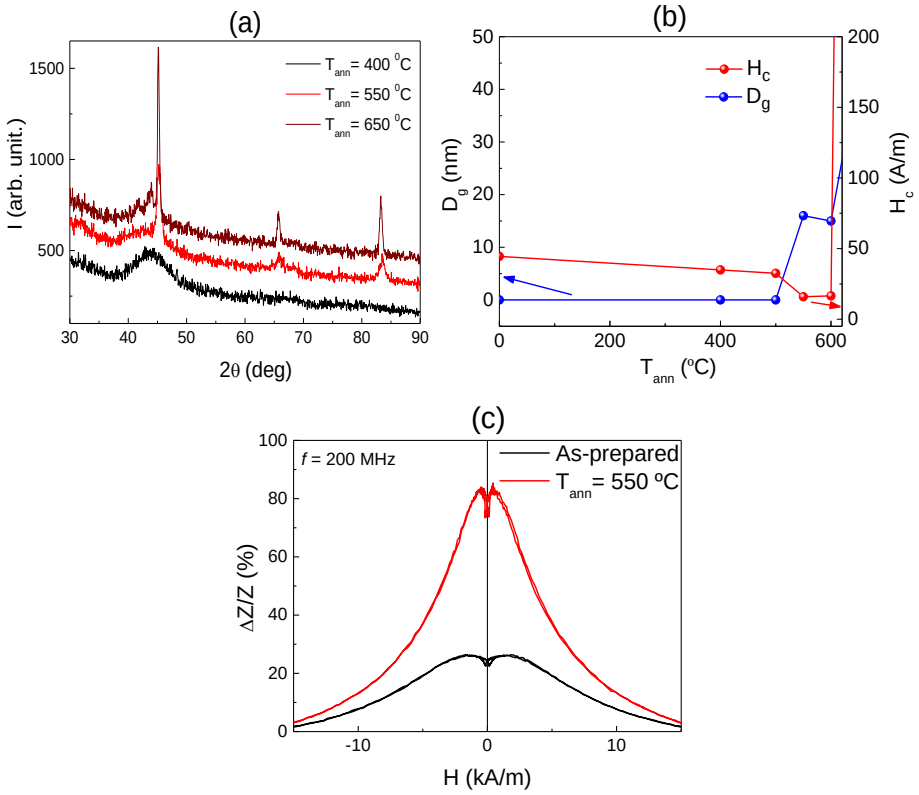

Figure 4.13. *XRD diffraction patterns of annealed $Fe_{70.8}Cu_1Nb_{3.1}Si_{14.5}B_{10.6}$ microwires (a), D_g (T_{ann}) and H_c (T_{ann}) dependencies (b) and GMI ratio dependencies (f = 200 MHz) of as-prepared and annealed at 550 °C (c) $Fe_{70.8}Cu_1Nb_{3.1}Si_{14.5}B_{10.6}$ microwires.*

Figure 4.13a shows the XRD diffraction patterns $Fe_{70.8}Cu_1Nb_{3.1}Si_{14.5}B_{10.6}$ amorphous glass-coated microwire with metallic nucleus and total diameters: *d*= 11.2 μm and *D*= 14.4 μm, respectively, annealed at different temperatures. The sample in as-prepared state and annealed at temperatures below $T_{ann} \leq$ 450 °C, maintains amorphous structure. After annealing at temperatures between 500-600 °C the beginning of crystallization can be appreciated, with the crystalline peak between 42-45° correspondent with α-Fe (Si) phase.

Various characteristics of the crystalline phase of the material can be determined by the shape of the crystalline peak, in particular, the full width at

the half maximum. By means of Debye Scherrer equation can be estimated the crystal main grain size D_g [23,24]:

$$D_g = k\lambda/\epsilon \cos 2\theta \quad (4.2)$$

being k a dimensionless shape factor with value close to unity, λ de wavelength, ϵ the full width at the half maximum of the crystalline peak and 2θ the angular position of the crystalline peak (Bragg angle).

Estimation of the average grain sizes of the nanocrystals embedded in the residual amorphous matrix (see *Figure 4.13b*) is below 20 nm.

Magnetic softening, reflected in the H_c decrease, together with the precipitation of small α-Fe (Si) grains (*Figure 4.13b*), correlate with the GMI ratio improvement observed in *Figure 4.13c* upon annealing and the consequent devitrification of the amorphous precursor.

Annealing at appropriate conditions that ensure the devitrification of *Finemet-type* amorphous microwires can be considered as an effective post-processing route for the optimization of the magnetic softness and GMI effect for this group of Fe-rich microwires, but deterioration and poor mechanical properties continue to be the main disadvantage in this type of microwires [25]. Therefore, we paid special attention to search of post-processing of microwires that allows maintaining amorphous structure.

4.2.2. Tuning of magnetic properties of amorphous microwires by furnace annealing

Below are presented some examples of the influence of conventional furnace annealing, focusing in the hysteresis loops of Fe-rich microwires of different compositions and on the domain wall dynamics and GMI effect and the combination of both magnetic properties in the same microwire.

4.2.2.1. Effect of furnace annealing on magnetic properties of FeBSiC microwires

Hysteresis loops character is not affected by the heat treatment, maintaining rectangular shape, as can be seen in *Figure 4.14a* and *Figure 4.15a* for $Fe_{75}B_9Si_{12}C_4$ microwires, only a slight decrease in H_c (t_{ann}) dependence is observed (*Figure 4.14b*). After conventional annealing at different temperatures (ranging from T_{ann} = 250 °C to T_{ann} = 375 °C), $Fe_{75}B_9Si_{12}C_4$ microwire hysteresis loops remain rectangular shaped (*Figure 4.14a)*, as typically observed for microwires with positive λ_s [2-4,11,12], with a slight H_c decrease.

The magnetic bistability origin is related to peculiar remagnetization process consisting of fast magnetization switching through a single DW propagation. DW propagation has been observed for this microwire in as-

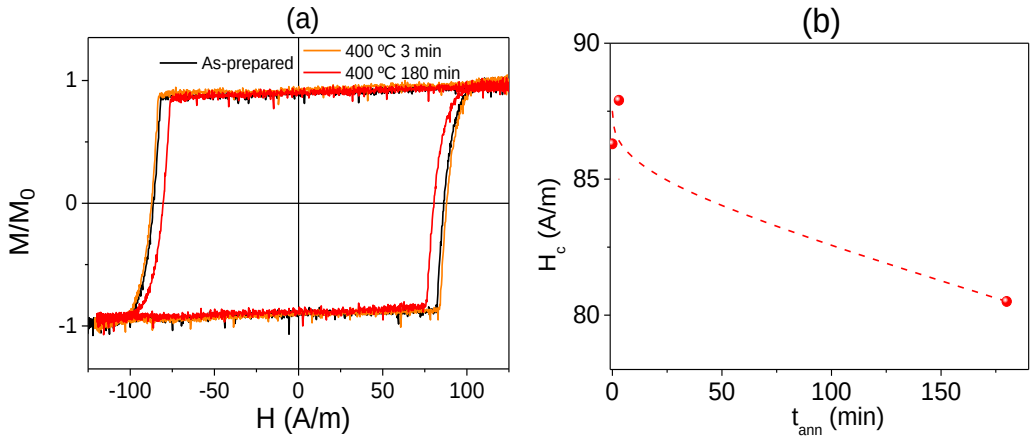

Figure 4.14. *Hysteresis loops of as-prepared and annealed at T_{ann} = 400 °C for different t_{ann} $Fe_{75}B_9Si_{12}C_4$ amorphous microwires (a) and H_c (t_{ann}) dependence (b).*

prepared and annealed states. In *Figure 4.15b* a noticeable increase in the DW velocity and mobility can be appreciated after the annealing. The DW dynamics exhibits an almost perfectly linear behavior for the *v(H)* dependence for this sample as-prepared and annealed.

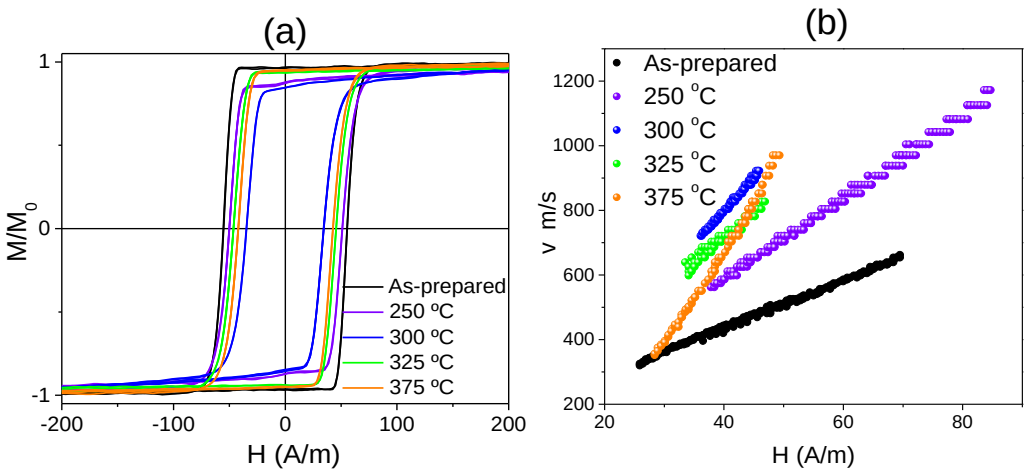

Figure 4.15. *Hysteresis loops (a) and v(H) dependence (b) of $Fe_{75}B_9Si_{12}C_4$ microwires as prepared and annealed during 60 min for different annealing temperatures.*

Such linear *v(H)* dependence below the Walker breakdown field, H_W, is attributed to a viscous DW propagation regime described in terms of DW mobility, *S,* (*eq. (1.2)*) [11,12].

It can be seen (*Figure 4.15b*) the influence of T_{ann} on *v* a *S* values consists in increase in *v* and *S* values increasing T_{ann} up to 375 °C. Similar DW velocity increase with the annealing temperature increase was recently reported elsewhere [11,12,26-28].

To study the Influence of annealing time, we select a temperature, T_{ann} = 325 °C, and vary the annealing time, $t_{ann,}$ as previously studied [2-4]. The results are presented below in *Figure 4.16*. Similar improvement as observed with increasing the annealing temperature is observed, for longer t_{ann} *v* and *S* values are higher.

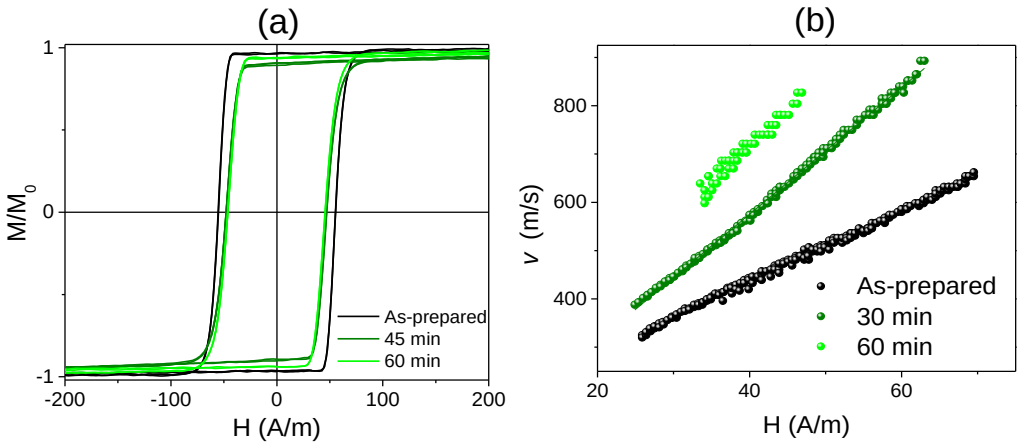

Figure 4.16. *Hysteresis loops (a) and v(H) dependence (b) of $Fe_{75}B_9Si_{12}C_4$ microwires as prepared and annealed at T_{ann} = 325 °C for different t_{ann}.*

On the other hand, magnetic microwires with rectangular hysteresis loops present poor GMI performance (*Figure 4.17*).

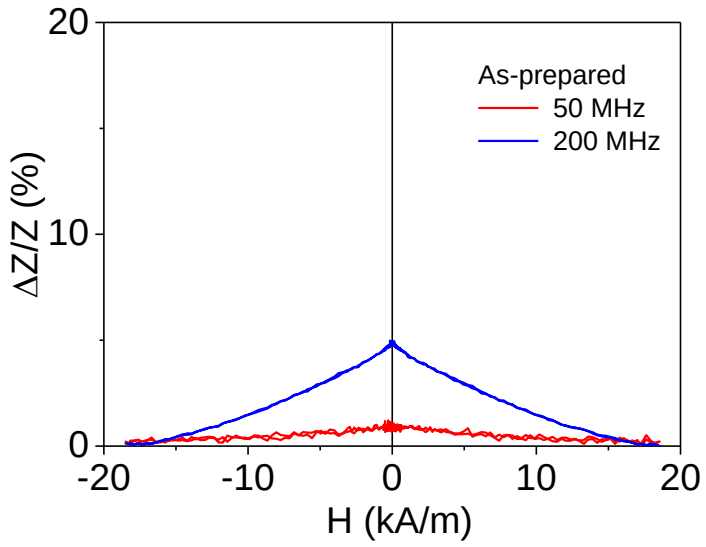

Figure 4.17. *ΔZ/Z(H) dependencies of as-prepared $Fe_{75}B_9Si_{12}C_4$ microwires measured at 50 and 200 MHz.*

4.2.2.2. Effect of furnace annealing on magnetic properties of Fe-Ni based microwires

Microwires based on Fe-Ni alloys present more complex behaviour, as previously reported [4,29,30]. In as-prepared state, as expected for microwires with positive λ_s, and discussed before from *Figure 4.4* and *Figure 4.5*, rectangular hysteresis loop is observed for Fe-Ni microwires. Here, we study the response of these microwires after conventional furnace annealing at 410 °C for t_{ann} ranging from 4 min up to 256 min. Annealing causes a coercivity increase for both samples studied (see *Figure 4.18* and *Figure 4.19*). The character of the hysteresis loop is not affected and maintains its rectangular shape. H_c (t_{ann}) tendency is not monotonic and presents a slight decrease for long annealing time, at t_{ann} = 128 min, for both microwires studied. For the case of $Fe_{49.6}Ni_{27.9}Si_{7.5}B_{15}$ (d = 14.2 μm, D = 33.85 μm and ρ = 0.42) sample a slight decrease is observed for short annealing time, not observed for $Fe_{62}Ni_{15.5}Si_{7.5}B_{15}$ microwires (d = 14.35 μm, D = 33.25 μm and ρ = 0.43), followed by H_c rising.

The lower H_c values obtained for $Fe_{49.6}Ni_{27.9}Si_{7.5}B_{15}$ microwire may be related to lower λ_s of this microwire [4,29,30].

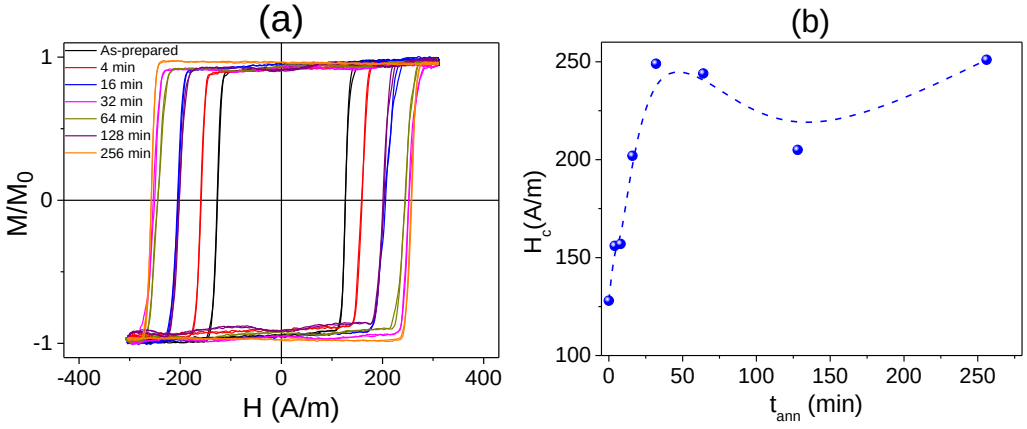

Figure 4.18. *Hysteresis loops of $Fe_{62}Ni_{15.5}Si_{7.5}B_{15}$ microwires as-prepared and annealed at T_{ann} = 410 °C for different t_{ann} (a) and H_c (t_{ann}) dependence (b).*

The magnetic hardening observed upon annealing for Fe-Ni microwires, in contrast with the behaviour of Fe compositions, in which is the common post-processing chosen for internal stresses relaxation, could be explain taking into account the beginning of the crystallization process. However, beginning of crystallization process can be disregard for the annealing treatments selected, as previous studies for similar Fe-Ni based microwires confirm that annealed at the same T_{ann} for longer annealing time (t_{ann} = 8 h) still maintain amorphous structure [29,30]. Then, H_c (t_{ann}) tendency should be related to the domain wall stabilization by directional atomic pair ordering [31,32], such as considered for amorphous materials composed of two or more ferromagnetic elements [32]. In fact, local nano-sized precipitations have been observed in Fe-Ni microwires subjected to annealing [30].

Curie temperature, T_c, of $Fe_{49.6}Ni_{27.9}Si_{7.5}B_{15}$ amorphous alloy (about 400 °C) is considerably lower than for $Fe_{62}Ni_{15.5}Si_{7.5}B_{15}$ alloy [10] and hence, for $Fe_{49.6}Ni_{27.9}Si_{7.5}B_{15}$ microwire the internal stresses relaxation plays a major role and DW stabilization is less appreciable as we will see below.

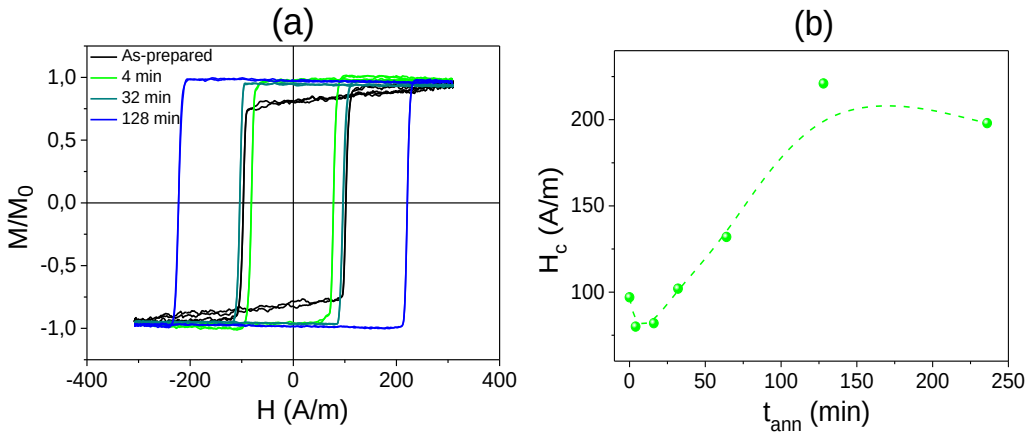

Figure 4.19. *Hysteresis loops of $Fe_{49.6}Ni_{27.9}Si_{7.5}B_{15}$ microwires as-prepared and annealed at T_{ann} = 410 °C for different annealing t_{ann} and H_c (t_{ann}) dependence (b).*

$Fe_{49.6}Ni_{27.9}Si_{7.5}B_{15}$ microwire chemical composition is close to the Invar-like composition, with Ni/Fe content of about 40/60. Invar-like crystalline materials possess low thermal expansion coefficients, related to their atomic

structure [33]. Taking into account short range order similarity of amorphous and crystalline materials [34], is reasonable to assume low internal stresses influence on the magnetic properties and hence on the DW dynamics for $Fe_{49.6}Ni_{27.9}Si_{7.5}B_{15}$ microwires.

Despite the magnetic hardening obtained for Fe-Ni based amorphous microwires upon annealing, this post-processing can be suitable to tailor the coercivity in this type of microwires.

v(H) dependence for $Fe_{62}Ni_{15.5}Si_{7.5}B_{15}$ microwire as-prepared and annealed in a conventional furnace at a fixed temperature of 410 °C for different t_{ann} is shown in *Figure 4.20a*, it can be observed the common linear dependence that can be described by *eq. (1.2)*. *S* dependence on t_{ann} is represented in *Figure 4.20b*. Upon annealing a noticeable increase of *v(H)* (for the same *H* values) and *S* is achieved. On the other hand, the minimum field for DW propagation observation, H_{min}, (that in magnetically bistable materials is associated to the coercivity) increases upon annealing (see *Figure 4.20a*).

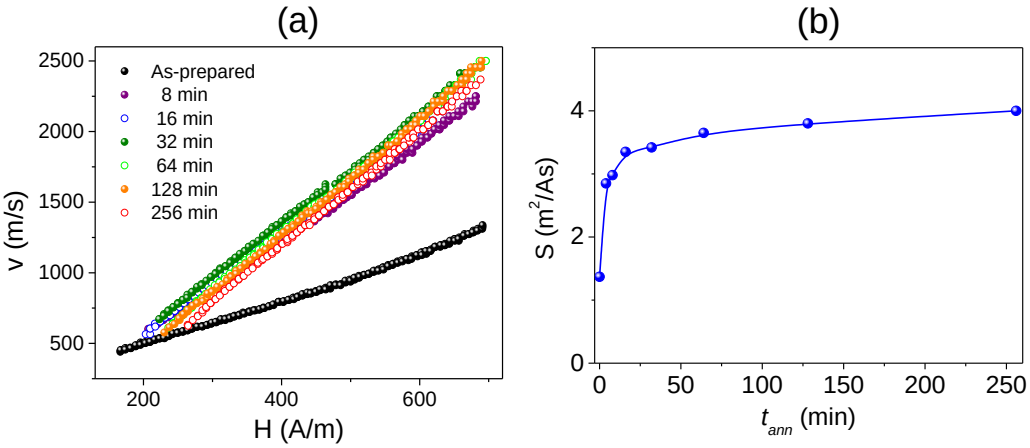

Figure 4.20. *v(H) dependence for as-prepared and annealed at 410 °C for different t_{ann} (a) and S(t_{ann}) dependence (b) $Fe_{62}Ni_{15.5}Si_{7.5}B_{15}$ microwires.*

This behaviour correlates with the H_c increase seen from the hysteresis loops presented before (*Figure 4.19*).

Domain wall mobility, *S,* is proportional to the domain wall width, δ_w [12,35,36]:

$$S \sim \delta_w \sim (A/K)^{1/2} \tag{4.3}$$

where *A* is the exchange stiffness constant and *K* is the magnetic anisotropy constant.

As discussed in *section 3.1*, in amorphous materials the main source of magnetic anisotropy is the magnetoelastic anisotropy, K_{me}, given by *eq. (1.1)*.

Consequently, if we assume that the magnetostriction coefficient of highly magnetostrictive microwires depends on annealing only slightly [35,36], we must assume that observed change in DW dynamics in Fe- and Fe-Ni rich microwires must be attributed to the stress relaxation.

The effect of applied stresses, σ_{app}, on the DW dynamics is shown in *Figure 4.21*. As predicted from aforementioned discussion, a decrease in *S*-

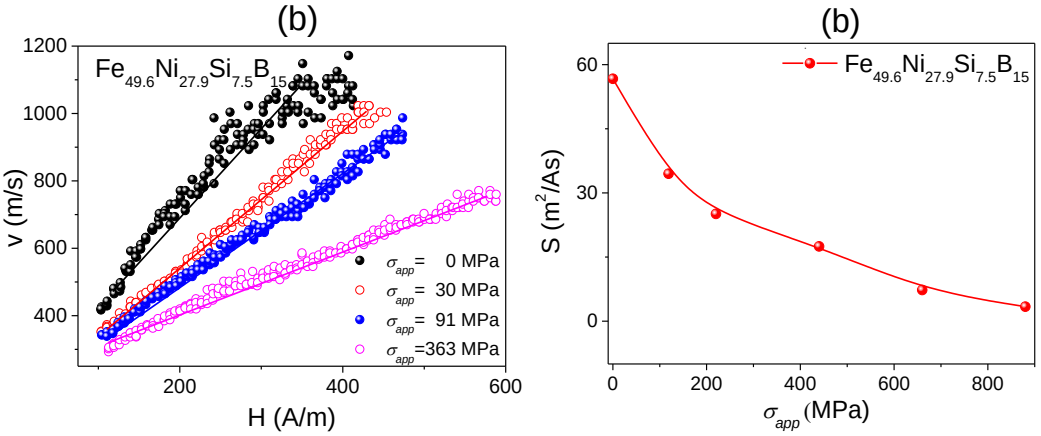

Figure 4.21. *Effect of different applied stresses on v(H) (a) and DW mobility as a function of the applied stress evaluated for* $Fe_{49.6}Ni_{27.9}Si_{7.5}B_{15}$ *microwire (b).*

values is observed with increase in σ_{app}

v(H) dependence and $S(t_{ann})$ for $Fe_{49.6}Ni_{27.9}Si_{7.5}B_{15}$ microwire annealed at the same conditions than $Fe_{62}Ni_{15.5}Si_{7.5}B_{15}$ sample can be seen in *Figure 4.22a* and *Figure 4.22b*, respectively. *Figure 4.22a* reflects in general lower *v(H)* values than those obtained for $Fe_{62}Ni_{15.5}Si_{7.5}B_{15}$ sample. For short t_{ann} a slight improvement in *v(H),* that correlates with H_c (t_{ann}) (*Figure 4.19*), can be

observed. However, for longer t_{ann} *v(H)* decreases. *S* (t_{ann}) presents the same tendency, an increase followed by a decrease for longer t_{ann}, being *S* values considerably high.

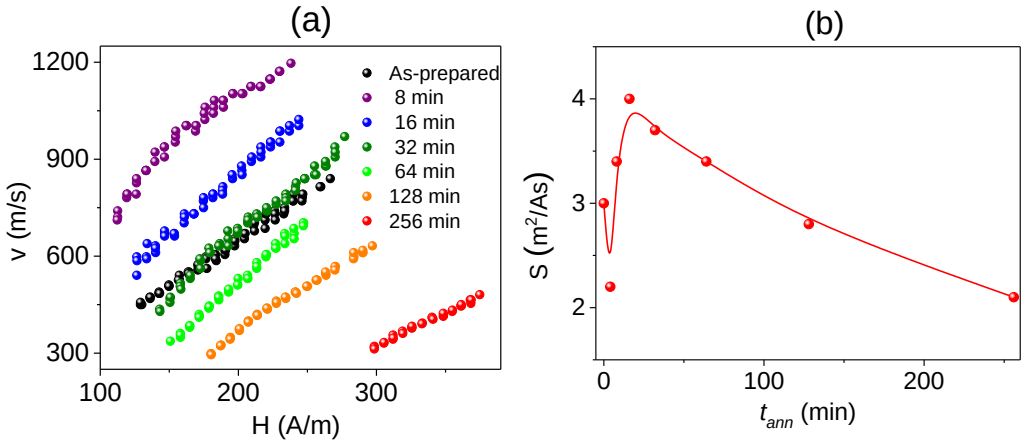

Figure 4.22. *v(H) dependence for as-prepared and annealed at 410 °C for different t_{ann} (a) and S (t_{ann}) dependence (b) $Fe_{49.6}Ni_{27.9}Si_{7.5}B_{15}$ microwires.*

Consequently, Fe-Ni- based microwires present effect of magnetic bistability and fast DW propagation. Annealing allows tuning the DW dynamics in Fe-Ni microwires. Considerable improvement in the DW velocity can be achieved for Fe-Ni-based microwires, less appreciable when the Ni content of the Fe-Ni based microwires is higher (as observed for $Fe_{49.6}Ni_{27.9}Si_{7.5}B_{15}$ microwire). Observed dependencies are related to different magnetoelastic anisotropies, DW stabilization and the difference in Curie temperatures.

On the other hand, similarly to Fe-rich microwires, Fe-Ni-base microwires present moderate GMI ratio (*Figure 4.23*).

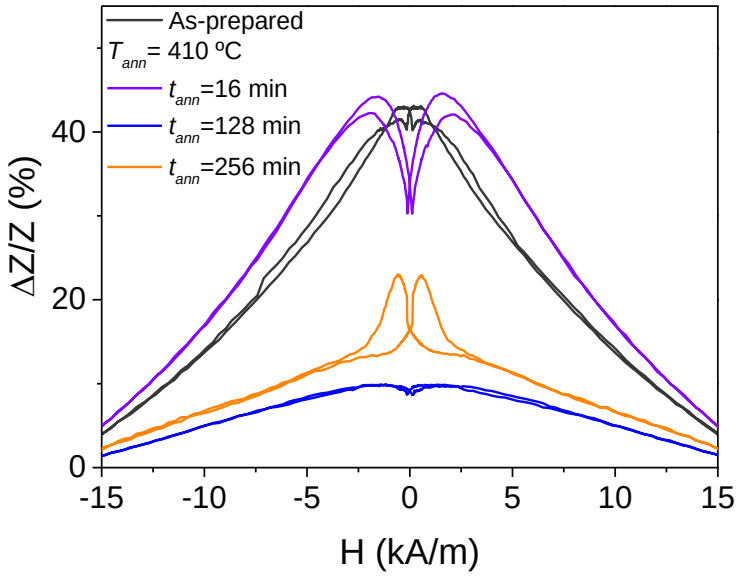

Figure 4.23. *GMI ratio measured in as-prepared (a) and annealed at 410 °C for 16 (b), 128 (c) and 256 (d) minutes* $Fe_{47.4}Ni_{26.6}Si_{11}B_{13}C_2$ *microwires measured at 600 MHz.*

4.2.3. Stress-annealing in FeBSiC microwires

4.2.3.1. Tuning of domain wall dynamics by stress-annealing

For amorphous glass coated microwires, the change in the magnetoelastic anisotropy (given by *eq. (1.1)*) by the stress relaxation induced by the annealing, being this the main source of magnetic anisotropy in absence of magnetocrystalline anisotropy, can explain the increase in the domain wall velocity and mobility.

Then, stress-annealing was performed in this $Fe_{75}B_9Si_{12}C_4$ microwire. In *Figure 4.24* it can be appreciated the disappearance of the rectangular shape of the hysteresis loop of as-prepared sample, that maintains up to 30 min of annealing time, with a more remarkable magnetic softening achieved increasing the annealing time, t_{ann}.

It must be take into account that the difference in the thermal expansion coefficients between the metallic nucleus and the glass coating is the responsible to induce most part of the internal stresses [3-5].

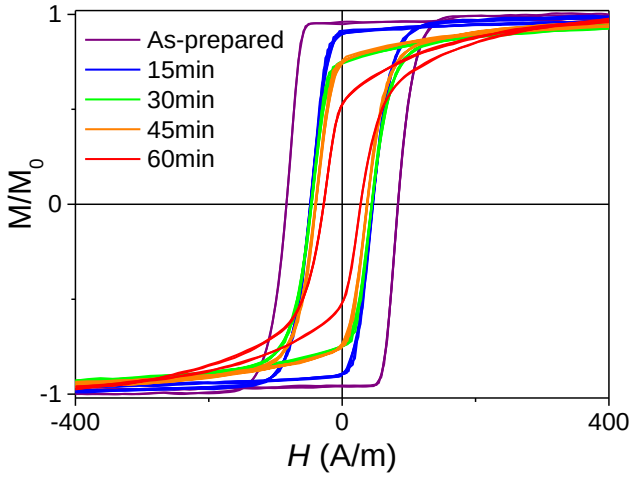

Figure 4.24. *Hysteresis loops of $Fe_{75}B_9Si_{12}C_4$ microwires as-prepared and stress-annealed with σ = 190 MPa at T_{ann} = 325 °C for different t_{ann}.*

v(H) dependence of stress-annealed samples (*Figure 4.25a*) reflects a drastic increase in the DW velocity and mobility increasing with the increase in the annealing time.

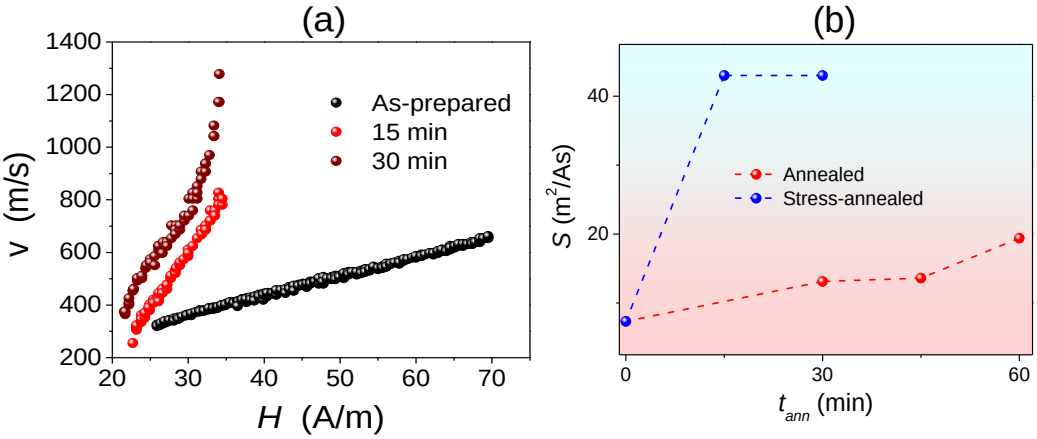

Figure 4.25. *v(H) dependence of as-prepared and stress-annealed* $Fe_{75}B_9Si_{12}C_4$ *microwires with σ = 190 MPa at T_{ann} = 325 °C for different t_{ann} (a) and $S(t_{ann})$ for $Fe_{75}B_9Si_{12}C_4$ microwires annealed at T_{ann}= 325 °C (b).*

Comparison of S (t_{ann}) values evaluated for conventional annealed and stress-annealed microwires is plotted in *Figure 4.25b*. $S \approx 7$ m^2/A·s for as-prepared sample substantially increases after annealing at 325 °C achieving $S \approx 10$ m^2/A·s, while after stress-annealing a more remarkable increase, up to $S \approx 40$ m^2/A·s, is obtained. This remarkable increase must be associated with transverse magnetic anisotropy induced by the stress annealing and reflected in the coercivity and remanent magnetization decrease (*Figure 4.24*).

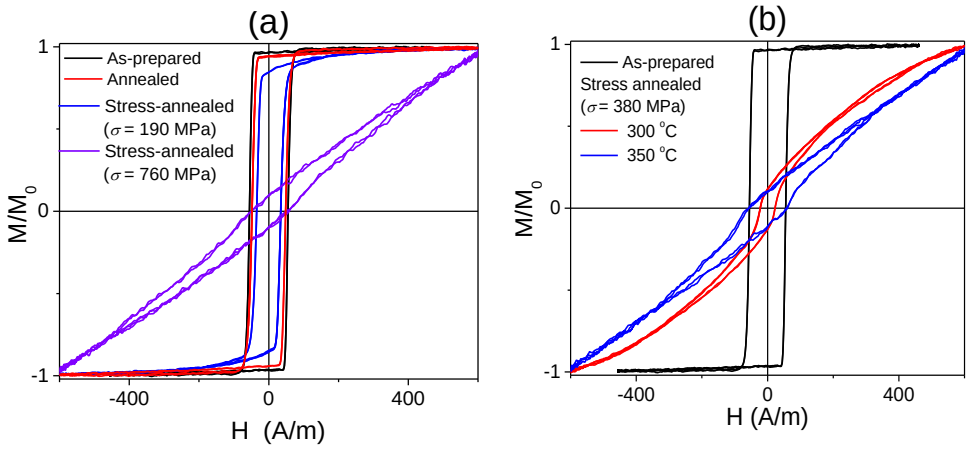

Figure 4.26. *Hysteresis loops of $Fe_{75}B_9Si_{12}C_4$ microwires as-prepared, annealed and stress-annealed at T_{ann}= 300 °C for t_{ann} = 60 min (a) and stress-annealed (σ = 380 MPa, t_{ann} = 30 min) at different temperatures (b).*

Stress-induced anisotropy can be tuned not only by modifying the annealing time but also changing the annealing temperature, T_{ann}, and the stress applied during the annealing, whose influence is studied in *Figure 4.27*. Stress-annealing at high enough T_{ann} and σ transforms the rectangular hysteresis loop into almost linear.

Considering that the magnetic domain structure of magnetic wires is assumed to be consisting of outer domain shell with transverse magnetization orientation and inner axially magnetized core [28,37], the domain structure modification can be evaluated from the squareness ratio, M_r/M_s, as described by *eq. (3.1)*.

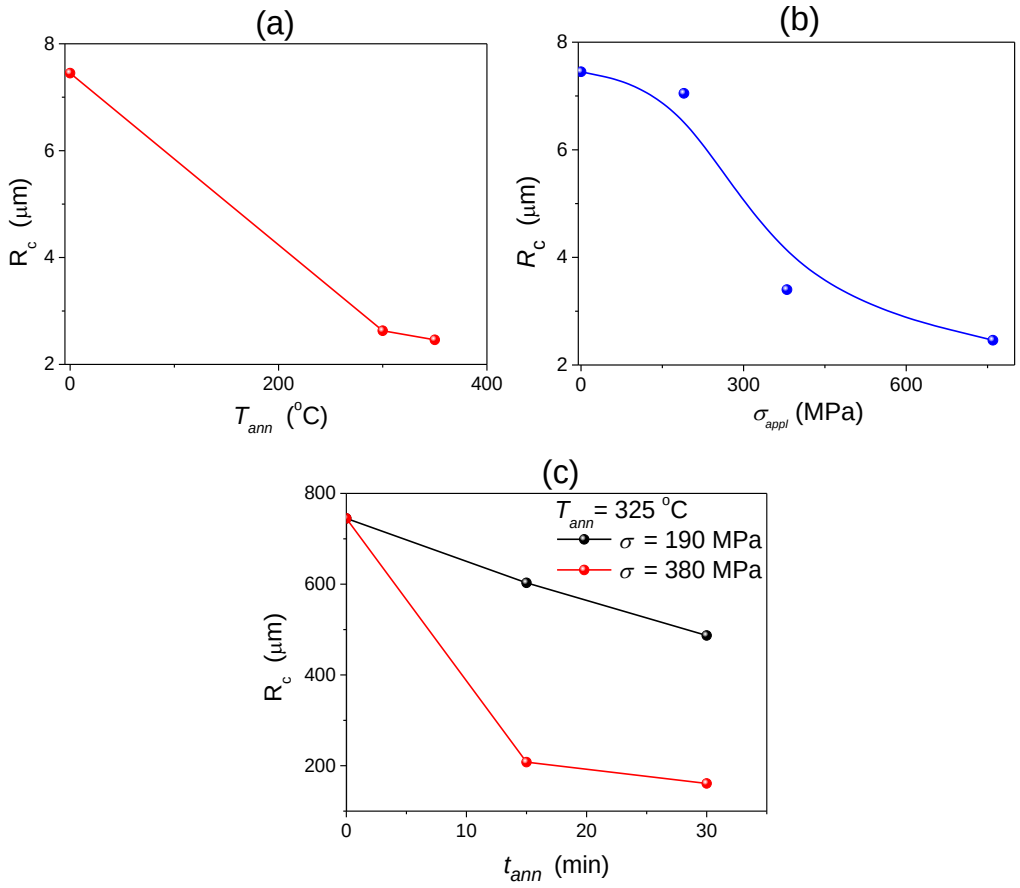

Figure 4.27. *Effect of annealing temperature (a), stress applied during annealing at T_{ann} = 300 °C (b) and annealing time (c) on R_c-values of studied microwire.*

In this way from M_r/M_s-values obtained from hysteresis loops presented in *Figure 4.27* we evaluated the dependence of the radius of inner axially magnetized core, R_c, on annealing conditions. As can be appreciated from *Figure 4.27*, R_c -values progressively decrease with increasing of σ_{appl}, T_{ann} and t_{ann} values.

At fixed annealing temperature the radius of inner axially magnetized core, R_c, is lower at higher applied stress (*Figure 4.27b,c*).

From aforementioned analysis, we can deduce that the stress-annealing allows the increase of the volume of outer domain shell with transverse magnetization orientation increase in expense of decreasing of the radius of inner axially magnetized core.

Consequently, beneficial effect of transverse magnetic anisotropy on DW velocity (see *Figure 4.25*) must be attributed to the increase of the volume of outer domain shell with transverse magnetic anisotropy.

One of the obstacles limiting applications of fast DW propagation observed in micro- and nano-wires is that the travelling DW is essentially not abrupt [38-40]. However, the characteristic width δ of a head-to-head DW is closely related to the magnetoelastic anisotropy [39]. Thus, the reduced head-to-head domain wall width δ/d (d is the metallic nucleus diameter) is determined by the value of the anisotropy constant K: for $K = 10^4$ erg/cm^3, $\delta/d \approx 13.5$ and for $K = 10^3$ erg/cm^3, $\delta/d = 40–50$ [39]. For these estimations, it was assumed that the whole volume of the metallic nucleus diameter presents axial magnetization.

In the present case, we are able to tune the volume of the inner axially magnetized core by annealing time and stress applied during the annealing (see *Figure 4.27*). Therefore, we may expect the modification of DW characteristic width δ upon stress annealing.

The characteristic DW width can be evaluated from the *EMF* signals generated by a head-to-head DW moving through the microwire [39].

The *EMF*, ε, generated within the turn of the pick-up coil by a change in the magnetic flux can be expressed as [39]:

$$\varepsilon(t) = \frac{\Delta\phi}{\Delta t} \tag{4.4}$$

where $\phi = BS$ is the magnetic flux, S is the area of the surface, $B = M + H$ is the magnetic induction, and M is the magnetization. Thus, the features (the amplitude and width) of the *EMF* peaks must be determined by $\frac{\partial M}{\partial t}$.

As can be appreciated from *Figure 4.28*, a decreasing of the *EMF* signal width from the pick-up coil can be appreciated after stress-annealing. The *EMF* signals, ε, have been compared for as-prepared and stress-annealed for

different t_{ann} samples (*Figure 4.28a*), as well as for as-prepared and those annealed under stress and without stress (*Figure 4.28b*).

Such changes are evidenced by the evaluation of the half-width, *W*, of the *EMF* signal with annealing time provided in *Figure 4.28c*. As can be appreciated, a decrease of half-width of the *EMF* signal after stress-annealing is evidenced.

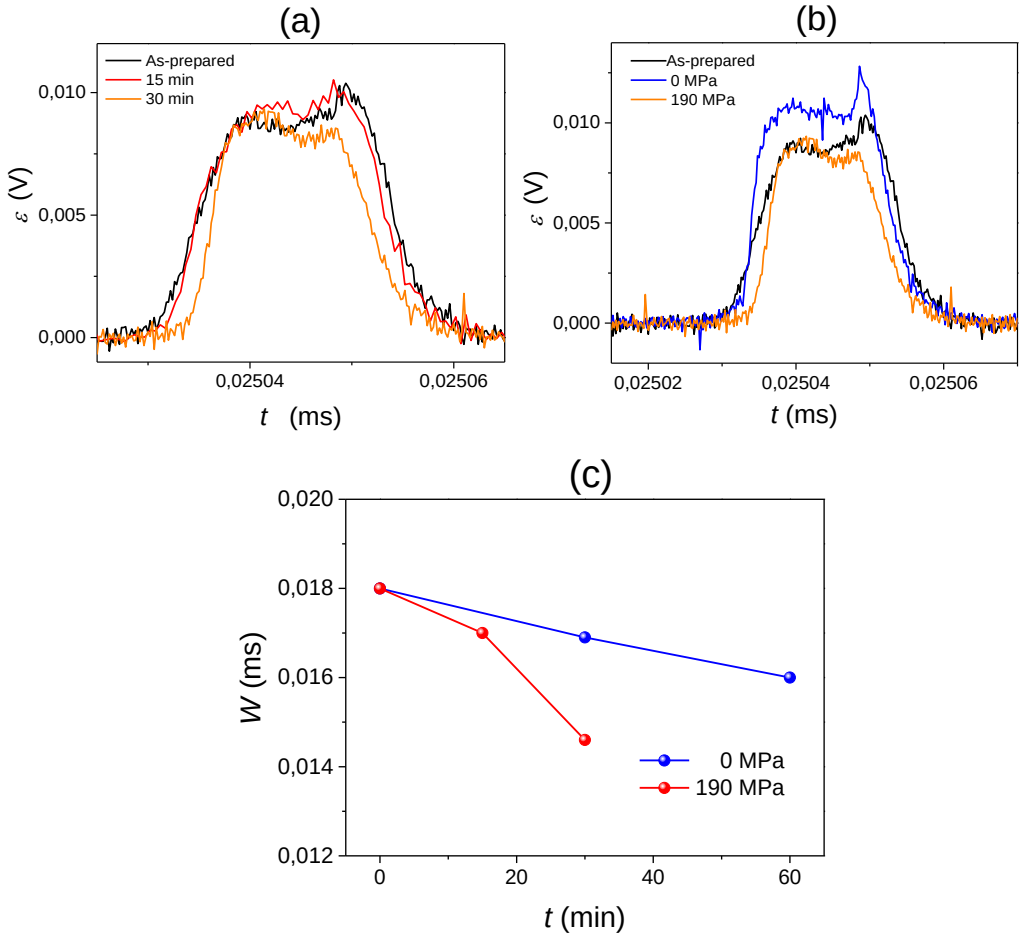

Figure 4.28. *EMF peaks induced by the magnetization change in pick-up coils measured for $Fe_{75}B_9Si_{12}C_4$ microwires as-prepared and stress-annealed (σ = 190 MPa) for different t_{ann} (a), as-prepared and annealed at T_{ann} = 325 °C for 30 min without stress and under stress (b) and dependence of the half-width of the EMF peaks with the annealing time (c).*

As discussed above, such decreasing of the half-width (full width at half maximum), *W*, must be associated either to the decreasing of the characteristic DW width or to the DW velocity increasing. The reason for such modifications can be stress-annealing induced transverse magnetic anisotropy as well as reduction of the volume of the inner axially magnetized core after stress-annealing. Indeed as mentioned above, the δ –values are determined by the magnetoelastic anisotropy and by the diameter of the axially magnetized core.

In order to separate these two factors we must analyze in more detail the *EMF* generated within the pick-up coil. Previously, the *EMF*, ε, generated within the pick-up coil turn when DW width, δ, is comparable with the distance to the coil turn, *z*, was analyzed [39]. The expression obtained in this case is [39]:

$$\varepsilon(t) = -QvR^2 \frac{\sqrt{\pi}}{2} \int dz_1 \frac{\langle \frac{\partial \alpha_z}{\partial z_1}(z_1 - vt) \rangle}{((z - z_1)^2 + R^2)^{3/2}} \tag{4.5}$$

where *R* is the radius of the coil turn, $v = -dz/dt$ is the domain wall velocity, $\frac{\partial \alpha_z}{\partial z_1}$ is the average linear density of the DW magnetic charge over the wire cross section and *Q* the magnetic charge.

The *eq. (4.5)* is rather complex. In the simplified case, when the characteristic domain wall width, δ, is small compared with the distance *z* from the coil turn to the DW position, the *eq. (4.5)* can be simplified as [39]:

$$\varepsilon(t) = -\frac{\sqrt{\pi}}{2} \frac{QvR^2}{(z + R^2)^{3/2}} \tag{4.6}$$

We can compare the *EMF* signals for as-prepared and stress-annealed samples if we consider the same coil parameters.

In this case the only difference in *EMF* values must be associated to the different DW velocity, *v*, values and difference in remanent magnetization of as-prepared and stress- annealed samples. The latter contributes through the magnetic charge, *Q*, given by [39]:

$$Q = 2M_r S \tag{4.7}$$

where S is the sample cross section and M_r – remanent magnetization. This is attributed to the fact that only the remagnetization reversal of the inner axially magnetized core contributes to the *EMF* signal.

These considerations allow us to evaluate if the difference in half-width of the *EMF* signal of as-prepared and stress- annealed (T_{ann} = 325 ^{o}C, σ_{appl} = 190 MPa, t_{ann} = 30 min) microwires is attributed only to different DW velocities or if DW shape change after stress annealing also takes place. Obtained velocities ratio taken from *Figure 4.25a* for H = 25 A/m for stress annealed and as-prepared samples (v_{sa} and v_{ap}, respectively) gives $v_{sa}/v_{ap} \approx 1.25$. However, considering the difference in the remanent magnetization (evaluated from *Figure 4.24*), the ratio $Q_{sa}\, v_{sa}/\, Q_{ap}\, v_{ap} \approx 0.98$ (where Q_{sa} and Q_{ap} are values for stress-annealed and as-prepared samples). While the W –values ratio, i.e., W_{sa}/W_{ap} (where W_{ap} and W_{sa} are the half-width of the *EMF* peaks for as-prepared and stress-annealed samples) is about 0.83.

Consequently, we can assume the characteristic DW width reduction in stress-annealed microwires.

4.2.3.2. Effect of stress-annealing on GMI effect of Fe-rich microwires

Similarly to Co-rich microwires, we used stress-annealing in order to improve the GMI effect. As shown above, stress-annealing allows to induce transverse magnetic anisotropy in Fe-rich microwires.

A remarkable GMI ratio improvement is observed upon stress-annealing of Fe-rich microwires (see *Figure 4.29*). As-compared to as-prepared microwire, stress-annealing (T_{ann} = 350 °C, t_{ann} = 60 min and σ_m = 190 MPa) allows an order of magnitude improvement of maximum GMI ratio, $\Delta Z/Z_{max}$, (see *Figure 4.29a* and *Figure 4.29b*). The other relevant feature is that stress-annealed

microwires present unusual *ΔZ/Z(H)* dependencies (see *Figure 4.29b*): low frequency *ΔZ/Z(H)* dependencies (10-50 MHz) are similar to that of as-prepared microwire, i.e., single peak dependence with a decay from H = 0. However, rising the frequency an additional maximum on *ΔZ/Z(H)* dependencies appears (*Figure 4.29b*). Therefore, at intermediate frequency range (100-300 MHz) *ΔZ/Z(H)* dependencies present irregular shape that recently has been interpreted as the superposition of the double-peak *ΔZ/Z(H)* dependence typical for transverse magnetic anisotropy and single-peak reported for axial magnetic anisotropy [4]. At elevated frequencies *ΔZ/Z(H)* dependencies present *ΔZ/Z(H)* dependence typical for the wires with transverse magnetic anisotropy (see *Figure 4.29c*).

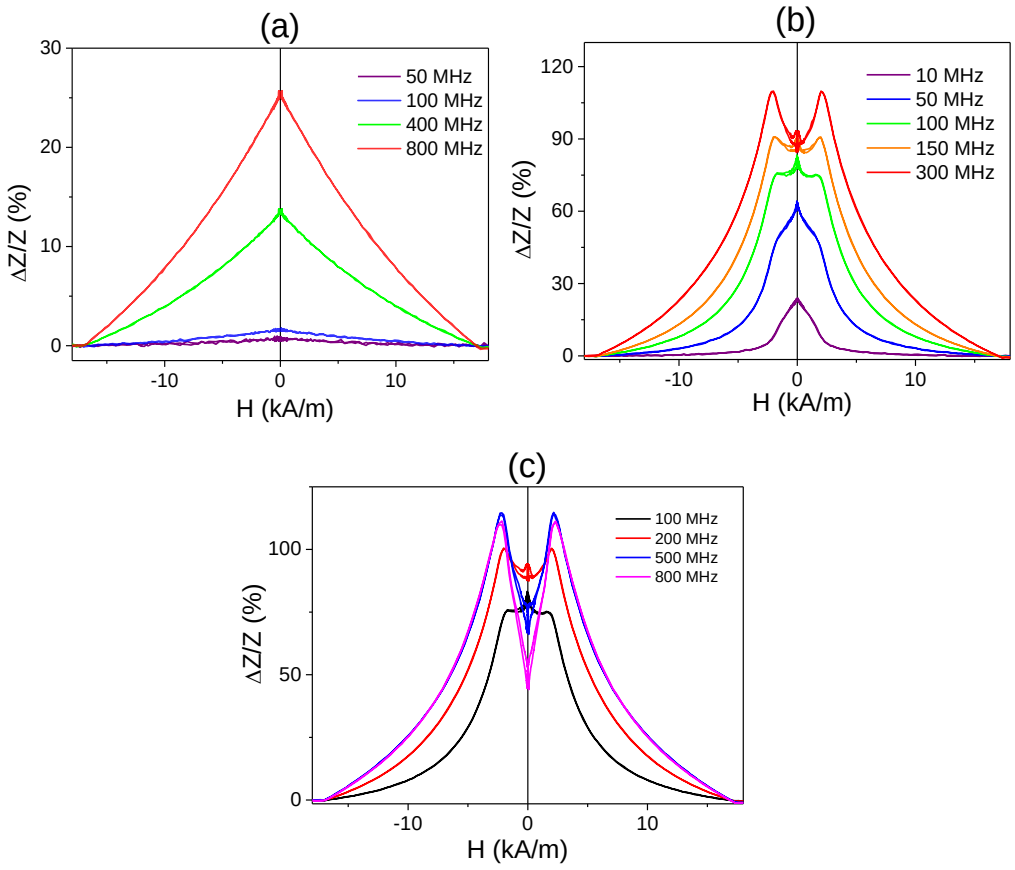

Figure 4.29. *ΔZ/Z(H) dependencies observed in as-prepared (a) and stress-annealed at T_{ann} =350 °C (for 60 min and σ_m = 190 MPa) $Fe_{75}B_9Si_{12}C_4$ microwires.*

Such frequency influence on *ΔZ/Z(H)* dependencies can be interpreted considering existence of inner axially magnetized domain inside the stress-annealed microwires and frequency dependence of the skin penetration depth, δ, as described in [4].

It is worth mentioning, that such irregularity can be observed in *ΔZ/Z(H)* dependencies for stress-annealed microwires at different annealing conditions. Thus, similar irregular dependencies have been observed for microwires annealed at 250 °C (*Figure 4.30a*) and 300 °C (*Figure 4.30b*) for 60 min and 900 MPa. However, the frequency range at which such unusual *ΔZ/Z(H)* dependencies are observed depend on stress- annealing conditions: for lower annealing temperature the frequency range (70-200 MHz) is shifted to lower frequencies.

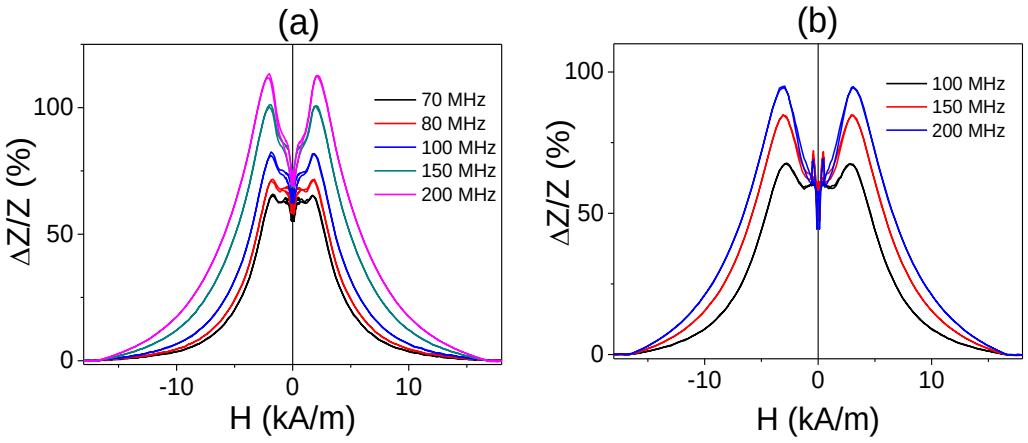

Figure 4.30. *ΔZ/Z(H) dependencies observed in stress-annealed at T_{ann} = 250 °C for 60 min and σ_m = 900 MPa (a) and T_{ann} = 300 °C for 60 min and σ_m = 900 MPa (b) $Fe_{75}B_9Si_{12}C_4$ microwires.*

From above presented results it is clear that the frequency is one of the important parameters allowing GMI ratio optimization. One of the parameters that can be used as a reference is the maximum GMI ratio, $\Delta Z/Z_{max}$. For as-prepared samples $\Delta Z/Z_{max}$ corresponds to H_m = 0, however, for the stress-annealed sample $\Delta Z/Z_{max}$ is observed at some field, $H_m \neq 0$. Frequency

dependence of maximum GMI ratio has been evaluated for as-prepared and one of the stress-annealed samples (T_{ann} = 350 °C, t_{ann} = 60 min, σ_m = 190 MPa).

From *Figure 4.31* it can be deduced that the proposed stress-annealing allows $\Delta Z/Z_{max}$ improvement. This improvement is most remarkable for the frequency band up to 200 MHz where $\Delta Z/Z_{max}$ of stress-annealed samples is 1-2 order superior than $\Delta Z/Z_{max}$ -values of as-prepared sample. Furthermore, in stress-annealed sample $\Delta Z/Z_{max}$ up to 120% is achieved at wide frequency range from 500 MHz up to 1 GHz.

The observed beneficial effect of stress-annealing must be related to stress-annealing induced magnetic anisotropy, which allows the transformation of the domain structure towards more favorable for the GMI effect optimization.

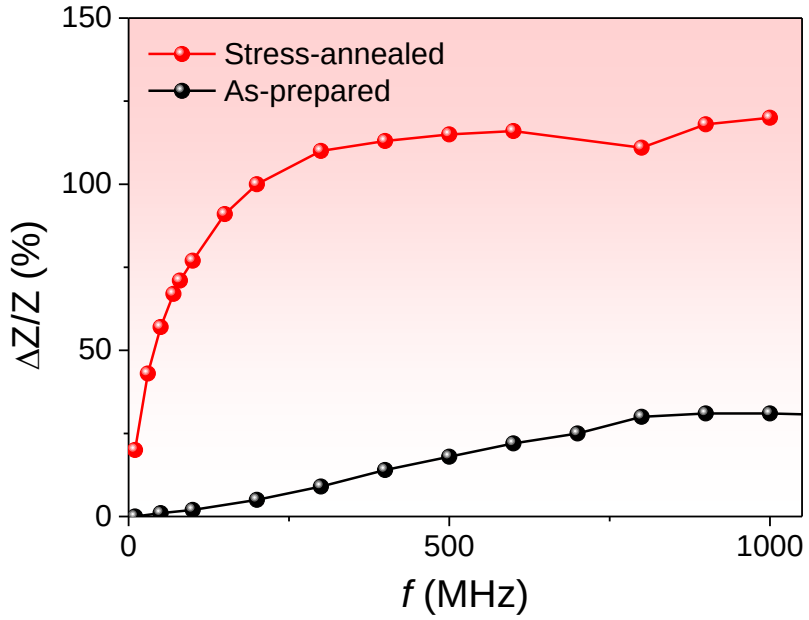

Figure 4.31. *Frequency dependence of maximum GMI ratio of as-prepared and stress-annealed (T_{ann} = 350 °C, t_{ann} = 60 min, σ_m = 190 MPa) microwires.*

4.2.3.3 Effect of stress-annealing on applied stress dependence of hysteresis loops of Fe-rich microwires

One of the most attractive applications of glass-coated microwires is related to stresses monitoring [41-43]. Accordingly, a design of magnetoelastic sensors and stress-sensitive composites based on stress dependent magnetic properties of microwires was reported.

Previously, tensile stress dependence of as-prepared Fe-rich microwires was studied [44,45]. As shown [44,45], generally the hysteresis loop maintains rectangular character, while an increase in H_c upon applied stress is observed [44,45].

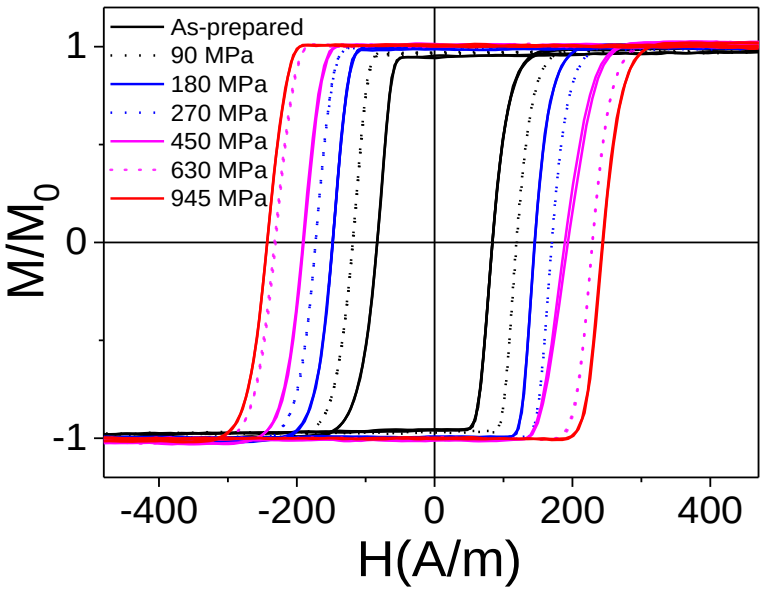

Figure 4.32. *Hysteresis loops of as-prepared and subjected to different applied stresses $Fe_{75}B_9Si_{12}C_4$ microwire.*

Below the stress-dependence of hysteresis loops and magnetic properties of as-prepared and stress-annealed Fe-rich microwires will be compared.

As-prepared and stress-annealed $Fe_{75}B_9Si_{12}C_4$ microwire was subjected to different applied stresses, for values of applied stress, σ, ranging from 90 to 945 MPa.

Under applied stress the hysteresis loop of $Fe_{75}B_9Si_{12}C_4$ microwire maintains its rectangular shape [41-46] with an increase in the coercive field, H_c, and switching field, H_s, upon increase in the applied stress, as can be seen in *Figure 4.32*. Coercive and switching field values are affected by the frequency, f, and amplitude of the magnetic field, H_0, [46,47] for this reason all the measurements were performed at fixed values of f and H_0.

Considering the following equation [44,45]:

$$H_S \propto \gamma \propto \frac{[A(3/2)\ \lambda_S\,(\sigma + \sigma_r)]^{1/2}}{cos\alpha} \tag{4.8}$$

with A the exchange energy constant, λ_S the saturation magnetostriction constant, σ_r, the residual tensile stresses and α the angle between the magnetization and the axial direction. For $\sigma > \sigma_r$ and $cos\ \alpha \approx -1$, H_s must be proportional to $\sigma^{1/2}$.

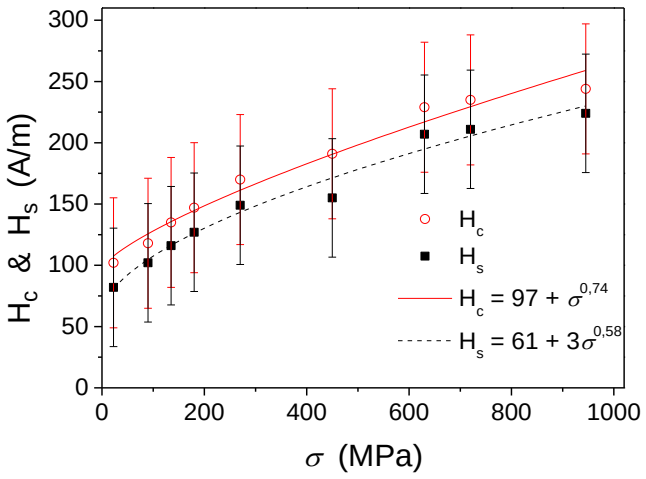

Figure 4.33. *Evaluated $H_c(\sigma)$ and $H_s(\sigma)$ dependencies for as-prepared $Fe_{75}B_9Si_{12}C_4$ microwires.*

As can be appreciated in *Figure 4.33*, in the present case H_s can be described rather well with $\sigma^{1/2}$ dependence. However, $H_c(\sigma)$ can be better described by $H_c = 94 + \sigma^{0,68}$ dependence. The difference between both fittings is not very significant, however we can consider that for the case of H_c (σ) dependence the contribution of the finite domain wall velocity can originate some difference in H_s and H_c –values.

It is worth mentioning, that $H_s \sim \sigma^{1/2}$ stress dependence has been previously reported for amorphous wires prepared by alternative (in-rotating-water) technique [47]. However, for conventional amorphous wires $H_s \sim \sigma^{1/2}$ dependence is observed only for high enough σ–values. At low σ region, below some threshold, a minimum of H_c is found for a certain σ–value [47]. The origin of this minimum on $H_c(\sigma)$ dependence observed for conventional wires was attributed to complex internal stresses. In the present case of glass-coated microwires the $H_c(\sigma)$ dependence is generally in agreement with predicted $H_s \sim \sigma^{1/2}$ for as-prepared microwires (see *Figure 4.33*).

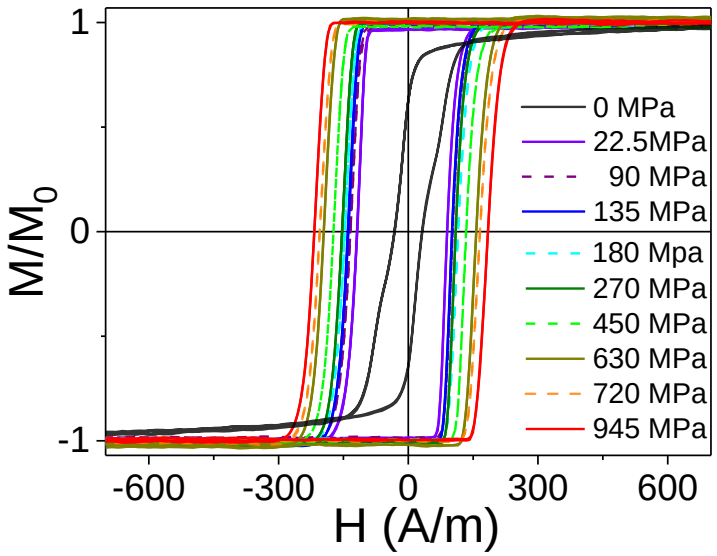

Figure 4.34. *Hysteresis loops of stress-annealed $Fe_{75}B_9Si_{12}C_4$ microwires upon stress application.*

Hysteresis loops of stress-annealed $Fe_{75}B_9Si_{12}C_4$ microwire present not only better magnetic softness with lower coercivity ($H_c \approx 35$ A/m) as compared

to as-prepared $Fe_{75}B_9Si_{12}C_4$ microwire (*Figure 4.34*), but also better stress-sensitivity. Indeed, upon application of even small tensile stress (22.5 MPa) the hysteresis loop undergoes a transformation to perfectly rectangular (see *Figure 4.34*). Upon this transformation a considerable coercivity growth up to $H_c \approx 100$ A/m and remanent magnetization, M_r/M_s, from 0.65 to 0.97 is observed.

Such perfectly rectangular character of hysteresis loops is maintained under further increase of applied stress (see *Figure 4.34*). The tensile stress dependence of $\sigma \geq 22.5$ MPa is similar to as-prepared sample: the hysteresis loops shape maintains rectangular character and an increase in coercivity, H_c, and switching filed, H_s, is observed (*Figure 4.34*).

Consequently, stress-annealed $Fe_{75}B_9Si_{12}C_4$ microwire presents stress-induced magnetic bistability.

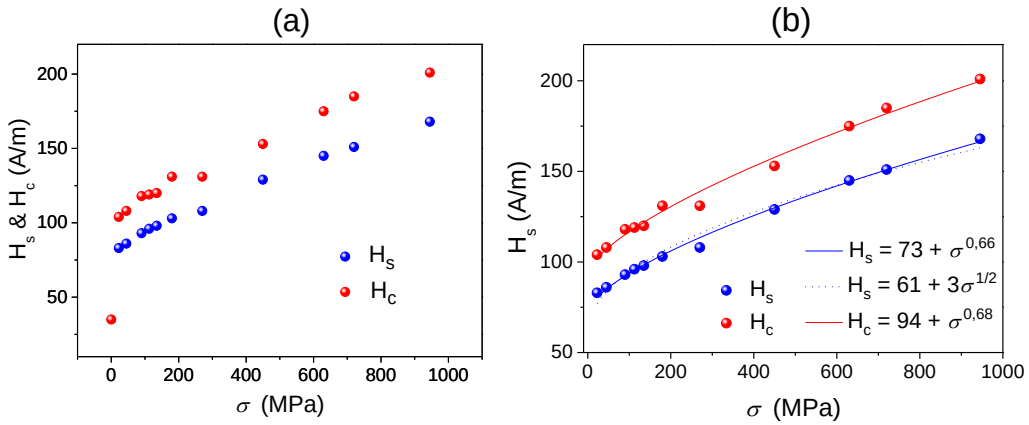

Figure 4.35. *Experimentally measured stress-dependence of H_c and H_s for stress-annealed $Fe_{75}B_9Si_{12}C_4$ microwires (a) and fittings for $H_c(\sigma)$ and $H_s(\sigma)$ dependencies (b).*

From observed $H_s(\sigma)$ dependence (see *Figure 4.35*) we can deduce that the stress-annealed $Fe_{75}B_9Si_{12}C_4$ microwire with stress-induced magnetic bistability can be described in terms of $\sigma^{1/2}$ law above some critical σ–value similarly to the wires and microwires with spontaneous magnetic bistability. Considering such $H_s \sim \sigma^{1/2}$ law we can assume that for applied magnetic field just above the switching field the magnetization process takes place mainly by the domain wall displacement in the inner axially magnetized core [46].

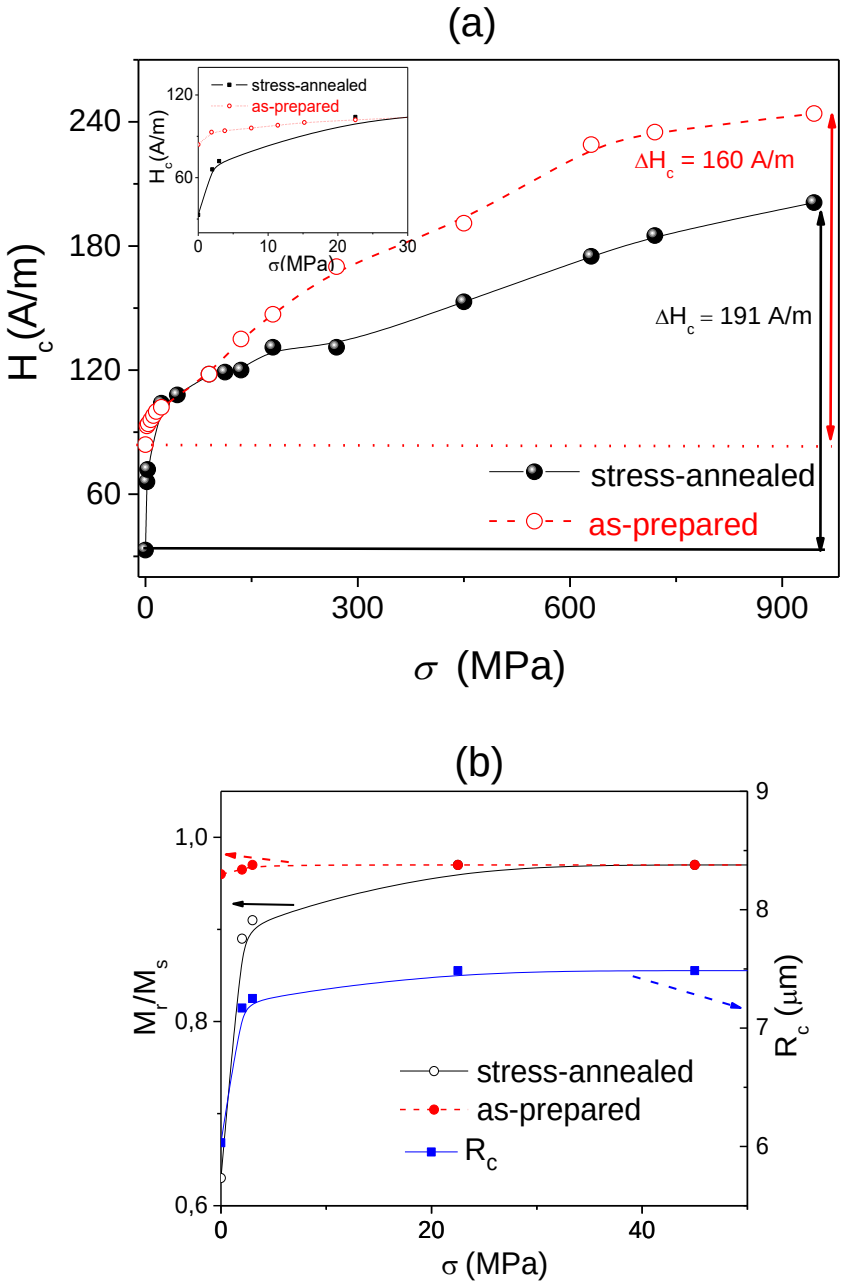

Figure 4.36. *Comparison of $H_c(\sigma)$ (a) and $M_r/M_s(\sigma)$ (b) dependencies in as-prepared and stress-annealed $Fe_{75}B_9Si_{12}C_4$ microwires.*

The advantage of proposed stress-annealing is such that this post-processing allows enhancement of the stress dependence of coercivity. The difference in H_c (σ) dependencies of as-prepared and stress-annealed $Fe_{75}B_9Si_{12}C_4$ microwire can be appreciated from *Figure 4.36a*. As clearly seen from *Figure 4.36a*, at the same amplitude of applied stress (950 MPa) the range

of change of coercivity, ΔH_c, for as-prepared $Fe_{75}B_9Si_{12}C_4$ sample is 160 A/m and for stress-annealed $Fe_{75}B_9Si_{12}C_4$ sample ΔH_c = 191 A/m. This difference is most remarkable for the range of low σ–values, making stress-annealing suitable for detection of low applied stresses. Similarly, squareness ratio, M_r/M_s, of stress-annealed $Fe_{75}B_9Si_{12}C_4$ sample presents more significant changes at low σ region.

Observed stress dependencies of the squareness ratio must be associated with changes of domain structure. Indeed, it is commonly accepted that the domain structure of Fe-rich microwires consists of inner axially magnetized core and outer shell with transverse magnetization easy direction [38,47].

As can be observed from *Figure 4.36b*, M_r/M_s ratio of stress-annealed $Fe_{75}B_9Si_{12}C_4$ sample rapidly increases upon applied stress. Considering *eq. (3.2)* we obtained R_c modification under applied stress influence from 6 up to almost 7.5 μm as depicted in *Figure 4.36b*. Consequently, we must assume change of domain structure in stress-annealed $Fe_{75}B_9Si_{12}C_4$ sample under influence of applied stresses in stress-annealed $Fe_{75}B_9Si_{12}C_4$ sample consisting of rising of the inner axially magnetized core radius from 6 up to almost 7.5 μm.

4.2.4. Reversibility of the stress-annealing anisotropy

As shown above, stress annealing of as-prepared $Fe_{75}B_9Si_{12}C_4$ microwires, allows the induction of transverse magnetic anisotropy that depends on the stress-annealing conditions. *Figure 4.37* compares the rectangular hysteresis loop of as prepared $Fe_{75}B_9Si_{12}C_4$ microwires with the hysteresis loops of the microwires annealed at a fixed T_{ann} = 350 °C and time t_{ann} = 60 min, under different applied stresses, σ, showing the gradual transformation of the hysteresis loop into linear and the increase in H_k (*Figure*

4.37) with increasing the stress-applied during the annealing, that correlates with the decrease of the squareness ratio, M_r/M_s.

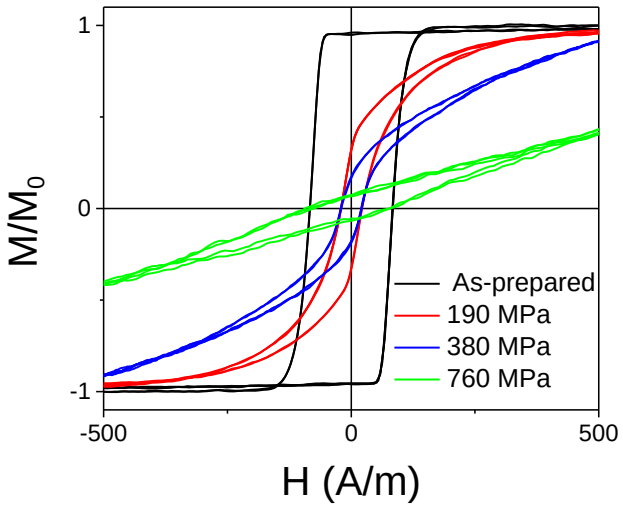

Figure 4.37. *Hysteresis loops of $Fe_{75}B_9Si_{12}C_4$ microwires as-prepared, stress-annealed at T_{ann} = 350 °C, t_{ann} = 60 min, under different applied stresses.*

H_c decreases at low applied stresses of 190 MPa and 380 MPa (inset of *Figure 4.38*) however for the higher stress applied H_c values are practically the same of as-prepared sample.

The radius of the inner axially magnetized core, R_c (as defined in *eq. (3.2)*), evaluated from M_r/M_s, shows a decrease with the increase in the applied stress during the stress-annealing *Figure 4.37*) that can be interpreted as the inner axially magnetized core reduction as the volume of microwire with transverse magnetic anisotropy grows.

To study the reversibility of the stress annealing anisotropy of a sample stress-annealed at a fixed σ, we performed a subsequent annealing without stress of the stress-annealed sample (SA) at the same temperature (T_{ann} = 350 °C) and for t_{ann} = 60 min, (SA + A), and a longer subsequent annealing, (SA + 2A), at the same temperature for t_{ann} = 150 min.

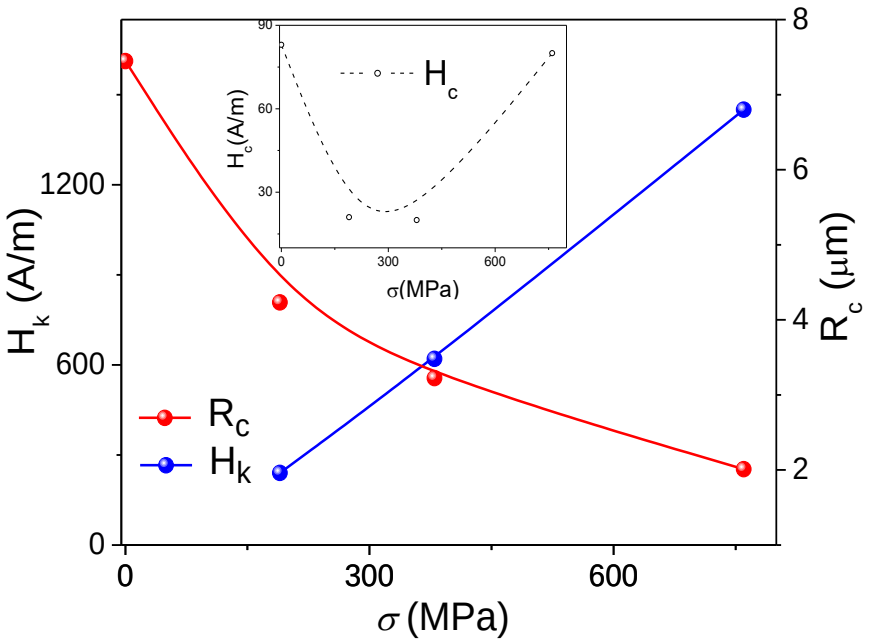

Figure 4.38. *H_k and R_c dependencies and H_c (on the inset) dependences on stress applied during the annealing. The lines in the figure are just guides for eyes.*

For the case of the microwire subjected to stress-annealing with σ = 190 MPa (hysteresis loops presented *in* *Figure 4.37* and *Figure 4.39a*) a partially recover of the stress-annealing anisotropy can be reached after the subsequent annealing. However, the hysteresis loop of microwire subjected to stress-annealing with σ = 76 MPa is less affected by subsequent annealing: it remains almost unchanged after subsequent annealing (see *Figure 4.39b*). As can be interpreted from M_r/M_s and R_c (t_{ann}) dependencies obtained from the hysteresis loops and represented in *Figure 4.40*, M_r/M_s and R_c values obtained after annealing (t_{ann} = 150 min) of stress- annealed with σ = 190 MPa sample reach values similar of those of as-prepared microwire. We can conclude that the subsequent annealing allows increasing the volume of the inner axially magnetized core.

Lower coercivity values of the sample subjected to longer subsequent annealing (t_{ann} = 150 min), as compared to as prepared sample, can be associated to the stress relaxation.

As observed from *Figure 4.39b,* hysteresis loops of the microwire stress-annealed with σ = 760 MPa followed by the subsequent annealing steps reflect much stronger induction of transverse magnetic anisotropy. The hysteresis loops of the microwire once subjected to stress-annealing do not change under subsequent annealing for t_{ann} = 60 min nor for longer t_{ann} = 150 min.

In R_c (t_{ann}) representation of *Figure 4.40*, comparing with sample stress-annealed with σ = 190 MPa, only a slight increase can be appreciated after the annealing procedures of the SA sample with σ = 760 MPa, for which the R_c (t_{ann}) dependence shows that after the stress annealing at those σ values most part of the microwire metallic nucleus possesses transverse magnetic anisotropy.

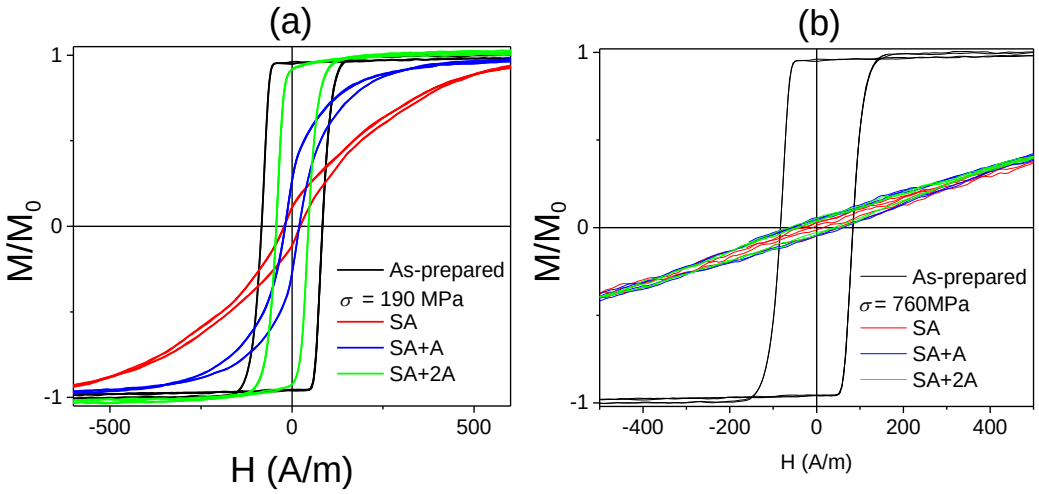

Figure 4.39. *Hysteresis loops of $Fe_{75}B_9Si_{12}C_4$ microwires as-prepared and stress annealed with σ = 190 MPa (a) and σ = 760 MPa (b) with subsequent annealing during 60 min and 150 min.*

The comparison between *Figure 4.37a* and *Figure 4.37b* and R_c (t_{ann}) dependence for both samples (*Figure 4.40)*, lead us to conclude that the increase in the applied stress during the stress annealing treatment implies a growth in the irreversible part of the stress-annealed induced magnetic anisotropy.

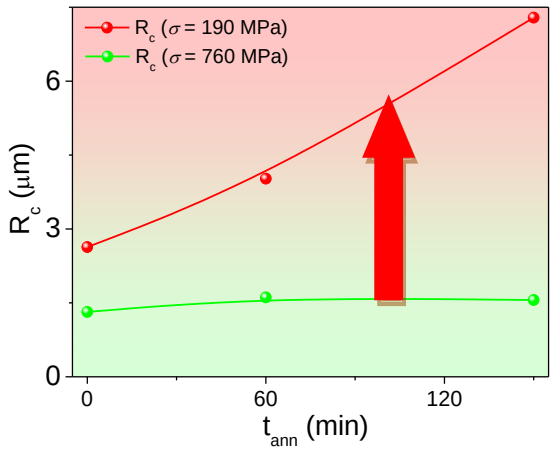

Figure 4.40. *Comparison of $R_c(t_{ann})$ dependence between samples stress-annealed upon σ = 190 and 760 MPa with subsequent annealing. The lines in the figure are just guides for eyes.*

One more advantage of Fe-rich microwire subjected to combined annealing (stress-annealing + subsequent annealing) is better GMI effect of such microwires.

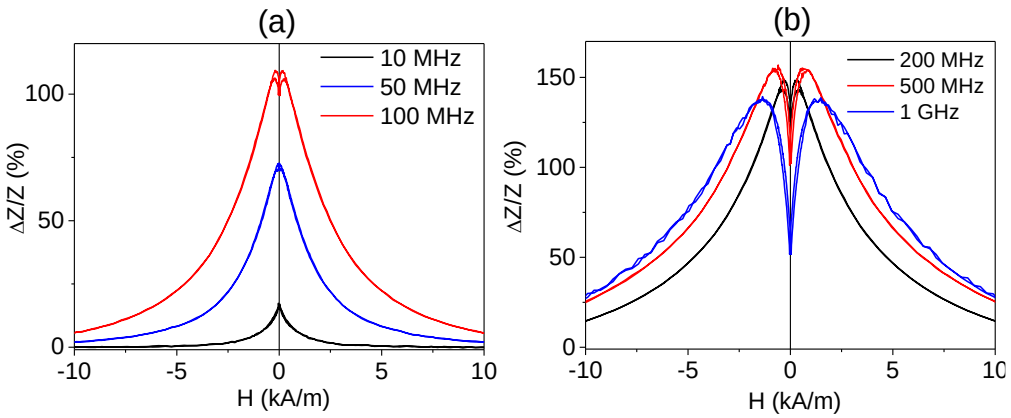

Figure 4.41. *ΔZ/Z(H) dependences of SA (σ = 190 MPa) and then annealed $Fe_{75}B_9Si_{12}C_4$ microwires measured at f ≤ 100 MHz (a) and at f ≥ 100 MHz (b).*

In spite of rectangular character of hysteresis loops of $Fe_{75}B_9Si_{12}C_4$ microwires stress annealed (SA) with σ = 190 MPa and then annealed at 350 °C for 150 min, such microwire present better GMI response as-compared to as-

prepared and even stress-annealed $Fe_{75}B_9Si_{12}C_4$ microwire: $\Delta Z/Z_{max}$ –values up to 150 % are recorded at 500 MHz (see *Figure 4.41*).

As shown in *Figure 4.41a* for $f \leq 80$ MHz the single peak $\Delta Z/Z(H)$ dependence is observed, while $f \geq 80$ MHz $\Delta Z/Z(H)$ dependence change from single-peak to double-peak type (see *Figure 4.41b*).

The proposed postprocessing consisting of stress-annealing followed by annealing allows suppressing the irregular $\Delta Z/Z(H)$ dependence observed in stress-annealed Fe-rich microwires (see *Figure 4.29*) by the subsequent annealing. One more example is provided in *Figure 4.42* and *Figure 4.43* for stress-annealing performed at σ = 760 MPa.

The stress-annealed (at σ = 760 MPa) $Fe_{75}B_9Si_{12}C_4$ microwire presents considerable GMI effect (see *Figure 4.42a and Figure 4.42b*) in spite of high transverse magnetic anisotropy that can be deduced from the hysteresis loops shown in *Figure 4.39*. As can be observed from *Figure 4.42a*, double-peak $\Delta Z/Z(H)$ dependencies are observed even for low frequencies (10-50 MHz). Rising the frequency, i.e., for intermediate frequencies ($100 \leq f \leq 200$ MHz) $\Delta Z/Z(H)$ dependencies present irregular shape (*Figure 4.42b*). Finally, for high frequencies ($f \geq 300$ MHz) again double peak $\Delta Z/Z(H)$ dependencies are observed (*Figure 4.42c*). Generally, observed $\Delta Z/Z_{max}$ –values are below 80%.

Higher $\Delta Z/Z_{max}$ –values (up to 120%) and double-peak $\Delta Z/Z(H)$ dependencies in a whole frequency range are observed for the $Fe_{75}B_9Si_{12}C_4$ microwire after SA (σ = 760 MPa) and then subsequently annealed (for 150 min) (see *Figure 4.43a* and *Figure 4.43b*).

From above presented experimental results we can deduce that annealing after stress annealing allows:

i) A remarkable GMI effect improvement as compared to as-prepared and even to stress-annealed Fe-rich microwires and

ii) Suppression of irregularities in $\Delta Z/Z(H)$ dependencies observed in all stress-annealed samples at intermediate frequencies (see *Figures 4.29, 4.41, 4.42* and *4.43*).

A beneficial influence of appropriate annealing after stress-annealing is evidenced from a comparison of the $\Delta Z/Z_{max}$ (f) dependencies presented in *Figure 4.44*. It is clearly seen that GMI effect improvement is observed in the whole frequency range. The highest $\Delta Z/Z_{max}$ ratio of about 160% is observed at 300 MHz (for the $Fe_{75}B_9Si_{12}C_4$ microwire SA at 190 MPa and then annealed) [48].

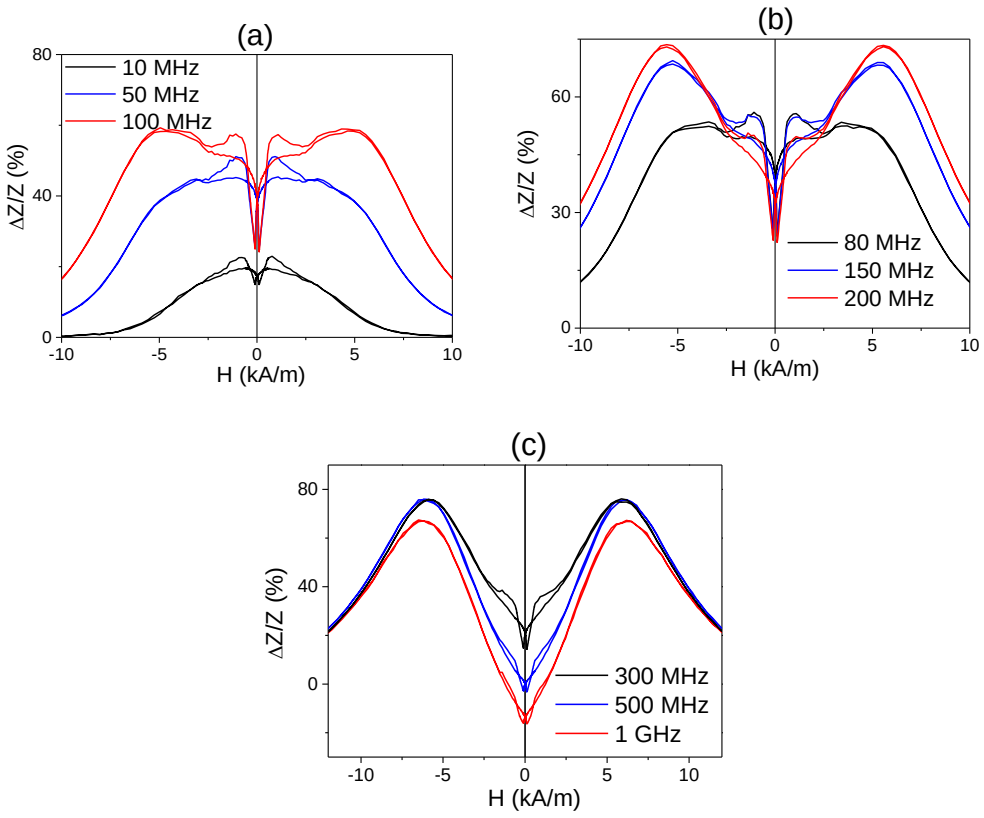

Figure 4.42. *ΔZ/Z(H) dependences of SA (σ = 760 MPa) $Fe_{75}B_9Si_{12}C_4$ microwire measured at f ≤ 100 MHz (a), 80 ≤ f ≤ 200 MHz (b) and at f ≥ 300 MHz (c).*

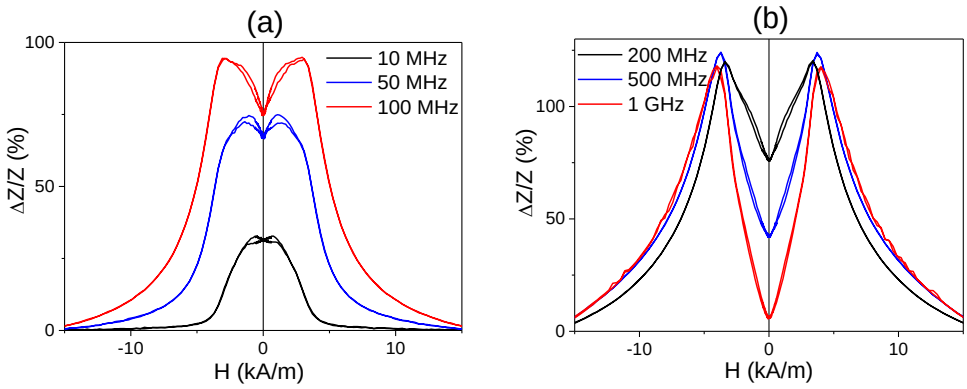

Figure 4.43. *ΔZ/Z(H) dependences of SA (σ = 760 MPa) + annealed $Fe_{75}B_9Si_{12}C_4$ microwire measured at f ≤ 100 MHz (a) and at f ≥ 200 MHz (b).*

In all the cases subsequent annealing allows $\Delta Z/Z_{max}$ –values improvement by up to 50%.

The observed beneficial effect of annealing on the GMI effect can be explained considering that annealing promotes the enhancement of circumferential anisotropy and, hence, suppresses the irregularities in the $\Delta Z/Z(H)$ dependencies.

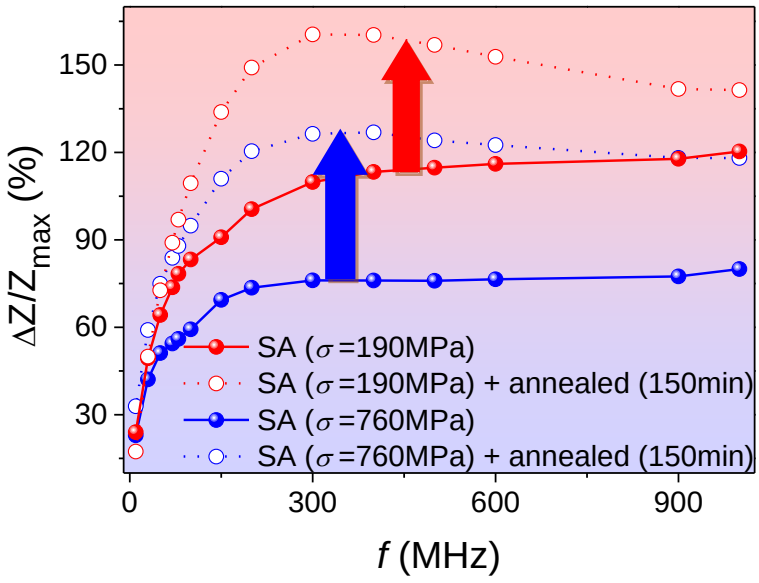

Figure 4.44. *$\Delta Z/Z_{max}(f)$ dependencies of SA and SA + annealed $Fe_{75}B_9Si_{12}C_4$ microwire for σ = 190 MPa and 760 MPa. The lines are just guides for eyes.*

4.2.5. GMI effect and DW propagation in "thick" glass-coated Fe-rich microwires

After annealing, at 550 °C the character of the hysteresis loop of $Fe_{71.7}B_{13.4}Si_{11}Nb_3Ni_{0.9}$ microwire does not change, as can be seen in *Figure 4.45*, although H_c experiments a slight increase, this magnetic hardening can be understood as the beginning of crystallization (as confirmed by the XRD pattern in *Figure 4.4c*). Then, we assumed that at lower annealing temperatures the microwire structure remains amorphous. Annealing at 300 °C causes a coercivity decrease, the magnetic softening in this case can be explained due to the internal stresses relaxation.

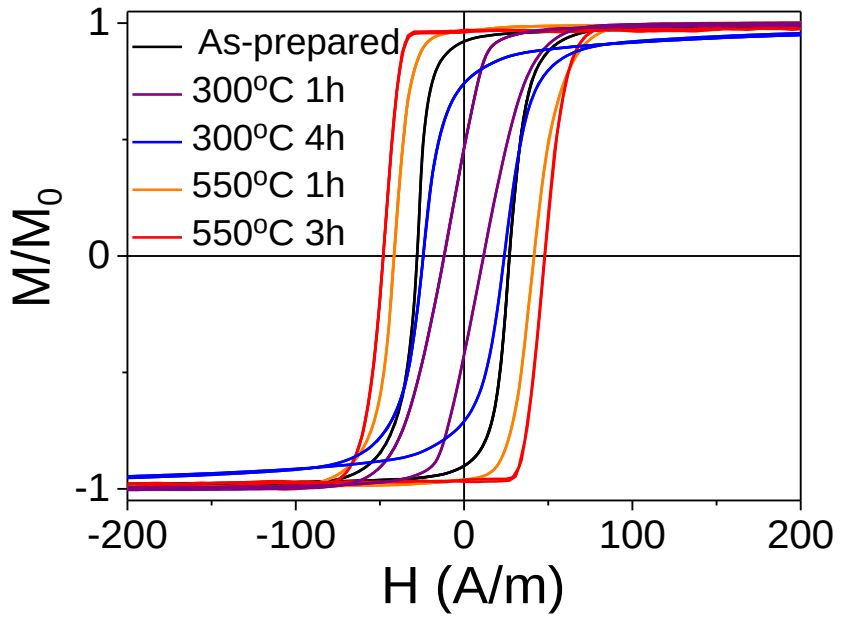

Figure 4.45. *Hysteresis loop of as-prepared $Fe_{71.7}B_{13.4}Si_{11}Nb_3Ni_{0.9}$ microwire and annealed at 550 °C and 300 °C for different t_{ann}.*

The bistable behaviour of the microwire as-prepared and annealed for short annealing time observed in *Figure 4.45*, suggests the possibility to observe single domain wall, DW, propagation, since it is observed for other Fe-rich microwires [35,36]. By means of the modified Sixtus-Tonks method (described in detail in Chapter 2) the velocity dependence on magnetic field *H*, *v(H),* was evaluated and it is presented in *Figure 4.45*. As-prepared microwire presents practically linear *v(H)* dependence and relatively high *v* values, up to

700 m/s, as compared to the reported for Fe-rich microwires of similar diameter obtained by in-rotating water quenching technique [49].

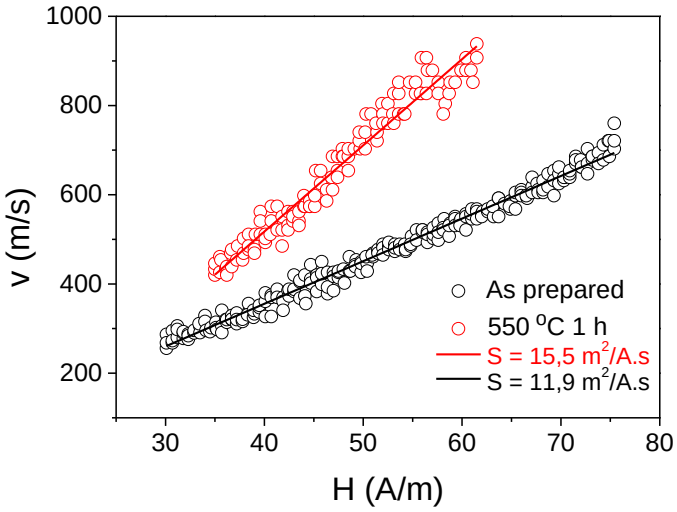

Figure 4.46. *DW velocity dependence on magnetic field, v(H), of as-prepared $Fe_{71.7}B_{13.4}Si_{11}Nb_3Ni_{0.9}$ microwires and annealed at 550 °C for t_{ann} = 1 h.*

The linear dependence of the DW velocity, *v(H)*, along the microwire [36-38,50], as a function of the magnetic field, in a viscous regime is described by *eq. (1.2)*.

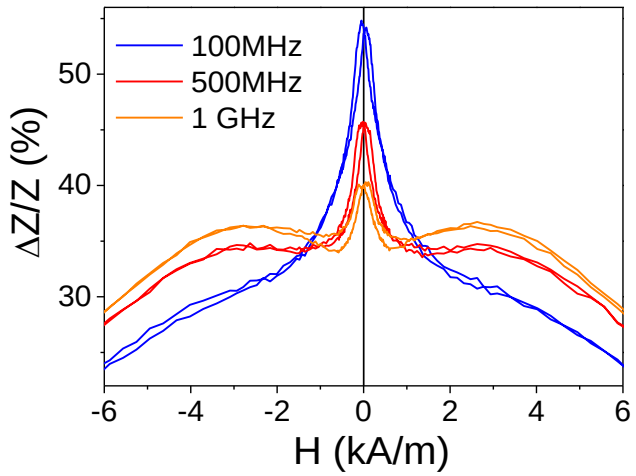

Figure 4.47. *GMI ratio dependence of as-prepared $Fe_{71.7}B_{13.4}Si_{11}Nb_3Ni_{0.9}$ microwire at different frequencies.*

From *eq. (1.2)*, *S* values are *S* ≈ 11,9 m^2/A·s for as-prepared sample, being higher than the values usually obtained for similar microwires in as-prepared state [28]. High *S*-values can be related to the effect of low magnetoelastic anisotropy of these microwires [28].

After annealing, DW velocity and mobility experiment an improvement, also reported for thinner Fe-rich microwires [28], b ut less appreciable than the one related to those, rising up to *v* ≈ 1000 m/s and *S* ≈15,5 m^2/A·s for annealed sample.

As-prepared $Fe_{71.7}B_{13.4}Si_{11}Nb_3Ni_{0.9}$ microwire presents relatively low GMI effect, *ΔZ/Z* ≈ 55% at 100 MHz (*Figure 4.47*). After annealing at 300 ℃ a significant improvement is appreciated. The largest increase is found for the sample annealed during t_{ann} = 4 h, *ΔZ/Z* ≈ 200%) as can be seen in *Figure 4.48*. This enhancement must be understood as a consequence of the stresses relaxation during the annealing. For longer t_{ann} the GMI ratio starts to decrease (*Figure 4.48a*).

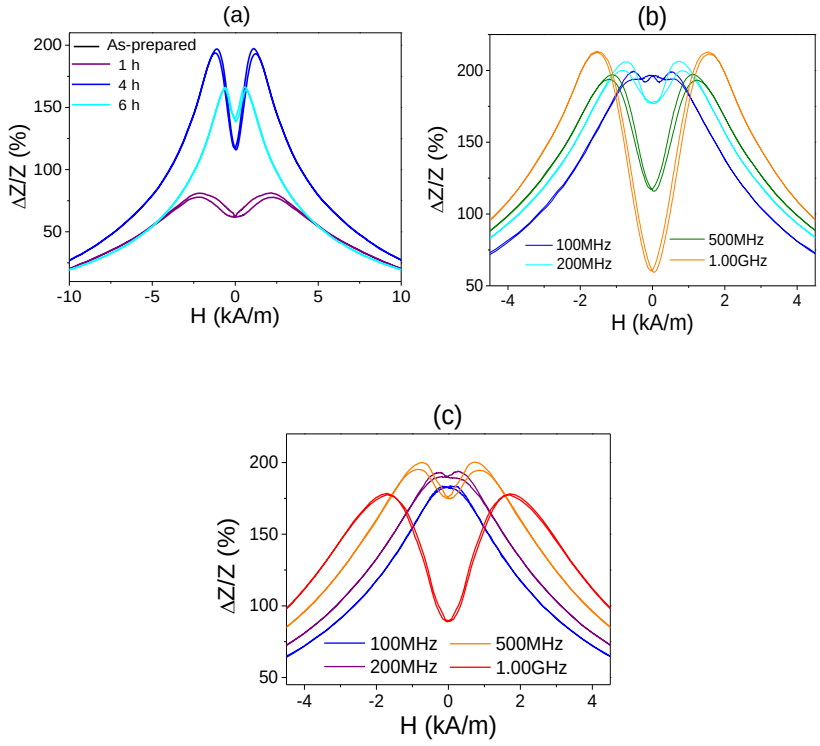

Figure 4.48. *GMI ratio dependence of $Fe_{71.7}B_{13.4}Si_{11}Nb_3Ni_{0.9}$ microwire annealed at 300 °C during for different t_{ann} (a), annealed at 300 °C during 4 h (b) and stress-annealed at 300 °C during 4 h with 400 MPa (c).*

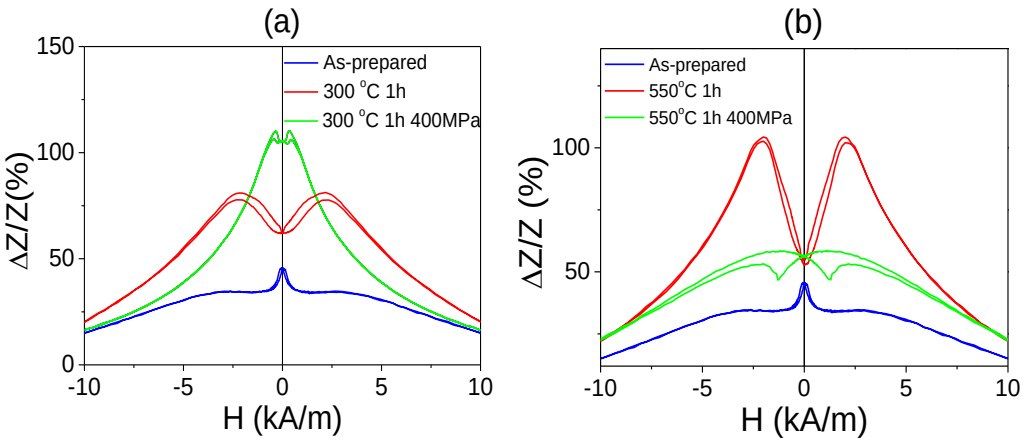

Figure 4.49. *GMI ratio dependence of as-prepared $Fe_{71.7}B_{13.4}Si_{11}Nb_3Ni_{0.9}$ microwire, annealed at 300 °C (a) and at 550 °C (b) for 1 h and stress annealed at the same conditions with 400 MPa measured at 500 MHz.*

However, stress-annealing at T_{ann} = 300 °C (1 h) allowed better GMI improvement (*Figure 4.49*). However, for higher annealing temperature (T_{ann} = 550 °C) we did not achieved GMI ratio improvement (*Figure 4.49b*).

Slight magnetic hardening after annealing at 550 °C (see *Figure 4.45*) can be related to beginning of the crystallization process. This assumption is confirmed by XRD pattern of as-prepared and annealed (at 550 °C) microwires described before (see *Figure 4.6*). Consequently, slight coercivity increasing observed after annealing at 550 °C must be attributed to the very beginning of crystallization of studied microwire upon annealing. For this reason, we must assume that for lower annealing temperatures the samples maintain the amorphous structure.

Aforementioned XRD results are consistent with the previously presented studies of as-prepared and annealed microwire performed by SEM: the SEM picture of as-prepared state is typical for amorphous samples (see *Figure 4.7a*). However, nano-sized crystallites can be appreciated in SEM image of annealed (T_{ann} = 550 °C, t_{ann} =3 h) sample (*Figure 4.7b*). From the SEM image

the crystallites size of about 25 nm can be estimated.

Figure 4.50 shows the maximum $\Delta Z/Z$ values obtained at every of the frequencies measured for the sample as-prepared and subjected under the different treatments. It should be noted that, this microwire even in as-prepared state presents simultaneously considerable GMI ratio and DW propagation (as presented in *Figures 4.46 and 4.48*), this combination of properties was only previously reported for cobalt rich microwires with induced magnetic stability after thermal treatment [4]. Post-processed samples exhibit high GMI ratio in a wide frequency range, in contrast to most Co-rich microwires that, for a given composition and magnetoelastic energy, possess an optimum frequency (about 200-300 MHz) [4].

High $\Delta Z/Z_{max}$ values obtained in a high frequency range is an attractive characteristic for modern industrial applications [4].

The advantage of the studied microwires is that at these annealing conditions (T_{ann} = 300 °C for t_{ann} = 4 h) the sample present amorphous structure and hence maintain good mechanical properties typical for amorphous materials.

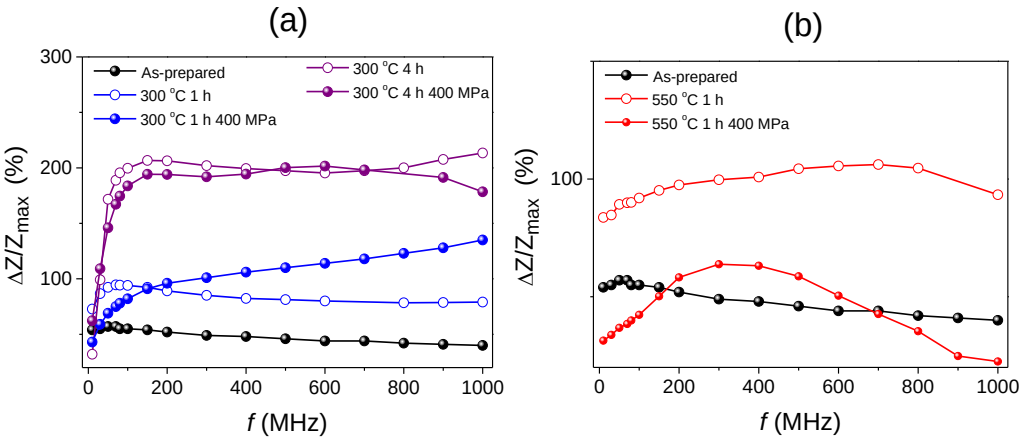

Figure 4.50. *$\Delta Z/Z_{max}(f)$ dependences of as-prepared and post-processed at different conditions $Fe_{71.7}B_{13.4}Si_{11}Nb_3Ni_{0.9}$ microwires.*

4.2.6. Graded magnetic anisotropy in Fe-rich microwires and its effect on DW dynamics

As shown in the previous sections, the stress-annealing induced anisotropy essentially depends on the stress-annealing conditions: annealing temperature, time and stress applied during the annealing and can be partially annealed out by subsequent furnace annealing [52]. Thus, this led us to design a post-processing consisting in stress-annealing at fixed stress and variable annealing temperature that allows creating a magnetic microwire with graded magnetic anisotropy [52,53].

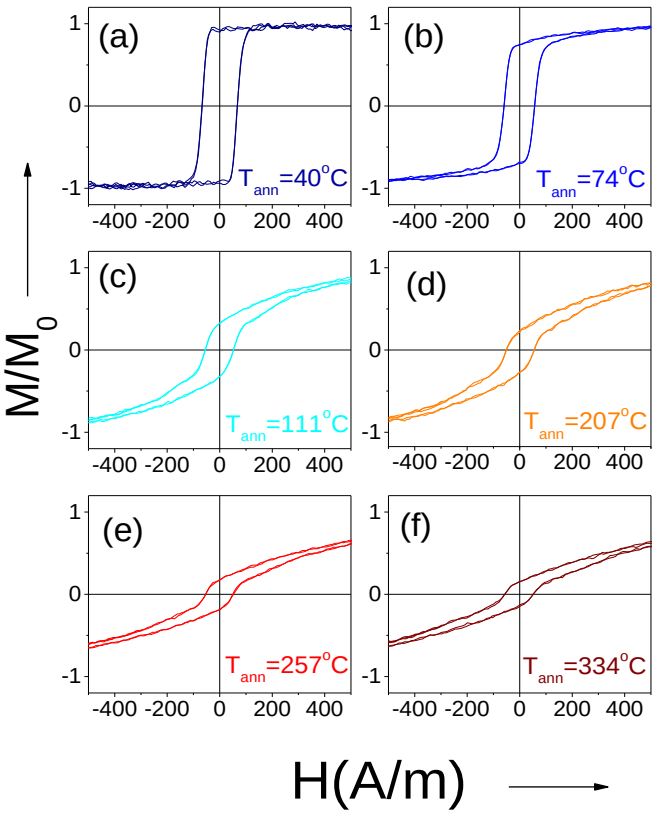

Figure 4.51. Local hysteresis loops of $Fe_{75}B_9Si_{12}C_4$ microwire stress-annealed at variable T_{ann} measured by a short pick-up coil along the microwire length.

This research was carried out employing a 30 cm long $Fe_{75}B_9Si_{12}C_4$ microwire (d = 15.2 μm, D = 17.2 μm) above studied. Stress-annealing at

variable temperature was performed in the same way as described in *Chapter 3* for Co-rich microwires. The microwire was inserted into a conventional furnace through the orifice and annealed in air atmosphere under tensile stress, $\sigma \approx 760$ MPa, created by a mechanical load attached to one end of the sample. The annealing temperature, T_{ann}, inside the furnace was set to 350 ºC.

Figure 4.51 shows the gradual change in the local hysteresis loop of the sample stress-annealed in the zone with variable T_{ann}, measured by a short pick-up coil movable along the microwire length. The hysteresis loop changes from perfectly rectangular in the part of the microwire stress-annealed at lower T_{ann} to almost linear in the part of the microwire stress-annealed at higher $T_{ann} \approx 350$ ºC. The linear local hysteresis loop obtained at $T_{ann} = 350$ ºC is rather similar to the bulk hysteresis loop obtained for the same T_{ann} (presented above in *Figure 4.37*).

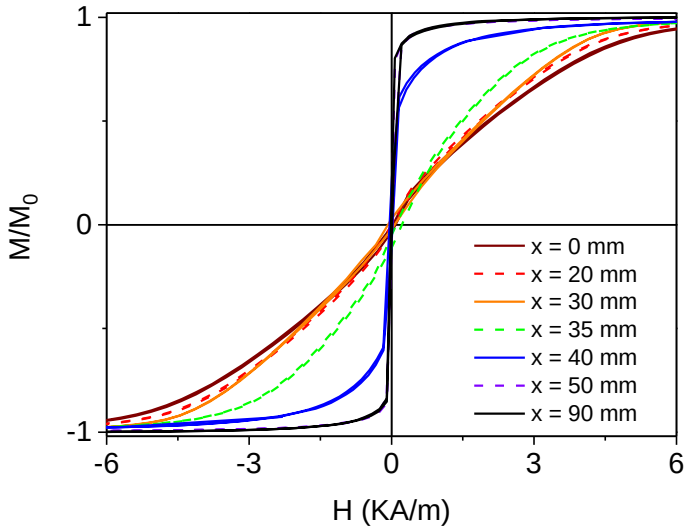

Figure 4.52. *Effect of stress-annealing at variable T_{ann} in the hysteresis loops of $Fe_{75}B_9Si_{12}C_4$ microwire measured at high field range along the microwire length.*

The hysteresis loops measured at high field presented in *Figure 4.52* reflect the macroscopic transverse anisotropy graded along the microwire length, with $H_k \approx 5$ kA/m observed for the sample end stress-annealed at 350 °C.

Obtained microwire, presents not only rather difference in the local hysteresis loops, but also variable squareness ratio, M_r/M_0, and coercivity, H_c, along the microwire length, L (see *Figure 4.53*).

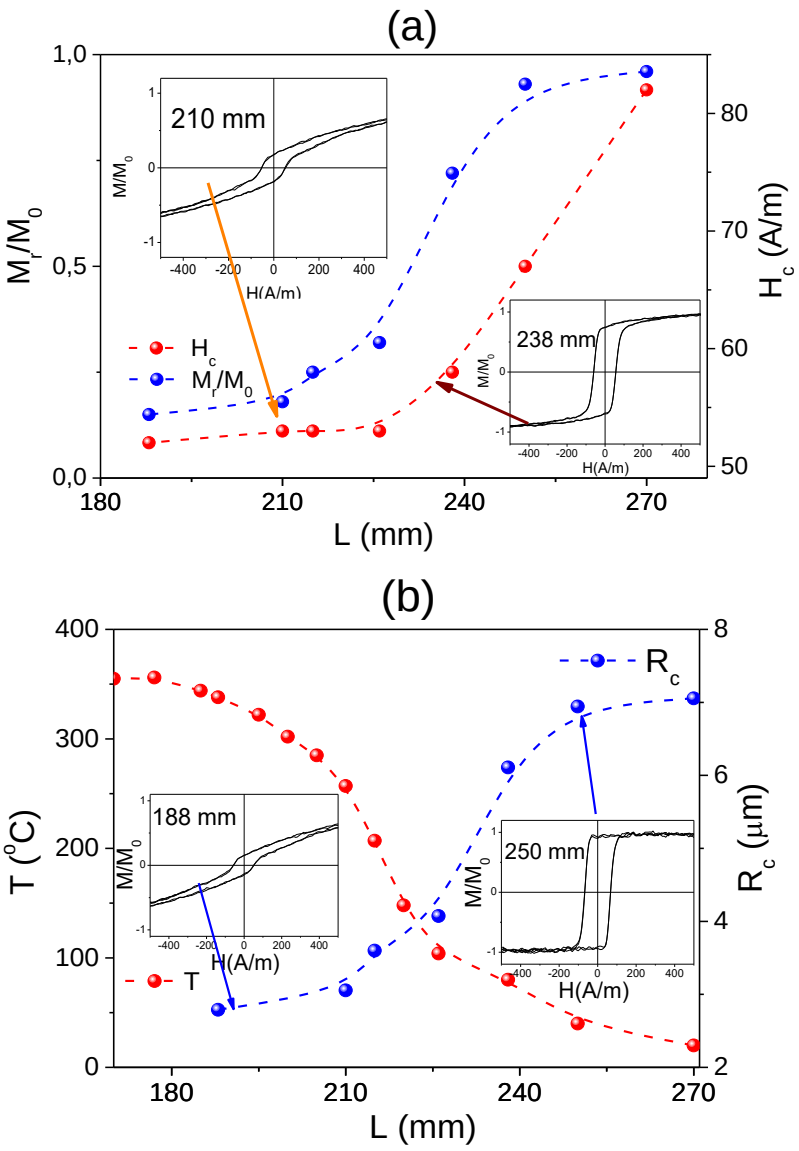

Figure 4.53. *M_r/M_0 (L) and H_c (L) dependences (a) and R_c (L) and T(L) profile (b) L. Local hysteresis loops recorded at different L are provided in the insets.*

Observed M_r/M_0 *(L)* dependence (*Figure 4.53a)* allows to evaluate the inner axially magnetized core radius, R_c, by means of *eq. 3.2.* R_c *(L)* dependence and its correlation with *T(L)* profile are provided in *Figure 4.53b*. Obtained R_c *(L),* M_r/M_0 *(L)* and H_c *(L)* dependencies and gradual change in hysteresis loop shape

reflect graded magnetic anisotropy obtained by stress-annealing at variable T_{ann}. From R_c *(L),* M_r/M_0 *(L)* and H_c *(L)* dependencies with the *T(L)* profile, M_r/M_0, H_c and R_c (T_{ann}) dependencies have been evaluated (see *Figure 4.54a* and *Figure 4.54b*).

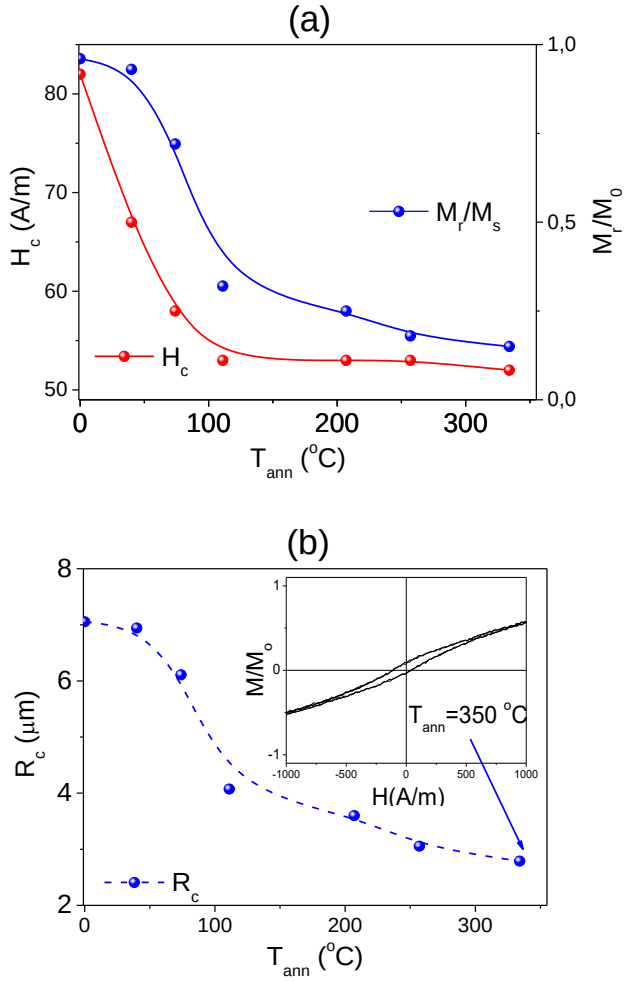

Figure 4.54. *M_r/M_0, H_c (a) and R_c (b) dependencies on T_{ann}. The local (L = 157 mm) hysteresis loop of the sample stress-annealed at T_{ann} = 350 °C is provided in the inset of (b).*

The observed dependencies of the squareness ratio, coercivity and radius of the inner axially magnetized core radius with the annealing temperature demonstrate the continuous magnetic anisotropy gradient along the microwire length, which should be attributed to the variable T_{ann} during the stress-annealing.

In the present case, the graded magnetic anisotropy appears as a continuous spatial distribution of magnetic anisotropy gradient over the microwire length subjected to stress-annealing at variable T_{ann}. Taking into account R_c dependences of the annealing temperature and the position in the microwire, obtained graded anisotropy can be attributed to a gradual modification of the domain structure i.e., an increase in the outer shell with transverse magnetic anisotropy in expense to a decrease in the inner core volume (see schematic picture in *Figure 4.55*).

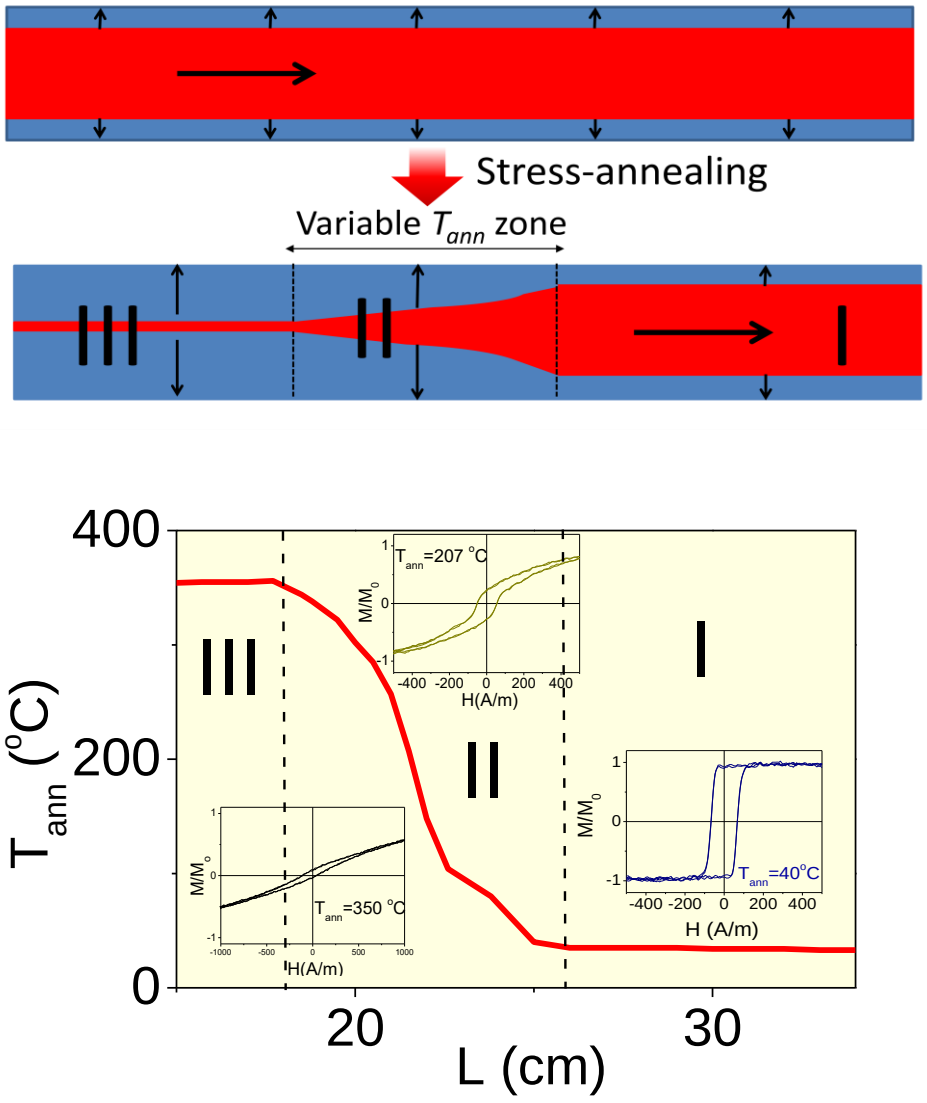

Figure 4.55. *Schematic picture of the graded magnetic anisotropy appearing as a continuous magnetic anisotropy gradient over the microwire length obtained by stress-annealing at variable T_{ann} compared with T(L) profile and local hysteresis loops at different L.*

According to the modification in the character of the local hysteresis loops along the sample length, can be identified three different zones in the microwire: zone *I* corresponding to either as-prepared or stress-annealed microwire at low T_{ann} (up to $T_{ann} \approx 74$ ºC) that correlates with almost perfectly rectangular hysteresis loops related to axial magnetic anisotropy. Zone *III*, for the section of the microwire stress-annealed at temperatures $T_{ann} \geq 334$ ºC where the local hysteresis loops are linear, associated to microwires with transverse magnetic anisotropy and zone *II*, for the section of the microwire stress-annealed at temperatures ranging from 74 ºC ≤ T_{ann} ≤ 334 ºC, where transverse and axial magnetic anisotropies superposition can be assumed (see *Figure 4.55*).

By modification of the stress-annealing conditions (T_{ann}, t_{ann} and σ) further tuning of the graded anisotropy can be achieved.

The transverse character of the magnetic anisotropy in the surface of the microwires is indirectly confirmed by the remarkable enhancement of the GMI effect observed after stress-annealing of Fe-rich microwires [38, 52].

As regarding the DW propagation, the DW velocity in the Walker model, *v*, is given by [57]:

$$v = \left(\frac{2\pi\gamma\Delta}{\alpha}\right) H \tag{4.9}$$

being γ the gyromagnetic ratio, α the magnetic damping parameter and Δ the DW width. The only variable parameters in *eq. (4.9)* are Δ and H. For this reason, as previously described, in a viscous regime, where *v(H)* dependence is linear, the DW propagation with a uniform velocity is usually assumed if H= const.

However, several methods allow the modification of Δ, such as the application of transverse field [55], as well as induced transverse magnetic anisotropy [38]. In consequence, we can expect rather different features of the DW propagation in a microwire with graded magnetic anisotropy. Therefore,

evaluation of the DW dynamics for obtained microwire with graded magnetic anisotropy is presented below in *Figures 4.56.*

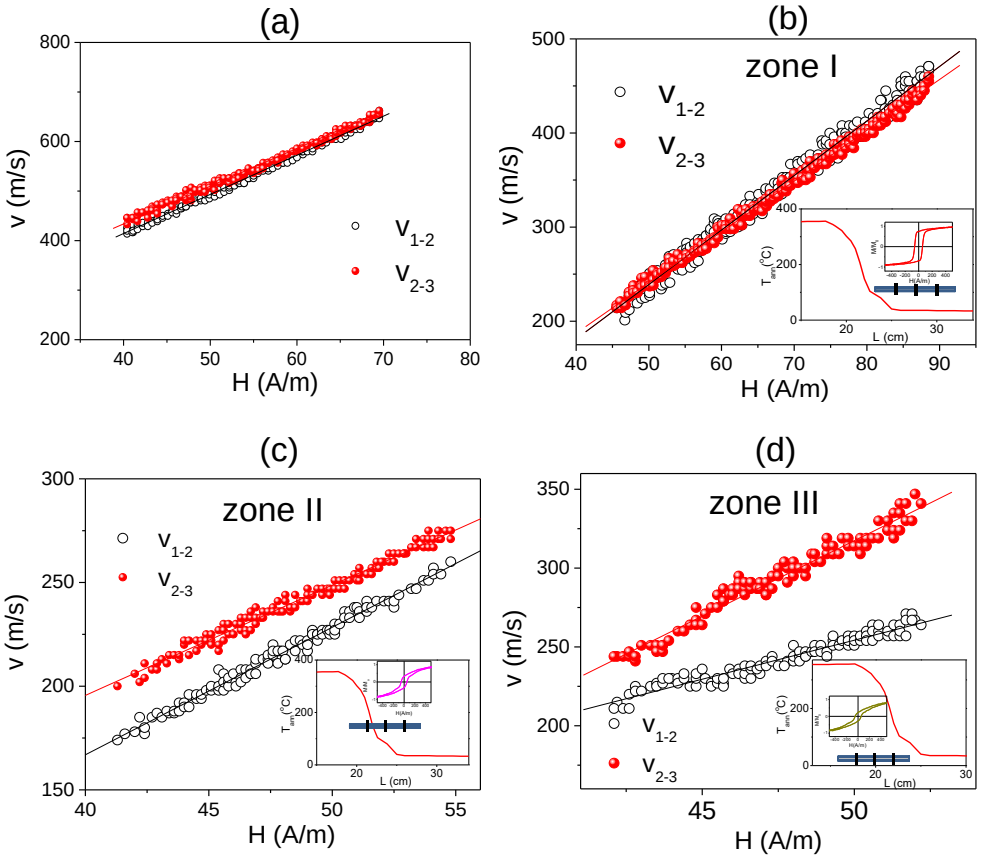

Figure 4.56. *v(H) dependencies of as-prepared (a) and stress-annealed at variable T_{ann} microwire measured at the different microwire zones (b-d) -the sample is inserted into the Sixtus-Tonks set-up from the side with stronger transverse magnetic anisotropy.*

Comparison of *v(H)* dependences of as-prepared and stress-annealed at variable T_{ann} microwire is shown in *Figures 4.56a-d*. The *v(H)* dependence of as-prepared sample is provided in *Figure 4.56a* and the *v(H)* dependence shown in *Figure 4.56b,c & d* corresponds to zone *I,* zones *II* and *III*, respectively. For the measurement the side of the sample with stronger transverse magnetic anisotropy is gradually inserted into the Sixtus-Tonks set-up consisting of 3 pick-up coils. *Figure 4.56a* and *4.56b*, show DW velocity values between the pair of pick-up coils 1-2 and 2-3, v_{1-2} and $v_{2-3,}$ respectively, that are almost identical, meaning that the DW travels with a constant velocity at a given *H* –

value in as-prepared sample as well as in the part of the sample with weak stress-annealing induced magnetic anisotropy. In contrast, for the microwire zones *II* and *III* $v_{2\text{-}3}$, values are considerably higher than $v_{1\text{-}2}$ values (*Figures 4.56c,d*). Such difference must be attributed to non-uniform DW propagation ($v \neq$const).

Faster DW propagation is obtained for the sample section with stronger transverse magnetic anisotropy, consistently with the reported influence of the stress-annealing induced magnetic anisotropy on DW dynamics. DW velocity improvement is related to the influence of the outer domain shell with transverse magnetic anisotropy (evidenced by R_c decrease observed in *Figure 4.54b* upon increase in T_{ann}) associated to stress-annealing induced transverse magnetic anisotropy [38]. Such induced magnetic anisotropy of transverse character is assumed to influence the DW dynamics in a similar way as the application of a transverse magnetic field [37,52,55].

Additional information can be obtained from the *EMF* signals, ε, induced by the travelling DW in the pick-up coils [38,39]. The time ε dependence, $\varepsilon(t)$, can provide information of the uniformity of the DW velocity, the DW shape, and even of the cross section of the region where DW propagates [38,39]. Experimental results on $\varepsilon(t)$ dependencies recorded for different sections of studied microwire sample are shown in *Figure 4.57* and *4.58*.

Figures 4.57a-h are obtained for the case when the microwire is gradually inserted from the zone *I* side into the measuring system from the side of the 3-rd pick-up coil, being *x* the length of microwire outside the primary coil end (see *Figure 4.57i*). This configuration allows the singe DW depinning and travel from the microwire region (from the end placed inside the magnetizing solenoid), which presents features of magnetic bistability and stress-annealing induced anisotropy either absent or rather small (see *Figure 4.57i*). However, the DW propagates in the region of the sample affected by stress-annealing at variable T_{ann} (when the sample is inserted sufficiently inside the solenoid).

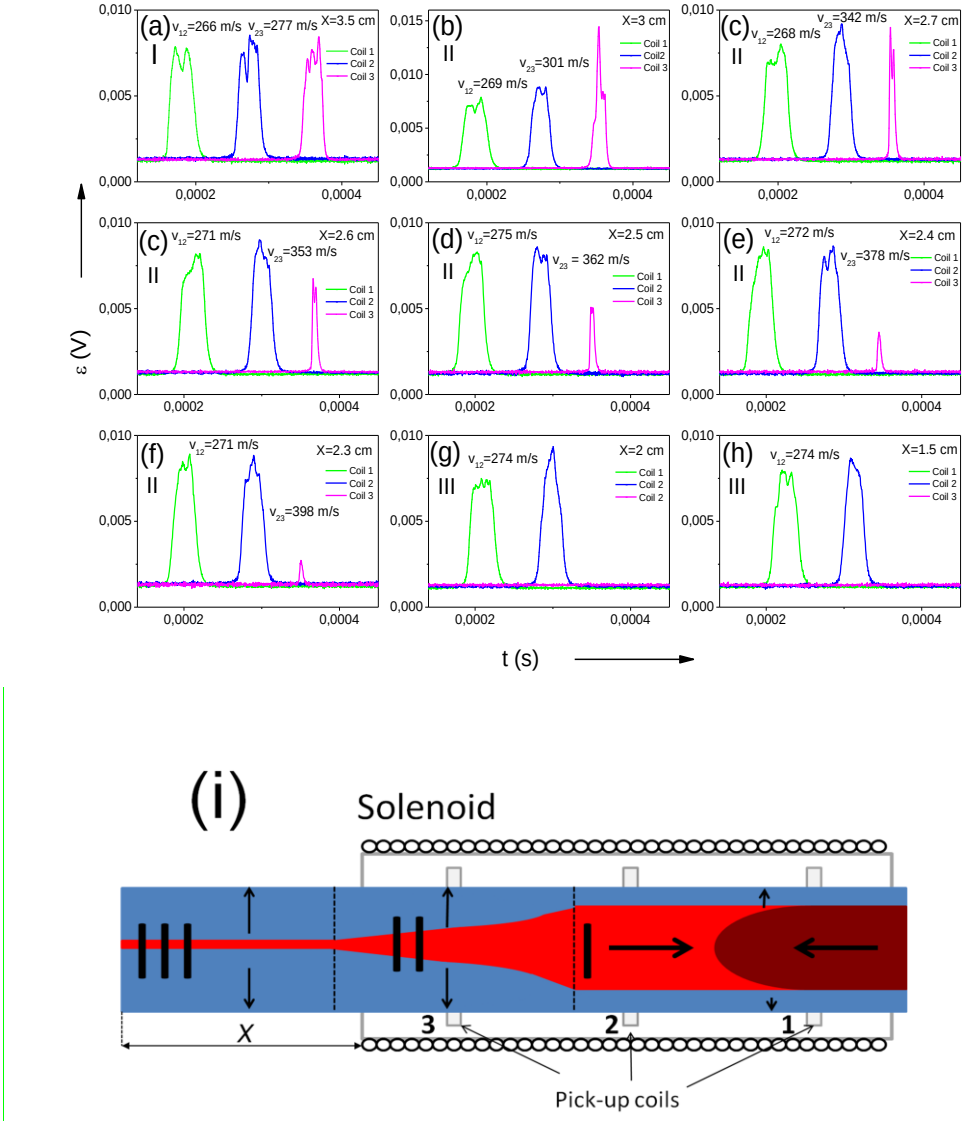

Figure 4.57. *EMF peaks induced by magnetization changes in the pick-up coils in stress-annealed at variable T_{ann} microwire from zones I (a), II (b-f) and III (g,h) when the sample is inserted into the measuring system from the microwire end with rectangular hysteresis loop. Schematic sketch of the DW propagation (i).*

Hence, the DW propagation is measured first for the zone *I*. Then, the sample from zones *II* and *III* step by step is inserted into the measuring system (from the 3-rd pick-up coil side). $\varepsilon(t)$ dependences obtained for the sample portion from the zone *I* are typical for the regular DW propagation with uniform velocity: travelling DW passes successively through the three pick-up coils (see

Figure 4.57a and 4.58a). The three *EMF* peaks present quite similar amplitude and shape and are separated by roughly the same time interval, *Δt,* indicating a single-DW propagation regime with DW travelling at constant velocity.

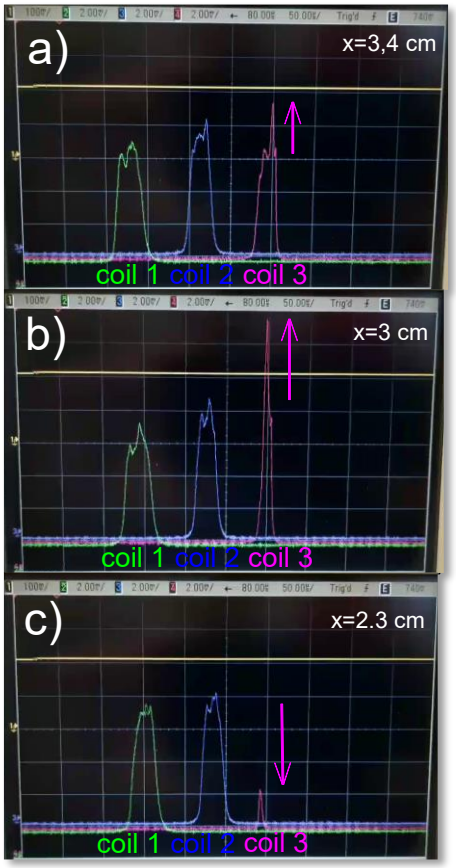

Figure 4.58. *Evolution of the EMF signals by magnetization changes in the pick-up coils for the microwire stress-annealed at variable T_{ann} when the sample is introduced in the measurement system from zone I end, with a length of sample outside the primary coil end of x = 3.4 cm (a), 3 cm (b) and 2.4 cm (c).*

When the zone *II* of the sample reaches the 3-rd pick-up coil (*Figure 4.57b and 4.57b*) can be observed that the signal from the 3-rd pick-up coil becomes much sharper (*Figure 4.57b and 4.57b*). The amplitude of *EMF* signal of the 3-rd pick-up coil first becomes higher and then decreases until vanishes when the sample moves further inside the measuring system (see *Figures 4.57c-h and 4.58c*). Such decrease is associated to a modification in the DW velocity (*Figure 4.56c*). Correspondingly, in the area with strong enough stress-annealing induced magnetic anisotropy the DW can be trapped.

The evolution with distance, *x*, of the *EMF* signal of the 3-rd pick-up coil and its half-width (full width at half maximum), *W*, are presented in *Figure 4.59a* and *4. 59b*, respectively. As clearly depicted in *Figure 4.59a*, the 3-rd *EMF* peak becomes sharper as the sample zone with stronger stress-annealing induced anisotropy is inserted inside the 3-rd pick-up coil. Such behaviour is also evidenced from *W(x)* representation shown in *Figure 4.59b*.

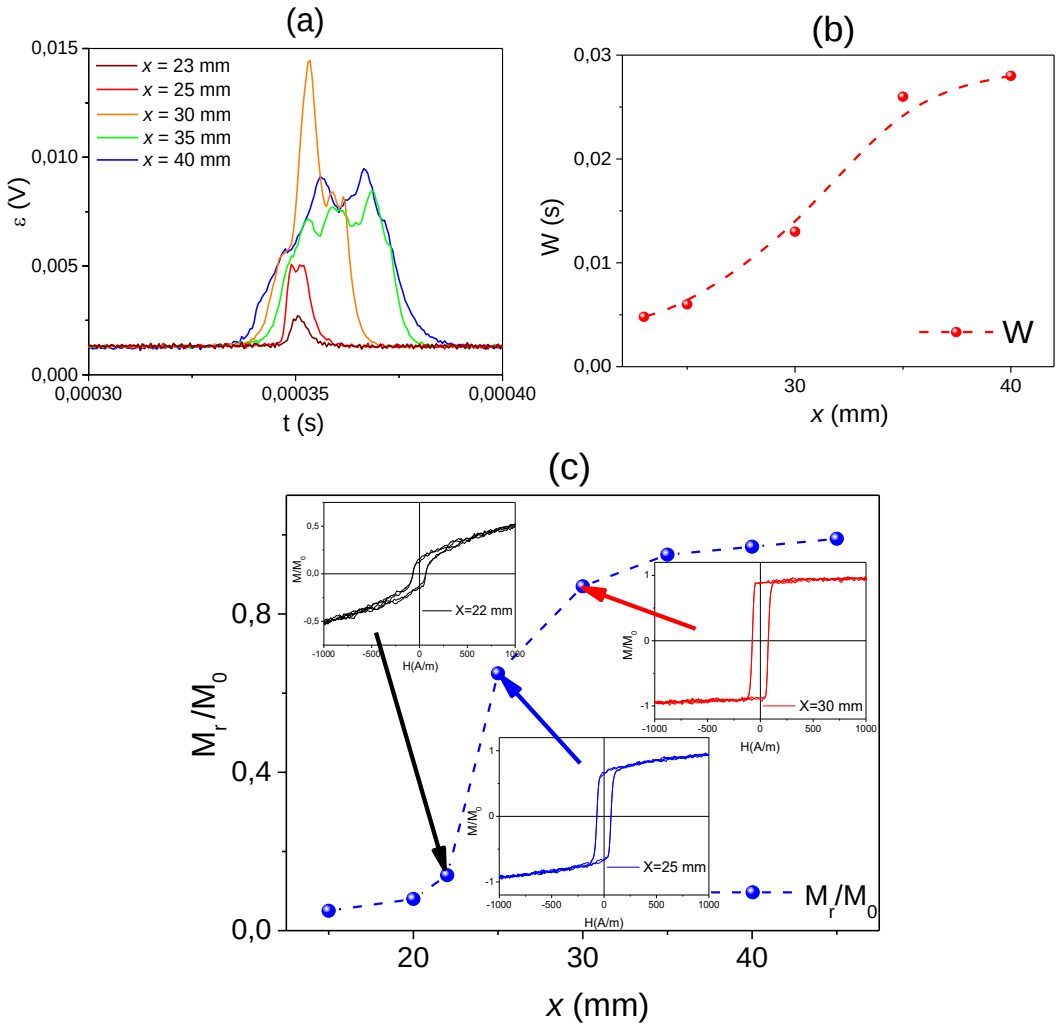

Figure 4.59. *Evolution of the EMF peak from the 3-rd pick-up coil with x (a), W(x) of the 3-rd EMF peak (b) and $M_r/M_0(x)$ dependence (c).*

Moreover, the *Δt* between the 2-nd and 3-rd pick-up coils becomes smaller, indicating faster DW velocity from the sample zone *II* (as also evidenced from *Figure 4.56d*).

Therefore, such evolution of the 3-rd *EMF* peak must be related with a decrease in the characteristic DW length, δ, or/and to the modification in the DW velocity.

Taking into account *equations (4.6) and (4.7)*, *EMF* signals detected by the 3-rd pick-up coils can be compared considering the same coil parameters and the fact that in this case, the difference *in EMF* signals must be attributed to the change in *Qv* product [38]. Consequently, the *EMF* modification observed *in Figure 4.58* and *4.59* must be associated either to different *v* values or the change in the magnetic charge *Q*.

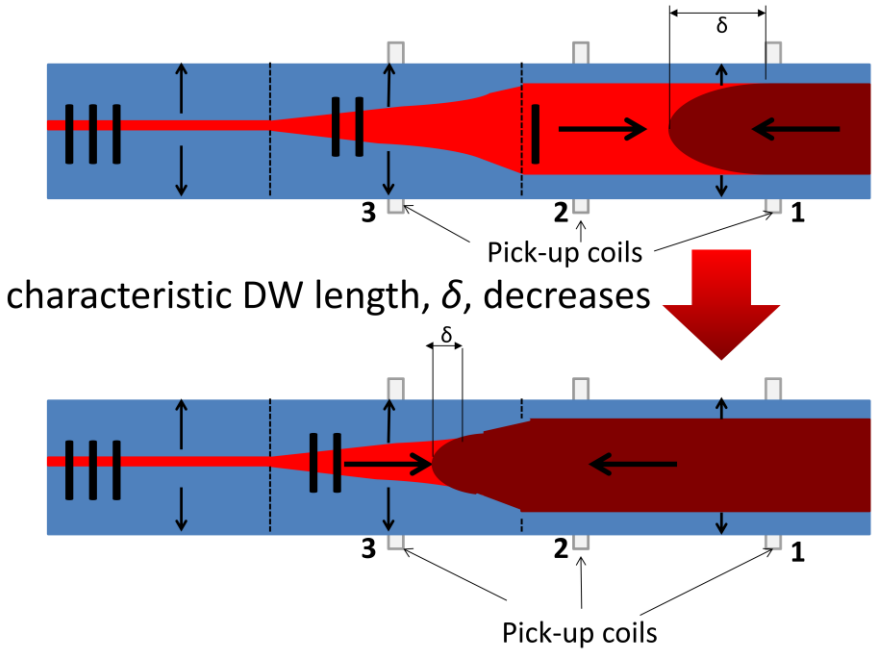

Figure 4.60. *Schematic illustration of the modification of the characteristic DW length in the zone of the sample with graded magnetic anisotropy.*

Previously, these effects have been separated from comparison of evolution of *Qv* and *W* [38,39]. In the present case, the DW propagation takes place in the sample zone with graded magnetic anisotropy, where M_r/M_0 gradually changes along the sample (see *Figure 4. 59c*). Accordingly, the DW velocity observed in zone *III* (*Figure 4.56d*) must be variable along the sample (i.e., different in each point of the sample from zone *III*). For H = 45 A/m the ratio between $v_{1\text{-}2}$ and $v_{2\text{-}3}$ values is $v_{1\text{-}2}/v_{2\text{-}3} \approx 0.85$ (see *Figure 4.56d*). On the

other hand, the average remanence ratio taken from *Figure 4.57c* $M_r/M_{0\,(1\text{-}2)}$ / $M_r/M_{0\,(2\text{-}3)} \approx 2$. Such simplified estimation gives as a result $Q_{1\text{-}2}\, v_{1\text{-}2} / Q_{2\text{-}3}\, v_{2\text{-}3} \approx 1.7$. Let us consider as $W_{1\text{-}2}$ and $W_{2\text{-}3}$ *W*-values for the zones *I* and *III*. Correspondingly, $W_{1\text{-}2}/W_{2\text{-}3}$ ratio evaluated from *Figure 4.59b* gives an average value $W_{1\text{-}2}/W_{2\text{-}3} \approx 4.5$. Thus, the difference observed in the 3-rd peak half-width cannot be explained only by different DW velocities in zones *I* and *III*.

Consequently, as schematically shown in *Figure 4.62*, a δ decrease can be assumed when the DW propagates in the zone with graded magnetic anisotropy. Such δ decrease is related to a decrease in the cross section of the inner axially magnetized core in which the DW is located, as well as by an increase in the magnetic anisotropy constant, *K*, due to stronger induced magnetic anisotropy. The δ –values are affected by *K*: the reduced head-to-head domain wall length, δ/d, (*d* is the metallic nucleus diameter) changes from $\delta/d \approx 13.5$ for $K = 10^3$ J/m^3 to $\delta/d = 40$–50 for $K = 10^2$ J/m^3 [39]. On the other hand, even at fixed magnetic anisotropy the DW length is affected by *d* values [39]. Accordingly, the decrease in δ/d in the microwire portion subjected to stress-annealing at high enough T_{ann} (see *Figure 4.60b*) must be attributed to the decrease in the inner core radius and higher magnetic anisotropy in stress-annealed sample section.

Above discussion suggests that DWs in amorphous microwires are quite wide: in amorphous Fe-rich microwires $\delta/d \sim 13.5 - 50$ [39], while for nanowires δ is of the order of the wire diameter, i.e., $\delta/d \sim 1 - 2$ [39]. This difference is fundamentally related to low magnetic anisotropy of amorphous microwires as well as low contribution of the exchange energy for microwires with thicker dimensions.

Substantially non uniform DW propagation in a medium with graded magnetic anisotropy together with the obtained decrease in DW length open the possibility to tune the DW features in magnetic microwires.

The other possibility to manipulate the DW dynamics of studied microwires is to create a local defect in the microwire by local stress-annealing. For this purpose we locally heated the microwire under applied tensile stress (σ = 90 MPa) for t_{ann} = 1 h, we used the annealing temperature equal to 250 ^{o}C.

Local nucleation field profiles (H_n (L) dependence) of as-prepared and locally stress-annealed sample are compared in *Figure 4.61a*. H_n (L) dependencies of both samples present similar features (i.e., local fluctuations

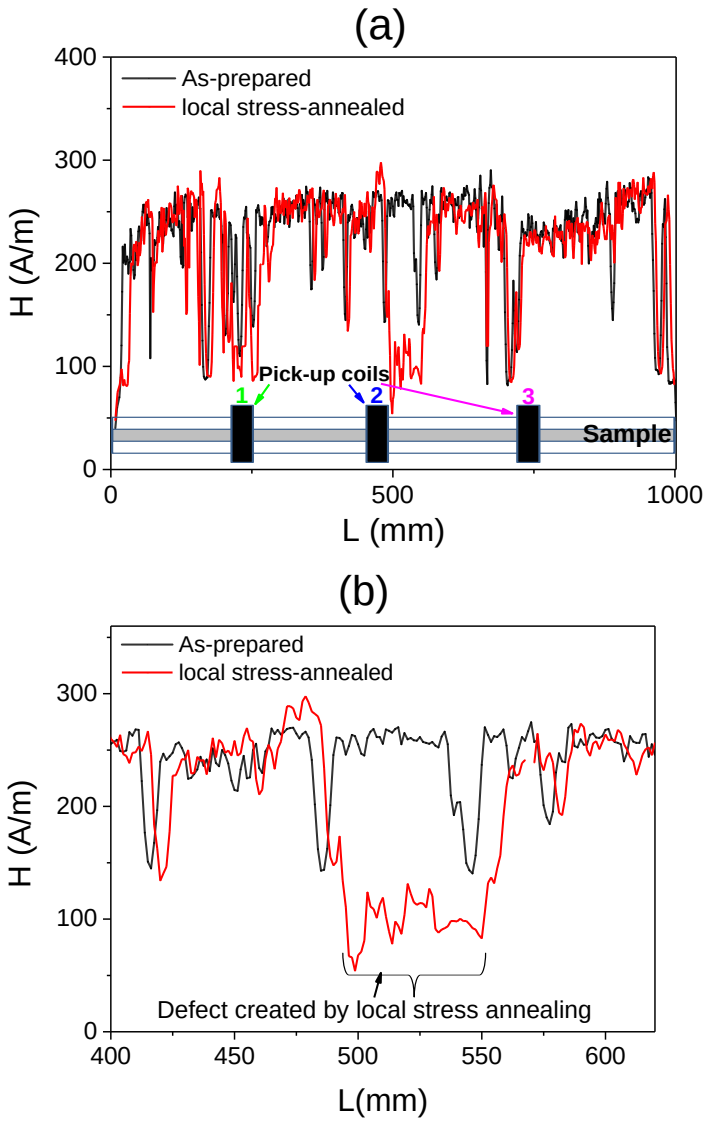

Figure 4.61. *Effect of local stress-annealing on local nucleation field distribution, $H_n(L)$, (a) and $H_n(L)$ distribution in the area affected by local stress-annealing (b) for $Fe_{75}B_9Si_{12}C_4$ microwire.*

at the same *L*-values). However, a region with lower H_n values is detected in the middle part of the locally stress-annealed sample (*Figure 4.61b*).

EMF peaks induced by the magnetization change in the pick-up coils for as-prepared and locally stress-annealed samples are presented in *Figure 4.62a* and *Figure 4.62b*, respectively. It can be appreciated the rather different character of the remagnetization process of locally stress-annealed sample from that of as-prepared sample: the *EMF* peaks sequence has changed. In locally stress-annealed sample the peaks in coil 1 and 2 appear almost simultaneously (*Figure 4.62b*), meaning that the DW passes almost simultaneously through coils 1 and 2. Considering the changes in the H_n (*L*) profile caused by local stress annealing we can assume that in this case the propagation of two DWs takes place: the first one travelling from the sample end (as also observed for as-prepared sample) and a second DW coming from the local defect created by the local stress-annealing.

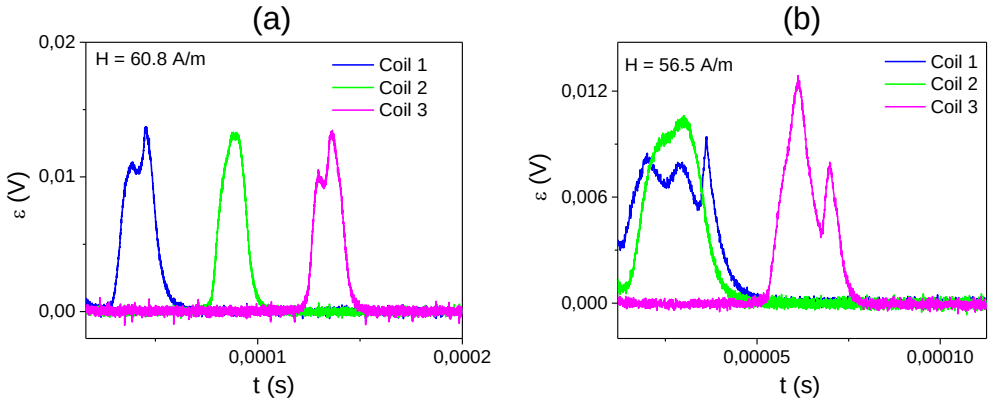

Figure 4.62. *EMF signals induced by magnetization changes in the pick-up coils in as-prepared (a) and locally stress-annealed (b) $Fe_{75}B_9Si_{12}C_4$ microwire.*

Previously, for the preparation of magnetic materials (e.g., thin films) with graded magnetic anisotropy, rather sophisticated techniques were employed, including changes in the chemical composition during the thin films deposition with subsequent annealing [56,57]. The graded magnetic anisotropy obtained in thin films appears as a continuous gradient over the film thickness. The generation of required spatial distribution of magnetic anisotropy was also

investigated for the engineering of DW dynamics by controllable nucleation and propagation of the reversed domains using model calculations [58].

Consequently, we proposed a rather simple method to design graded magnetic anisotropy in magnetic microwires by stress-annealing at fixed applied stress and variable annealing temperature. The obtained medium presents an artificially modified inner axially magnetized core radius, which serves as a gate for DW propagation, allowing engineering of DW dynamics in Fe-rich microwires by graded magnetic anisotropy. Therefore, non uniform velocity of single DW propagation is assumed in graded magnetic anisotropy medium. Furthermore, in the section of the microwire with sufficiently strong stress-annealing induced magnetic anisotropy, the DW can be trapped. On the other hand, the section with moderate stress-annealing induced magnetic anisotropy presents faster DW propagation and a decrease in the DW length.

4.3. Concluding remarks

Generally, Fe and Fe-Ni based microwires present rectangular hysteresis loops and therefore single domain wall propagation can be observed in such microwires. Domain wall dynamics can by substantially improved by furnace annealing allowing internal stresses relaxation.

Although as-prepared Fe-rich amorphous microwires exhibit low GMI ratio and rectangular hysteresis loops, stress-annealing, Joule heating, and combined stress-annealed followed by conventional furnace annealing can substantially improve the GMI effect (by more than an order of magnitude). On the other hand, Fe-rich microwires with moderate stress-annealing induced anisotropy can present both GMI effect and single domain wall propagation.

We demonstrated that the stress-annealing induced anisotropy is partially reversible: part of such stress-annealing induced anisotropy can be annealed out.

The stress-annealing induced anisotropy depends on stress-annealing conditions: temperature, stress and time. The dependence of stress-annealing induced anisotropy on stress-annealing conditions allowed to obtain microwires with graded magnetic anisotropy: a gradual modification of hysteresis loops consisting of variable squareness ratio and coercivity along the microwire length is achieved in microwires subjected to stress annealing with a temperature gradient. We found that the domain wall propagation in a microwire with graded magnetic anisotropy is substantially non uniform. Domain wall can be trapped in the microwire region with strong enough stress-annealing induced magnetic anisotropy. On the other hand, faster domain wall propagation and a decrease in the domain wall length are observed in the region with moderate stress-annealing induced magnetic anisotropy. Beneficial effect of stress-annealing on the domain wall dynamics is associated with the induced transverse magnetic anisotropy in the outer domain which affects the

travelling domain wall in a similar way as application of transversal bias magnetic field.

Amorphous Fe-rich glass coated microwires with metallic nucleus diameter of about 100 μm can be prepared using the Taylor-Ulitovsky method. Such microwires after appropriate annealing can present combination of both high GMI effect and single domain wall propagation.

4.4. References

[1] A. Zhukov, M. Ipatov, V. Zhukova, Chapter 2 - Advances in Giant Magnetoimpedance of Materials, in: H. of M.M., K.H.J. Buschow Ed., Elsevier, (2015) pp. 139–236, doi:10.1016/bs.hmm.2015.09.001.

[2] A. Zhukov, M. Ipatov, P. Corte-León, L.G.- Legarreta, M. Churyukanova, J.M. Blanco, J. Gonzalez, S. Taskaev, B. Hernando, V. Zhukova, Giant magnetoimpedance in rapidly quenched materials, J. Alloys Compd. 814 (2020) 152225, doi:10.1016/j.jallcom.2019.152225.

[3] H. Chiriac, T.-A. Óvári, S. Corodeanu, G. Ababei, Interdomain wall in amorphous glass-coated microwires, Phys. Rev. B 76 (2007) 214433, doi:10.1103/PhysRevB.76.214433.

[4] V. Zhukova, P. Corte-Leon, J.M. Blanco, M. Ipatov, L. Gonzalez-Legarreta, A. Gonzalez, A. Zhukov, Development of Magnetically Soft Amorphous Microwires for Technological Applications (Review), Chemosensors 10 (2022) 26, doi:10.3390/chemosensors10010026.

[5] H. Chiriac, T.-A. Óvári, Gh. Pop, F. Barariu, Internal stresses in highly magnetostrictive glass-covered amorphous wires, J. Magn. Magn. Mater. 160 (1996) 237-238.

[6] A. Zhukov, M. Churyukanova, S. Kaloshkin, V. Sudarchikova, S. Gudoshnikov, M. Ipatov, A. Talaat, J.M. Blanco, V. Zhukova, Magnetostriction of Co–Fe-Based Amorphous Soft Magnetic Microwires, J. Electron. Mater. 45 (2016) 226–234, doi:10.1007/s11664-015-4011-2.

[7] A. Zhukov, V. Zhukova, J.M. Blanco, J. Gonzalez, Recent research on magnetic properties of glass-coated microwires, J. Magn. Magn. Mater. 294 (2005) 182–192, doi:10.1016/j.jmmm.2005.03.033.

[8] A. Zhukov, M. Ipatov, J.M. Blanco, A. Chizhik, A. Talaat, V. Zhukova, Fast Magnetization Switching in Amorphous Microwires, Acta Phys. Pol. 126 (2014) 7-11, doi:10.12693/APhysPolA.126.7.

[9] G. Herzer, Amorphous and Nanocrystalline Soft Magnets, in: G.C. Hadjipanayis Ed., Proc. NATO Adv. Study Inst. Magn. Hysteresis Nov. Mater., pp. 711–730, Springer Netherlands, Dordrecht (1997), doi:10.1007/978-94-011-5478-9_77.

[10] M. Churyukanova, V. Semenkova, S. Kaloshkin, E. Shuvaeva, S. Gudoshnikov, V. Zhukova, I. Shchetinin, A. Zhukov, Magnetostriction investigation of soft magnetic microwires, Phys. Status Solidi A 213(2) (2016) 363–367, doi:10.1002/pssa.201532552.

[11] V. Zhukova, J.M. Blanco, M. Ipatov, A. Zhukov, Magnetic properties and domain wall propagation in FeNiSiB glass-coated microwires, J. Appl. Phys. 115 (2014) 17A309, doi:10.1063/1.4862717.

[12] A. Zhukov, J.M. Blanco, M. Ipatov, A. Talaat, V. Zhukova, Engineering of domain wall dynamics in amorphous microwires by annealing, J. Alloys Compd. 707 (2017) 35–40.

[13] H. Chiriac, T.-A. Óvári, M. Takajo, J. Yamasaki, A. Zhukov, Domain Structure of 'Thick' Amorphous Microwires with Nearly Zero Magnetostriction, MRS Proc. 674 (2001) U7.7, doi:10.1557/PROC-674-U7.7.

[14] V.V. Molokanov, A.N. Shalygin, P.P. Umnov, T.R. Chueva, N.V. Umnova, S.V. Simakov, Conditions for Obtaining "Thick" Amorphous Wires by the Ulitovsky–Taylor Method, Inorg. Mater. Appl. Res. 10 (2019) 463–466.

[15] F. Qin, H.-X. Peng, Ferromagnetic microwires enabled multifunctional composite materials, Prog. Mater. Sci. 58 (2013) 183–259.

[16] V. Zhukova, P. Corte-Leon, J.M. Blanco, M. Ipatov, J. Gonzalez, A. Zhukov, Electronic Surveillance and Security Applications of Magnetic Microwires, Chemosensors 9 (2021) 100, doi:10.3390/ chemosensors9050100.

[17] J. Arcas, C. Gómez-Polo, A. Zhukov, M. Vázquez, V. Larin, A. Hernando, Magnetic properties of amorphous and devitrified FeSiBCuNb glass-coated microwires, Nanostructured Mater. 7 (1996) 823–834, doi:10.1016/S0965-9773(96)00054-2.

[18] P. Marín, M. Vázquez, J. Arcas, A. Hernando, Thermal dependence of magnetic properties in nanocrystalline FeSiBCuNb wires and microwires, J. Magn. Magn. Mater. 203 (1999) 6–11, doi:10.1016/S0304-8853(99)00173-0.

[19] A. Talaat, V. Zhukova, M. Ipatov, J.J. Del Val, J.M. Blanco, L. Gonzalez-Legarreta, B. Hernando, M. Churyukanova, A. Zhukov, Engineering of magnetic softness and magnetoimpedance in Fe-rich microwires by nanocrystallization, JOM 68 (2016) 1563–1571.

[20] R. Hasegawa, Applications of Amorphous Magnetic Alloys BT - Properties and Applications of Nanocrystalline Alloys from Amorphous Precursors, in: B. Idzikowski, P. Švec, M. Miglierini Eds., pp. 189–198, Springer Netherlands, Dordrecht (2005).

[21] V. Zhukova, M. Ipatov, P. Corte-Leon, J.M. Blanco, E. Zanaeva, A.I. Bazlov, J. Jiang, D.V. Louzguine-Luzgin, J. Olivera, A. Zhukov, Excellent magnetic properties of $(Fe_{0.7}Co_{0.3})_{83.7}Si_4B_8P_{3.6}Cu_{0.7}$ ribbons and microwires, Intermetallics 117 (2020) 106660, doi:10.1016/j.intermet.2019.106660.

[22] V. Zhukova, A. Talaat, M. Ipatov, J.J. del Val, J.M. Blanco, L. Gonzalez-Legarreta, B. Hernando, R. Varga, P. Klein, A. Zhukov, Optimization of Soft Magnetic Properties in Nanocrystalline Fe-Rich Glass-Coated Microwire, JOM 67(9) (2015) 2108-2116.

[23] B.D. Cullity, S.R. Stock, Elements of x-ray diffraction, Prentice Hall, Up. Saddle River, NJ. (2001) 388.

[24] A. Talaat, V. Zhukova, M. Ipatov, J.M. Blanco, P. Klein, R. Varga, L. Gonzalez-Legarreta, B. Hernando, A. Zhukov, Magnetic Properties of Nanocrystalline Microwires, J. Electr. Mater. 45(1) (2016) 212-218, doi:10.1007/s11664-015-3966-3.

[25] V. Zhukova, A.F. Cobeño, A. Zhukov, A.R. de Arellano Lopez, J.M. Blanco, V. Larin, J. Gonzalez, S. López-Pombero, Correlation between magnetic and mechanical properties of devitrified glass-coated $Fe_{71.8}Cu_1Nb_{3.1}Si_{15}B_{9.1}$ microwires, J. Magn. Magn. Mater. 249 (2002) 79–84, doi:10.1016/S0304-8853(02)00509-7.

[26] A. Zhukov, K. Chichay, A. Talaat, V. Rodionova, J.M. Blanco, M. Ipatov, V. Zhukova, Manipulation of magnetic properties of glass-coated microwires by annealing, J. Magn. Magn. Mater. 383 (2015) 232–236, doi:10.1016/j.jmmm.2014.10.003.

[27] K. Chichay, V. Zhukova, V. Rodionova, M. Ipatov, A. Talaat, J.M. Blanco, J. Gonzalez, A. Zhukov, Tailoring of domain wall dynamics in amorphous microwires by annealing, J. Appl. Phys. 113 (2013) 17A318, doi:10.1063/1.4795617.

[28] V. Zhukova, P. Corte-Leon, L. González-Legarreta, A. Talaat, J.M. Blanco, M. Ipatov, J. Olivera, A. Zhukov, Review of Domain Wall Dynamics Engineering in Magnetic Microwires, Nanomaterials 10 (2020) 2407, doi:10.3390/nano10122407.

[29] A. Zhukov, M. Churyukanova, S. Kaloshkin, V. Semenkova, S. Gudoshnikov, M. Ipatov, A. Talaat, J.M. Blanco, V. Zhukova, Effect of annealing on magnetic properties and magnetostriction coefficient of Fe–Ni-based amorphous

microwires, J. Alloys Compd. 651 (2015) 718–723, doi:10.1016/j.jallcom.2015.08.151.

[30] V. Zhukova, O.A. Korchuganova, A.A. Aleev, V.V. Tcherdyntsev, M. Churyukanova, E.V. Medvedeva, S. Seils, J. Wagner, M. Ipatov, J.M. Blanco, S.D. Kaloshkin, A. Aronin, G. Abrosimova, N. Orlova, A. Zhukov, Effect of annealing on magnetic properties and structure of Fe-Ni based magnetic microwires, J. Magn. Magn. Mater. 433 (2017) 278–284, doi:10.1016/j.jmmm.2017.03.028.

[31] J. Yamasaki, K. Mohri, K. Watari, K. Narita, Domain wall induced anisotropy during annealing in amorphous ribbons, IEEE Trans. Magn. 20 (1984) 1855–1857, doi:10.1109/TMAG.1984.1063345.

[32] J. Becker, F. Luborsky, J. Walter, Magnetic moments and curie temperatures of $(Fe, Ni)_{80}(P, B)_{20}$ amorphous alloys, IEEE Trans. Magn. 13 (1977) 988–991, doi:10.1109/TMAG.1977.1059499.

[33] D.G. Rancourt, M.-Z. Dang, Relation between anomalous magnetovolume behavior and magnetic frustration in Invar alloys, Phys. Rev. B. 54 (1996) 12225–12231, doi:10.1103/PhysRevB.54.12225.

[34] P.H. Gaskell, On the structure of simple inorganic amorphous solids, J. Phys. C Solid State Phys. 12 (1979) 4337–4368, doi:10.1088/0022-3719/12/21/004.

[35] V. Zhukova, J.M. Blanco, V. Rodionova, M. Ipatov, A. Zhukov, Domain wall propagation in micrometric wires: Limits of single domain wall regime, J. Appl. Phys. 111 (2012) 07E311.

[36] V. Zhukova, J.M. Blanco, M. Ipatov, A. Zhukov, Magnetoelastic contribution in domain wall dynamics of amorphous microwires, Phys. B Condens. Matter. 407 (2012) 1450–1454, doi:10.1016/j.physb.2011.09.124.

[37] V. Zhukova, J.M. Blanco, M. Ipatov, M. Churyukanova, S. Taskaev, A. Zhukov, Tailoring of magnetoimpedance effect and magnetic softness of Fe-rich glass-coated microwires by stress- annealing, Sci. Rep. 8 (2018) 3202, doi:10.1038/s41598-018-21356-3.

[38] P. Corte-León, J.M. Blanco, V. Zhukova, M. Ipatov, J. Gonzalez, M. Churyukanova, S. Taskaev, A. Zhukov, Engineering of Magnetic Softness and Domain Wall Dynamics of Fe-rich Amorphous Microwires by Stress- induced Magnetic Anisotropy, Sci. Rep. 9 (2019) 12427, doi:10.1038/s41598-019-48755-4.

[39] S.A. Gudoshnikov, Yu.B. Grebenshchikov, B.Ya. Ljubimov, P.S. Palvanov, N.A. Usov, M. Ipatov, A. Zhukov, J. Gonzalez, Ground state magnetization distribution and characteristic width of head to head domain wall in Fe-rich amorphous microwire, Phys. Status Solidi A 206(4) (2009) 613–617.

[40] P.A. Ekstrom, A. Zhukov, Spatial structure of the head-to-head propagating domain wall in glass-covered FeSiB microwire, J. Phys. D: Appl. Phys. 43 (2010) 205001.

[41] A. Zhukov, A.F. Cobeño, J. Gonzalez, J.M. Blanco, P. Aragoneses, L. Dominguez, Magnetoelastic sensor of level of the liquid based on magnetoelastic properties of Co-rich microwires, Sens. Actuat. A Phys. 81/1-3 (2000) 129-133.

[42] D. Praslička, J. Blažek, M. Šmelko, J. Hudák, A. Čverha, I. Mikita, R. Varga, A. Zhukov, Possibilities of Measuring Stress and Health Monitoring in Materials Using Contact-Less Sensor Based on Magnetic Microwires, IEEE Trans. Magn. 49 (2013) 128–131, doi: 10.1109/TMAG.2012.2219854.

[43] A. Allue, P. Corte-León, K. Gondra, V. Zhukova, M. Ipatov, J.M. Blanco, J. Gonzalez, M. Churyukanova, S. Taskaev, A. Zhukov, Smart composites with embedded magnetic microwire inclusions allowing non-contact stresses and temperature monitoring, Compos. -A: Appl. Sci. Manuf. 120 (2019) 12-20,

doi:10.1016/j.compositesa.2019.02.014.
[44] P. Aragoneses, J.M. Blanco, A.F. Cobeño, L. Dominguez, J. Gonzalez, A. Zhukov, V. Larin, Stress Dependence of the Switching Field in Co-rich Amorphous Microwires, J. Magn. Magn Mat. 196-197 (1999) 248-250.
[45] P. Aragoneses, J.M. Blanco, L. Dominguez, J.González, A. Zhukov, M.Vázquez, The Stress dependence of the switching field in glass-coated amorphous microwires, J. Phys. D: Applied Phys. 31 (1998) 3040-3045.
[46] A. Zhukov, M. Vázquez, J. Velázquez, C. García, R. Valenzuela, B. Ponomarev, Frequency dependence of coercivity in rapidly quenched amorphous materials, Mater. Sci. Eng. A. 226–228 (1997) 753–756, doi:10.1016/S0921-5093(97)80079-2.
[47] P. Corte-Leon, V. Zhukova, M. Ipatov, J.M. Blanco, J. Gonzalez, M. Churyukanova, J.M. Baraibar, S. Taskaev, A. Zhukov, Stress dependence of the magnetic properties of glass-coated amorphous microwires, J. Alloys Compd. 789 (2019) 201-208, doi:10.1016/j.jallcom.2019.03.044.
[48] P. Corte-Leon, V. Zhukova, J.M. Blanco, M. Ipatov, S. Taskaev, M. Churyukanova, J. Gonzalez, A. Zhukov, Engineering of magnetic properties and magnetoimpedance effect in Fe-rich microwires by reversible and irreversible stress-annealing anisotropy, J. Alloys Compd. 855 (2021) 157460, doi:10.1016/j.jallcom.2020.157460.
[49] I. Ogasawara, S. Ueno, Preparation and properties of amorphous wires, IEEE Trans. Magn. 31 (1995) 1219–1223, doi:10.1109/20.364811.
[50] V. Zhukova, J.M. Blanco, M. Ipatov, R. Varga, J. Gonzalez, A. Zhukov, Domain wall propagation in Fe-rich microwires, Phys. B Condens. Matter. 403 (2008) 382–385, doi:10.1016/j.physb.2007.08.055.
[51] V. Zhukova, J.M. Blanco, M. Ipatov, A. Zhukov, Effect of transverse magnetic field on domain wall propagation in magnetically bistable glass-coated amorphous microwires, J. Appl. Phys. 106 (2009) 113914, doi:10.1063/1.3266009.
[52] V. Zhukova, J.M. Blanco, P. Corte-Leon, M. Ipatov, M. Churyukanova, S. Taskaev, A. Zhukov, Grading the magnetic anisotropy and engineering the domain wall dynamics in Fe-rich microwires by stress-annealing, Acta Mater. 155 (2018) 279-285, doi:10.1016/j.actamat.2018.05.068.
[53] P. Corte-León, V. Zhukova, J.M. Blanco, A. Chizhik, M. Ipatov, J. Gonzalez, A. Fert, A. Alonso, A. Zhukov, Engineering of domain wall propagation in magnetic microwires with graded magnetic anisotropy, Appl. Mater. Today (2021) 101263, doi:10.1016/j.apmt.2021.101263.
[54] N.L. Schryer, L.R. Walker, The motion of 180° domain walls in uniform dc magnetic fields, J. Appl. Phys. 45(12) (1974) 5406-5421.
[55] A. Kunz, S.C. Reiff, Enhancing domain wall speed in nanowires with transverse magnetic fields, J. Appl. Phys. 103 (2008) 07D903.
[56] Jai-Lin Tsai, Hsin-Te Tzeng, Bing-Fong Liu, Magnetic properties and microstructure of graded Fe/FePt films, J. Appl. Phys. 107 (2010) 113923.
[57] C.L. Zha, R.K. Dumas, Y.Y. Fang, V. Bonanni, J. Nogués, J. Åkerman, Continuously graded anisotropy in single $(Fe_{53}Pt_{47})_{100-x}Cu_x$ films, Appl. Phys. Lett. 97 (2010) 182504.
[58] R. Skomski, T.A. George, D.J. Sellmyer, Nucleation and wall motion in graded media, J. Appl. Phys. 103 (2008) 07F531.

5. Application: Magnetic microwire inclusions in smart composites allowing non-contact stress and temperature monitoring

Thin and flexible glass-coating provides new functionalities, as previously mentioned, such as improved mechanical and corrosive properties, adherence with polymeric matrices and biocompatibility [1-3]. These mentioned features of glass-coated microwires allow better use of the advantages of amorphous materials in a number of emerging applications opening new opportunities for development of novel applications, such as non-destructive stresses monitoring, biomedical applications, magnetoelastic sensors and smart composites with tunable magnetic permittivity [4-8]. The other advantages of glass-coated microwires are low dimensionality and excellent mechanical properties [1]. Particularly, the stress dependence of hysteresis loops and GMI effect, which is proposed for the mechanical stresses monitoring in fiber reinforced composites (FRC) containing microwires inclusions or using magnetoelastic sensors based on stress dependence of various magnetic properties [4-8].

Glass-coated $Fe_{75}B_9Si_{12}C_4$ (metallic nucleus diameter, d = 15.2 μm, total diameter, D = 17.2 μm, $\rho = d/D$ = 0.88) and $Fe_{3.8}Co_{65.4}Ni_1B_{13.8}Si_{13}Mo_{1.35}C_{1.65}$ (d = 18,8 μm, D = 22,2 μm) microwires with positive and low negative magnetostriction coefficients, λ_s, respectively, prepared by Taylor-Ulitovsky technique, have been employed in this study. λ_s –values of studied $Fe_{75}B_9Si_{12}C_4$ and $Fe_{3.8}Co_{65.4}Ni_1B_{13.8}Si_{13}Mo_{1.35}C_{1.65}$ microwires are about 35 x 10^{-6} and -1 x 10^{-6}, respectively, as presented before.

As studied in the previous chapter, as-prepared $Fe_{75}B_9Si_{12}C_4$ microwires present rectangular hysteresis loops [9]. Under applied stresses the character of hysteresis loops of as-prepared Fe-rich microwires does not change [10]. However, magnetic softness and external stresses sensitivity of as-prepared Fe-rich microwires can be considerably improved by stress-annealing [9,10].

Stress-annealed Fe-rich microwires can present higher sensitivity to external stresses [10]. Therefore, $Fe_{75}B_9Si_{12}C_4$ microwires were stress-annealed in a conventional furnace at 300 ^oC under 190 MPa. As previously reported, $Fe_{75}B_9Si_{12}C_4$ microwires stress-annealed at these conditions present good magnetic softness and considerable GMI effect [9].

On the other hand, from previous studies and as it is reviewed in this work, it is known that as-prepared Co-rich microwires typically present good magnetic softness and hence high GMI effect [11]. Additionally, previously is shown that the composite materials with embedded Co-rich microwires can present field tunability of effective permittivity and enhanced sensitivity to external stimuli, like temperature or stress [12]. Therefore, we expect that Fiber Reinforced Composites, FRCs, containing $Fe_{3.8}Co_{65.4}Ni_1B_{13.8}Si_{13}Mo_{1.35}C_{1.65}$ microwires with low negative vanishing magnetostriction coefficient can be sensitive to stresses.

The stress has been applied during the annealing as well as during the sample cooling with the furnace. The value of applied stresses (evaluated using *eq. 2.1*) was up to 450 MPa.

Wire arrays were fabricated using prepared glass coated amorphous wires embedded in the thermoset matrix polymerization and placed inside the glass tube (*Figure 5.1a*). We used a vinylester resin (DERAKANE 8084) resin, accelerated with Cobalt Octoate (0,3 pph) and catalyzed with Methyl Ethyl Ketona (MEK 60%, 1,5 pph).

DERAKANE 8084 epoxy vinyl ester resin is an elastomer modified resin designed to offer increased adhesive strength, superior resistance to abrasion and severe mechanical stress, while giving greater toughness and elongation.

The liquid resin properties are the following; its density at 25 °C is of 1.02 g/ml, its dynamic viscosity at 25 °C is of 360 MPa and its styrene content is of 40%.

During the polymerization process of the resin, volume shrinkage occurs (8.2%) and solid cured resin is obtained. The mechanical properties of the cured resin are the

following: tensile strength of 76 MPa, tensile modulus of 2.9 GPa, and tensile elongation of 8-10%.

All technical resin information can be found in its technical data sheet (Document 1820 V5 F2, Language ES "draft", © 2017 Ashland Inc.).

5.1. Effect of the matrix polymerization in the hysteresis loops of the microwire inclusions of the composite material

Consequently, we studied the evolution of the hysteresis loop of $Fe_{3.8}Co_{65.4}Ni_1B_{13.8}Si_{13}Mo_{1.35}C_{1.65}$ microwire embedded in the thermoset resin during its polymerization inside the glass tube with the pick-up coil (*Figure 5.1a*).

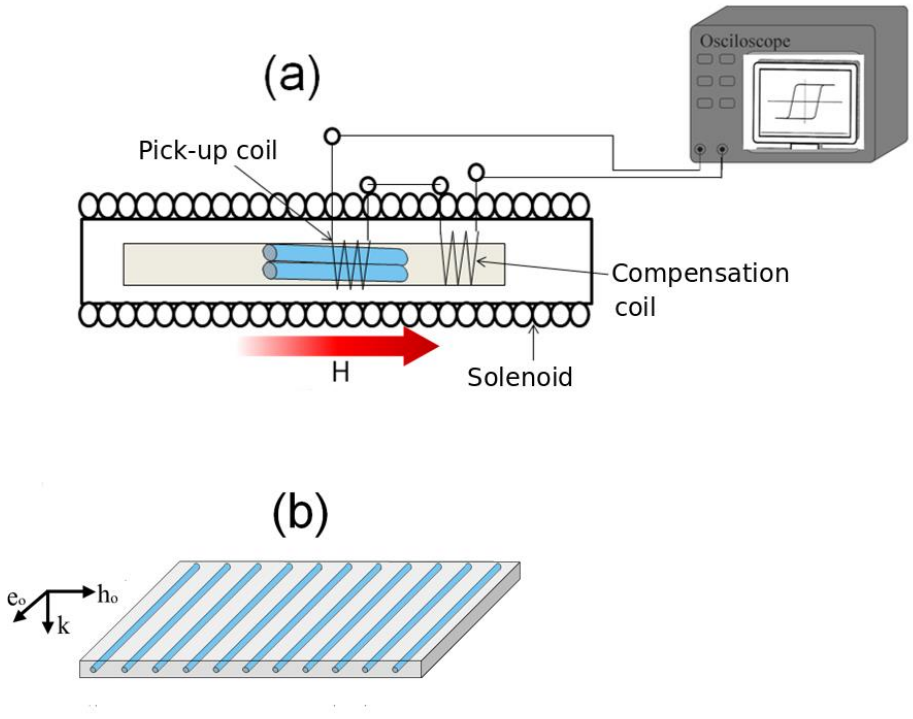

Figure 5.1. *Sketch of a system allowing measurements of the hysteresis loops of linear array consisting of glass coated amorphous wires embedded in the polymerizing composite and placed inside the glass tube (a) and of a FRC with embedded microwires (b).*

The polymerizing matrix provides external stimuli for the microwire inclusions (*Figure 5.1b*), which affects the magnetic properties and the GMI effect of microwires.

We performed two kinds of in-situ experiments when glass-coated microwires: 1) were place in a thermoset matrix during its polymerization and 2) were embedded in a polymerized composite.

Hysteresis loops of both kinds of microwires are shown in *Figure 5.2*. As can be appreciated from *Figure 5.2a*, $Fe_{3.8}Co_{65.4}Ni_1B_{13.8}Si_{13}Mo_{1.35}C_{1.65}$ microwire presents almost linear hysteresis loop with a good magnetic softness (coercivity, $H_c \approx 10$ A/m). It is worth mentioning that the hysteresis loop of microwire placed inside the linear array remains almost the same as for free single microwire (see *Figure 5.2a*). Stress-annealed (employed for in-situ experiments) $Fe_{75}B_9Si_{12}C_4$ microwire also presents low coercivity ($H_c \approx 40$ A/m) (*Figure 5.2b*). However, the hysteresis loop character is different to that of Co-rich microwire.

Hysteresis loops of the arrays containing the microwires have been measured in situ using the fluxmetric method during the time period of 120 min. The temperature has been measured by a standard thermocouple.

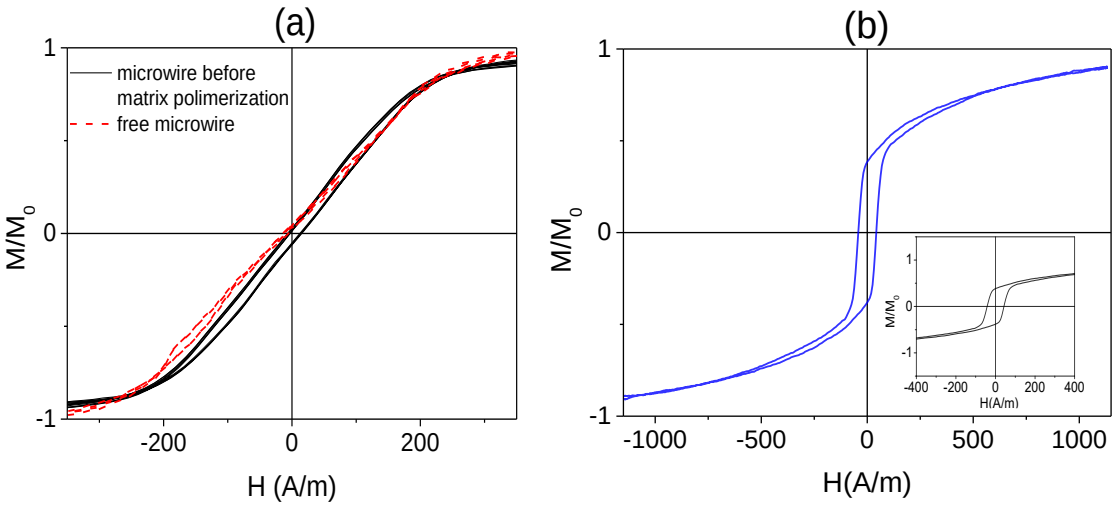

Figure 5.2. *Hysteresis loops of $Fe_{3.8}Co_{65.4}Ni_1B_{13.8}Si_{13}Mo_{1.35}C_{1.65}$ (a) and stress-annealed $Fe_{75}B_9Si_{12}C_4$ (b) microwires.*

In the first series of experiments we measured the evolution of the hysteresis loops of the linear microwire (of both Co-rich and Fe-rich compositions) array during the thermoset matrix polymerization. These results are represented by the changes of the hysteresis loops with the polymerization time, *t* (*Figure 5.3*).

We observed change of shape of the hysteresis loops of the array containing $Fe_{3.8}Co_{65.4}Ni_1B_{13.8}Si_{13}Mo_{1.35}C_{1.65}$ microwires, namely: linear character of the hysteresis loop observed in $Fe_{3.8}Co_{65.4}Ni_1B_{13.8}Si_{13}Mo_{1.35}C_{1.65}$ magnetic microwire becomes rectangular during the matrix polymerization. This change of the hysteresis loop character in array of $Fe_{3.8}Co_{65.4}Ni_1B_{13.8}Si_{13}Mo_{1.35}C_{1.65}$ microwires is observed after approximately t = 20 min (*Figure 5.3*). Observed change of hysteresis loops can be represented by the evolution of the coercivity, H_c, and magnetic anisotropy field, H_k, obtained directly from the hysteresis loops. As can be observed from *Figure 5.4a*, magnetic anisotropy field presents non-monotonic dependence on time of polymerization, while coercivity grows from 6 to 35 A/m (*Figure 5.4b*).

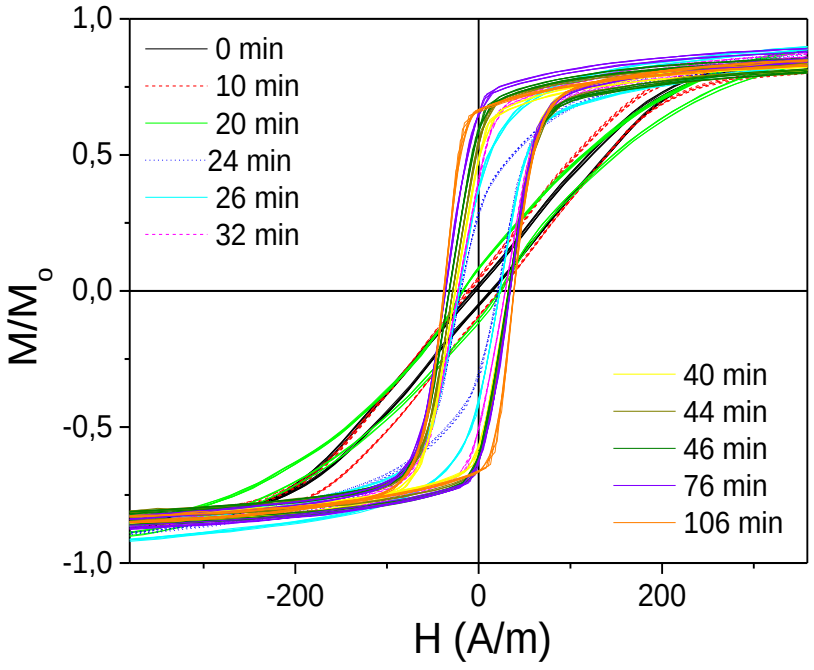

Figure 5.3. *Effect of the matrix polymerization on hysteresis loops of the array containing the* $Fe_{3.8}Co_{65.4}Ni_1B_{13.8}Si_{13}Mo_{1.35}C_{1.65}$ *microwires.*

Similarly, remarkable change of the hysteresis loops of array containing $Fe_{75}B_9Si_{12}C_4$ microwires upon polymerization is observed (*Figure 5.5*). In this case, initially the hysteresis loop presents almost rectangular shape with $H_c \approx 40$ A/m. Upon thermoset matrix polymerization the hysteresis loop becomes more inclined and finally changes to linear (see *Figure 5.5a*). Evolution of coercivity on polymerization time presents non-monotonic dependence with maximum about 40 min, see *Figure 5.5b*). Finally, for long *t*-values the hysteresis loops become almost anhysteretic and the coercivity drops to 3 A/m. Then, in this case the variation of magnetic properties is even more remarkable than for the case of the arrays containing Co-rich microwires.

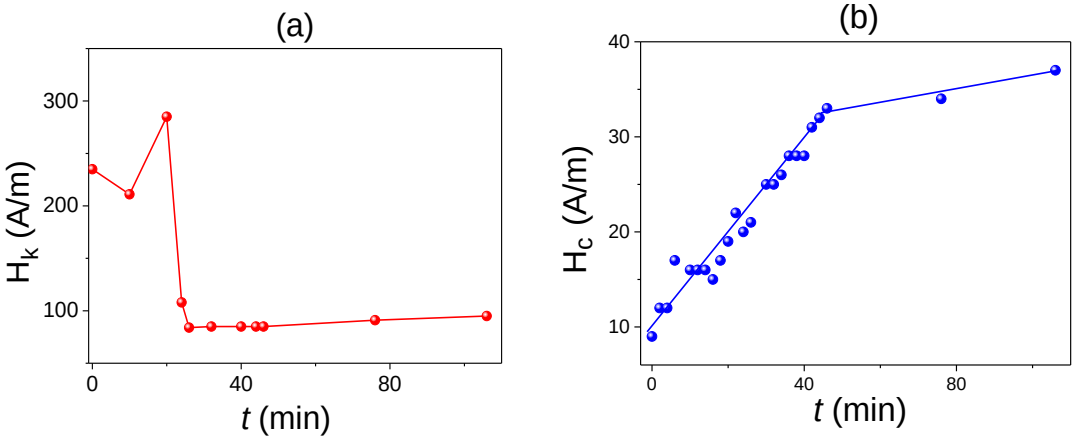

Figure 5.4. *Time dependence of the anisotropy field (a) and coercivity (b) of the array containing* $Fe_{3.8}Co_{65.4}Ni_1B_{13.8}Si_{13}Mo_{1.35}C_{1.65}$ *microwires inside the glass tube.*

5.2. Effect of the matrix polymerization in the electromagnetic parameters of the FRC with embedded microwires

The second detection method involves measurements of the transmission, *T*, and reflection, *R*, parameters of the composite containing Co-rich microwires ($Fe_{3.8}Co_{65.4}Ni_1B_{13.8}Si_{13}Mo_{1.35}C_{1.65}$) using the free space system.

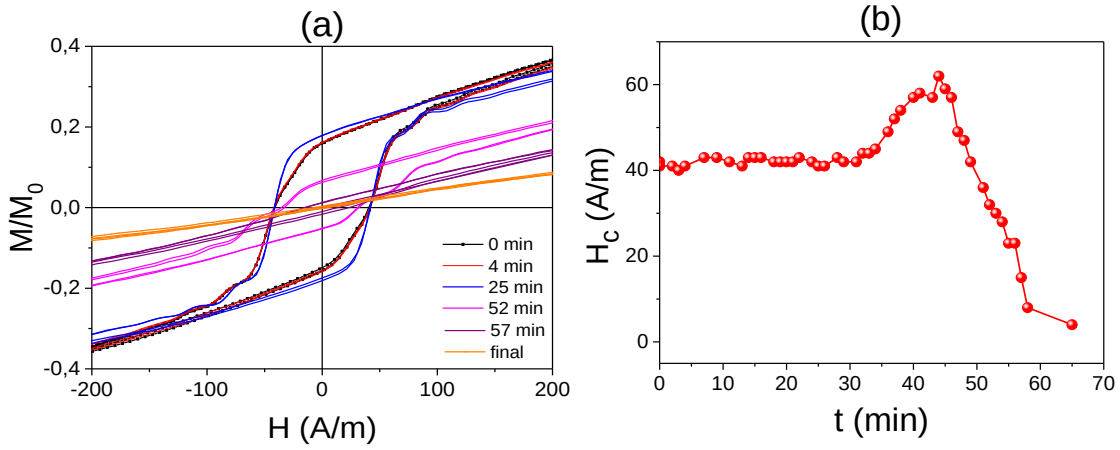

Figure 5.5. *Evolution of hysteresis loops (a) and coercivity (b) of linear array containing $Fe_{75}B_9Si_{12}C_4$ stress-annealed microwires.*

As can be appreciated from *Figure 5.6*, considerable variation of the *T*-parameter is observed in the range of 4-7 GHz (*Figure 5.6a*). Similarly, to H_k *(t)* dependence obtained for linear array containing $Fe_{3.8}Co_{65.4}Ni_1B_{13.8}Si_{13}Mo_{1.35}C_{1.65}$ microwires a non-monotonic variation of *T*-parameter upon polymerization is observed (*Figure 5.6a*). Additionally, some changes of *R*-parameter are also observed in a wide frequency range (*Figure 5.6b*).

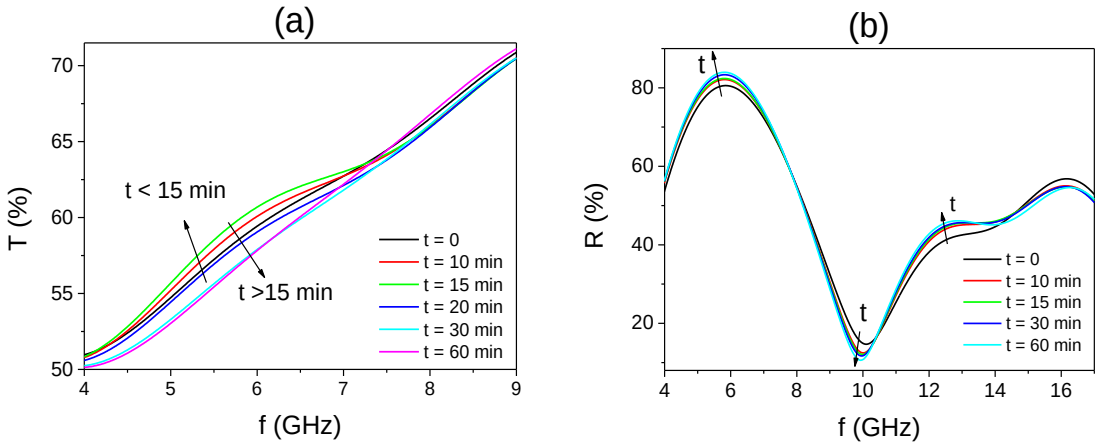

Figure 5.6. *Transmission, T, (a) and reflection, R, (b) parameters measured using free-space system during the composite polymerization.*

Observed changes of magnetic properties can be related to two main phenomena arising during the composite matrix polymerization: heating and mechanical stresses.

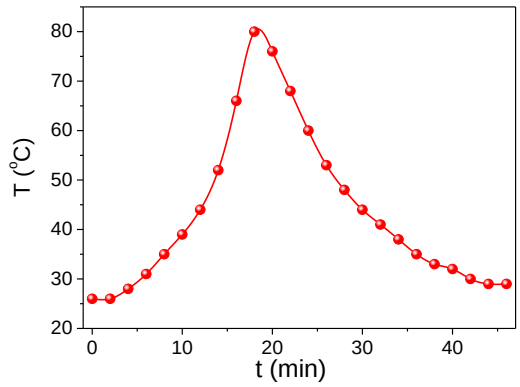

***Figure 5.7.** Temperature evolution upon the polymerization.*

In order to evaluate the heating we measured the temperature by means of a thermocouple. As can be observed from *Figure 5.7*, the matrix polymerization produces a heating of the composite up to 80 °C. For the present geometry (linear array of microwires with polymerizing composite inside the glass-tube) the heating takes place up to *t* = 20 min (when the temperature, *T*, achieves about 80 °C) followed

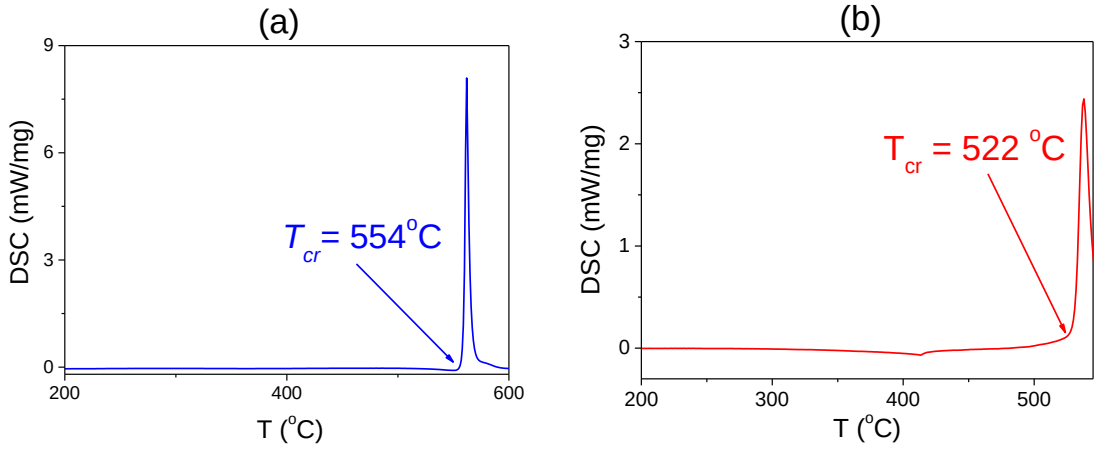

***Figure 5.8.** DSC curves of as-prepared $Fe_{3.8}Co_{65.4}Ni_1B_{13.8}Si_{13}Mo_{1.35}C_{1.65}$ (a) and stress-annealed $Fe_{75}B_9Si_{12}C_4$ (b) microwires.*

by cooling down to almost ambient temperature at *t* ≈ 50 min (when *T* ≈ 30 °C).

Structure and crystallization temperature of studied microwires have been evaluated by the DSC method. Both studied samples at 80 °C maintain amorphous character. The crystallization temperatures, T_{cr}, (determined as the beginning of the first crystallization peak) evaluated by the DSC of microwire are about 554 and 522 °C respectively (see *Figure 5.8a,b*).

Additionally, all studied microwires present XRD picture typical for completely amorphous materials. The XRD of microwires embedded in the polymerized matrix present broad halo typical for completely amorphous materials (see *Figure 5.9a,b*). Therefore, we must pay attention on the magnetoelastic behaviour of both microwires.

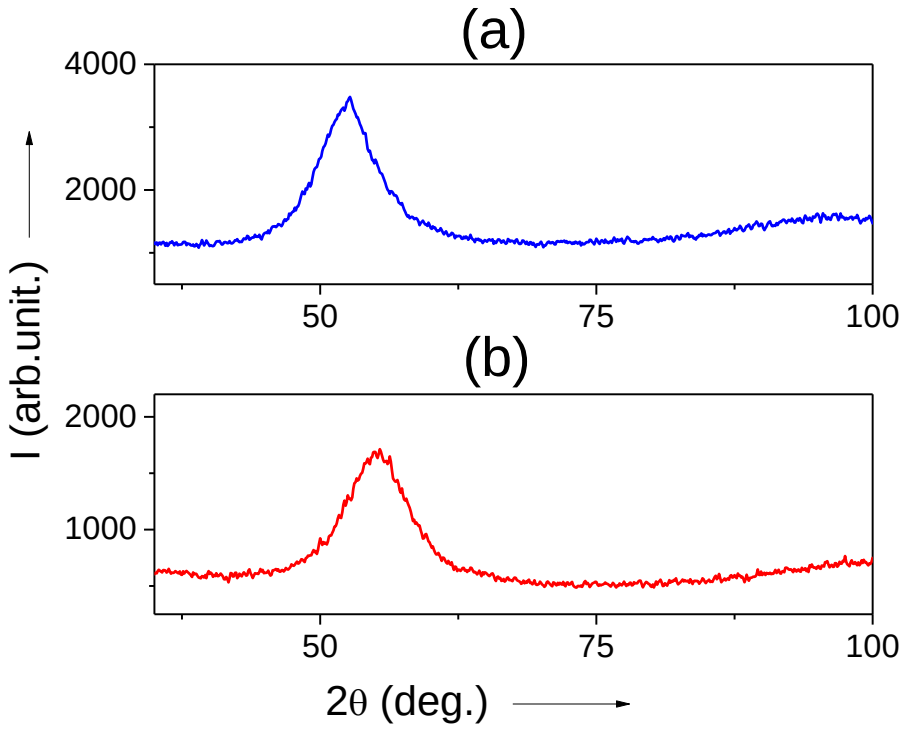

Figure 5.9. *XRD, picture of the $Fe_{3.8}Co_{65.4}Ni_1B_{13.8}Si_{13}Mo_{1.35}C_{1.65}$ (a) and $Fe_{75}B_9Si_{12}C_4$ (b) microwires embedded in the polymerized matrix.*

5.3. Effect of the composite matrix polymerization process in the internal stresses of the microwires

The second phenomenon affecting the hysteresis loops during the resin polymerization are the mechanical stresses affecting to the metallic nucleus of the microwire. Matrix polymerization is accompanied by change of density and shrinkage. Although generally the internal stresses arising during the matrix polymerization are complex and distributed in non-homogeneously distributed inside the matrix [13] an important fact is that the matrix shrinks as it cools. Additionally, studied system consisting of glass-coated metallic microwires inside the polymerizing matrix presents different thermal expansion coefficients of metallic nucleus, glass-coating and the matrix consisting of vinylester (Derakane 8084) resin accelerated with Cobalt Octoate and catalyzed with Methyl Ethyl Ketona. However, we can assume that the shrinkage of the matrix produces compressive stresses in magnetic nucleus of glass-coated microwires.

In order to confirm this assumption, we evaluated the influence of applied tensile stresses on the hysteresis loops of both employed microwires. As shown in *Figure 5.10a*, the hysteresis loop shape of as-prepared $Fe_{3.8}Co_{65.4}Ni_1B_{13.8}Si_{13}Mo_{1.35}C_{1.65}$ microwire (with low negative λ_s -value) maintains linear shape under applied tensile stresses. However, magnetic anisotropy field, H_k, of as-prepared $Fe_{3.8}Co_{65.4}Ni_1B_{13.8}Si_{13}Mo_{1.35}C_{1.65}$ microwire rises under application of tensile stresses (see *Figure 5.10a*). An increase of magnetic anisotropy field, H_k, of $Fe_{3.8}Co_{65.4}Ni_1B_{13.8}Si_{13}Mo_{1.35}C_{1.65}$ microwire upon tensile stresses (proportional to the mechanical load, *P*, attached to the microwire) is depicted in *Figure 5.11*. In fact the influence of applied stresses on hysteresis loops of Co-rich microwires is poorly studied. However, from evolution of the GMI ratio upon tensile stresses [4] such H_k rising upon tensile stresses can be predicted in Co-rich microwires.

Almost non-hysteretic loops of Co-rich microwires (with $\lambda_s < 0$) with a well-defined transverse circular anisotropy have been attributed to magnetisation process running by quasi-reversible magnetisation rotation from the circumferential to the

axial direction as increasing the axial applied magnetic field [14]. Such circular magnetic anisotropy is induced by the internal stresses (mostly of tensile character) generated during the fabrication [14,15]. To explain the influence of applied stresses it is necessary to consider the negative λ_s-values and the fact that the applied stress induces additional circular magnetoelastic anisotropy responsible for the linear hysteresis loop.

In contrast, the hysteresis loops of stress-annealed $Fe_{75}B_9Si_{12}C_4$ microwires ($\lambda_s > 0$) upon application of tensile stress, the hysteresis loop becomes perfectly rectangular (*Figure 5.10b*). Additionally, growth of coercivity, upon applied stresses (*Figure 5.10*) and mechanical load, *P*, (*Figure 5.11*) can be appreciated. Previously, H_c rising upon applied tensile stresses, σ, was interpreted considering that the coercivity is proportional to the energy required to form the domain wall involved in the magnetization reversal [16]. In this case, the coercive field was associated to the switching field, H_s, that is the value of the applied magnetic field to remagnetize the inner core [16]. Experimentally observed in Fe-rich microwires H_s (σ) dependence follows a $\sigma^{1/2}$ law [16] previously predicted for amorphous wires [16], which is generally in agreement with the results of the *Figure 5.10b*.

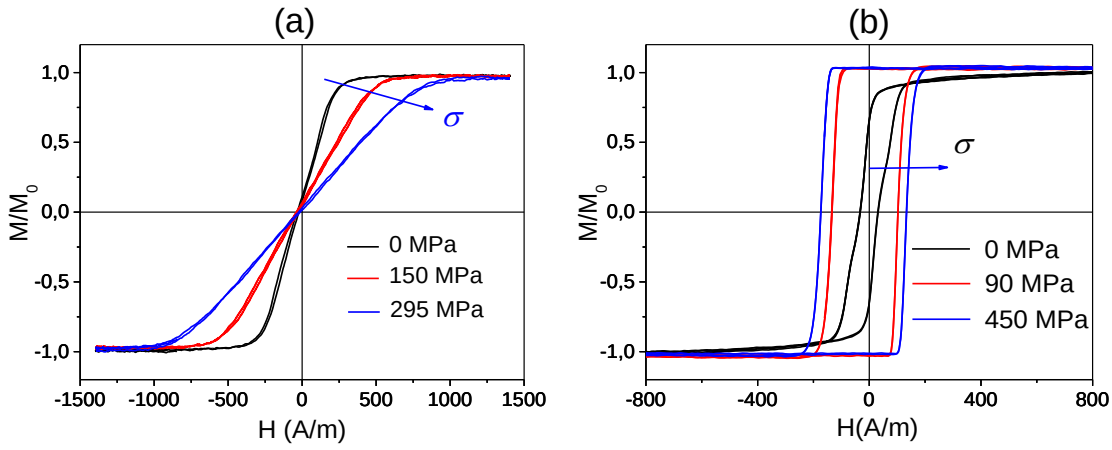

Figure 5.10. *Evolution of the hysteresis loops of $Fe_{3.8}Co_{65.4}Ni_1B_{13.8}Si_{13}Mo_{1.35}C_{1.65}$ (a) and stress-annealed $Fe_{75}B_9Si_{12}C_4$ (b) microwires.*

Previously, the recovery of the rectangular hysteresis loop typical in stress-annealed Fe-rich microwires [17] upon tensile stresses was explained by the increasing of the longitudinal stress component under the tensile stress application and consequently the alignment of the easy magnetization axis along the highest stress component in the microwires with $\lambda_s > 0$ [16].

Observed dependencies generally present the behavior opposite to those observed during the polymerization process. Particularly, linear hysteresis loop of linear array containing the $Fe_{3.8}Co_{65.4}Ni_1B_{13.8}Si_{13}Mo_{1.35}C_{1.65}$ microwires becomes rectangular during the matrix polymerization. Moreover, as shown in *Figure 5.4*, this transformation of hysteresis loops is associated to magnetic anisotropy field decrease upon the polymerization. However, observed H_k *(t),* H_c *(t)* and *T (t)* dependencies are non- monotonic: some increase of H_k at t = 20 min and T up to t = 15 min (at $f \approx$ 4-7 GPa) must be related to the heating.

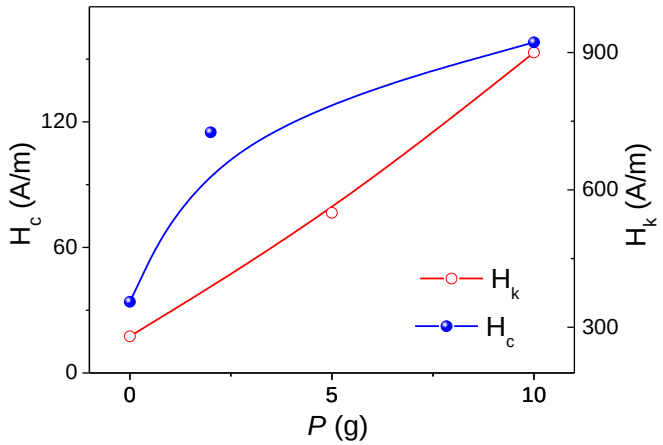

Figure 5.11. *Variation of H_k of $Fe_{3.8}Co_{65.4}Ni_1B_{13.8}Si_{13}Mo_{1.35}C_{1.65}$ microwire and H_c of $Fe_{75}B_9Si_{12}C_4$ microwire upon application of a mechanical load, P.*

Similarly, coercivity behaviour of $Fe_{75}B_9Si_{12}C_4$ microwires upon application of tensile stress is opposite to that observed upon polymerization: under the influence of tensile stresses the hysteresis loop becomes perfectly rectangular, while during the FRC polymerization the on the hysteresis loop changes from rectangular to linear.

To understand the effect of polymerization on magnetic properties of glass-coated microwires we must consider the character of the internal mechanical stresses. As mentioned before, the main part of the mechanical stresses is originated by the difference in the thermal expansion coefficients of metallic alloy and glass-coating. The main part of the metallic nucleus of the microwire (up to $r \sim 0.85\ R$, where R is the metallic nucleus radius, r- metallic nucleus radius) has tensile stresses [15,18]. Therefore, the difference in thermal expansion coefficients of metallic alloy and glass-coating upon heating becomes smaller allowing the reduction of the internal stresses. This assumption has been recently confirmed by direct observation of the heating effect on hysteresis loop of Co-rich microwires with vanishing magnetostriction coefficient [14]. The transformation of the hysteresis loop from linear to rectangular upon heating was explained by the easy anisotropy direction change from circumferential to axial upon heating.

However, after the initial heating observed for about the first 20 min, the matrix is cooled during further polymerization (see *Figure 5.7*). Accordingly, one can expect the opposite trend towards an increase in internal stresses inside the ferromagnetic core, which are responsible for the evolution of magnetic properties during polymerization.

The other factor affecting the magnetic properties of the microwire inclusions during matrix polymerization is aforementioned matrix shrinkage.

From previous knowledge on internal stresses arising during the matrix polymerization [19] it is known that such stresses are complex and distributed non-homogeneously inside the matrix and especially in the inclusions inside the

polymerized matrix. In first approximation we can consider that the matrix shrinks during the polymerization.

Therefore, we can assume the compression stresses acting upon glass-coated microwires. The properties of the main constituents, i.e., the matrix, the glass coating and the metallic nucleus of the microwires are quite different. Therefore, the stresses must be non-uniformly distributed within the microwire inclusions. Generally, such compression acting upon the glass coating should reduce the internal stresses inside the metallic nucleus. Thus, the matrix shrinkage will act similarly to the matrix heating. However, in order to understand the polymerization effect, we must consider both effects simultaneously: a temperature change (which includes initial heating followed by cooling) and a matrix shrinkage.

Thus, taking into account the obtained experimental results on the effect of applied stresses on the hysteresis loop of individual microwires and on the polymerization effect, it can be concluded that the observed in-situ evolution of the hysteresis loop of arrays consisting of Co and Fe-rich microwires, as well as the transmission and reflection parameters at polymerization should be attributed to the matrix shrinkage and the temperature variation during the polymerization.

A schematic (rather simplified) picture illustrating the effect of the polymerization process on the stress distribution is shown in *Figure 5.12*. It should be noted that shrinkage of the matrix, as well as heating and cooling occur simultaneously. The observed non-monotonic H_c, H_k (*Figure 5.4*) and T dependencies (*Figure 5.6*) should be attributed to the cumulative effect of all processes during matrix polymerization.

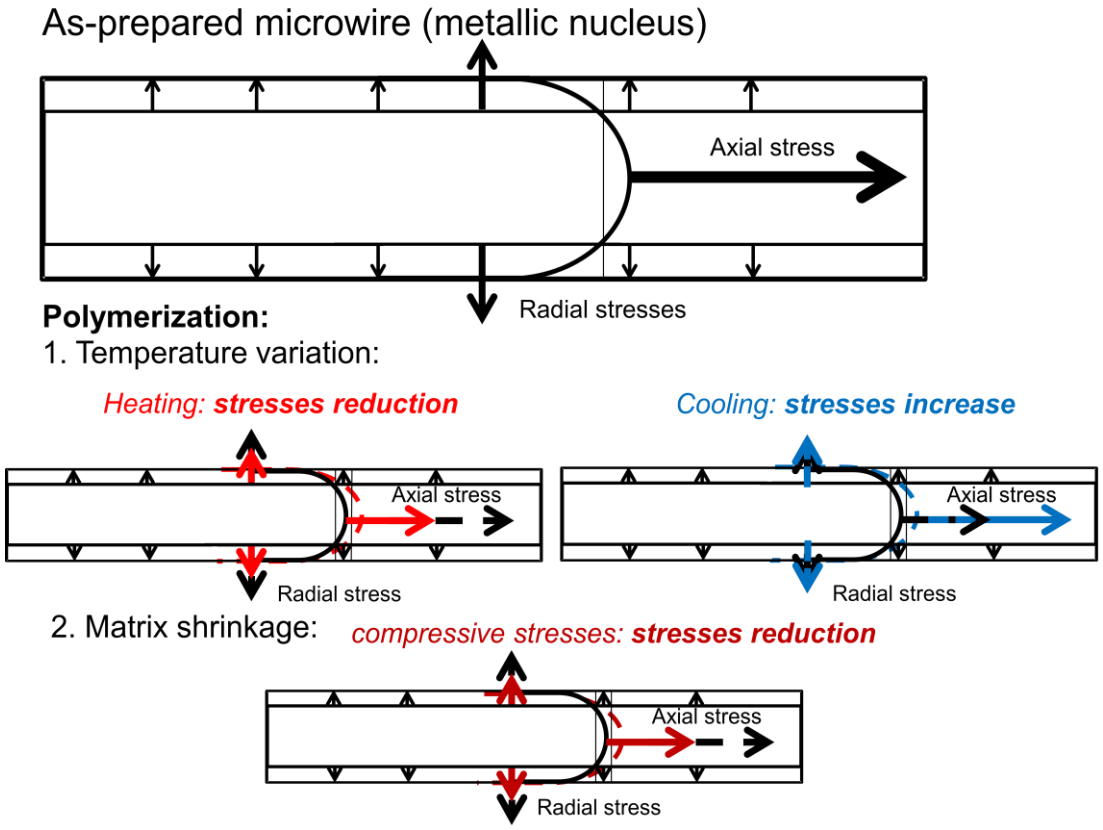

Figure 5.12. *Schematic picture illustrating the effect of the polymerization process on the stress distribution inside the metallic nucleus of glass-coated microwire.*

It is worth mentioning, that due to the mismatch in the properties of their constituents, composite are prone to build-up of residual stresses. In consequence, it can be helpful to identify what happened in the microwire/polymer interface.

The adhesion in the interface between the microwire and the matrix in the composite was checked using the Hitachi TM-1000 scanning electronic microscope, SEM, as well as using recently described adhesion test [6]. Using mentioned technique as well as SEM microscopy (see *Figure 5.13*) we observed quite good adhesion between the polymeric matrix and glass-coating. When a microwire is drawn out of a polymerized matrix, the applied stress above 60 MPa is necessary for breaking the interface between the metallic nucleus and the glass coating. However the interface between the glass nucleus and the matrix was not destroyed.

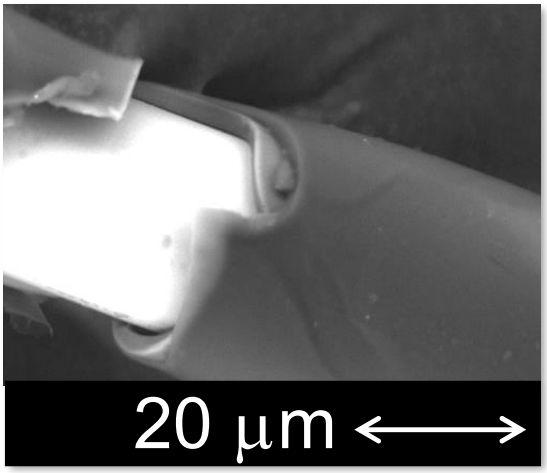

Figure 5.13. *SEM image of studied glass-coated microwire inside the polymeric matrix.*

Above, we described the use of magnetic microwires for in-situ monitoring of the matrix polymerization. Eventually, the same technique can be used for the remote monitoring of stress or temperature not only during the polymerization, but also for real time non-destructive monitoring of local stresses and temperature during the exploitation of the composites.

Concluding remarks

We propose a novel sensing technique for non-destructive and non-contact monitoring of the composites utilizing ferromagnetic glass-coated microwire inclusions with magnetic properties sensitive to tensile stress and temperature.

To demonstrate it we have studied in-situ the impact of matrix polymerization on the evolution of the hysteresis loop of arrays consisting of Co- and Fe-rich microwires as well as the transmission and reflection parameters of the composites with microwire inclusions.

A remarkable change in the hysteresis loops shape of linear microwire arrays is observed. For the arrays containing Co-rich microwires we observed transformation of the linear hysteresis loop to rectangular shape and a coercivity increasing from 6 to 35 A/m. Even more remarkable changes of the hysteresis loops of the arrays containing stress-annealed Fe-rich microwires consisting of a change of the hysteresis loop from rectangular to linear shape and a coercivity drop from 40 A/m to 3 A/m are observed. The effect of applied tensile stresses on the hysteresis loops of both studied microwires is the opposite to that observed during the composite polymerization.

Additionally, we observed considerable variation of the *T*-parameter (in the range of 4-7 GHz) and *R*-parameter upon composite polymerization using the free space technique.

Observed dependencies are discussed considering the matrix shrinkage during the polymerization and heating during the matrix polymerization and their influence on magnetic properties of glass-coated microwires.

Obtained experimental results yield new and important insights suitable for development of novel sensing technique for non-destructive and non-contact monitoring of the FRCs utilizing ferromagnetic glass-coated microwire inclusions.

Consequently, a novel sensing technique for non-destructive and non-contact monitoring of the composites utilizing ferromagnetic glass-coated microwire inclusions

with quite soft magnetic properties and tunable magnetic permittivity sensitive to tensile stress and temperature is proposed.

5.4. References

[1] T. Goto, M. Nagano, N. Wehara, Mechanical properties of amorphous Fe80P16C3B1 filament produced by glass-coated melt spinning, Trans. JIM 18 (1977) 759-764.

[2] D. Kozejova, L. Fecova, P. Klein, R. Sabol, R. Hudak, I. Sulla, D. Mudronova, J. Galik, R. Varga, Biomedical applications of glass-coated microwires, J. Magn. Magn. Mater. 470 (2019) 2-5, doi:10.1016/j.jmmm.2017.11.004.

[3] A. Talaat, J. Alonso, V. Zhukova, E. Garaio, J.A. García, H. Srikanth, M.H. Phan, A. Zhukov, Ferromagnetic glass-coated microwires with good heating properties for magnetic hyperthermia, Sci. Rep. 6 (2016) 39300.

[4] A.F. Cobeño, A. Zhukov, J.M. Blanco, V. Larin, J. Gonzalez, Magnetoelastic sensor based on GMI of amorphous microwire, Sens. Actuators A 91 (2001) 95-98.

[5] D. Praslička, J. Blažek, M. Šmelko, J. Hudák, A. Čverha, I. Mikita, R. Varga, A. Zhukov, Possibilities of Measuring Stress and Health Monitoring in Materials Using Contact-Less Sensor Based on Magnetic Microwires, IEEE Trans. Magn. 49(1) (2013) 128-131.

[6] M. Churyukanova, S. Kaloshkin, E. Shuvaeva, A.Stepashkin, M. Zhdanova, A. Aronin, O. Aksenov, P. Arakelov, V. Zhukova, A. Zhukov, Non-contact method for stress monitoring based on stress dependence of magnetic properties of Fe-based microwires, J. Alloys Compd. 748(5) (2018) 199-205.

[7] J. Olivera, M. González, J.V. Fuente, R. Varga, A. Zhukov, J.J. Anaya, An Embedded Stress Sensor for Concrete SHM Based on Amorphous Ferromagnetic Microwires, Sensors 14 (2014) 19963-19978.

[8] F.X. Qin, H.X. Peng, M.H. Phan, L.V. Panina, M. Ipatov, A. Zhukov, Effects of wire properties on the field-tunable behaviour of continuous-microwire composites, Sens. Actuators A 178 (2012) 118–125.

[9] V. Zhukova, J.M. Blanco, M. Ipatov, M. Churyukanova, S. Taskaev, A. Zhukov, Tailoring of magnetoimpedance effect and magnetic softness of Fe-rich glass-coated microwires by stress- annealing, Sci. Rep. 8 (2018) 3202, doi:10.1038/s41598-018-21356-3.

[10] P. Corte-Leon, V. Zhukova, M. Ipatov, J.M. Blanco, J. Gonzalez, M. Churyukanova, J.M. Baraibar, S. Taskaev, A. Zhukov, Stress dependence of the magnetic properties of glass-coated amorphous microwires, J. Alloys Compd. 789 (2019) 201-208, doi:10.1016/j.jallcom.2019.03.044.

[11] A. Talaat, V. Zhukova, M. Ipatov, J.M. Blanco, J. Gonzalez, A. Zhukov, Impact of Stress Annealing on the Magnetization Process of Amorphous and Nanocrystalline Co-Based Microwires, Materials 12 (2019) 2644, doi:10.3390/ma12162644.

[12] L. Panina, M. Ipatov, V. Zhukova, J. Gonzalez, A. Zhukov, Tuneable composites containing magnetic microwires, chapter 22, pp. 431-460 in Book: Metal, ceramic and polymeric composites for various uses, Ed. John Cuppoletti, 2011, doi:10.5772/21423 (ISBN 978-953-307-1098-3) InTech - Open Access Publisher (www.intechweb.org), Janeza Trdine, 9, 51000 Rijeka, Croatia.

[13] J.A. Nairn, P. Zoller, Matrix solidification and the resulting residual thermal stresses in composites. J. Mater. Sci. 20(1) (1985) 355–67.

[14] V. Zhukova , P. Corte-Leon, J.M. Blanco, M. Ipatov, L. Gonzalez-Legarreta, A. Gonzalez, A. Zhukov, Development of Magnetically Soft Amorphous Microwires for Technological Applications (Review), Chemosensors (10) (2022) 26, doi:10.3390/chemosensors10010026.

[15] J. Velázquez, M. Vazquez, A. Zhukov, Magnetoelastic anisotropy distribution in glass-coated microwires, J. Mater. Res. 11 (10) (1996) 2499-2505.

[16] P. Aragoneses, J.M. Blanco, L. Dominguez, J. González, A. Zhukov, M. Vázquez, The Stress dependence of the switching field in glass-coated amorphous microwires, J. Phys. 31 (1998) 3040-3045.
[17] V. Zhukova, V.S. Larin, A. Zhukov, Stress induced magnetic anisotropy and giant magnetoimpedance in Fe-rich glass/coated magnetic microwires, J.Appl. Phys. 94 (2) (2003) 1115-1118, doi:10.1063/1.1585113.
[18] H. Chiriac, T.A. Ovari, A. Zhukov, Magnetoelastic anisotropy of amorphous microwires, J. Magn. Magn. Mater. 254-255 (2003) 469-471.
[19] A. Allue, P. Corte-León, K. Gondra, V. Zhukova, M. Ipatov, J.M. Blanco, J. Gonzalez, M. Churyukanova, S. Taskaev, A. Zhukov, Smart composites with embedded magnetic microwire inclusions allowing non-contact stresses and temperature monitoring, Compos. - A: Appl. Sci. Manuf., 120 (2019) 12-20, doi:10.1016/j.compositesa.2019.02.014.

6. Conclusions and future outlook

Following the guidelines established in the introduction, this thesis has been devoted to the optimization of the magnetic properties of Co and Fe-based glass-coated microwires fabricated by the Taylor Ulitovsky technique, including: improvement of magnetic softness, increase in the giant magnetoimpedance (GMI) effect and fast domain wall (DW) dynamics control. The experimental results for the different post-processing routes selected allow us to extract the following conclusions:

❖ Co-based amorphous glass-coated microwires:

1. Co-based microwires with nearly-zero magnetostriction coefficient can present excellent magnetic softness and GMI effect even in as-prepared state.
2. Conventional annealing at sufficiently high temperature (350 °C) leads to magnetic hardening. Despite the magnetic hardening, increase in the GMI effect is obtained with a change in the shape of the *ΔZ/Z(H)* curve, from double-peak to single-peak dependence.
3. Stress-annealing allows obtaining better magnetic softness as-compared with furnace annealing, although higher temperatures and stresses values are needed than for Fe-rich microwires. $Co_{69.2}Fe_{3.6}Ni_1B_{12.5}Si_{11}Mo_{1.5}C_{1.2}$ microwires stress-annealed with σ = 472 MPa showed a decrease in the coercivity that is more noticeable as the temperature increases (up to 350 °C). GMI ratio improvement is observed, although similar $\Delta Z/Z_{max}$ values are observed for stress-annealing at fixed applied stress and different annealing temperatures.
   The samples stress-annealed present higher $\Delta Z/Z_{max}$ –values at higher frequencies. In addition, we have noted that short annealing treatments (t_{ann} = 10 min) also can produce beneficial effect.

4. Remarkable GMI effect improvement (up to 650%) and extremely magnetic softness (H_c ≈ 2 A/m) is obtained for $Co_{67}Fe_{3.9}Ni_{1.5}B_{11.5}Si1_{4.5}Mo_{1.6}$ microwire after Joule heating. Optimal Joule heating conditions for maximizing the GMI ratio are found to be I = 40 mA, t_{ann} = 5 min. The optimum frequency shifts from 300 MHz for as-prepared sample to 200 MHz in current-annealed samples.
5. $Co_{69.2}Fe_{4.1}B_{11.8}Si_{13.8}C_{1.1}$ microwire exhibits higher GMI ratio after Joule heating as compared with stress-annealing. Pointing out the beneficial effect of Joule heating for Co-based microwires.
6. The effect of applied tensile stress studied for $Co_{65.4}Fe_{3.8}Ni_1B_{13.8}Si_{13}Mo_{1.35}C_{1.65}$ microwire showed a linear H_k (σ) dependence.
7. Co-rich microwires with magnetic bistability induced by annealing exhibit DW propagation. DW velocity increase upon application of tensile stress is observed in studied $Co_{69.2}Fe_{4.1}B_{11.8}Si_{13.8}C_{1.1}$ microwire. Stress-annealing of Co-rich microwires with induced magnetic bistability allows further improvement of the DW velocity and mobility values.
8. Graded magnetic anisotropy is attained in Co-based $Co_{64.04}Fe_{5.71}B_{15.88}Si_{10.94}Cr_{3.4}Ni_{0.03}$ (d = 95 μm, D = 130 μm) and $Co_{66}Cr_{3.5}Fe_{3.5}B_{16}Si_{11}$ (d = 20.1 μm, D = 24.8 μm) microwires stress-annealed under a temperature gradient, reflected on the gradual modification of the hysteresis loops along the sample length.

❖ Fe-based glass-coated microwires:

1. Hysteresis loops of $Fe_{70}B_{15}Si_{10}C_5$ amorphous glass-coated microwires of different diameters of the metallic nucleus and glass coating showed the influence of the internal stresses. Coercivity and switching field decrease as ρ ratio increases.
2. Devitrification of Finemet-type (FeSiBNbCu) amorphous microwires after annealing results in enhancement of the magnetic softness, but

the deterioration of the mechanical properties leads to look for post-processing that allows maintain the amorphous state.

3. Internal stresses relaxation after furnace annealing of $Fe_{75}B_9Si_{12}C_4$ and Fe-Ni microwires gives rise to an improvement of the DW velocity with increasing annealing temperature and time.
4. Stress-annealing of $Fe_{70}B_{15}Si_{10}C_5$ microwires (d = 15.2 μm, D = 17.2 μm) allowed:
   - Remarkable increase in DW mobility associated with induced transverse magnetic anisotropy.
   - At high enough T_{ann} and σ, the rectangular hysteresis loop transforms into almost linear.
   - Noticeable maximum GMI ratio improvement of an order of magnitude is observed due to the induced transverse magnetic anisotropy.
   - At elevated frequencies (above 500 MHz) $\Delta Z/Z(H)$ dependences present double-peak shape typical of microwires with transverse magnetic anisotropy.
   - Enhancement of the stress dependence of coercivity, and therefore the stress sensitivity.
5. Stress-annealing induced anisotropy depends on stress-annealing conditions: temperature, stress and time. Such induced anisotropy is partially reversible: part of the stress-annealing induced anisotropy was annealed out by subsequent furnace annealing after stress-annealing, obtaining a substantial improvement of the GMI effect.
6. Fe-rich microwires with moderate stress-annealing induced anisotropy can present both GMI effect and single domain wall propagation.
7. "Thick" $Fe_{71.7}B_{13.4}Si_{11}Nb_3Ni_{0.9}$ microwire (d = 103 μm, D = 158 μm) presents simultaneously considerable GMI ratio and DW propagation even in as-prepared state. Furnace annealing allows an enhancement in the DW velocity and mobility. Conventional furnace annealing and stress-annealing at temperatures below crystallization allow GMI ratio

improvement in a wide frequency range. The largest increase is found for the sample annealed at 300 °C during t_{ann} = 4 h, $\Delta Z/Z \approx 200\%$.

8. Microwires with graded magnetic anisotropy were obtained by stress-annealing treatment at fixed applied stress and variable annealing temperature. Such microwires present the following features:
   - Local hysteresis loops of the microwire gradually change its character along the microwire length correlating with the anisotropy induced in each section of the microwire.
   - Non-uniform DW propagation. DW trapping is observed in the microwire region with strong enough stress-annealing induced magnetic anisotropy. Faster DW propagation and a decrease in the DW length are obtained in the region with moderate stress-annealing induced magnetic anisotropy.

❖ Applications:

A novel sensing technique is proposed for non-destructive and non-contact stress and temperature monitoring of composites consisting of ferromagnetic glass-coated microwire inclusions added in a polymeric matrix.

❖ Future outlook:

Although the described routes for optimizing the magnetic properties allowed a significant improvement in magnetic softness and an increase in the GMI coefficient, further efforts are needed to find suitable post-processing methods for greater improvement.

Recently, it was demonstrated a substantial improvement in the GMI ratio and DW dynamics in Fe-rich amorphous microwires subjected to Joule heating, proving

that there are still many other possibilities for further tuning of the magnetic properties.

The unique combination of magnetic properties (such as a high GMI effect and fast magnetization switching related to a single and large Barkhausen jump) in the same magnetic microwires properly post-processed, is potentially suitable for completely new applications that are expected to be developed.

7. Conclusiones (Spanish)

Siguiendo las pautas establecidas en la introducción, esta tesis se ha dedicado a la optimización de las propiedades magnéticas de microhilos recubiertos de vidrio ricos en Co y en Fe fabricados por la técnica de Taylor Ulitovsky, incluyendo: mejora del comportamiento magnético blando, aumento de la magnetoimpedancia gigante (GMI) y control de la dinámica de paredes de dominio (DW). Los resultados experimentales para las diferentes rutas de posprocesado seleccionadas nos permiten extraer las siguientes conclusiones:

❖ Microhilos amorfos recubiertos de vidrio basados en Co:

1. Los microhilos basados en Co con un coeficiente de magnetostricción casi nulo pueden presentar un excelente comportamiento magnético blando y efecto GMI incluso en el estado en que se prepararon.
2. El recocido convencional a una temperatura suficientemente alta (350 °C) conduce al endurecimiento magnético. A pesar del endurecimiento magnético, se obtiene un aumento en el efecto GMI con un cambio en la forma de la curva de dependencia $\Delta Z/Z(H)$, pasando de forma de doble pico a pico único.
3. El recocido bajo tensión permite obtener un mejor comportamiento magnético blando en comparación con el recocido en horno, aunque se necesitan temperaturas y valores de tensión más altos que para los microhilos ricos en Fe. Los microhilos $Co_{69.2}Fe_{3.6}Ni_1B_{12.5}Si_{11}Mo_{1.5}C_{1.2}$ recocidos bajo tensión, con σ = 472 MPa, mostraron una disminución en la coercitividad que es más notoria a medida que aumenta la temperatura (hasta 350 °C). Se observa una mejora en la relación GMI, aunque se observan valores $\Delta Z/Z_{max}$ similares para el recocido bajo tensión a una tensión aplicada fija y diferentes temperaturas de recocido.

Las muestras recocidas bajo tensión presentan valores más altos de $\Delta Z/Z_{max}$ a frecuencias más altas. Además, se ha observado que los tratamientos de recocido cortos (t_{ann} = 10 min) también pueden producir un efecto beneficioso.

4. Se obtiene una mejora notable del efecto GMI (hasta 650%) y un comportamiento magnético extremadamente blando ($H_c \approx 2$ A/m) para el microhilo $Co_{67}Fe_{3.9}Ni_{1.5}B_{11.5}Si1_{4.5}Mo_{1.6}$ después del calentamiento por efecto Joule. Se encuentra que las condiciones óptimas de calentamiento por efecto Joule para maximizar la relación GMI en esta muestra son I = 40 mA, t_{ann} = 5 min. La frecuencia óptima cambia de 300 MHz para las muestras sin tratar a 200 MHz en muestras recocidas con corriente.
5. El microhilo $Co_{69.2}Fe_{4.1}B_{11.8}Si_{13.8}C_{1.1}$ exhibe una relación GMI más alta después del calentamiento por efecto Joule en comparación con el resultado tras recocido bajo tensión. Señalando el efecto beneficioso del calentamiento por efecto Joule para microhilos ricos en Co.
6. El efecto de la aplicación de una tensión de tracción estudiado para el microhilo $Co_{65.4}Fe_{3.8}Ni_1B_{13.8}Si_{13}Mo_{1.35}C_{1.65}$ mostró una dependencia lineal de $H_k(\sigma)$.
7. Los microhilos ricos en Co con biestabilidad magnética inducida por recocido muestran propagación de paredes de dominio. Se observa un aumento de la velocidad de las paredes de dominio tras la aplicación de tensión de tracción en el microhilo $Co_{69.2}Fe_{4.1}B_{11.8}Si_{13.8}C_{1.1}$ estudiado. El recocido con tensión de microhilos ricos en Co con biestabilidad magnética inducida permite una mayor mejora de los valores de velocidad y movilidad de las paredes de dominio.
8. Se logra anisotropía magnética graduada en microhilos ricos en Co $Co_{64.04}Fe_{5.71}B_{15.88}Si_{10.94}Cr_{3.4}Ni_{0.03}$ (d = 95 μm, D = 130 µm) y $Co_{66}Cr_{3.5}Fe_{3.5}B_{16}Si_{11}$ (d = 20.1 μm, D = 24.8 μm) recocidos bajo tensión y bajo un gradiente de temperatura, esta anisotropía graduada se refleja en la variación gradual de los ciclos de histéresis a lo largo de la longitud de las muestras.

❖ Microhilos recubiertos de vidrio basados en Fe:

1. Los ciclos de histéresis de microhilos amorfos recubiertos de vidrio $Fe_{70}B_{15}Si_{10}C_5$ de diferentes diámetros del núcleo metálico y el recubrimiento de vidrio mostraron la influencia de las tensiones internas. La coercitividad y el campo de conmutación disminuyen a medida que aumenta el ratio ρ.
2. La desvitrificación de microhilos amorfos de tipo Finemet (FeSiBNbCu) después del recocido da como resultado una mejora del comportamiento magnético blando, pero el deterioro de las propiedades mecánicas lleva a buscar un posprocesado que permita mantener el estado amorfo.
3. La relajación de las tensiones internas después del recocido en horno de microhilos $Fe_{75}B_9Si_{12}C_4$ y Fe-Ni da lugar a una mejora de la velocidad de paredes de dominio con el aumento de la temperatura y el tiempo de recocido.
4. Tras recocido bajo tensión de microhilos $Fe_{70}B_{15}Si_{10}C_5$ (d = 15.2 μm, D = 17.2 μm) se han obtenido:
   - Incremento notable en la movilidad de las paredes de dominio asociado a la anisotropía magnética transversal inducida.
   - Para T_{ann} y σ lo suficientemente altos, el ciclo de histéresis rectangular se transforma en casi lineal.
   - Se observa una mejora notable del ratio GMI máximo de un orden de magnitud debido a la anisotropía magnética transversal inducida.
   - A frecuencias elevadas (superiores a 500 MHz) las dependencias *ΔZ/Z(H)* presentan la forma de doble pico típica de microhilos con anisotropía magnética transversal.
   - Mejora de la dependencia coercitividad con la tensión aplicada y, por lo tanto, de la sensibilidad a la tensión.

5. La anisotropía inducida por el recocido bajo tensión depende de las condiciones de recocido: temperatura, tensión y tiempo. Esta anisotropía inducida es parcialmente reversible: parte de la anisotropía inducida por el recocido bajo tensión fue revertida mediante un posterior recocido en horno después del recocido bajo tensión, obteniendo una mejora sustancial del efecto GMI.
6. Los microhilos ricos en Fe con anisotropía inducida por recocido con tensión moderada pueden presentar tanto efecto GMI como propagación de paredes de dominio único.
7. El microhilo $Fe_{71.7}B_{13.4}Si_{11}Nb_3Ni_{0.9}$ "grueso" (d = 103 μm, D = 158 μm) presenta simultáneamente efecto GMI y propagación de paredes de dominio considerables, incluso sin tratamiento de posprocesado. El recocido en horno permite una mejora en la velocidad y movilidad de paredes de dominio. El recocido en horno convencional y el recocido bajo tensión a temperaturas por debajo de la cristalización permiten mejorar el ratio GMI en un amplio rango de frecuencias. El mayor incremento se encuentra para la muestra recocida a 300 °C durante t_{ann} = 4 h, $\Delta Z/Z \approx 200\%$.
8. Se obtuvieron microhilos con anisotropía magnética graduada mediante tratamiento de recocido bajo tensión a una tensión aplicada fija y temperatura de recocido variable. Dichos microhilos presentan las siguientes características:
    - Los ciclos de histéresis locales del microhilo cambian gradualmente de carácter a lo largo de la longitud del microhilo en correlación con la anisotropía inducida en cada sección del microhilo.
    - Propagación de paredes de dominio no uniforme. Se observa “atrapamiento” de las paredes de dominio en la región del microhilo con suficientemente fuerte anisotropía magnética inducida por el recocido con tensión debido a la variación de temperatura de recocido a lo largo de la longitud del microhilo.

- Se obtiene una propagación de paredes de dominio más rápida y una disminución en la longitud de la pared de dominio en la región con moderada anisotropía magnética inducida por recocido de tensión.

❖ Aplicaciones:

Se propone una nueva técnica de detección para el control remoto y no destructivo de la tensión y la temperatura de materiales compuestos consistentes en inclusiones de microhilos ferromagnéticos recubiertos de vidrio añadidos en una matriz polimérica.

❖ Perspectivas de futuro:

Aunque las rutas descritas para optimizar las propiedades magnéticas permitieron una mejora significativa en el comportamiento magnético blando y un aumento en el coeficiente GMI, se necesitan más esfuerzos para encontrar métodos de posprocesado adecuados que permitan una mayor mejora.

Recientemente, se demostró una mejora sustancial en la relación GMI y el control de la dinámica de paredes de dominio en microhilos amorfos ricos en Fe sometidos a calentamiento por efecto Joule, lo que demuestra que todavía hay muchas otras posibilidades para un mayor ajuste de las propiedades magnéticas.

La combinación única de propiedades magnéticas (como efecto GMI alto y una conmutación de magnetización rápida relacionada con un único y gran salto de Barkhausen) en los mismos microhilos magnéticos correctamente posprocesados, es potencialmente adecuada para aplicaciones completamente nuevas que se esperan desarrollar.

List of publications

i. Publications related to this work

[1] **P. Corte-León**, V. Zhukova, J.M. Blanco, M. Ipatov, A. Fert, J. Gonzalez, A. Zhukov, Domain wall propagation in Fe-rich magnetic microwires with graded magnetic anisotropy, AIP Adv. 12 (2022) 035228, doi:10.1063/9.0000324.

[2] A. Gonzalez, V. Zhukova, M. Ipatov, **P. Corte-León**, J.M. Blanco, A. Zhukov, Effect of Joule heating on GMI and magnetic properties of Fe-rich glass-coated microwires, AIP Adv. 12 (2022) 035021, doi:10.1063/9.0000290.

[3] **P. Corte-León**, V. Zhukova, J.M. Blanco, A. Irigaray, A. Gonzalez, M. Ipatov, A. Zhukov, Graded magnetic anisotropy in Co-rich microwires, AIP Adv. 12 (2022) 035215, doi:10.1063/9.0000315.

[4] A. Gonzalez, V. Zhukov, **P. Corte-Leon**, A. Chizhik, M. Ipatov, J.M. Blanco, A. Zhukov, Tuning of Magnetoimpedance Effect and Magnetic Properties of Fe-Rich Glass-Coated Microwires by Joule Heating, Sensors 22 (2022) 1053.

[5] **P. Corte-Leon**, L. Gonzalez-Legarreta, M.Ipatov, J.M. Blanco, A. Gonzalez, V. Zhukova, Advanced functional magnetic microwires for technological applications, Arcady Zhukov, J. Phys. D: Appl. Phys. (Accepted) (2022), doi:10.1088/1361-6463/ac4fd7.

[6] V. Zhukova, **P. Corte-León**, J.M. Blanco, M. Ipatov, L. Gonzalez-Legarreta, A. Gonzalez, A. Zhukov, Development of Magnetically Soft Amorphous Microwires for Technological Applications, Chemosensors 10 (2022) 26.

[7] V. Zhukova, **P. Corte-León**, J.M. Blanco, M. Ipatov, A. Gonzalez, A. Zhukov, Development of Co-Rich Microwires with Graded Magnetic Anisotropy, Sensors 22(1) (2022) 187.

[8] **P. Corte-León**, V. Zhukova, J.M. Blanco, A. Chizhik, M. Ipatov, J. Gonzalez, A. Fert, A. Alonso, A. Zhukov, Engineering of domain wall propagation in magnetic microwires with graded magnetic anisotropy, Appl. Mater. Today 26 (2021) 101263, ISSN 2352-9407.

[9] A. Zhukov, L. Gonzalez-Legarreta, **P. Corte-Leon**, M. Ipatov, J.M. Blanco, J. Gonzalez, V. Zhukova, Tailoring of Magnetic Softness and Magnetoimpedance of Co-Rich Microwires by Stress Annealing, Phys. Status Solidi A 218 (2021) 2100130.

[10] **P. Corte-León**, V. Zhukova, M. Ipatov, J.M. Blanco, A. Zhukov, Effect of Joule heating on giant magnetoimpedance effect and magnetic properties of Co-rich microwires, J. Alloys Compd. 883 (2021) 160778, ISSN 0925-8388, (2021).

[11] V. Zhukova, **P. Corte-León**, J.M. Blanco, M. Ipatov, J. Gonzalez, A. Zhukov, Electronic Surveillance and Security Applications of Magnetic Microwires, Chemosensors 9 (2021) 100.

[12] **P. Corte-León**, V. Zhukova, J.M. Blanco, M. Ipatov, S. Taskaev, J. González, A. Zhukov, Development of iron-rich microwires with a unique combination of magnetic properties, Scr. Mater. 195 (2021) 113726.

[13] **P. Corte-León**, V. Zhukova, J.M. Blanco, M. Ipatov, J. Gonzalez, A. Zhukov, Engineering of magnetic properties and magnetoimpedance effect in Fe-rich microwires by reversible and irreversible stress-annealing anisotropy, J. Alloys Compd. 855(2) (2021) 157460, doi:10.1016/jallcom.2020.157460.

[14] **P. Corte-León**, V. Zhukova, A. Chizhik, J.M. Blanco, M. Ipatov, L. González-Legarreta, A. Zhukov, Magnetic Microwires with Unique Combination of Magnetic Properties Suitable for Various Magnetic Sensor Applications, Sensors 20(24) (2020) 7203.

[15] V. Zhukova, **P. Corte-León**, L. González-Legarreta, A. Talaat, J.M. Blanco, M. Ipatov, J. Olivera, A. Zhukov, Review Domain Wall Dynamics Engineering in Magnetic Microwires, Nanomaterials 10 (2020) 2407.

[16] V. Zhukova, **P. Corte-León**, M. Ipatov, J.M. Blanco, J. Olivera, A. Zhukov, Magnetic properties and applications of glass-coated ferromagnetic microwires, AEMAC 4(4) (2020) 107-113, ISSN 2531-0739.

[17] A. Allue, **P. Corte-León**, K. Gondra, V. Zhukova, M. Ipatov, J.M. Blanco, J. Gonzalez, A. Zhukov, Smart composites with magnetic microwire inclusions allowing non-contact stress and temperature monitoring, AEMAC 4(4) (2020) 114-119, ISSN 2531-0739.

[18] V. Zhukova, **P. Corte-León**, L. González-Legarreta, A. Talaat, J.M. Blanco, M. Ipatov, J. Olivera, A. Zhukov, Optimization of Magnetic Properties of Magnetic Microwires by Post-Processing, Processes 8(8) (2020) 1006, doi:10.3390/pr8081006.

[19] A. Chizhik, J. Gonzalez, A. Zhukov, P. Gawroński, M. Ipatov, **P. Corte-Leon**, J.M. Blanco, V. Zhukova, Reversible and non-reversible transformation of magnetic structure in amorphous microwires, Nanomaterials 10 (2020) 1450, doi: 10.3390/nano10081450

[20] **P. Corte-Leon**, V. Zhukova, M. Ipatov, J.M. Blanco, J. Gonzalez, M. Churyukanova, S. Taskaev, A. Zhukov, The effect of annealing on magnetic properties of "Thick" microwires, J. Alloys Compd. 831 (2020) 150992.

[21] D. González-Alonso, L. González-Legarreta, **P. Corte-Leon**, V. Zhukova, M. Ipatov, J.M. Blanco, A. Zhukov, Magnetoimpedance Response and Field Sensitivity in Stress-Annealed Co-Based Microwires for Sensor Applications, Sensors 20(11) (2020) 3227.

[22] L. Gonzalez-Legarreta, **P. Corte-Leon**, V. Zhukova, M. Ipatov, J.M. Blanco, J. Gonzalez, A. Zhukov, Optimization of magnetic properties and GMI effect of Thin Co-rich Microwires for GMI Microsensors, Sensors 20(6) (2020) 1558.

[23] L. Gonzalez-Legarreta, **P. Corte-León**, V. Zhukova, M. Ipatov, J.M. Blanco, Margarita Churyukanova, Sergey Taskaev, Arcady Zhukov, Route of magnetoimpedance and domain walls dynamics optimization in Co-based microwires, J. Alloys Compd. 830 (2020) 154576.

[24] A. Zhukov, M. Ipatov, **P. Corte-Leon**, L. Gonzalez-Legarreta, J.M. Blanco, V. Zhukova, Soft magnetic microwires for sensor applications, J. Magn. Magn. Mater. 498 (2020) 166180.

[25] V. Zhukova, **P. Corte-Leon**, L. González-Legarreta, M. Ipatov, A. Talaat, J.M. Blanco, J. Gonzalez, J. Olivera, A. Zhukov, Stress-Induced Magnetic Anisotropy Enabling Engineering of Magnetic Softness GMI Effect and Domain Wall Dynamics of Amorphous Microwires, Phys. Met. 121 (2020) 316-321.

[26] **P. Corte-León**, L. Gonzalez-Legarreta, V. Zhukova, M. Ipatov, J.M. Blanco, M. Churyukanova, S. Taskaev, A. Zhukov, Controlling the domain wall dynamics in Fe-, Ni-and Co-based magnetic microwires, J. Alloys Compd. 834 (2020) 155170.

[27] **P. Corte-Leon**, V. Zhukova, J.M. Blanco, L. González-Legarreta, M. Ipatov, A. Zhukov, Stress-induced magnetic anisotropy enabling engineering of magnetic softness of Fe-rich amorphous microwires, J. Magn. Magn. Mater. 510(15) (2020) 166939.

[28] A. Zhukov, M. Ipatov, **P. Corte-León**, J.M. Blanco, L. Gonzalez-Legarreta, V. Zhukova, Routes for optimization of giant magnetoimpedance effect in magnetic microwires, IEEE Instrum. Meas. Mag. 23(1) (2020) 56-63.

[29] **P. Corte-León**, A. Talaat, V. Zhukova, M.Ipatov, J.M. Blanco, J. González, A. Zhukov, Stress-Induced Magnetic Anisotropy Enabling Engineering of Magnetic Softness and GMI Effect of Amorphous Microwires, Appl. Sci. 10 (2020) 981.

[30] V. Zhukova, A. Talaat, **P. Corte-León**, J.M. Blanco, M. Ipatov, A. Zhukov, Engineering of magnetic properties and domain wall dynamics in Fe-Ni-based amorphous microwires by annealing, AIP Adv. 10 (2020) 015130.

[31] **P. Corte-León**, L. Gonzalez-Legarreta, M. Churyukanova, J.M. Blanco, J. Gonzalez, S. Taskaev, B. Hernando, V. Zhukova, Giant Magnetoimpedance in Rapidly Quenched Materials, A. Zhukov, M. Ipatov, J. Alloys Compd. 814(25) (2020) 152225, doi: 10.1016/j.jallcom.2019.152225.

[32] A. Zhukov, L. Gonzalez-Legarreta, M. Ipatov, **P. Corte-León**, J.M. Blanco, V. Zhukova, Giant magnetoimpedance effect at GHz frequencies in amorphous microwires, AIP Adv. 9, (2019) 125333.

[33] V. Zhukova, **P. Corte-León**, M. Ipatov, J.M. Blanco, L. Gonzalez-Legarreta, A. Zhukov, Development of Magnetic Microwires for Magnetic Sensor Applications, Sensors 19(21) (2019) 4767.

[34] **P. Corte-León**, V. Zhukova, M. Ipatov, J.M. Blanco, J. Gonzalez, L. Dominguez, M. Churyukanova, A. Zhukov, High frequency giant magnetoimpedance effect of a stress-annealed Fe-rich glass-coated microwire, J. Alloys Compd. 802(25) (2019) 112-117.

[35] **P. Corte-León**, J.M. Blanco, V. Zhukova, M. Ipatov, J. Gonzalez, M. Churyukanova, S. Taskaev, A. Zhukov, Engineering of Magnetic Softness and Domain Wall Dynamics of Fe-rich Amorphous Microwires by Stress-induced Magnetic Anisotropy, Sci. Rep. 9(1) (2019) 1-14.

[36] A. Zhukov, **P. Corte-León**, L. Gonzalez-Legarreta, M. Ipatov, A. Talaat, J.M. Blanco, J. Gonzalez, V. Zhukova, Magnetic microwires for sensor applications, Adv. Mater. Lett. 10(5) (2019) 305-311.

[37] **P. Corte-León**, V. Zhukova, M. Ipatov, J.M. Blanco, J. Gonzalez, A. Zhukov, Magnetic properties of "thick" glass-coated Fe-rich microwires, AIP Adv. 9 (2019) 035017.

[38] **P. Corte-León,** V. Zhukova, M. Ipatov, J.M. Blanco, J. Gonzalez, M. Churyukanova, J.M. Baraibar, S. Taskaev, A. Zhukov, Stress dependence of the magnetic properties of glass-coated amorphous microwires, J. Alloys Compd. 789 (2019) 201-208, doi:10.1016/j.jallcom.2019.03.044.

[39] A. Allue, **P.Corte-León**, K. Gondra, V. Zhukova, M. Ipatov, J.M. Blanco, J. Gonzalez, M. Churyukanova, S. Taskaev, A. Zhukov, Smart composites with embedded magnetic microwire inclusions allowing non-contact stresses and temperature monitoring, Compos. Part A Appl. 120 (2019) 12-20 doi:10.1016/j.compositesa.2019.02.014.

[40] **P. Corte-León**, V. Zhukova, M. Ipatov, J.M. Blanco, J. Gonzalez, A. Zhukov, Engineering of magnetic properties of Co-rich microwires by Joule heating, Intermetallics 105 (2019) 92-98, doi:10.1016/j.intermet.2018.11.013.

[41] **P. Corte-León**, V. Zhukova, M. Ipatov, J.M. Blanco, J. González, A. Zhukov, Optimization of GMI Effect and Magnetic Properties of Co-Rich Microwires by Joule Heating, IEEE Trans. Magn. 55(2) (2019) 2000404, doi:10.1109/TMAG.2018.2868895.

[42] **P. Corte-León**, J.M. Blanco, M. Ipatov, J. Gonzalez, V. Zhukova, Engineering of Magnetic Properties of Fe-Rich Microwires by Stress Annealing, Arcady Zhukov, IEEE Trans. Magn. 55(2) (2019) 2000504, doi:10.1109/TMAG.2018.2866452.

[43] A. Chizhik, J. Gonzalez, **P. Corte-Leon**, A. Zhukov, A. Stupakiewicz, Route of Tuning of Magnetic Properties in Magnetic Microwires, IEEE Magn. Lett. 9 (2018) 1405304, doi: 10.1109/LMAG.2018.2860940.

[44] V. Zhukova, J.M. Blanco, **P. Corte-Leon**, M. Ipatov, M. Churyukanova, S. Taskaev, A. Zhukov, Grading the magnetic anisotropy and engineering the domain wall dynamics in Fe-rich microwires by stress-annealing, Acta Mater. 155 (2018) 279-285, doi: 10.1016/j.actamat.2018.05.068.

[45] V. Zhukova, **P. Corte-León**, M. Ipatov, A. Talaat, J.M. Blanco, J. Olivera, J. Gonzalez, A.P. Zhukov, Tailoring of magnetic softness and GMI effect in Fe-rich thin magnetic wires, AIP Adv. 8(5) (2018) 056102, doi:10.1063/1.5004701.

[46] A. Zhukov, M. Ipatov, J.M. Blanco, **P. Corte-León**, J. Olivera, J. Gonzalez, V. Zhukova, Engineering of Magnetic Properties of Magnetic Microwires, Acta Phys. Pol. A 133(3) (2018) 321-328, doi:10.12693/APhysPolA.133.321.

ii. Other publications

[1] A. Chizhik, **P. Corte-León**, V. Zhukova, J. Gonzalez, A. Zhukov, MOKE studies of magnetic microwires with longitudinally distributed properties, J. Magn. Magn. Mater. 547 (2022) 168824.

[2] A. Chizhik, J. Gonzalez, A. Zhukov, **P. Corte-Leon**, V. Zhukova, P. Gawroński, A. Stupakiewicz, Influence of Combined Mechanical Stress on Magnetic Structure in Magnetic Microwires, J. Magn. Magn. Mater. 513 (2020) 166974.

[3] C. Garcia, V. Zhukova, S.Shevyrtalov, M. Ipatov, **P. Corte-Leon**, A. Zhukov, Tuning of magnetic properties in Ni-Mn-Ga Heusler-type glass-coated microwires by annealing, J. Alloys Compd. 838(15) (2020) 155481.

[4] V. Zhukova, M. Ipatov, **P. Corte-León**, J.M. Blanco, E. Zanaeva, A. I. Bazlov, J. Jiang, D.V. Louzguine-Luzgin, J. Olivera, A. Zhukov, Excellent magnetic properties of $(Fe_{0.7}Co_{0.3})_{83.7}Si_4B_8P_{3.6}Cu_{0.7}$ ribbons and microwires, Intermetallics 117 (2020) 10660.

[5] **P. Corte-Leon**, V. Zhukova, L. Domínguez, J.M. Blanco, M. Ipatov, A. Chizhik, A. Zhukov, J. Gonzalez, Giant magnetoimpedance and magneto-optical Kerr effects in $(Co_{63}Ni_{37})_{75}Si_{15}B_{10}$ amorphous ribbon, Intermetallics 125 (2020) 106925, doi: 10.1016/j.internet.2020.106925.

[6] M. Churyukanova, S. Kaloshkin, E. Shuvaeva, A. Mitra, A.K. Panda, R.K. Roy, P. Murugaiyan, **P. Corte-León**, V. Zhukova, A. Zhukov, The effect of heat treatment on magnetic and thermal properties of Finemet-type ribbons and microwires, J. Magn. Magn. Mater. 492 (2019) 165598.

[7] A. Chizhik, A. Zhukov, **P. Corte-León**, J.M. Blanco, J. Gonzalez, P. Gawronski, Torsion induced acceleration of domain wall motion in magnetic microwires, J. Magn. Magn. Mater. 489(1) (2019) 165420.

[8] A. Zhukov, M. Ipatov, J.J. del Val**,** **P.Corte-León**, J. Gonzalez, A. Granovsky, V. Zhukova, Effect of annealing on magnetic properties of Ni–Mn–Ga glass-coated microwires, J. Mater. Res. 33(15) (2018) 2148-2155, doi:10.1557/jmr.2018.105.

iii. Book Chapters

[1] A. Zhukov, M. Ipatov, J.M. Blanco, **P. Corte-Leon**, V. Zhukova, Heusler-type glass-coated microwires: Fabrication, characterization, and properties in Magnetic Nano-and Microwires, Woodhead Publishing Series in Electronic and Optical Materials, (Ed. Manuel Vázquez), pp. 255-294, Elsevier (2020).

[2] A. Zhukov, M. Ipatov, **P. Corte-León**, J.M. Blanco, V. Zhukova, Advanced functional magnetic microwires for magnetic sensors suitable for biomedical applications in Magnetic Materials and Technologies for Medical Applications, Woodhead Publishing Series in Electronic and Optical Materials, (Ed. A.M. Tishin), Elsevier (2021).

iv. Conference proceedings

[1] A. Zhukov, **P. Corte-León**, L. Gonzalez-Legarreta, M. Ipatov, J.M. Blanco, V. Zhukova, Optimization of Giant Magnetoimpedance Effect in Fe-rich Microwires, 2018 International Conference on Electromagnetics in Advanced Applications (ICEAA), IEEE Xplore pp. 134-137, 2018, doi:10.1109/ICEAA.2018.8520524.

[2] A. Zhukov, **P. Corte-León**, M. Ipatov, J.M. Blanco, J. Gonzlez, V. Zhukova, Engineering of Giant Magnetoimpedance Effect in Co-rich Microwires by Joule heating, 2018 International Conference on Electromagnetics in Advanced Applications (ICEAA), IEEE Xplore pp. 130-133, 2018, doi:10.1109/ICEAA.2018.8520420.

[3] **P.Corte-León**, L. Gonzalez-Legarreta, V. Zhukova, M. Ipatov, J. Gonzalez, J.M. Blanco, A. Zhukov, Tunning the Giant Magnetoimpedance Effect in Fe-rich Magnetic Microwires by Stress-annealing, Proceedings of The Ninth International Conference on Sensor Device Technologies and Applications, SENSORDEVICES 2018, IARIA, pp. 6-11, 2018, ISBN: 978-1-61208-660-6.

[4] **P. Corte-León**, L. Gonzalez-Legarreta, V. Zhukova, M. Ipatov, J. Gonzalez, J.M. Blanco, A. Zhukov, Optimization of Giant Magnetoimpedance Effect in Co-rich Magnetic Microwires, Proceedings of The Ninth International Conference on Sensor Device Technologies and Applications, SENSORDEVICES 2018, IARIA, pp.1-5, 2018, ISBN**:** 978-1-61208-660-6.

v. Conference participation

- "ImagineNano2018 International Event - Nanospain2018 Conference", Bilbao, Spain, 13-15 March.
  Poster presentation: P. Corte-León, V. Zhukova, M. Ipatov, J.M. Blanco, J. González, A. Zhukov, "Engineering of magnetic properties of Co-rich microwires by Joule heating"

- ESRW18, 8th Early Stage Researchers Whorkshop in Nanoscience, Instituto IMDEA Nanociencia, 2018, Madrid, Spain, 13-14 June.
  Oral presentation: P. Corte-Leon, V. Zhukova, M. Ipatov, J. M. Blanco, J. Gonzalez, A. Zhukov**,** "Engineering of magnetic properties of Co-rich microwires by Joule heating"

- ISMANAM 2018, 25th International Symposium on Metastable, Amorphous and Nanostructured Materials, Roma, Italy, 2-6 July.
  Poster presentation: P. Corte-Leon, V. Zhukova, M. Ipatov, J. M. Blanco, J. Gonzalez, A. Zhukov, "The Effect of annealing on Magnetic Properties of Thick Microwires",

- Jornada de Jóvenes Investigadores en Magnetismo at the Spanish Magnetism Club and the Spanish Chapter of the IEEE Magnetics Society Annual Joint Meeting, Gijón, Spain, 29-30 November 2018.
  Oral presentation: P. Corte-Leon, V. Zhukova, M. Ipatov, J.M. Blanco, J. Gonzalez, A. Zhukov, "Non-contact monitoring of composite polymerization through the impact on magnetic properties of magnetic microwire inclusions"

- 2019 JOINT MMM-INTERMAG, Washington, DC, USA, 14-18 January.
  Oral presentation: A. Chizhik, A. Zhukov, J. Gonzalez, **P. Corte-Leon,** "Multi-parameters Optimization of Magnetic Properties in Microwires for Sensor Application"

  Poster presentation: P. Corte-Leon, V. Zhukova, M. Ipatov, J.M. Blanco, J. Gonzalez, A. Zhukov, "The Effect of annealing on Magnetic Properties of "Thick" Microwires"

- 10th International Conference on Fine Particle Magnetism ICFPM2019, Gijón, Spain, 26-31 May 2019.
  Oral presentation: P. Corte-Leon, V. Zhukova, M. Ipatov, J.M. Blanco, J. Gonzalez, A. Zhukov, "Stress dependence of the magnetic properties of glass-coated amorphous microwires"

- The 2020 Around-the-Clock Around the Globe Magnetics Conference, IEEE Magnetics Society, 27 August 2020, (online).
  Oral presentation: P. Corte-León, V. Zhukova, J.M. Blanco, M. Ipatov, S. Taskaev, M. Churyukanova, J. González, A. Zhukov, "Engineering of magnetic properties and magnetoimpedance effect in Fe-rich microwires by reversible and irreversible stress-annealing anisotropy"

- 150th ANNUAL MEETING & EXHIBITION, TMS 2021 Virtual, March 15-18, 2021.
  Oral presentation: P. Corte-León, L. Gonzalez-Legarreta, V. Zhukova, M. Ipatov, J.M. Blanco, A. Zhukov, "Engineering of magnetic properties of Co-rich microwires by post-processing"

Oral presentation: P. Corte-León, V. Zhukova, J.M. Blanco, M. Ipatov, S. Taskaev, M. Churyukanova, J. Gonzalez, A. Zhukov, "Engineering of magnetic properties and magnetoimpedance effect in Fe-rich microwires by reversible and irreversible stress-annealing anisotropy"

- 2022 JOINT MMM-INTERMAG, New Orleans, LA, USA, 10-14 January.
  Oral presentation: P. Corte-León, V. Zhukova, J.M. Blanco, M. Ipatov, A. Zhukov, "Domain wall propagation in Fe-rich magnetic microwires with graded magnetic anisotropy"
  Oral presentation: P. Corte-León, V. Zhukova, J.M. Blanco, M. Ipatov, A. Zhukov, "Graded magnetic anisotropy in Co-rich microwires"

vi. Scholar fellowships and research stays abroad

- **2019:** (June 2nd - July 2nd) UPV/EHU Mobility fellowship for one month stay realized at Department of Physics, Universidad Técnica Federico Santa María, Valparaíso, Chile.

- **2021:** (February 1st – April 16th) stay realized at the Department of Applied Magnetism and Nanomaterials of the Institute of Experimental Physics of the Slovak Academy of Sciences, Košice, Eslovaquia.